

MÖSSBAUER SPECTRA OF INORGANIC COMPOUNDS: BONDING AND STRUCTURE

G. M. Bancroft

Chemistry Department, University of Western Ontario, London, Canada

and

R. H. Platt

University Chemical Laboratory, University of Cambridge, Cambridge, England

I. Preface	59
II. Introduction	60
A. The Mössbauer Effect	60
B. Isomer and Center Shift	61
C. Quadrupole Splitting	63
D. The Additivity Model for Quadrupole Splittings	71
III. Fingerprint Uses	89
A. Oxidation States and Inequivalent Mössbauer Atoms	89
B. Decomposition Reactions	94
C. The Effect of Temperature and Pressure on the Electronic Structure of Iron Compounds	95
D. Site Populations in Silicate Minerals	97
E. Preparation of Novel Compounds	100
F. Frozen Solution Studies	101
IV. Bonding and Structure	103
A. Sn ^{IV} Compounds	103
B. Fe ^{II} Low-Spin Compounds	166
C. Ru ^{II} and Ir ^{III} Compounds	184
D. Iodine Compounds	187
E. Sn ^{II} Compounds	201
F. Other Oxidation States of Iron	208
G. Other Mössbauer Isotopes	227
References	241

I. Preface

The Mössbauer effect, discovered by R. L. Mössbauer in 1957 (413) began to be widely applied to chemical problems after it was shown in 1960 that ⁵⁷Fe exhibited this phenomenon (369). In the last ten years, Mössbauer spectroscopy has become a powerful and versatile probe in many areas of chemistry. The great fraction of Mössbauer research has been carried out using ⁵⁷Fe and ¹¹⁹Sn. However, over thirty other isotopes exhibit the effect (411) and chemically interesting information has been obtained on compounds of Ni, Kr, Ru, Sb, Te, I, Xe, W, Ir, Au,

Np, and many of the rare earths, although the use of several of the above isotopes presents considerable experimental difficulties and inconvenience.

Despite the great growth of Mössbauer research in inorganic chemistry in the last ten years and the number of books (14, 110, 247, 270, 274, 412, 536, 559) and reviews (175, 198, 235, 277, 297, 324, 437, 516, 577), the technique has largely remained in the hands of the specialists. It is our intention in this chapter to review critically recent Mössbauer studies which illustrate the use of this technique first, in rather simple fingerprint applications, and second, in the determination of the structure and bonding in inorganic compounds. Hopefully, this will hasten the advance of Mössbauer spectroscopy as a routine method in inorganic chemistry departments and industry.

We severely limit the scope of this chapter by neglecting not only the basic physics of the experiment and how it arises (247), but also experimental details (110). We will also just discuss the use of two Mössbauer parameters, the isomer or center shift and quadrupole splitting, and neglect magnetic splitting and magnetic effects. Useful bonding information can be obtained from magnetic splittings (357), but the overwhelming majority of inorganic compounds do not show magnetic splitting at temperatures of 77°K (liquid N₂) and above.

In a chapter of this scope it is neither feasible nor desirable to attempt to give a comprehensive account of every pertinent paper or to include a catalog of all Mössbauer data. Rather we have tried to present a critical account of the major areas in which Mössbauer spectroscopy has been applied recently to the problems of structure and bonding for all isotopes except the rare earths and actinides and to include enough data for the reader to judge the scope and limitations of this spectroscopy. Annual surveys of the Mössbauer literature are available in the excellent series of articles by Greenwood (298). For ¹¹⁹Sn Mössbauer spectroscopy, two very recent compilations of data have been published (437, 577).

II. Introduction

A. THE MÖSSBAUER EFFECT

Mössbauer spectroscopy can be likened to ultraviolet spectroscopy. Both techniques employ a source of radiation, an absorber and a detector. In Mössbauer spectroscopy, we consider transitions between nuclear energy levels with the emission and absorption of γ rays; whereas, in ultraviolet spectroscopy, we consider the transitions between electronic energy levels with the emission and absorption of ultraviolet radiation.

To observe resonance, a range of source photon energies is scanned: in ultraviolet by the use of a prism or grating, and in Mössbauer by employing the Doppler effect. The energy of the γ ray (E_γ) is varied by the well-known Doppler formula

$$\Delta E = (v/c)E_\gamma$$

where ΔE = change in energy of γ photon, v = velocity of source relative to absorber, and c = velocity of light. As in ultraviolet, absorption is plotted versus the energy of source photon (usually in velocity units for Mössbauer). Different compounds of one isotope give different spectra, i.e., the nuclear energy levels are sensitive to the extranuclear environment. These differences in spectra can be attributed to the hyperfine interactions—the interactions between the nuclear charge distribution and the extranuclear electric and magnetic fields. These hyperfine interactions give rise to the isomer shift (I.S.), the quadrupole splitting (Q.S.), and the magnetic Zeeman splitting. As mentioned previously, we will be concerned with the first two parameters.

B. ISOMER AND CENTER SHIFT

The isomer shift results from the electrostatic interaction between the charge distribution of the nucleus and those electrons which have a finite probability of being found in the region of the nucleus. The above interaction results in a slight shift of both ground and excited nuclear energy levels in a compound relative to those in the free atom. The shifts will be different in source and absorber and a Doppler velocity will have to be supplied to the source or absorber to observe resonance, i.e., for resonance

$${}^sE_\gamma \pm (v/c) {}^sE_\gamma = {}^aE_\gamma,$$

where ${}^sE_\gamma$ and ${}^aE_\gamma$ are the source and absorber transition energies, respectively.

However, a similar shift in energy levels can arise from the second-order Doppler (S.O.D.) shift which arises from the thermal motion of the Mössbauer atoms (319, 360). The observed center or chemical shift (C.S.) is a resultant of both the isomer shift and S.O.D. shift; although the latter is usually much smaller than the isomer shift and is usually neglected. The center shift (C.S.) will be used in this chapter, although other terms such as chemical or chemical isomer shift are also commonly used.

The isomer shift can be computed classically by considering the effect of the overlap of s electron density with the nuclear charge density.

First-order perturbation theory (75, 247) gives the isomer shift δ as:

$$\delta = K \frac{\delta R}{R} \{[\Psi(O)_s]_a^2 - [\Psi(O)_s]_s^2\} \quad (1)$$

where $[\Psi(O)_s]_a^2$ and $[\Psi(O)_s]_s^2$ are the total s electron densities at the absorber and source atoms, respectively, K is a constant for a given isotope, and $\delta R = R_{\text{ex}} - R_{\text{gr}}$, where R_{ex} and R_{gr} are the radius of the excited and ground nuclear states, respectively. The isomer shift depends on a nuclear factor $\delta R/R$ and an extranuclear factor—the s electron densities. For some isotopes such as ^{57}Fe , δR is negative and, thus, if $[\Psi(O)_s]_a^2 < [\Psi(O)_s]_s^2$, then a positive shift is observed. For other isotopes,

TABLE I
 s ELECTRON DENSITIES AT THE IRON NUCLEUS FOR
DIFFERENT d CONFIGURATIONS^a

d Electron configuration	Electron density at iron nucleus (atomic units)
d^8	11,878.6
d^7	11,879.1
d^6	11,879.5
d^5	11,881.3
d^4	11,885.2
d^3	11,892.0

^a From Refs. (160, 555).

such as ^{119}Sn , δR is positive and, thus, if $[\Psi(O)_s]_a^2 > [\Psi(O)_s]_s^2$, a positive shift is observed. For a given source, e.g., ^{57}Co in Pd, an increase in I.S. is observed when the s electron density in absorbers decreases.

Although changes in isomer shift are due to variations in s electron density, differences in isomer shifts are observed on addition or removal of p or d electrons which do not themselves interact with the nuclear charge density. Hartree-Fock calculations for different d^n configurations by Watson (Table I) (160, 555) show that a decrease in the number of Fe $3d$ electrons causes a marked increase in the $3s$ electron density at the nucleus. This trend arises indirectly via the $3s$ electrons which spend a fraction of their time further from the nucleus than the $3d$ electrons, causing the $3s$ electrons to expand, and thus reduce the s electron density at the nucleus. On this basis, one would expect that a d^6 ion (Fe^{2+}) would have a larger isomer shift than a d^5 ion (Fe^{3+}).

In a molecule, the picture becomes more complex because the s , p , and d electron densities will be modified by covalent bonding (553). For example, in ^{57}Fe , the two important bonding interactions, σ bonding and π back-bonding, contribute both to a $4s$ population and a change in the d -orbital population from the free ion value. Isomer shifts have been calculated for a variety of $3d$ and $4s$ configurations for ^{57}Fe , but for a variety of reasons, these calculations are not entirely satisfactory (216). For our purposes, it is usually extremely useful just to obtain *relative* changes in valency orbital populations from *relative* isomer shifts, keeping in mind that an increase in $4s$ density decreases the isomer shift, whereas an increase in $3d$ density increases the isomer shift.

For ^{119}Sn , the sign of $\delta R/R$ was in dispute for some time. However, this is now known to be positive (381), and the isomer shift will thus increase with an increase in s electron density, but decrease with an increase in p electron density. Lees and Flinn have derived an equation for the isomer shift relative to Mg_2Sn as a function of the number of $5s$ and $5p$ electrons (designated n_s and n_p , respectively) (381):

$$\text{I.S.} = -2.36 + 3.01n_s - 0.20n_s^2 - 0.17n_s n_p \quad (2)$$

Similar equations have been derived for other isotopes (498, 510). These equations indicate that the isomer shift should be much more sensitive to the s electron density than the p electron density, and could be used in conjunction with Q.S. data to obtain both n_s and n_p . It would be expected that covalent tin ($5s\ 5p^3$) would have a more positive shift than "ionic" Sn^{IV} compounds, which can, for convenience, be classified as having the electronic configuration $4d^{10}$, and that the isomer shift in Sn compounds will vary with the covalent character of its bonds.

C. QUADRUPOLE SPLITTING

If the nucleus is not spherical, as assumed above, and $I > \frac{1}{2}$, the interaction of noncubic extranuclear electric fields with the nuclear charge density results in a splitting of the nuclear energy levels. For example, for ^{57}Fe and ^{119}Sn , the $I = \frac{3}{2}$ level splits into two, while the $I = \frac{1}{2}$ level remains degenerate (Fig. 1). A characteristic two-line spectrum is obtained (Fig. 1) from the two allowed transitions. The separation of the peaks is the quadrupole splitting (Q.S.), and the centroid of the two peaks relative to the source is the center shift. For noninteger nuclear spins the quadrupole interaction results in $I + \frac{1}{2}$ levels, but for integer spins, it is possible to obtain $2I + 1$ levels, and the degeneracy is completely removed. If I is large for ground and excited states, then complex

spectra can be observed, and it becomes more difficult to obtain the hyperfine parameters (252, 345, 568).

The magnitude of the quadrupole splitting is proportional to the electric field gradient (EFG) tensor which interacts with the quadrupole moment of the nucleus. While the isomer shift measures the s electron density at the nucleus, the EFG tensor measures the distortion from

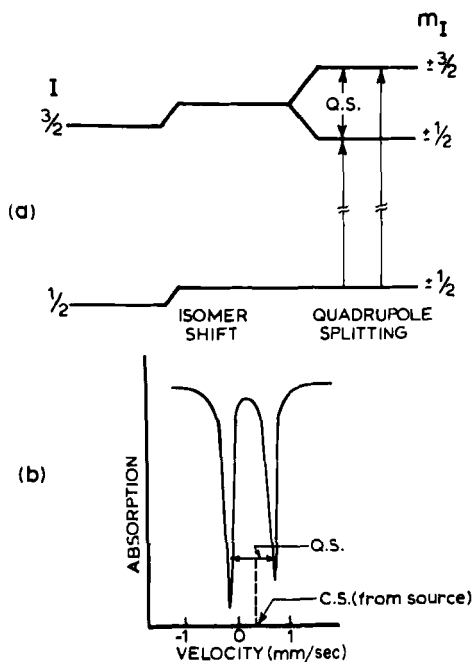


FIG. 1. (a). Nuclear energy levels, the isomer shift, and quadrupole splitting for $I_{gr} = \frac{1}{2}$, $I_{ex} = \frac{3}{2}$. (b) Resultant Mössbauer spectrum.

cubic symmetry of the electron distribution and ligands about the Mössbauer atom.

The EFG tensor has nine components which arise in the following way (136). The electric field at the Mössbauer nucleus is the negative gradient of the potential V and the EFG is the gradient of the electric field E .

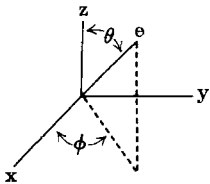
$$\text{EFG} = \nabla E = - \begin{bmatrix} V_{xx} & V_{xy} & V_{xz} \\ V_{yx} & V_{yy} & V_{yz} \\ V_{zx} & V_{zy} & V_{zz} \end{bmatrix} \quad (3)$$

where

$$V_{xx} = \frac{\partial^2 V}{\partial x^2}, \quad V_{xy} = \frac{\partial^2 V}{\partial x \partial y}, \text{ etc.}$$

If we assume that the EFG is set up by point charges, e , the contribution of one point charge to each component of the EFG tensor is given by the expressions in Table II (136). The polar coordinates are defined in the

TABLE II
COMPONENTS OF ELECTRIC FIELD GRADIENT TENSOR FOR
A POINT CHARGE OF 1 PROTONIC CHARGE e

Components	Coordinates
$V_{xx} = er^{-3}(3 \sin^2 \theta \cos^2 \phi - 1)$ $V_{yy} = er^{-3}(3 \sin^2 \theta \sin^2 \phi - 1)$ $V_{zz} = er^{-3}(3 \cos^2 \theta - 1)$ $V_{xy} = V_{yx} = er^{-3}(3 \sin^2 \theta \sin \phi \cos \phi)$ $V_{xz} = V_{zx} = er^{-3}(3 \sin \theta \cos \theta \cos \phi)$ $V_{yz} = V_{zy} = er^{-3}(3 \sin \theta \cos \theta \sin \phi)$	

normal fashion. The above tensor can be reduced to diagonal form if the coordinate axes are properly chosen so that the EFG can be completely specified by the three components V_{xx} , V_{yy} , and V_{zz} .^{*} However, even these three are not independent, since

$$V_{xx} + V_{yy} + V_{zz} = 0 \quad (4)$$

There are, then, only two independent parameters and these are normally chosen to be V_{zz} and η , where $\eta = (V_{xx} - V_{yy})/V_{zz}$. The EFG axes are chosen so that $|V_{zz}| \geq |V_{yy}| \geq |V_{xx}|$, thus constraining η to have values between 0 and 1. Many of the properties of the EFG tensor can be deduced from the symmetry properties of the crystal. For example, if a molecule has a fourfold axis of symmetry (as in *trans*-MA₂B₄) (where M is a Mössbauer isotope), then this axis is chosen to be the Z direction of the EFG tensor. A rotation of 90° about the Z axis produces no change in the EFG tensor, and it follows that $V_{xx} = V_{yy}$ and $\eta \equiv 0$. However, in some cases of interest (e.g. *cis*-MA₂B₄), the Z EFG axes do not coincide with the highest symmetry axes of the molecule. The proper

* The initial axes will be distinguished from the principal EFG axes in this article by using small letters x , y , z , and V_{xx} , V_{yy} , V_{zz} , etc., for the former, but X , Y , Z and V_{XX} , V_{YY} , V_{ZZ} for the latter.

choice of EFG axes is illustrated later in this article for many cases of interest (Table IV).

For the $I = \frac{3}{2}$ case (^{57}Fe and ^{119}Sn), the Q.S. can be expressed as:

$$\Delta \equiv \text{Q.S.} = \frac{1}{2}e^2qQ(1 + \eta^2/3)^{1/2} \quad (5)$$

where Q is the quadrupole moment of the nucleus, $eq = V_{zz} = -$ the Z component of the EFG, and $e =$ protonic charge $= 4.80 \times 10^{-10}$ e.s.u. Either q or V_{zz} is normally referred to as the field gradient. It should be kept in mind that the signs of q and the Z component of the EFG are different.

Ideally, we would like to obtain three pieces of information from a measurement of the quadrupole splitting: the magnitude of q and η , and the sign of q . It should be noted that like $\delta R/R$, Q can be either positive or negative, and thus q and the Q.S. may not have the same sign. If the $\pm \frac{3}{2}$ state is at high energy (as in Fig. 1), the sign of the Q.S. is positive. For Mössbauer nuclei such as ^{57}Fe and ^{119}Sn , a two-line spectrum is obtained, and the Q.S. easily measured. By the nature of Eq. (5), it is obvious that both q and η cannot be calculated from a measurement of the Q.S. Also, the sign of the Q.S. cannot generally be determined from a powder spectrum since the $\pm \frac{3}{2}$ and $\pm \frac{1}{2}$ lines are of very similar intensity and cannot be distinguished. Techniques for measuring the sign of Q (and q) and estimating η for ^{57}Fe and ^{119}Sn will be discussed later in this section.

For convenience, assume that $\eta = 0$ and express q as*:

$$q = (1 - \gamma_\infty) q_{\text{lat}} + (1 - R) q_{\text{val}} \quad (35I) \quad (6)$$

where (a) R and γ_∞ are the Sternheimer antishielding factors, (b) q_{lat} , the contribution from the external ligand charges Z_i , is given by

$$q_{\text{lat}} = \sum_i \frac{Z_i(3 \cos^2 \theta_i - 1)}{r_i^3} \quad (7)$$

and (c) q_{val} , the valence contribution from the valence electrons equals

$$- \sum_{\substack{\text{valence} \\ \text{electrons}}} \langle 3 \cos^2 \theta_i - 1 \rangle \langle r^{-3} \rangle \quad (8)$$

Table III gives the contribution to q_{val} from p and d electrons. The Sternheimer factors take into account the effect of q_{val} or q_{lat} on the inner

* The maximum value of $(1 + \eta^2/3)^{1/2} = 1.15$ so that a large η makes little difference to the magnitude of the Q.S.

nonvalence electrons and result in magnifying any contribution to q from the valence electrons or lattice, without changing the sign.

Both q_{lat} and q_{val} terms can, in principle, be calculated using Eqs. (7) and (8) if the crystal structure and the valence orbital populations are known. However, it is usually difficult to assign charges to different atoms in the structure (17) and valence orbital populations are usually not known and are difficult to calculate. In addition, the value of Q is often not accurately known for most isotopes making it difficult to compare calculated and observed splittings.

TABLE III
VALUES OF $V_{zz}/e(=q)$ FOR p AND d ELECTRONS

Wavefunction	V_{zz}/e	Wavefunction	V_{zz}/e
p_x	$+\frac{2}{5}\langle r^{-3} \rangle_p$	d_{z^2}	$-\frac{4}{7}\langle r^{-3} \rangle_d$
p_y	$+\frac{2}{5}\langle r^{-3} \rangle_p$	$d_{x^2 - y^2}$	$+\frac{4}{7}\langle r^{-3} \rangle_d$
p_z	$-\frac{4}{5}\langle r^{-3} \rangle_p$	d_{xy}	$+\frac{4}{7}\langle r^{-3} \rangle_d$
		d_{xz}	$-\frac{2}{7}\langle r^{-3} \rangle_d$
		d_{yz}	$-\frac{2}{7}\langle r^{-3} \rangle_d$

Because of these (and other) difficulties, more semiempirical methods such as the additivity model are used to rationalize Q.S. values, but before discussing the additivity model, it seems appropriate to examine features of the field gradient more closely.

If the electron and ligand charge distributions have cubic symmetry, both q_{val} and q_{lat} , respectively, will be zero. For example, the q_{val} contribution from p electrons can be written using Eq. (8) and Table III:

$$q_{\text{val}} = K_p[-N_{p_z} + \frac{1}{2}(N_{p_x} + N_{p_y})]^* \quad (9)$$

where $K_p = +\frac{4}{5}\langle r^{-3} \rangle_p$ and N = orbital populations. It is evident from Eq. (9) that if the three p orbitals are equally populated, then $q_{\text{val}} = 0$. If $N_{p_z} > \frac{1}{2}(N_{p_x} + N_{p_y})$, then q_{val} is negative; if $N_{p_z} < \frac{1}{2}(N_{p_x} + N_{p_y})$, q_{val} will then be positive. A concentration of negative charge along the Z EFG axis gives a negative q . Similarly for d electrons

$$q_{\text{val}} = K_d[-N_{d_{z^2}} + N_{d_{x^2 - y^2}} + N_{d_{xy}} - \frac{1}{2}(N_{d_{xz}} + N_{d_{yz}})] \quad (10)$$

* This is the result of the Townes-Dailey treatment for quadrupole splittings. For a discussion of the assumptions and approximations see Lucken (391).

where $K_d = +\frac{4}{7}\langle r^{-3} \rangle_d$. If the component orbitals of the t_{2g} and/or the e_g levels have equal populations, then $q_{\text{val}} = 0$.

Similarly for q_{lat} , it can easily be shown using Eq. (7) that an octahedral or tetrahedral array of charges of equal magnitude gives $q_{\text{lat}} = 0$. Compressing the axial ligands in the octahedral case gives a negative q_{lat} ; compressing the equatorial ligands gives a positive q_{lat} . Again a concentration of negative charge along the Z EFG axis gives a negative q .

It is convenient now to divide q_{val} into two contributions:

$$q_{\text{val}} = q_{\text{C.F.}} + q_{\text{M.O.}} \quad (11)$$

where $q_{\text{C.F.}}$ is the valence contribution considering a crystal field model with no overlap of ligand and metal orbitals, and $q_{\text{M.O.}}$ is the valence contribution considering bonding between metal and ligands.

The $q_{\text{C.F.}}$ term is dominant in transition metal ions such as Fe^{2+} high spin or Fe^{3+} low spin in which the t_{2g} and/or e_g levels are not fully or half populated. In many other cases of interest, I and Te compounds, Sn^{IV} , Fe^{II} low spin, Ru^{II} , and Ir^{III} , the Q.S. can be attributed to $q_{\text{M.O.}}$ (and possibly q_{lat}). To illustrate the value of the above separation, consider Fe^{II} low spin, where the major part of the Q.S. is due to $q_{\text{M.O.}}$, and Fe^{II} high spin, where the major part of the Q.S. is due to $q_{\text{C.F.}}$. For Fe^{II} low spin (t_{2g}^6) (44), if there is no covalent bonding, $N_{d_{xy}} = \frac{1}{2}(N_{d_{xx}} + N_{d_{yy}})$ and $q_{\text{C.F.}} = 0$. Consider a hypothetical species *trans*- $[\text{FeA}_2\text{B}_4]^{2+}$, where A and B are neutral ligands, and suppose that any Q.S. is due to the differences in π back-bonding capacity of A and B. If A is a better π acceptor than B, then more electron density will be withdrawn along the Z axes than along the X or Y axes and $N_{d_{xy}} > \frac{1}{2}(N_{d_{xx}} + N_{d_{yy}})$ and $q_{\text{M.O.}}$ is positive; if A is a poorer π acceptor than B, then $N_{d_{xy}} < \frac{1}{2}(N_{d_{xx}} + N_{d_{yy}})$ and $q_{\text{M.O.}}$ is negative. The quadrupole splittings for many other isotopes can also be rationalized by considering the electron imbalance about the Mössbauer isotope given by Eqs. (9) and (10).

Quadrupole splittings which arise from a $q_{\text{M.O.}}$ term normally vary little with temperature. Any small variation with temperature is due to small changes in bond lengths.

In contrast to the above situation, the fourth electron in the t_{2g} level in Fe^{2+} high spin ($t_{2g}^4e_g^2$) normally gives rise to a large $q_{\text{C.F.}}$ term which is more temperature dependent (351). If the Fe^{2+} is surrounded by a perfect octahedron of point charges, then the degeneracy of the t_{2g} levels is not removed, and the extra electron spends an equal time in all three of the t_{2g} orbitals and $q_{\text{val}} = 0$, because $N_{d_{xy}} = \frac{1}{2}(N_{d_{xx}} + N_{d_{yy}}) = 1.33$. However, this system is inherently subject to a Jahn-Teller distortion

which removes the degeneracy of the t_{2g} and e_g levels. If the axial ligands are compressed slightly, then the sixth electron preferentially occupies the d_{xy} orbital and a large positive $q_{C.F.}$ results. This field gradient is normally very temperature dependent because the splitting of the t_{2g} levels is usually of the order of kT . Thus, the d_{xz} and d_{yz} orbitals are Boltzmann populated, and this Boltzmann population decreases on lowering the temperature. For the axial compression, $q_{C.F.}$ can be expressed as

$$q_{C.F.} = \frac{4}{7} \langle r^{-3} \rangle \left[\frac{1 - e^{-\Delta_3/kT}}{1 + 2e^{-\Delta_3/kT}} \right] \quad (12)$$

where Δ_3 is the energy separation between d_{xy} and (d_{xz} , d_{yz}), and k is Boltzmann's constant. Thus, the maximum value of $q_{C.F.}$ due to one d electron ($\frac{4}{7} \langle r^{-3} \rangle$) is decreased owing to thermal population; and as T decreases, $q_{C.F.}$ increases ($e^{-\Delta_3/kT}$ decreases).

Spin-orbit coupling decreases the Q.S. from the above value (351). The $q_{M.O.}$ and q_{lat} terms are usually much smaller than $q_{C.F.}$, but both usually decrease the observed quadrupole splitting from that expected just from the $q_{C.F.}$ term.

A similar type of treatment is applicable to Fe^{III} (281, 283) low spin. In other cases of interest, such as Fe^0 (d^8), and Fe^{-I} (d^9), it is usually not possible to separate contributions from $q_{M.O.}$ and $q_{C.F.}$. Quadrupole splittings for a large number of compounds in the above valency states have remained largely unexplained since detailed molecular orbital calculations are needed.

From the above discussion, it is apparent that more bonding information can be obtained on ions having symmetric ground states (Fe^{II} and Sn^{IV}), since the major part of the Q.S. is due to $q_{M.O.}$ and "complications" from $q_{C.F.}$ do not enter the picture. However, information of considerable structural and bonding interest can still be obtained for ions such as Fe^{2+} high spin, and these will be discussed in later sections.

The Sign of the Quadrupole Splitting

As we have discussed previously, it is often desirable to determine the sign of the Q.S. and q , but for ^{57}Fe and ^{119}Sn it is not possible by taking the usual powder spectrum to obtain the sign of the Q.S. and q . For ^{57}Fe , Q is positive, whereas for ^{119}Sn , Q is negative. Thus, a measured positive Q.S. would correspond to a positive q for ^{57}Fe , but a negative q for ^{119}Sn .

There are two methods which are normally used to obtain the sign of q . The first involves obtaining spectra of a sample with all crystallites oriented in one known way relative to the direction of the gamma beam

(5, 121); the second involves measuring the spectrum of a polycrystalline sample at 4°K in a large magnetic field (132, 136). Because of the difficulties in obtaining single crystals in a known orientation, the second method is usually the most useful and will be briefly described here.

On application of a large magnetic field to a powdered sample, the degeneracy of the nuclear levels is completely removed. The EFG axes take all orientations with respect to the magnetic field, and a large

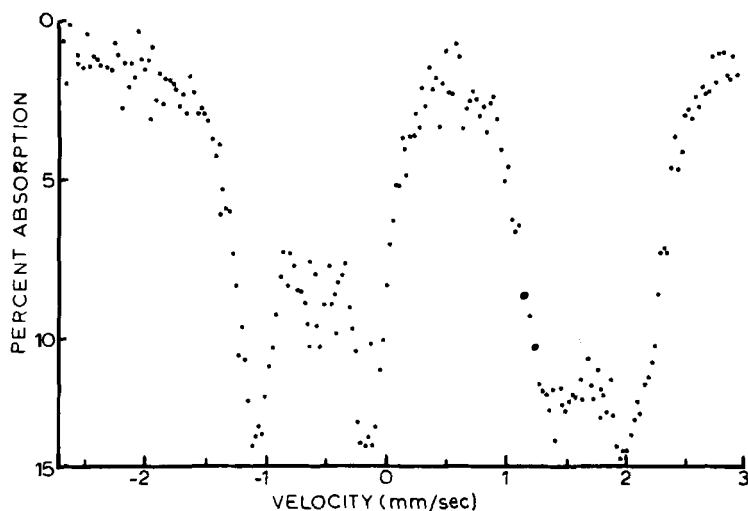


FIG. 2. Effect of a magnetic field on an ^{57}Fe powder spectrum—the Mössbauer spectrum of ferrocene at 4.2°K in an applied longitudinal magnetic field of 40 kgauss (132). The doublet lies to positive velocities and V_{zz} and q are positive.

number of superimposed spectra are observed. For $\eta = 0$ or a small value, the two-line zero field spectrum splits into a doublet and a triplet (Fig. 2), with the doublet being due to the $+\frac{1}{2} \rightarrow +\frac{3}{2}$ and $-\frac{1}{2} \rightarrow -\frac{3}{2}$ transitions. For ^{57}Fe , then, if the doublet lies to positive velocity, the sign of both Q.S. and q is positive. If η approaches 1, the spectrum goes from the doublet-triplet structure to a symmetric triplet-triplet structure. Using detailed computation, an estimate of η can be made (136). Orientation of the crystallites or an anisotropic f factor can markedly alter the spectrum and lead to difficulties in detailed interpretation, especially for small quadrupole splittings (<0.50 mm/sec), but the sign can still usually be obtained.

For ^{119}Sn , a doublet-quartet structure is observed (265, 438) in an

applied magnetic field, and the sign of the Q.S. is positive (q negative) if the doublet is at positive velocities.

D. THE ADDITIVITY MODEL FOR QUADRUPOLE SPLITTINGS

The interpretation of the quadrupole splittings of Sn^{IV} , Fe^{II} low spin, and Fe^{II} compounds has been greatly facilitated by application of the additivity model [for example, see Refs. (36, 44, 122, 406, 440, 442)] and it should prove to be useful for Fe^{III} high spin, Ir^{III} , Ru^{II} , W^0 , W^{VI} , and a number of other Mössbauer atoms. In this model, use is made of the basic premise that the quadrupole splitting can be regarded to a first approximation as the sum of independent contributions, one for each ligand bound to the metal atom. The additivity model is expected to apply for compounds of transition metal ions whose t_{2g} and/or e_g subshells are filled or half-filled, e.g., Fe^{II} (t_{2g}^6) or Ir^{III} (t_{2g}^6), or for compounds of main group ions whose s and p shells are empty [e.g., Sn^{IV} ($4d^{10}$) or Te^{VI} ($4d^{10}$)] in the free ion.

In the above cases, $q_{\text{C.F.}} = 0$, and quadrupole splittings will be purely a function of the nature and distribution of the ligand bonds. For other compounds (e.g., Fe^{II} high spin, Fe^{III} low spin, Fe^0), the $q_{\text{C.F.}}$ term obscures the dependence of the quadrupole splitting on the nature of the M-L bonds. In other cases (Sn^{II} compounds), the inherent asymmetric occupation of the valence orbitals ($\text{Sn}^{\text{II}} = 5s^{2-x}5p^x$) obscures the dependence of the Q.S. on the M-L bond types.

In this section, we will explore the consequences of additivity and attempt to relate the various formulations of the additivity model. The agreement between theory and experiment will be assessed later using the extensive Q.S. data for Sn^{IV} and Fe^{II} low-spin compounds. The use of the additivity treatment in predicting structures of compounds and bonding properties of ligands will be discussed.

1. Point Charge Formalism

The simplest formulation of an additive EFG is the point charge model, in which each ligand is assigned a charge, the magnitude of which represents the contribution of that ligand to the EFG. Since the EFG is expressed in terms of separate contributions, q_{val} and q_{lat} (Section II, C), these two contributions are usually represented by separate charges.

Thus, for a compound containing n ligands bound to a metal atom, $\text{M}(\text{A}, \text{B}, \text{C}, \dots \text{N})$, the nine components of the EFG tensor, V_{rs} , written in terms of the axes defined in Table II, are given by the equations:

$$V_{xx} = e \sum_L [L](3 \sin^2 \theta_L \cos^2 \phi_L - 1) \quad (13.1)$$

$$V_{yy} = e \sum_L [L](3 \sin^2 \theta_L \sin^2 \phi_L - 1) \quad (13.2)$$

$$V_{zz} = e \sum_L [L](3 \cos^2 \theta_L - 1) \quad (13.3)$$

$$V_{xy} = V_{yx} = e \sum_L 3[L] \sin^2 \theta_L \sin \phi_L \cos \phi_L \quad (13.4)$$

$$V_{xz} = V_{zx} = e \sum_L 3[L] \sin \theta_L \cos \theta_L \cos \phi_L \quad (13.5)$$

$$V_{yz} = V_{zy} = e \sum_L 3[L] \sin \theta_L \cos \theta_L \sin \phi_L \quad (13.6)$$

where

$$[L] = \frac{C_1(1-R)}{r_1^3} + \frac{C_L(1-\gamma)}{r_L^3} \quad (14)$$

In Eqs. (13.1)→(13.6) C_1 and C_L are the equivalent charges at distances r_1 and r_L , representing the valence and lattice contributions of the generic ligand L, respectively. The angles θ_L and ϕ_L , together with r_1 and r_L , form the spherical polar coordinates of the charges C_1 and C_L relative to the Z axis of the EFG tensor. The summation is made over all ligands.

Expressions for the relative values of V_{zz} and η expected for various idealized structural types may be derived in terms of the parameters $[L]$. The axes are chosen so as to diagonalize the EFG tensor and preserve the ordering convention $|V_{zz}| \geq |V_{yy}| \geq |V_{xx}|$. Expressions obtained for common structural types are summarized in Table IV.

A more elegant treatment of the point charge model has been described by Clark (119), who calculated the contribution of a ligand (L), to the total EFG tensor assuming that the Z axis is directed along the metal–ligand bond. If the bond has cylindrical symmetry, a “ $C_{\infty v}$ bond,” it may be represented by a point, and the contribution to the EFG at the nucleus is given by the tensor

$$\begin{bmatrix} -\frac{1}{2}q_L & 0 & 0 \\ 0 & -\frac{1}{2}q_L & 0 \\ 0 & 0 & q_L \end{bmatrix} \quad (15)$$

This tensor is the partial field gradient (p.f.g.)_L of ligand L. The parameter q_L , in point charge formalism is equal to

$$\frac{2C_1(1-R)}{r_1^3} + \frac{2C_L(1-\gamma)}{r_L^3} \quad (16)$$

and, hence, comparing Eqs. (13.3), (14), and (16), the Z component of (p.f.g.)_L = 2[L]e. The total EFG tensor of a molecule may be calculated

by placing each ligand, in turn, on the Z axis, writing down its (p.f.g.)_L, and then rotating the tensor, (p.f.g.)_L, to its true position. The contributions from each ligand are then summed. For example, the EFG tensors calculated for octahedral *trans*- and *cis*- MA₄B₂ species are

$$\begin{bmatrix} -(q_B - q_A) & 0 & 0 \\ 0 & -(q_B - q_A) & 0 \\ 0 & 0 & 2(q_B - q_A) \end{bmatrix} \quad (17.1)$$

and

$$\begin{bmatrix} \frac{1}{2}(q_B - q_A) & 0 & 0 \\ 0 & \frac{1}{2}(q_B - q_A) & 0 \\ 0 & 0 & -(q_B - q_A) \end{bmatrix} \quad (17.2)$$

respectively, which give the same 2 : -1 ratio found in Table IV.

The expressions in Table IV allow the relative quadrupole splittings for various structural types to be compared using the expression:

$$\Delta = \frac{1}{2}eV_{zz}Q(1 + \eta^2/3)^{1/2} \quad (18)$$

In any such comparison, we tacitly assume that the [L] of a ligand is a constant in all compounds of a given valence state, e.g., Sn^{IV}. This, of course, would not be expected to hold exactly, but the expressions in Table IV are found to give a good semiquantitative guide to relative quadrupole splittings. As discussed later in this section, it is more convenient and accurate to assign separate [L] values to a ligand for different coordination numbers.

2. Molecular Orbital Approaches

Although the point charge model may be anticipated to be a reasonably accurate guide to lattice effects, it is obviously rather a crude and unrealistic approximation to the asymmetries of metal-ligand bonding interactions. Attempts have been made, therefore, to gain a clear understanding of additive electron field gradients arising from bonding interactions.

Bancroft *et al.* (44), in considering the quadrupole splittings of low-spin Fe^{II} six-coordinate compounds, have described a model based on a suggestion by McClure (393) for the interpretation of electronic spectra. In this treatment, instead of representing the valence contribution of a ligand to the EFG as a point charge, the effect of the ligand upon the populations of the iron atomic orbitals is considered. Thus, σ donation will populate the 4s, 4p, 3d_{z²}, and 3d_{x²-y²} orbitals, while

TABLE IV

POINT CHARGE MODEL EXPRESSIONS FOR THE COMPONENTS OF THE EFG TENSOR FOR SOME COMMON STRUCTURES^a

Code No. ^b	Structure	Components of EFG ^c
1	$ \begin{array}{c} Z \\ \\ B \\ \\ M \cdots X \\ / \quad \quad \backslash \\ B \quad B \quad B \end{array} $	$V_{ZZ} = V_{XX} = V_{YY} = 0$
2	$ \begin{array}{c} Z \\ \\ A \\ \\ M \cdots X \\ / \quad \quad \backslash \\ B \quad B \quad B \end{array} $	$V_{ZZ} = \{2[A] - 2[B]\} e$ $V_{YY} = \{-[B] + [A]\} e$ $V_{XX} = \{-[B] + [A]\} e$ $\eta = 0$
3 ^d	$ \begin{array}{c} z \\ \\ A \\ \\ M \\ / \quad \quad \backslash \\ A \quad B \quad B \end{array} $	$V_{ZZ} = \{2[A] - 2[B]\} e$ $V_{YY} = \{2[B] - 2[A]\} e$ $V_{XX} = 0$ $\eta = 1$
4 ^e	$ \begin{array}{c} z \\ \\ A \\ \\ M \\ / \quad \quad \backslash \\ B \quad C \quad C \end{array} $	$V_{zz} = \{2[A] - \frac{2}{3}([B] + 2[C])\} e$ $V_{yy} = \{-[A] - [B] + 2[C]\} e$ $V_{xx} = \{-[A] + \frac{2}{3}[B] - \frac{2}{3}[C]\} e$ $V_{xz} = V_{zx} = \left\{ \frac{\sqrt{2}}{3} (-2[B] + 2[C]) \right\} e$ $V_{xy} = V_{yx} = V_{yz} = V_{zy} = 0$ $\eta \neq 0$ $\Delta = \frac{1}{2} e^2 Q (\frac{4}{3} P^2 + 2Q^2)^{1/2}$ $P = [A] + [B] - 2[C]$ $Q = [A] - [B]$ Sign = sign of P
5 ^g	$ \begin{array}{c} z \\ \\ A \\ \\ M \\ / \quad \quad \backslash \\ D \quad B \quad C \end{array} $	$V_{zz} = \{2[A] - \frac{2}{3}([B] + [C] + [D])\} e$ $V_{yy} = \{-[A] - [B] + [C] + [D]\} e$ $V_{xx} = \{-[A] + \frac{2}{3}[B] - \frac{1}{3}([C] + [D])\} e$ $V_{yz} = V_{zy} = \left\{ \frac{\sqrt{2}}{\sqrt{3}} ([C] - [D]) \right\} e$ $V_{zx} = V_{xz} = \left\{ \frac{\sqrt{2}}{3} (-2[B] + [C] + [D]) \right\} e$ $V_{xy} = V_{yx} = \left\{ \frac{2}{\sqrt{3}} ([C] - [B]) \right\} e$ $\eta \neq 0$

TABLE IV—continued

Code No. ^b	Structure	Components of EFG ^c
6 ^h	$ \begin{array}{c} \text{Z} \\ \\ \text{B} \\ \\ \text{B} \diagup \text{M} \text{---} \text{B X} \\ \\ \text{B} \end{array} $	$ \begin{aligned} V_{ZZ} &= \{4[\text{B}]^{\text{tba}} - 3[\text{B}]^{\text{tbe}}\} e \\ V_{YY} &= \{\tfrac{3}{2}[\text{B}]^{\text{tbe}} - 2[\text{B}]^{\text{tba}}\} e \\ V_{XX} &= \{\tfrac{3}{2}[\text{B}]^{\text{tbe}} - 2[\text{B}]^{\text{tba}}\} e \\ \eta &= 0 \end{aligned} $
7 ^h	$ \begin{array}{c} \text{X} \\ \\ \text{B} \\ \\ \text{B} \diagup \text{M} \text{---} \text{A Z} \\ \\ \text{B} \end{array} $	$ \begin{aligned} V_{ZZ} &= \{2[\text{A}]^{\text{tbe}} - 2[\text{B}]^{\text{tba}} - \tfrac{1}{2}[\text{B}]^{\text{tbe}}\} e \\ V_{YY} &= \{-[\text{A}]^{\text{tbe}} - 2[\text{B}]^{\text{tba}} + \tfrac{5}{2}[\text{B}]^{\text{tbe}}\} e \\ V_{XX} &= \{-[\text{A}]^{\text{tbe}} + 4[\text{B}]^{\text{tba}} - 2[\text{B}]^{\text{tbe}}\} e \\ \eta &\neq 0 \end{aligned} $
8 ^h	$ \begin{array}{c} \text{Z} \\ \\ \text{B} \\ \\ \text{B} \diagup \text{M} \text{---} \text{B X} \\ \\ \text{A} \end{array} $	$ \begin{aligned} V_{ZZ} &= \{2[\text{A}]^{\text{tba}} - 3[\text{B}]^{\text{tbe}} + 2[\text{B}]^{\text{tba}}\} e \\ V_{YY} &= \{-[\text{A}]^{\text{tba}} + \tfrac{3}{2}[\text{B}]^{\text{tbe}} - [\text{B}]^{\text{tba}}\} e \\ V_{XX} &= \{-[\text{A}]^{\text{tba}} + \tfrac{3}{2}[\text{B}]^{\text{tbe}} - [\text{B}]^{\text{tba}}\} e \\ \eta &= 0 \end{aligned} $
9 ^h	$ \begin{array}{c} \text{Z} \\ \\ \text{B} \\ \\ \text{A} \diagup \text{M} \text{---} \text{B X} \\ \\ \text{A} \end{array} $	$ \begin{aligned} V_{ZZ} &= \{-2[\text{A}]^{\text{tbe}} - [\text{B}]^{\text{tbe}} + 4[\text{B}]^{\text{tba}}\} e \\ V_{YY} &= \{\tfrac{5}{2}[\text{A}]^{\text{tbe}} - [\text{B}]^{\text{tbe}} - 2[\text{B}]^{\text{tba}}\} e \\ V_{XX} &= \{-\tfrac{1}{2}[\text{A}]^{\text{tbe}} + 2[\text{B}]^{\text{tbe}} - 2[\text{B}]^{\text{tba}}\} e \\ \eta &\neq 0 \end{aligned} $
10 ^h	$ \begin{array}{c} \text{Z} \\ \\ \text{A} \\ \\ \text{B} \diagup \text{M} \text{---} \text{B X} \\ \\ \text{B} \\ \\ \text{A} \end{array} $	$ \begin{aligned} V_{ZZ} &= \{4[\text{A}]^{\text{tba}} - 3[\text{B}]^{\text{tbe}}\} e \\ V_{YY} &= \{-2[\text{A}]^{\text{tba}} + \tfrac{3}{2}[\text{B}]^{\text{tbe}}\} e \\ V_{XX} &= \{-2[\text{A}]^{\text{tba}} + \tfrac{3}{2}[\text{B}]^{\text{tbe}}\} e \\ \eta &= 0 \end{aligned} $
11	$ \begin{array}{c} \text{Z} \quad \text{Y} \\ \quad \\ \text{B} \quad \text{B} \\ \quad \\ \text{B} \diagup \text{M} \diagdown \text{B} \\ \quad \\ \text{B} \quad \text{X} \end{array} $	$V_{ZZ} = V_{XX} = V_{YY} = 0$
12	$ \begin{array}{c} \text{Z} \quad \text{Y} \\ \quad \\ \text{A} \quad \text{B} \\ \quad \\ \text{B} \diagup \text{M} \diagdown \text{B} \\ \quad \\ \text{B} \quad \text{X} \\ \\ \text{A} \end{array} $	$ \begin{aligned} V_{ZZ} &= \{4[\text{A}] - 4[\text{B}]\} e \\ V_{YY} &= \{2[\text{B}] - 2[\text{A}]\} e \\ V_{XX} &= \{2[\text{B}] - 2[\text{A}]\} e \\ \eta &= 0 \end{aligned} $

continued

TABLE IV—*continued*POINT CHARGE MODEL EXPRESSIONS FOR THE COMPONENTS OF THE EFG TENSOR
FOR SOME COMMON STRUCTURES^a

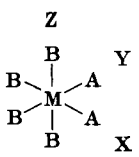
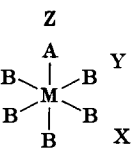
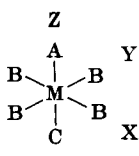
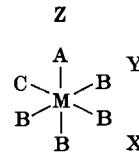
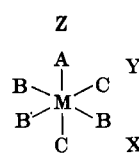
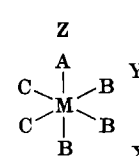
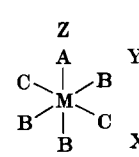
Code No. ^b	Structure	Components of EFG ^c
13		$V_{zz} = \{2[B] - 2[A]\} e$ $V_{yy} = \{[A] - [B]\} e$ $V_{xx} = \{[A] - [B]\} e$ $\eta = 0$
14		$V_{zz} = \{2[A] - 2[B]\} e$ $V_{yy} = \{[B] - [A]\} e$ $V_{xx} = \{[B] - [A]\} e$ $\eta = 0$
15		$V_{zz} = \{2[A] + 2[C] - 4[B]\} e$ $V_{yy} = \{2[B] - [A] - [C]\} e$ $V_{xx} = \{2[B] - [A] - [C]\} e$ $\eta = 0$
16		$V_{zz} = \{2[A] - [B] - [C]\} e$ $V_{xx} = \{-[B] + 2[C] - [A]\} e$ $V_{yy} = \{2[B] - [C] - [A]\} e$ $\eta \neq 0$
17		$V_{zz} = \{2[A] + [C] - 3[B]\} e$ $V_{xx} = \{3[B] - 2[C] - [A]\} e$ $V_{yy} = \{[C] - [A]\} e$ $\eta \neq 0$
18		$V_{zz} = \{2[A] - 2[C]\} e$ $V_{yy} = \{[C] - [A]\} e$ $V_{xx} = \{[C] - [A]\} e$ $\eta = 0$
19		$V_{zz} = \{2[A] - 2[C]\} e$ $V_{xx} = \{4[C] - 3[B] - [A]\} e$ $V_{yy} = \{3[B] - 2[C] - [A]\} e$ $\eta \neq 0$

TABLE IV—continued

Code No. ^b	Structure	Components of EFG ^c
20		$V_{zz} = \{4[A] - 2[B] - 2[C]\} e$ $V_{yy} = \{[C] + [B] - 2[A]\} e$ $V_{xx} = \{[C] + [B] - 2[A]\} e$ $\eta = 0$
21		$V_{zz} = \{4[A] - 2[B] - 2[C]\} e$ $V_{xx} = \{4[B] - 2[C] - 2[A]\} e$ $V_{yy} = \{4[C] - 2[B] - 2[A]\} e$ $\eta \neq 0$
22		$V_{zz} = \{[B] + [C] - 2[A]\} e$ $V_{xx} = \{[C] + [A] - 2[B]\} e$ $V_{yy} = \{[B] + [A] - 2[C]\} e$ $\eta \neq 0$
23		$V_{zz} = V_{yy} = V_{xx} = 0$
24		$V_{zz} = \{3[A] - 3[B]\} e$ $V_{xx} = \{3[B] - 3[A]\} e$ $V_{yy} = 0$ $\eta = 1$

^a These expressions are taken from Refs. (29, 39, 44, 55, 122, 234, 440, 442).

^b When referring to a structure in the text, the code number will be prefixed by table number.

^c The choice of axes is indicated on the diagram of the structure or in a footnote. In all cases, except 4 and 5 this choice of axes serves to diagonalize the EFG tensor. The ordering of the axes to preserve the convention $|V_{zz}| \geq |V_{yy}| \geq |V_{xx}|$ will depend on the [L] values. Thus, the final choice of axes may not be the same as given here, i.e., V_{zz} may become V_{xx} or V_{yy} , etc.

^d The X axes coincide with the C_2 symmetry axis, and the Y and Z axes lie in the symmetry planes.

^e The Y axis is perpendicular to the symmetry plane, while the X and Z axes lie in the plane. The orientation of the X and Z axes depends on the relative magnitudes of [A], [B], and [C], and the tensor must be diagonalized separately for each case considered.

^f This expression gives the magnitude of the quadrupole splitting and is obtained from the symmetrized parameters of Clark (120).

^g The EFG tensor must be diagonalized for each example considered.

^h The superscripts tbe and tba refer to trigonal-bipyramidal equatorial and trigonal-bipyramidal axial bonds, respectively.

π bonding will reduce the populations of the d_{xy} , d_{xz} , and d_{yz} orbitals. The effect of a particular ligand, L, on the iron atomic orbital populations will depend on (a) the σ -donating (σ_L) and π -withdrawing (π_L) capacities of the ligands and (b) the relative involvement of the atomic orbitals in the Fe-L bond which for σ bonding is proportional to the squares of the coefficients of the hybrid orbitals:

$$h_{1,2} = 1/\sqrt{6} s \pm 1/\sqrt{2} p_z + 1/\sqrt{3} d_{z^2} \quad (19.1)$$

$$h_{3,4} = 1/\sqrt{6} s \pm 1/\sqrt{2} p_x - 1/\sqrt{12} d_{z^2} + \frac{1}{2} d_{x^2-y^2} \quad (19.2)$$

$$h_{5,6} = 1/\sqrt{6} s \pm 1/\sqrt{2} p_y - 1/\sqrt{12} d_{z^2} - \frac{1}{2} d_{x^2-y^2} \quad (19.3)$$

The π orbitals (d_{xy} , d_{yz} , d_{xz}) have equal π -bonding power in the three principal directions of the EFG tensor which lie along the M-L bonds.

TABLE V

RELATIVE CHARGE DENSITIES IN p AND d ORBITALS OF THE SIX OCTAHEDRAL σ BONDING HYBRIDS^a

Ligand	p_x	p_y	p_z	$d_{x^2-y^2}$	d_{z^2}
L_z	0	0	$\frac{1}{2}$	0	$\frac{1}{3}$
L_z	0	0	$\frac{1}{2}$	0	$\frac{1}{3}$
L_x	$\frac{1}{2}$	0	0	$\frac{1}{4}$	$\frac{1}{12}$
L_x	$\frac{1}{2}$	0	0	$\frac{1}{4}$	$\frac{1}{12}$
L_y	0	$\frac{1}{2}$	0	$\frac{1}{4}$	$\frac{1}{12}$
L_y	0	$\frac{1}{2}$	0	$\frac{1}{4}$	$\frac{1}{12}$

^a From Ref. (44).

The normalized relative amounts of charge density in a given bonding direction are summarized in Table V. We neglect the $4p$ contributions, since the dependence of V_{rs} upon $\langle r^{-3} \rangle$ will result in a much smaller contribution to the EFG from $4p$ orbitals.

The relative populations of the $3d$ orbitals may be computed as σ_L or π_L multiplied by the appropriate coefficient in Table V. For example, a ligand, L, on the Z axis will increase the population of the $3d_{z^2}$ orbital by an amount proportional to $\frac{1}{3}\sigma_L$ and decrease the population of the d_{xz} and d_{yz} orbitals by an amount proportional to π_L . As an illustration of the method, Table VI contains the relative changes in effective

population of each $3d$ orbital from t_{2g}^6 configuration for *trans*- and *cis*- FeA_2B_4 species. Substitution into Eq. (10) gives the expressions

$$q_{\text{trans}}\alpha[-2(\pi_B + \pi_A) + (\frac{2}{3}\sigma_B - \frac{2}{3}\sigma_A)]^* \quad (20.1)$$

$$q_{\text{cis}}\alpha[+\pi_B - \pi_A - \frac{1}{3}\sigma_B + \frac{1}{3}\sigma_A] \quad (20.2)$$

TABLE VI

RELATIVE CHANGES IN ORBITAL POPULATIONS FOR *trans*- AND *cis*- MA_2B_4

Ligand	p_x	p_y	p_z	$d_{x^2-y^2}$	d_{z^2}
<i>trans</i> - MA_2B_4^a					
L_z	0	0	$\frac{1}{2}\sigma_A$	0	$\frac{1}{3}\sigma_A$
L_z	0	0	$\frac{1}{2}\sigma_A$	0	$\frac{1}{3}\sigma_A$
L_x	$\frac{1}{2}\sigma_B$	0	0	$\frac{1}{4}\sigma_B$	$\frac{1}{12}\sigma_B$
L_x	$\frac{1}{2}\sigma_B$	0	0	$\frac{1}{4}\sigma_B$	$\frac{1}{12}\sigma_B$
L_y	0	$\frac{1}{2}\sigma_B$	0	$\frac{1}{4}\sigma_B$	$\frac{1}{12}\sigma_B$
L_y	0	$\frac{1}{2}\sigma_B$	0	$\frac{1}{4}\sigma_B$	$\frac{1}{12}\sigma_B$
Total	σ_B	σ_B	σ_A	σ_B	$\frac{2}{3}\sigma_A + \frac{1}{3}\sigma_B$
<i>cis</i> - MA_2B_4^a					
L_z	0	0	$\frac{1}{2}\sigma_B$	0	$\frac{1}{3}\sigma_B$
L_z	0	0	$\frac{1}{2}\sigma_B$	0	$\frac{1}{3}\sigma_B$
L_x	$\frac{1}{2}\sigma_A$	0	0	$\frac{1}{4}\sigma_A$	$\frac{1}{12}\sigma_A$
L_x	$\frac{1}{2}\sigma_B$	0	0	$\frac{1}{4}\sigma_B$	$\frac{1}{12}\sigma_B$
L_y	0	$\frac{1}{2}\sigma_A$	0	$\frac{1}{4}\sigma_A$	$\frac{1}{12}\sigma_A$
L_y	0	$\frac{1}{2}\sigma_B$	0	$\frac{1}{4}\sigma_B$	$\frac{1}{12}\sigma_B$
Total	$\frac{1}{2}(\sigma_A + \sigma_B)$	$\frac{1}{2}(\sigma_A + \sigma_B)$	σ_B	$\frac{1}{2}(\sigma_A + \sigma_B)$	$\frac{1}{3}\sigma_A + \frac{1}{2}\sigma_B$

^a From Ref (44). See Table IV, species 12 and 13 for the correct assignment of axes.

and a similar treatment for FeAB_5 gives

$$q_{\text{AB}_5}\alpha[-\pi_B + \pi_A - \frac{1}{3}\sigma_B + \frac{1}{3}\sigma_A] \quad (20.3)$$

Clearly Eqs. (20.1)–(20.3), give the same $q_{\text{trans}} : q_{\text{cis}} : q_{\text{AB}_5}$ ratios calculated from the point charge model (Table IV) and lend confidence to the application of the simple additivity relationship in Table IV to the quadrupole splitting of low-spin Fe^{II} compounds.

* In the original equations in Bancroft *et al.* (44), the above σ_L values were multiplied by four. This constant does not affect the relative values.

For Sn^{IV} species, the situation is more complex as the range of structures to be considered spans four-, five-, and six-coordinate compounds. A simple but general molecular orbital theory for an additive EFG has been described and applied to Sn^{IV} compounds (122). The model is closely related to the ideas used in the interpretation of NQR spectroscopy (391) and to the model of Bancroft *et al.* (44) described above. In the first instance only σ bonding will be considered as π -bonding effects are not thought to make an important contribution to the EFG of Sn^{IV} compounds (see Section IV, A, 1a).

For the general closed shell molecule with n ligands $\text{M}(\text{A}, \text{B}, \dots \text{N})$, the total wavefunction of the valence electrons can be written

$$\Psi = |\Psi_1^\alpha \Psi_1^\beta \Psi_2^\alpha \Psi_2^\beta \dots \Psi_n^\alpha \Psi_n^\beta| \quad (21)$$

where $\Psi_1, \Psi_2, \dots \Psi_n$ are n valence molecular orbitals containing $2n$ valence electrons. The symbol $|\)$ denotes a Slater determinant and α, β denote $m_s = +\frac{1}{2}, -\frac{1}{2}$ respectively.

The components V_{rs} of the EFG tensor at M are given by the diagonal matrix elements of the EFG tensor operator acting upon Ψ and may be written in terms of one-electron matrix elements.

$$\begin{aligned} V_{rs} &= (\Psi_1^\alpha \Psi_1^\beta \dots \Psi_n^\beta | \sum_{\text{el}} \mathcal{V}_{rs} | \Psi_1^\alpha \Psi_1^\beta \dots \Psi_n^\beta) \\ &= 2 \sum_{L=A}^N (1 - R_L) (\Psi_L | \mathcal{V}_{rs} | \Psi_L) \end{aligned} \quad (22)$$

where $\mathcal{V}_{rs} = -er^{-5}(3x_r x_s - r^2 \delta_{rs})$.

In Eq. (22), \sum_{el} denotes the summation over all electrons, e is the protonic charge, and R_L is the appropriate Sternheimer factor, $x_r x_s = x, y, z$ and $\delta_{rs} = \text{Kronecker delta}$ (i.e., $\delta_{xy} = 0$; $\delta_{xx} = 1$).

The molecular orbital may be transformed into a set of localized orbitals α_L ($L = \text{A}, \text{B}, \dots \text{N}$), chosen so that each α_L is, so far as possible, localized in the region of the M-L axis. The Slater determinant [Eq. (21)] and V_{rs} remain unchanged by such a unimodular transformation and, hence,

$$\begin{aligned} V_{rs} &= 2 \sum_{L=A}^N (1 - R_L) (\alpha_L | \mathcal{V}_{rs} | \alpha_L) \\ &= \sum_{L=A}^N V_{rs}(L) \end{aligned} \quad (23)$$

If the orbital α_L is to a large extent localized in the M-L bond axis, $V_{rs}(L)$ will depend mainly on the properties of the ligand, L. In this case the total EFG is simply the tensor sum of approximately independent

contributions and these localized orbitals provide a natural framework for a discussion of additive electric field gradients. If the tensor $V_{rs}(\mathbf{L})$ is written in terms of the local axes (i.e., axes referring to the M-L bond) with Z directed along the M-L bond, then $V_{rs}(\mathbf{L})$ form the elements of the "partial field gradient" due to L, (p.f.g.)_L, encountered earlier in Clark's treatment of the point charge model.

It is also convenient if the localized orbitals are equivalent orbitals. The members of a set of equivalent orbitals can be permuted among themselves by the operations of the point group or one of its subgroups. The set of localized orbitals α_L may span one or more sets of equivalent orbitals. In the first case, the orbitals are unique and it follows from the definition of equivalent orbitals that *different members of the same set of equivalent orbitals give rise to the same (p.f.g.)_L*.

As a further approximation the localized orbitals may be considered as a linear combination of a metal orbital h_L and a ligand orbital χ_L .

$$\alpha_L = c_1 h_L + c_2 \chi_L \quad (24)$$

The orbitals α_L , h_L , and χ_L may all be taken as real, so that c_1 and c_2 are also real. The metal orbital is an appropriate equivalent orbital formed from the metal atomic orbitals and is called a "hybrid orbital." The matrix element in Eq. (23) may be written

$$(\alpha_L | \mathcal{V}_{rs} | \alpha_L) = c_1^2 (h_L | \mathcal{V}_{rs} | h_L) + 2c_1 c_2 (h_L | \mathcal{V}_{rs} | \chi_L) + c_2^2 (\chi_L | \mathcal{V}_{rs} | \chi_L) \quad (25)$$

The first and third terms of Eq. (25) may be identified with the valence and lattice contributions to the EFG represented in the point charge model by the equivalent charges C_1 and C_L [Eq. (14)], respectively. As V_{rs} depends on $\langle r^{-3} \rangle$ (*vide infra*), the three terms will fall off roughly as $1:10^{-1}:10^{-2}$. Hence, only a small contribution from the lattice is expected (although this may be inflated by an order of magnitude due to Sternheimer effects) and the second and third terms of Eq. (25) may be neglected. In this case, using the local axes (X, Y, and Z) and taking the Z axis along the M-L bond

$$V_{zz}(\mathbf{L}) = 2(1 - R_L)(h_L | \mathcal{V}_{zz} | h_L) c_1^2 = 2[\mathbf{L}]e \quad (26)$$

The above expression is sufficient for a $C_{\infty v}$ (119) bond, but for a bond without axial symmetry

$$\eta_L = \frac{(h_L | \mathcal{V}_{XX} - \mathcal{V}_{YY} | h_L)}{(h_L | \mathcal{V}_{zz} | h_L)} \quad (27)$$

where X and Y are chosen so as to diagonalize $V(\mathbf{L})$.

For tin(IV) compounds the structures of interest are tetrahedral, octahedral, and trigonal-bipyramidal. For tetrahedral and octahedral systems, the appropriate metal hybrids h_L ($5sp^3$ and $5sp^3d^2$, respectively) span a single equivalent set, whereas the trigonal-bipyramidal hybrids span two sets (apical and equatorial) as the $5s$ and $5d_{z^2}$ may participate in both apical and equatorial bonds. In Table VII are given typical

TABLE VII

CALCULATION OF PARTIAL FIELD GRADIENTS IN IMPORTANT STRUCTURAL TYPES^{a,b}

Tetrahedral

$$h_z^{\text{tet}} = \frac{1}{2}s + \frac{\sqrt{3}}{2}p_z$$

$$[L]^{\text{tet}} = -\frac{2}{15}\langle r^{-3} \rangle_p \sigma_L^{\text{tet}}$$

Octahedral

$$h_z^{\text{oct}} = \frac{1}{\sqrt{6}}s + \frac{1}{\sqrt{2}}p_z + \frac{1}{\sqrt{3}}d_{z^2}$$

$$[L]^{\text{oct}} = \left(-\frac{1}{3}\langle r^{-3} \rangle_p - \frac{2}{21}\langle r^{-3} \rangle_d - \frac{\sqrt{2}}{3\sqrt{5}}\langle r^{-3} \rangle_{sd} \right) \sigma_L^{\text{oct}}$$

Trigonal-bipyramidal

Apical

$$h_z^{\text{tba}} = \frac{1}{\sqrt{2}}\cos\theta s + \frac{1}{\sqrt{2}}p_z + \frac{1}{\sqrt{2}}\sin\theta d_{z^2}$$

$$[L]^{\text{tba}} = \left(-\frac{1}{3}\langle r^{-3} \rangle_p - \frac{1}{7}\sin^2\theta\langle r^{-3} \rangle_d - \frac{1}{\sqrt{5}}\sin\theta\cos\theta\langle r^{-3} \rangle_{sd} \right) \sigma_L^{\text{tba}}$$

Equatorial

$$h_z^{\text{tbe}} = \frac{1}{\sqrt{3}}\sin\theta s + \frac{\sqrt{2}}{\sqrt{3}}p_z + \frac{1}{2\sqrt{3}}\cos\theta d_{z^2} - \frac{1}{2}\cos\theta d_{x^2-y^2}$$

$$[L]^{\text{tbe}} = \left(-\frac{4}{15}\langle r^{-3} \rangle_p + \frac{1}{21}\cos^2\theta\langle r^{-3} \rangle_d - \frac{1}{3\sqrt{5}}\cos\theta\sin\theta\langle r^{-3} \rangle_{sd} \right) \sigma_L^{\text{tbe}}$$

$$\eta_L^{\text{tbe}} = \left| \frac{15\cos^2\theta\langle r^{-3} \rangle_d - 21\sqrt{5}\cos\theta\sin\theta\langle r^{-3} \rangle_{sd}}{28\langle r^{-3} \rangle_p - 5\cos^2\theta\langle r^{-3} \rangle_d + 7\sqrt{5}\cos\theta\sin\theta\langle r^{-3} \rangle_{sd}} \right|$$

^a tet = tetrahedral, oct = octahedral, tba = trigonal-bipyramidal-apical, tbe = trigonal-bipyramidal-equatorial.

^b From Ref. (121).

hybrids for each structural type; the nonequivalence of the trigonal-bipyramidal hybrids is accommodated by use of the parameter θ ($0 < \theta < 2\pi$) to describe the distribution of s and d_{z^2} character between apical and equatorial hybrids.

Also in Table VII are given the partial field gradient parameters, $[L]$ [N.B., the Z component of $(p.f.g.)_L = 2[L]e$], obtained by substitution of the expressions h_L into Eqs. (26) and (27). The radial averages $\langle r^{-3} \rangle_p$, $\langle r^{-3} \rangle_d$, and $\langle r^{-3} \rangle_{sd}$ are equal to the appropriate radial integrals, corrected for Sternheimer effects, for example,

$$\langle r^{-3} \rangle_{sd} = (1 - R_{sd}) \int_0^\infty \rho_s(r)(r^{-3})\rho_d(r)r^2 dr \quad (28)$$

where $\rho_s(r)$ and $\rho_d(r)$ are the radial parts of the $5s$ and $5d$ wave functions. The empirical parameter $\sigma_L^{\text{superscript}}$ is proportional to $2c_1^2$. Assuming that Sternheimer effects are constant, calculations of the integrals $\langle r^{-3} \rangle_p$, $\langle r^{-3} \rangle_d$, and $\langle r^{-3} \rangle_{sd}$ for the valence orbitals of tin (using Herman Skillman wave functions) indicate that the ratios $\langle r^{-3} \rangle_{sd} : \langle r^{-3} \rangle_p$ and $\langle r^{-3} \rangle_d : \langle r^{-3} \rangle_p$ are of order of magnitude 10^{-3} and 10^{-2} , respectively (122). Thus, terms in $\langle r^{-3} \rangle_{sd}$ and $\langle r^{-3} \rangle_d$ can be neglected. The $[L]$ values in Table VII then reduce to

$$[L]^{\text{tet}} = -\frac{3}{10} \langle r^{-3} \rangle_p \sigma_L^{\text{tet}} \quad (29.1)$$

$$[L]^{\text{oct}} = -\frac{1}{5} \langle r^{-3} \rangle_p \sigma_L^{\text{oct}} \quad (29.2)$$

$$[L]^{\text{tba}} = -\frac{1}{5} \langle r^{-3} \rangle_p \sigma_L^{\text{tba}} \quad (29.3)$$

$$[L]^{\text{tbe}} = -\frac{4}{15} \langle r^{-3} \rangle_p \sigma_L^{\text{tbe}} \quad (\eta_L^{\text{tbe}} = 0) \quad (29.4)$$

Equations (29.1)–(29.4), together with the properties of equivalent orbitals, lead to some important conclusions. First, the equivalence of the octahedral and tetrahedral hybrid orbitals means that the additivity model should provide a good rationalization of the relative quadrupole splittings found for compounds restricted to *one* of these coordination numbers. In these cases, the relative quadrupole splittings can be compared using the equations in Table IV and Eq. (18), where the appropriate $[L]$ value is defined in Eq. (29). However, it is clear from Eqs. (29.1)–(29.4) that different values must be used for $[L]^{\text{oct}}$ and $[L]^{\text{tet}}$ and, hence, quadrupole splittings for four- and six-coordinate compounds cannot be directly compared. Equations (29.1)–(29.4) imply that the ratio $[L]^{\text{oct}}/[L]^{\text{tet}}$ is equal to 0.67 ($\sigma_L^{\text{oct}}/\sigma_L^{\text{tet}}$). If, as might be expected, ($\sigma_L^{\text{oct}}/\sigma_L^{\text{tet}}$) does not differ greatly from unity, $[L]^{\text{oct}}$ should be approximately 70% of $[L]^{\text{tet}}$. This ratio is close to that found experimentally. For five-coordinate compounds, the equations in Table IV may be used,

but separate $[L]^{tba}$ and $[L]^{tbe}$ values must be employed; this is often neglected in a simple point charge approach (442).

From Eqs. (29.1)–(29.4) it is clear that tabulation of quantities proportional to $[L]^{superscript}$ for a set of ligands is equivalent to tabulation of corresponding $\sigma_L^{superscript}$ values. But it is also evident from Eqs. (29.1)–(29.4) and Table IV, that a constant quantity may be added to or subtracted from $\sigma_L^{superscript}$ without altering the magnitudes of the calculated quadrupole splittings. For example, consider a tetrahedral R_3SnX species. Substitution of expressions for $[R]^{tet}$ and $[X]^{tet}$ into the appropriate additivity expressions in Table IV gives

$$V_{ZZ} = \frac{3}{5} \langle r^{-3} \rangle_p (\sigma_R^{tet} - \sigma_X^{tet}) e \quad (30)$$

V_{ZZ} depends on the difference of $\sigma_R^{tet} - \sigma_X^{tet}$ and it is, therefore, not possible to determine absolute $[L]^{superscript}$ values direct from quadrupole splitting data. The best that can be done for tetrahedral and octahedral compounds is to evaluate parameters related to

$$[L]^{tet} - [X]^{tet} \quad \text{and} \quad [L]^{oct} - [X]^{oct} \quad (31)$$

where X is some standard ligand. For five-coordinate compounds one may evaluate parameters related only to

$$[L]^{tba} - [X]^{tba} \quad \text{and} \quad [L]^{tbe} - \frac{4}{3}[X]^{tba} \quad (32.1)$$

or, alternatively,

$$[L]^{tba} - \frac{3}{4}[X]^{tbe} \quad \text{and} \quad [L]^{tbe} - [X]^{tbe} \quad (32.2)$$

The above five-coordinate conditions are perhaps more meaningful if written in terms of σ_L , in which cases the quantities which may be evaluated are related to

$$-\frac{1}{5} \langle r^{-3} \rangle_p (\sigma_L^{tba} - \sigma_X^{tba}) \quad \text{and} \quad -\frac{4}{15} \langle r^{-3} \rangle_p (\sigma_L^{tbe} - \sigma_X^{tba}) \quad (33.1)$$

or, alternatively,

$$-\frac{1}{5} \langle r^{-3} \rangle_p (\sigma_L^{tba} - \sigma_X^{tbe}) \quad \text{and} \quad -\frac{4}{15} \langle r^{-3} \rangle_p (\sigma_L^{tbe} - \sigma_X^{tbe}) \quad (33.2)$$

It is perhaps appropriate to point out the relationship of this treatment to that of Bancroft *et al.* (44). For low-spin Fe^{II} compounds, the equivalent orbitals for the σ bonds are the d^2sp^3 hybrids formed from the $3d_z^2$, $3d_{x^2-y^2}$, $4s$, and $4p$ iron atomic orbitals. Neglecting contributions from $4p$ orbitals or cross-terms

$$[L]^\sigma = \frac{-2}{21} \langle r^{-3} \rangle_{3d} \sigma_L^{oct} \quad (34)$$

where $[L]^\sigma$ is related to the parameter σ_L of Bancroft (44) by the relationship

$$[L]^\sigma = -\frac{2}{3}\sigma_L \quad (35)$$

In order to consider π bonding in low-spin Fe^{II} using this model, it is necessary to form 12 localized π orbitals (2 per M-L axis). Symmetry considerations, however, show that for the case of low-spin Fe^{II} octahedrally coordinated by ligands with empty π orbitals, it is not possible to write a general set of localized orbitals. Although this result does not preclude additivity of π contributions in special cases, it does suggest that there is no theoretical justification for writing a π -bonding contribution to the total EFG as a partial field gradient parameter (π_L), which is completely independent of the other ligands. In other words, some deviations from strict additivity might be expected for the π -bonding contribution to the EFG of low-spin Fe^{II} compounds.

The calculations so far described in this section have referred to regular geometries, whereas in practice, distortions from a regular geometry will be anticipated. Attempts have been made to calculate the effect of distortions using a point charge model (29, 64, 288, 402). In this case, changes in V_{rs} arising from changes in the orientation of the M-L axis are calculated assuming that $[L]$ values remain constant. This method yields equations for V_{zz} which differ in the relative magnitudes of the coefficients of $[L]$. For example, for a tetrahedral MA_3B molecule distorted as in Fig. 3, but preserving C_{3v} symmetry,

$$V_{zz} = \{2[B]^{\text{tet}} - 3(1 - 3\cos^2\alpha)[A]^{\text{tet}}\}e \quad (36)$$

where α is defined in Fig. 3. Similar results are obtained for MA_2B_2 systems.

The application of the point charge model to distorted systems does not seem realistic as the expression for a given bond orbital α_L will be expected to change with orientation of the bond. The equivalence of the orbitals will, therefore, be lost and constant $[L]$ values can no longer be assigned.

The molecular orbital model of Clark *et al.* [122] has been extended to consider distortions of SnA_3B (Fig. 3) and SnA_2B_2 (Fig. 3) species. The distortion of SnA_3B preserves C_{3v} symmetry, whereas that of SnA_2B_2 preserves C_{2v} symmetry, and the angles α and β are related by the equations

$$\text{for } \text{SnA}_3\text{B}: 2.19 \geq \alpha \geq \frac{1}{2}\pi \quad \cos\beta = \frac{1}{2}(3\cos^2\alpha - 1) \quad (37.1)$$

$$\text{for } \text{SnA}_2\text{B}_2: \frac{1}{2}\pi \geq \alpha \geq \frac{1}{4}\pi \quad \cos^2\beta = 1 - \cot^2\alpha \quad (37.2)$$

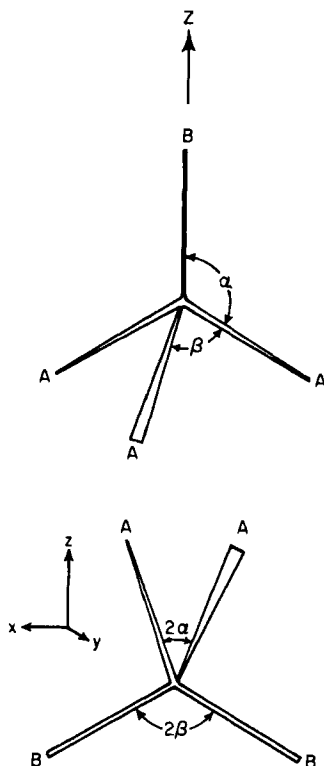


FIG. 3. Distortions of the SnA_3B and SnA_2B_2 compounds from tetrahedral symmetry ($I\bar{2}2$). See Eqs. (37.1) and (37.2).

The calculated values of Δ are

$$\text{for } \text{SnA}_3\text{B}: \Delta_1(\alpha) = f_1(\alpha) \Delta_1^{\text{tet}} \quad (38.1)$$

$$\text{for } \text{SnA}_2\text{B}_2: \Delta_2(\alpha) = f_2(\alpha) |\Delta_2^{\text{tet}}| \text{sgn } \{Q\} \quad (38.2)$$

where $f_1(\alpha)$ and $f_2(\alpha)$ are functions of angle α , plotted in Figs. 4a and 4b. For SnA_2B_2 , η is also a function of α and it is plotted as a broken line in Fig. 4b.

Equations (38.1) and (38.2) show that in contrast to the point charge model, Δ remains proportional to $[\text{B}]^{\text{tet}} - [\text{A}]^{\text{tet}}$. Thus, for $[L]$ values calculated from observed quadrupole splittings on the basis of an idealized geometry, the values obtained will be *apparent* values equal to $|f(\alpha)|$ times the value for exact tetrahedral geometry. The *true* partial field gradient parameters will be different from these apparent values.

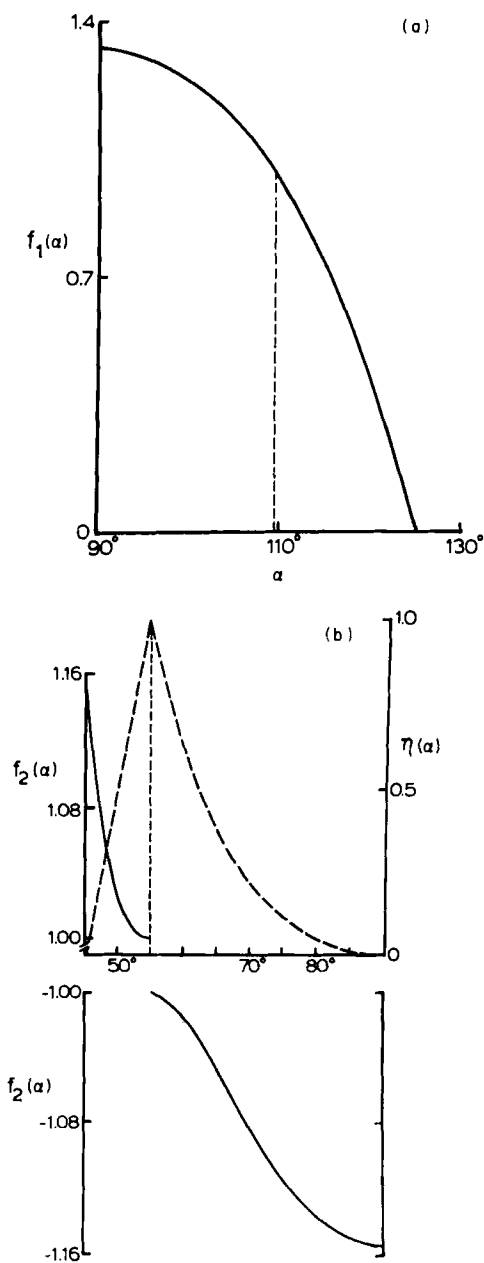


FIG. 4. $f(\alpha)$ [Eqs. (38.1) and (38.2)] plotted for distorted SnA_3B and SnA_2B_2 structures (122). (a) $f_1(\alpha)$ for SnA_3B species versus α . (b) $f_2(\alpha)$ for SnA_2B_2 species versus α . η is also a function of α , and it is plotted as broken line.

The compounds in Table VIII provide a test for this treatment as structural and Mössbauer information are available. Further, the values for α and β satisfy the appropriate Eq. (37) almost exactly. The ratios of Q.S. (ii) : Q.S. (i) and Q.S. (iii) : Q.S. (i) calculated directly from observed quadrupole splittings are 0.77 and 0.68. If the quadrupole splittings are corrected to "tetrahedral values," the ratios become 1.67 and 1.23, respectively. However, the predicted ratio is 0.87 (assuming $[\text{Cl}]^{\text{tet}} = [\text{Br}]^{\text{tet}}$), which is in much closer agreement with the uncorrected value.

TABLE VIII

MÖSSBAUER QUADRUPOLE SPLITTING AND STRUCTURAL DATA FOR SOME TETRAHEDRAL COMPOUNDS SHOWING DISTORTIONS FROM IDEALIZED GEOMETRY

Code	Compound ^a	α^b	β^b	Ref.	Δ^c (mm/sec)	Ref.
(i)	$[\text{cpFe}(\text{CO})_2]_2\text{SnCl}_2$	47.0	64.3	(426)	+2.38	(64, 288, 331)
(ii)	$[\text{cpFe}(\text{CO})_2]\text{SnCl}_3$	119.2	98.3	(296)	+1.81	(29, 64, 288, 331)
(iii)	$[\text{cpFe}(\text{CO})_2]\text{SnBr}_3$	117.7	100.2	(407)	1.60	(64)
(iv)	$\text{Me}_3\text{SnMn}(\text{CO})_5$	111.6	107.3	(80)	0.75	(29, 431, 569)
(v)	$[\text{Mn}(\text{CO})_5]_3\text{SnCl}$	101.0	116.5	(543)	1.55	(364)

^a cp = π -Cyclopentadienyl.

^b Average of nominally equal angles; see Fig. 3 for definition.

^c An average of the data has been taken.

Similarly a value of $\frac{1}{2}e^2|Q| ([\text{Me}]^{\text{tet}} - [\text{Cl}]^{\text{tet}})$ may be calculated from (iv) and (v) (Table VIII), to be equal to -1.13 mm/sec if no corrections for distortions are made or -1.02 mm/sec if corrections are applied. The uncorrected value is close to the value of -1.37 mm/sec obtained in Section IV, A, 1, b.

The overall conclusions therefore are that small distortions from regular geometry are best ignored when applying the additivity model. One possible explanation is that whereas the quadrupole splitting weights the portion of the bond close to the metal nucleus, bond angle data weights the portion roughly midway between.

Finally, it should be noted that additive electric field gradients are, in fact, manifestations of underlying special symmetry features, which have been elegantly elucidated by Clark (119).

III. Fingerprint Uses

Any spectroscopic parameter such as the center shift and quadrupole splitting which is sensitive to the electronic or molecular structure of a compound is capable of providing the chemist with two general types of information: the characterization of the type of atom or molecule by comparison of the spectroscopic parameter with those of known species (the so-called fingerprint technique), and the elucidation of bonding and structure. The first of these will be reviewed quite briefly in this section, while perhaps the more important application—structure and bonding—will be discussed in some detail in Section IV.

The fingerprint application is very useful in the following ways: to indicate the purity of a compound; to characterize the oxidation state of, and the coordination environment about the Mössbauer atom; to detect inequivalent Mössbauer atoms in compounds or minerals, and to estimate the amount of each Mössbauer atom present; and to identify the compounds or species in a complex mixture.

Unlike many other spectroscopic experiments, the line shapes in Mössbauer spectra are normally very well-behaved Lorentzians making the spectra amenable to detailed computer processing. Thus, if the peak or peaks are slightly asymmetric, or if there is a slight shoulder on one of them, one can usually be confident that there is a Mössbauer atom present which is causing this asymmetry or shoulder.

A. OXIDATION STATES AND INEQUIVALENT MÖSSBAUER ATOMS

Mössbauer spectra are often very useful to characterize the oxidation state of the Mössbauer atom, especially in chemically difficult situations. The very different C.S. values for some of the different oxidation states of iron indicate that these should be diagnostic (Table IX). Any gross deviation of this parameter from the expected value might indicate

TABLE IX
CENTER SHIFTS (C.S.) FOR HIGH-SPIN IRON COMPOUNDS
RELATIVE TO NITROPRUSSIDE^{a,b}

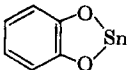
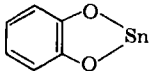
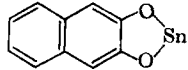
Oxidation state	+1	+2	+3	+4	+6
Center shift	~+2.2	~+1.4	~+0.7	~+0.2	~-0.6

^a From Ref. (297).

^b Data in mm/sec at room temperature.

undesirable reactions. An excellent example concerns the Mössbauer spectra of high-spin Fe^{II} chelates of salicylaldoxime, salicylaldehyde, and others. The first and subsequent reported spectra of these compounds gave C.S. (~ 0.60 mm/sec) and small Q.S. values characteristic of Fe^{III} compounds (236, 376, 532), but these parameters were still attributed to the expected Fe^{II} species with a large degree of π back-bonding. However, recent work (177) conclusively shows that the above compounds are, in fact, oxidation products of Fe^{II} compounds, which give normal Fe^{II} C.S. of about 1.4 and 2.5 mm/sec, respectively. Preparation of the Fe^{II} compounds must be carried out in a vacuum system.

TABLE X
CENTER SHIFTS OF Sn^{II} AND Sn^{IV} COMPOUNDS

Compound	C.S. ^a	Ref.
1. α -Tin	+2.10	
2. 	+2.95	(50)
3. 	+3.13	(50)
4. 	+3.08	(50)
5. $(\text{C}_5\text{H}_5)_2\text{Sn}$	+3.73	(317)
6. $(\text{Ph}_2\text{Sn})_n$	+1.42	(280)
7. $(\text{Bu}_2\text{Sn})_n$	+1.55	(280)
8. $[(\text{C}_5\text{H}_5)_2\text{Sn}]_n$	+0.72	(317)

^a Data in mm/sec, relative to SnO_2 or BaSnO_3 .

Mössbauer spectra are very useful here, because the Fe^{II} and Fe^{III} compounds cannot be readily distinguished by magnetic measurements or chemical analyses.

For a number of other Mössbauer isotopes, $\delta R/R$ [Eq. (1)] is large enough so that different oxidation states give measurably different center shifts. For example, the difference in center shift for the +3 and +5 oxidation states of ^{121}Sb is over 10 mm/sec (62, 496, 522), and this large difference has been used to estimate the amount of Sb^{III} and Sb^{V}

in nonstoichiometric oxides and sulfides of antimony, such as Sb_2O_4 and Sb_2S_3 (62, 71, 522). Similarly, for ^{119}Sn Mössbauer, Sn^{II} compounds invariably give higher C.S. values than α -tin, whereas Sn^{IV} compounds give lower C.S. values than α -tin. For example, in Table X, compounds 2–5 are clearly Sn^{II} species (50, 317), while compounds 6, 7, and 8 are Sn^{IV} species with polymeric structures.

For ^{129}I (90, 310, 445), ^{127}I (205, 361, 452), ^{129}Xe (451, 453, 454), and ^{125}Te (219, 266, 361, 545) the C.S. is usually sensitive enough to determine oxidation states in chemically difficult situations [for a summary of results, see Shenoy and Ruby (510)]. Similarly, ^{197}Au (49, 108, 222), ^{193}Ir (495, 552), ^{237}Np (458), ^{99}Ru (128, 130, 362, 470, 471), and ^{151}Eu (197, 272), to name a few, often give diagnostic C.S. values. The above isotopes, partly because of sensitivity of the C.S., are among the most widely studied species at the present time.

However, there are a number of situations where Mössbauer cannot distinguish between oxidation states readily. For low-spin iron compounds containing strong π -acceptor groups such as CO, the C.S. values have a fairly small range for oxidation states from +2 to -2 (110). Thus, $\text{K}_3\text{Fe}^{\text{III}}(\text{CN})_6$ and $\text{K}_4\text{Fe}^{\text{II}}(\text{CN})_6$ have remarkably similar center shifts (76, 238, 239). Similarly, in a study of Ir compounds (562) the center shift values for $\text{IrCl}(\text{CO})[\text{P}(\text{C}_6\text{H}_5)_3]_2$ and $\text{XYIrCl}(\text{CO})[\text{P}(\text{C}_6\text{H}_5)_3]_2$, where

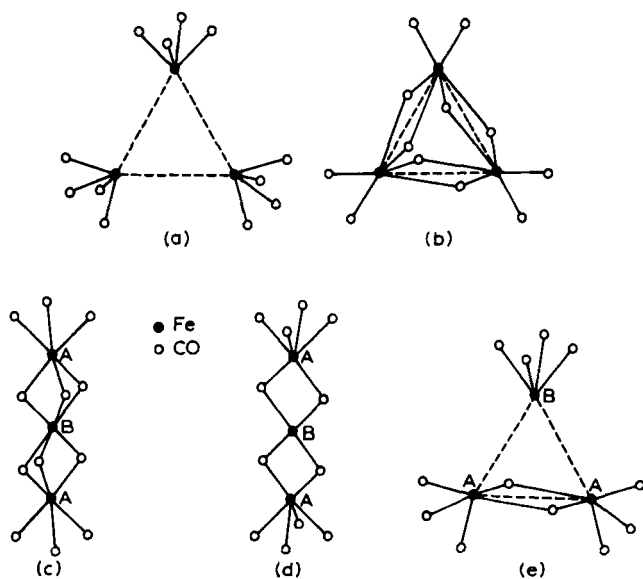


FIG. 5. Possible structures for $\text{Fe}_3(\text{CO})_{12}$ (218).

X, Y = Cl, H, Br, etc., were remarkably similar despite the formal Ir oxidation states of +1 and +3, respectively.

The Mössbauer effect has been widely used for compounds containing two or more Mössbauer atoms to determine whether they are equivalent. This information is usually very useful for structural predictions. The first and most notable contribution in this area is given by the Mössbauer spectrum of $\text{Fe}_3(\text{CO})_{12}$ (218). Until a definitive crystal structure was published recently (557), several different structures were proposed on the basis of incomplete X-ray work and infrared data. These structures were based either on a triangle of Fe atoms or a linear array of Fe atoms (Fig. 5). The Mössbauer spectrum of $\text{Fe}_3(\text{CO})_{12}$ (Fig. 6) clearly

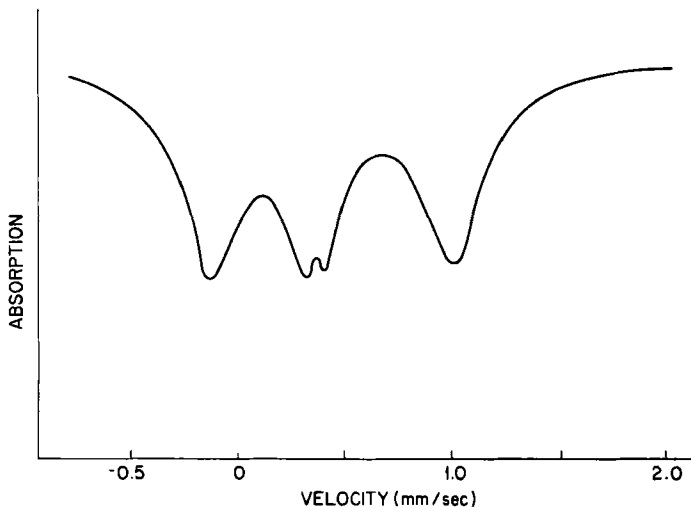


FIG. 6. Mössbauer spectrum of $\text{Fe}_3(\text{CO})_{12}$ (293).

indicates that there are two distinguishable (to Mössbauer) iron atoms present, with the outer peaks due to one type of iron atom (Fe_A) and a narrow doublet due to Fe_B . From the areas, it is apparent that $\text{Fe}_A:\text{Fe}_B \sim 2:1$. Linear structures of the type shown in Fig. 5c,d would be consistent with this spectrum, but the spectrum of the $\text{Fe}_3(\text{CO})_{11}\text{H}^-$ anion, which is very similar to that of $\text{Fe}_3(\text{CO})_{12}$ (Table XI), rules out a linear structure. If there are any bridging carbonyls in a linear structure, it is not possible to replace any CO group by H and leave two iron atoms equivalent. The above evidence strongly suggests that $\text{Fe}_3(\text{CO})_{12}$ has an unsymmetrical triangular structure, with one iron atom coordinated to the same atoms in both $\text{Fe}_3(\text{CO})_{12}$ and the hydride, since the para-

meters for iron atom A in both the parent molecule and the anion are very similar. One structure which is consistent with this evidence is given in Fig. 5e. The H^- substitutes for a bridging carbonyl, leaving atoms A equivalent, but the C.S. is decreased somewhat from that in $Fe_3(CO)_{12}$. The very similar parameters for Fe_B in both structures are consistent with the identical nearest neighbors for Fe_B in both structures. There are other unsymmetrical triangular structures which would fit the above evidence, but the recent X-ray structure (557) confirms that $Fe_3(CO)_{12}$ has the structure shown in Fig. 5e.

TABLE XI
MÖSSBAUER PARAMETERS FOR $Fe_3(CO)_{12}$ AND $NaFe_3(CO)_{11}H$
AT 298°K^a

Compound	Fe atom	C.S. ^b	Q.S.
$Fe_3(CO)_{12}$	A	+0.34	1.05
	B	+0.32	<0.20
$Na[Fe_3(CO)_{11}H]$	A	+0.26	1.32
	B	+0.28	<0.20

^a Relative to nitroprusside (mm/sec).

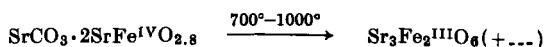
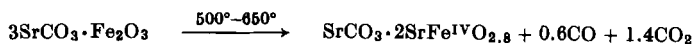
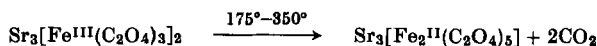
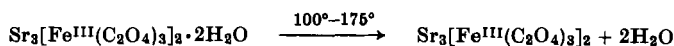
^b From Ref. (218).

There are a number of other examples, where the observation of more than the expected number of lines for one Mössbauer atom has been very useful in structural elucidation: e.g., $I_2Cl_4Br_2$ (445), and a host of polynuclear iron compounds (223, 224, 295, 370) to name a few. However, it should be emphasized that if a polynuclear compound gives rise to apparently one set of absorptions, this negative evidence cannot be taken as proof of equivalence. For example, the crystal structure of $[(\pi-C_5H_5)_2Fe_2(CO)_3]_2DPPA$ (102) shows that the two iron atoms are inequivalent with a DPPA molecule ($Ph_2PC\equiv CPPH_2$) linking two $Fe_2(CO)_3(\pi-C_5H_5)_2$ units. One iron atom is bound to a C_5H_5 , a terminal CO, and two bridging CO, whereas the other is bound to a C_5H_5 and the two bridging CO, but a terminal P on the DPPA. However, the Mössbauer spectrum (102, 104) shows only one narrow doublet with line widths of 0.24 and 0.26 mm/sec, which might suggest that the two irons are equivalent. Similarly, a previous Mössbauer prediction of the equivalence of iron atoms in $C_8H_{10}Fe_2(CO)_6$ (206) has recently been shown incorrect by an X-ray study (143). For many such spectra, detailed computation becomes important for detecting any line broadening or asymmetry which could be due to an overlap of Lorentzians.

B. DECOMPOSITION REACTIONS

Mössbauer spectroscopy has been particularly valuable in several studies for following reactions in the solid state. The information from Mössbauer spectra can often not be obtained by other techniques, but it is usually important to use Mössbauer in conjunction with other techniques.

The classic example in this area of research is the elucidation of the complex decomposition scheme of $\text{Sr}_3[\text{Fe}^{\text{III}}(\text{C}_2\text{O}_4)_3]_2 \cdot 2\text{H}_2\text{O}$ using mainly C.S. values as a guide to the oxidation state of iron (Table IX) and weight losses from thermal analyses (253). Table XII shows that the C.S. varies from the initial value of 0.65 mm/sec (Fe^{III}), to 1.44 mm/sec (Fe^{II}) after heating to 200°C, to 0.60 mm/sec (Fe^{III}) at 400°C, to 0.27 (Fe^{IV}) and 0.82 mm/sec (Fe^{III}) at temperatures of 700°C and above. A mechanism which is consistent with these oxidation states of iron and the weight loss data is:



In a similar fashion, using Mössbauer to distinguish between the oxidation states of iron, the thermal decomposition of $\text{K}_3\text{Fe}^{\text{III}}(\text{C}_2\text{O}_4)_3 \cdot 3\text{H}_2\text{O}$ (31) and $\text{Fe}(\text{C}_2\text{O}_4) \cdot 2\text{H}_2\text{O}$ (314) have been followed. The $\text{FeSO}_4 + \text{KCN}$ reaction has also been studied using Mössbauer (308).

The effect of external radiation on compounds containing Mössbauer atoms has been recently studied. The radiation-induced decomposition of $\text{K}_3\text{Fe}(\text{C}_2\text{O}_4)_3 \cdot 3\text{H}_2\text{O}$ proceeds stoichiometrically to either $\text{K}_2\text{Fe}^{\text{II}}(\text{C}_2\text{O}_4)_2(\text{H}_2\text{O})_2$ (30) or $\text{K}_6\text{Fe}_2^{\text{II}}(\text{C}_2\text{O}_4)_5$ in vacuum and air, respectively. Other studies (309, 560) indicate that Fe^{III} is formed in Fe^{II} compounds during irradiation. In $\text{Fe}(\text{acac})_3$ (32), the large line width is reduced substantially on irradiation, and this has been attributed to a relaxation mechanism.

TABLE XII
ROOM TEMPERATURE MÖSSBAUER PARAMETERS FOR THE
THERMAL DECOMPOSITION OF $\text{Sr}_3[\text{Fe}(\text{C}_2\text{O}_4)_3]_2 \cdot 2\text{H}_2\text{O}^a$

Temperature of heating (°C)	C.S. ^b	Q.S.	Assignment
25	+0.65	0.44	$\text{Sr}_3[\text{Fe}^{\text{III}}(\text{C}_2\text{O}_4)_3]_2 \cdot 2\text{H}_2\text{O}$
200	+1.44	2.3	$\text{Sr}_3\text{Fe}_2^{\text{II}}(\text{C}_2\text{O}_4)_5$
400	+0.60	0.70	$\text{SrCO}_3 \cdot \text{Fe}_2^{\text{III}}\text{O}_3$
600	+0.44	0.74	
700	+0.27	~0	$\text{SrCO}_3 \cdot 2\text{SrFe}^{\text{IV}}\text{O}_{2.8}(\text{A})$
	+0.82	~0	$\text{Sr}_3\text{Fe}_2^{\text{III}}\text{O}_6(\text{B})$
1000	+0.23	~0	(A)
	+0.75	~0	(B)

^a Relative to nitroprusside (mm/sec).

^b From Ref. (253).

C. THE EFFECT OF TEMPERATURE AND PRESSURE ON THE ELECTRONIC STRUCTURE OF IRON COMPOUNDS

Mössbauer spectroscopy has been used to study a number of very interesting changes in the electronic state of the iron atom in Fe^{II} and Fe^{III} compounds at low temperatures and high pressures. A large number of Mössbauer and magnetic studies of high spin-low spin equilibria in Fe^{II} and Fe^{III} compounds have been undertaken (73, 145, 195, 287, 356, 373-375, 482). For example, in the series of Fe^{II} bisphenanthroline complexes, $\text{Fe}(\text{phen})_2\text{X}_2$, if $\text{X} = \text{Cl}^-$, Br^- , I^- , or other ligands low in the spectrochemical series, high-spin compounds are obtained having, first, the large C.S. and Q.S. (Table XIII) characteristic of Fe^{II} high-spin compounds and, second, large magnetic moments ($\mu = 5.0$ – 5.3 B.M.) slightly higher than those expected for four unpaired electrons. In contrast, if X is CN^- or NO_2^- , then low-spin compounds are obtained with the small C.S. and Q.S. characteristics of Fe^{II} low-spin compounds (Table XIII) and the very small magnetic moments expected for no unpaired electrons. For intermediate ligands such as NCS or NCS_e (374, 375), the high- and low-spin configurations are of very similar energy and in the thermally accessible range. Thus, $\text{Fe}(\text{phen})_2(\text{NCS})_2$ is high spin at room temperature, but low spin at liquid N_2 temperatures. Using Mössbauer spectra, magnetic suscepti-

bilities, and other spectral techniques, König and Madeja (375) have presented evidence that for $\text{Fe(phen)}_2\text{mal} \cdot 7\text{H}_2\text{O}$ and $\text{Fe(phen)}_2\text{F}_2 \cdot 4\text{H}_2\text{O}$, Fe is surprisingly in the intermediate $S = 1$ state.

Other, more subtle changes in the ligand environment lead to a similar high spin-low spin equilibria. In a study of octahedral Fe^{II} chelates based on the hydrotris(1-pyrazolyl)borate ligand, Jesson *et al.* (356) have shown that the H,H- and CH_3, CH_3 -substituted complexes are low spin and high spin, respectively, over the temperature range 295 to

TABLE XIII
MÖSSBAUER PARAMETERS FOR $\text{Fe(phen)}_2\text{X}_2$ AND RELATED COMPOUNDS^a

Compound	Temperature (°K)	C.S. ^b	Q.S.	Type of spin
$\text{Fe(phen)}_2(\text{NO}_2)_2$	293	0.53	0.38	Low
$\text{Fe(phen)}_2\text{Cl}_2$	293	1.21	3.00	High
$\text{Fe(phen)}_2(\text{NCS})_2$	293	1.23	2.67	High
	77	0.62	0.34	Low
$\text{Fe(phen)}_2(\text{NCS}_2)_2$	293	1.28	2.52	High
	77	0.60	0.18	Low
$\text{Fe(phen)}_2\text{mal} \cdot 7\text{H}_2\text{O}$	293	0.59	0.18	Intermediate
	77	0.52	0.18	
$\text{Fe(phen)}_2\text{F}_2 \cdot 4\text{H}_2\text{O}$	293	0.58	0.21	Intermediate
	77	0.55	0.16	

^a Relative to nitroprusside (mm/sec).

^b From Refs. (374, 375).

4°K, whereas the CH_3 , H-substituted complex is high spin at 295°K, but reverts to low spin near 150°. Goodgame and Machado (287) have shown that $\text{Fe(pyim)}_3(\text{ClO}_4)_2$ forms two geometrical isomers, one low spin and the other giving high spin-low spin equilibria over the temperature range studied.

In many of these studies, the energy separation between the 5T_2 and 1A_1 states has been determined, although recent evidence (373) suggests that this energy separation is strongly temperature dependent.

Drickamer and co-workers (48, 107, 196, 230, 250, 251, 385, 386, 435) have done a great deal of interesting work on the effect of high pressure on a wide variety of iron-containing chemicals, and these studies again indicate the great diagnostic use of Mössbauer for detecting different types of iron atoms. Many of these studies indicate that Fe^{III} reduces to

Fe^{II} with increasing pressure. The phenomenon is reversible with some hysteresis. Typical spectra of $\text{Fe}(\text{acac})_3$ are shown in Fig. 7 (107) indicating that the initial Fe^{III} species is reduced partially to Fe^{II} on application of large pressures. On releasing the pressure, the Fe^{II} peaks disappear. The Fe^{III} to Fe^{II} reduction involves an electron transfer from a nonbonding ligand level to an antibonding $3d$ level on the iron. The $3d$ orbitals spread with increasing pressure, lowering their energy relative to the ligand levels, thus permitting the thermal transfer of an electron from ligand to metal.

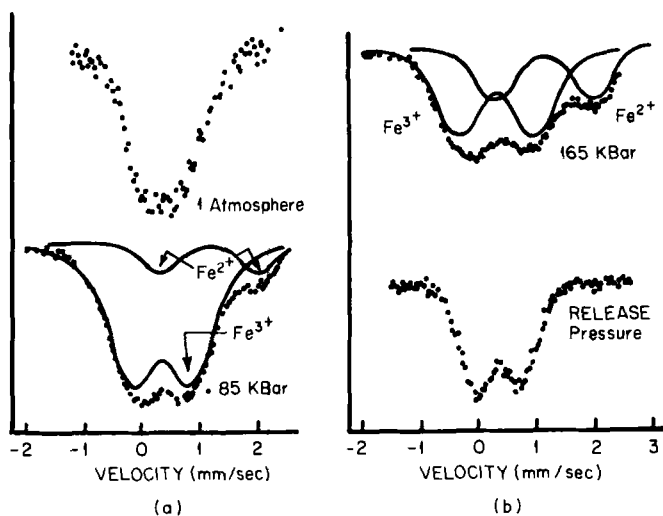


Fig. 7. Mössbauer spectra of $\text{Fe}(\text{acac})_3$ (107). Note the Fe^{II} peaks after pressure is applied, and the return to a pure Fe^{III} spectrum after release of pressure.

Similarly, Fe^{IV} in $\text{SrFeO}_{2.86}$ is reduced reversibly to Fe^{III} , whereas the Fe^{VI} in BaFeO_{4-x} is reduced irreversibly to Fe^{IV} with perhaps some Fe^{III} (435), presumably again by ligand to metal charge transfer.

These studies should be of the greatest importance in understanding not only the electronic structure of iron compounds, but also the mechanism of reduction of iron in the earth's interior.

D. SITE POPULATIONS IN SILICATE MINERALS

Mössbauer spectroscopy has been applied as a fingerprint technique to a wide range of iron-containing minerals, and a great deal of useful

information has been obtained. The most significant and important studies center around the determination of Fe^{2+} site populations and $\text{Fe}^{3+}/\text{Fe}^{2+}$ ratios in silicate minerals (20, 21, 23–26, 40, 181, 200, 221, 264, 311, 343, 474, 503, 549, 550 and references]. Most silicate minerals such as orthopyroxenes $[(\text{FeMg})_2\text{Si}_2\text{O}_6]$ have two or more cation sites into which Fe^{2+} and Mg^{2+} can enter (172). In orthopyroxenes, there are two such sites; the distorted M2 site, and the more regularly octahedral M1 site. X-Ray diffraction measurements (263) first showed that Fe^{2+} orders in the M2 position, i.e., it prefers the M2 position over the M1

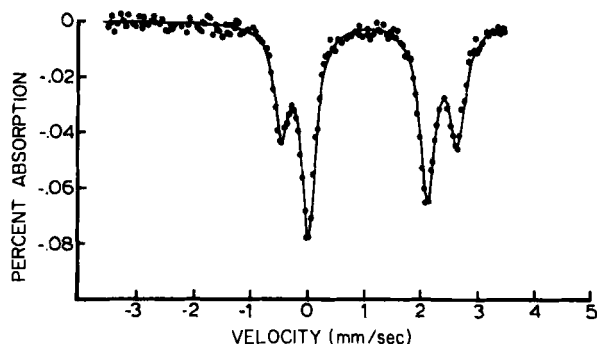


FIG. 8. Mössbauer spectrum of an orthopyroxene of approximate composition $(\text{Fe}_{0.57}\text{Mg}_{0.43})\text{Si}_2\text{O}_6$ at 80°K (549). The outer two peaks are due to Fe^{2+} in M1, while the inner two peaks are due to Fe^{2+} in M2.

position. Thus, in an orthopyroxene of composition $(\text{Fe}_{0.5}\text{Mg}_{0.5})_2\text{Si}_2\text{O}_6$, about 85% of the Fe^{2+} enters the M2 position. Since the amount of ordering should be temperature dependent, the determination of site populations has become of great interest not only for determining crystal chemical relationships, but also as a potential geothermometer.

Mössbauer spectroscopy offers a convenient, rapid, and accurate method for obtaining Fe^{2+} site populations, since structurally different Fe^{2+} ions (such as Fe^{2+} in M2 and M1 above) often give distinctive spectra (Fig. 8). The area (A) under a peak is proportional to the amount (n) of Fe^{2+} in each site, i.e., $A_{\text{M2}}/A_{\text{M1}} = n_2/n_1$. The first quantitative results reported in 1966 for orthopyroxenes, anthophyllites, and cumingtonites (23, 40) have led to the determination of site populations in a large range of iron-containing minerals such as pyroxenes (25, 311, 503, 549, 550), biotites (343), and other amphiboles (24). Although there are difficulties in obtaining accurate site populations for some minerals (21), the excellent agreement between Mössbauer and X-ray results

(Table XIV) suggests that accurate values can be obtained for most minerals.

In addition to Fe^{2+} ratios, $\text{Fe}^{3+}/\text{Fe}^{2+}$ ratios in minerals can easily be obtained (24, 181), and these are, in general, in good agreement with the corresponding ratios from chemical analysis (Table XV). Wet chemical methods for obtaining these ratios are often inaccurate, and the nondestructive Mössbauer method should become a standard method for determining this ratio.

Virgo and Hafner (311, 549, 550) and Saxena and Ghose (503) have obtained Fe^{2+} site populations for a large number of natural and syn-

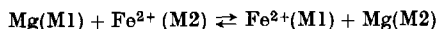
TABLE XIV

COMPARISON OF X-RAY AND MÖSSBAUER SITE POPULATIONS IN SILICATE MINERALS

Mineral	Total Fe^{2+} per formula unit	Fe^{2+} site populations (per formula unit)			
		Mössbauer	Ref.	X-ray	Ref.
Orthopyroxene	1.06	M2 = 0.87	(550)	M2 = 0.90	(263)
		M1 = 0.19		M1 = 0.15	
Glaucophane	0.61	M3 = 0.28	(24)	M3 = 0.29	(436)
		M1 = 0.33		M1 = 0.32	
Grunerite	6.13	M4 = 1.96	(26)	M4 = 1.97	(228)
		M123 ^a = 4.17		M123 = 4.13	
Anthophyllites	1.61	M4 = 1.39	(40)	—	
		M123 = 0.22		—	
	1.47	—		M4 = 1.30	(229)
		—		M123 = 0.17	
Cummingtonites	2.48	M4 = 1.65	(26)	—	
		M123 = 0.83		—	
	2.50	—		M4 = 1.50	(231)
				M123 = 1.29	
		—		M4 = 1.74	(262)
				M123 = 0.58	

^a M123 refers to Fe^{2+} per formula unit in M1 + M2 + M3.

thetic pyroxenes and determined both preliminary thermodynamic and kinetic data for the exchange reaction:



A number of papers have appeared recently which discuss the kinetics and thermodynamics of the above type of exchange reaction (305, 414, 503, 538 and references). These papers and the experimental papers mentioned above indicate the great potential of site population determinations for determining the highest temperature of formation of orthopyroxenes and kinetics of cooling, although the low activation energies for forward and reverse reactions may make such determinations very difficult.

TABLE XV
COMPARISON OF MÖSSBAUER AND CHEMICAL ANALYSES
VALUES FOR % Fe^{3+} /TOTAL IRON^a

Mineral	% $\text{Fe}^{3+}/(\text{Fe}^{2+} + \text{Fe}^{3+})$	
	Mössbauer	Chemical analyses
Howieite	24	20
Deerite	37	37
Crocidolite	41	41
Glaucophane	28	32
Crossite	37	40

^a From Refs. (24, 27).

E. PREPARATION OF NOVEL COMPOUNDS

It is apparent from the previous discussion that the vast majority of Mössbauer spectra have been taken with a constant standard single-line source with the absorber as the compound under study. However, a number of interesting papers have appeared in which a standard single-line absorber has been used with the source compound being of interest. Because the source is radioactive, extensive rearrangement of the electrons and bond breaking may occur on the Mössbauer time scale (the half-life of the excited state). As a result, the observed Mössbauer spectrum may not reflect the initial electronic and/or ligand environment about the Mössbauer atom. The differences in spectra can be very useful to the radiochemist in investigating the effect of the radioactive process [for example, see (225, 248, 249, 272, 352, 358, 398, 541)], but we are

concerned here with the situations where the spectrum does reflect the initial electronic and ligand environment on the Mössbauer lifetime.

The classic studies in this area have been undertaken by the Perlows (450, 451, 453, 454), who have produced a number of ^{129}Xe compounds by the β decay of iodine compounds prepared with ^{129}I . For example, the spectra of XeCl_4 (451), XeCl_2 (453), and XeBr_2 (454) were obtained after the decay of KICl_4 , KICl_2 , and KIBr_2 , respectively, using a standard Xe absorber such as a xenon clathrate. These compounds have to be stable for longer than the lifetime of the nuclear excited state ($\sim 10^{-9}$ sec) in order to be "observed."

Somewhat similar experiments have been undertaken using ^{83}Kr Mössbauer (322, 444, 497). Using $^{83}\text{SeO}_2$ as a source ($^{83}\text{Se} \rightarrow ^{83}\text{Kr}$) and a krypton clathrate HQ-Kr as absorber, evidence has been presented (322) for the existence of a bona fide Kr-O bond. However, using $\text{K}^{83}\text{BrO}_3$ as source (444) ($^{83}\text{Br} \rightarrow ^{83}\text{Kr}$), no evidence was found for the existence of a KrO_3 species, in contrast to the production of XeO_3 from KIO_3 and its observation by Mössbauer (450).

Some source work (495) using ^{193}Os compounds as sources and single-line ^{193}Ir absorbers have also provided interesting results. The 73-keV excited nuclear energy level of ^{193}Ir is populated in the β decay of ^{193}Os . As in the $^{129}\text{I} \rightarrow ^{129}\text{Xe}$ transition, the majority of the Os atoms should end up in a valence state which is higher by unity than the parent Os atom. The spectra of OsO_4 , $\text{K}_2\text{OsO}_4 \cdot 2\text{H}_2\text{O}$, and $\text{Os}(\text{C}_5\text{H}_5)_2$ sources appear to be characteristic of IrO_4^+ , IrO_4^- , and $\text{Ir}(\text{C}_5\text{H}_5)_2^+$, respectively, and provide valuable information on unknown and highly unstable iridium species.

In other forms of radioactive decay, more substantial electronic rearrangement takes place. For example, ^{57}Co captures an orbital electron to give ^{57}Fe . $\text{Co}^{\text{III}}(d^6)$ should yield $\text{Fe}^{\text{III}}(d^5)$ if the resulting Auger process does not disturb the molecular structure. In most cases, a mixture of charge states are obtained (225, 248, 249, 352, 541), and in other cases, the absorptions are not characteristic of Fe^{II} or Fe^{III} species and very broad lines are observed. Yet, for interesting Co compounds such as vitamin B_{12} and Co^{II} phthalocyanine (422, 423), the spectra are characteristic of Fe^{II} with apparently very little, if any, fragmentation. The potential uses and advantages of such emission spectra have been discussed (423).

F. FROZEN SOLUTION STUDIES

The Mössbauer effect cannot be observed in a liquid, but Mössbauer spectra of glasses and smectic liquid crystals have been observed. Thus,

it is possible to obtain valuable information on the structure of a molecule in solution, or the structure of the solvent, by taking a spectrum of a glass at, for example, 80°K. There are, however, several difficulties which should be emphasized. First, one is often not sure whether a true glass has been obtained, or whether the solid has crystallized. Microcrystalline domains are very difficult to detect. Second, it is sometimes possible that the solvent may coordinate to the Mössbauer atom in unexpected situations. For example, Sn often coordinates to solvent molecules which are normally very "weak" ligands. In other cases, Mössbauer spectra are used to study solvent coordination. Mössbauer spectra of five-coordinate bis(*N,N*-diethyldithiocarbamato)iron(III) chloride $[\text{Fe}(\text{dte})_2\text{Cl}]$ and related compounds show a large Q.S. of about 2.7 mm/sec in the solid state, but a Q.S. value of about 0.8 mm/sec in solvents such as dimethylformamide (178). By contrast the six-coordinate $\text{Fe}(\text{dte})_3$ compound gives a small Q.S. of about 0.6 mm/sec both in solution and solid. These results, and other spectroscopic evidence, strongly indicate that the coordination about the Fe^{III} changes from five in the solid to six in solution.

Solution Mössbauer spectra of Sn compounds of the type $\text{R}'\text{SnR}_3$ ($\text{R} = \text{C}_2\text{H}_5, \text{C}_6\text{H}_5$; $\text{R}' = 4\text{-thiopyridone, thiophenol}$) have also been very helpful in determining the coordination number about the Sn atom—both in solid and solution (424).

In an interesting Mössbauer study of the pH dependence of the species in an aqueous solution of $\text{NH}_4\text{Fe}^{\text{III}}\text{EDTA}$ (15), the Mössbauer spectrum changes markedly from pH 6.8 to 3.9. By comparison with solid spectra, the species at pH 6.8 and 3.9 have been assigned to $[\text{Fe}^{\text{III}}(\text{EDTA}(\text{OH}))]^{2-}$ and $\text{Fe}^{\text{III}}(\text{EDTA})^-$, respectively.

In other studies, the use of frozen solution spectra has not provided as much useful information. In a study of $[\pi\text{-C}_5\text{H}_5\text{Fe}(\text{CO})_2]\text{SnCl}_3$ and related compounds (331), reasonably conclusive evidence was not obtained as to whether the short Fe–Sn bond was due to intermolecular stacking forces or the specific nature of the chemical bonds. In another area, $\text{Fe}_3(\text{CO})_{12}$ supposedly has a different structure in solution than in the solid (461), but recent attempts to observe a different spectrum in solution than in the solid have not met with success (38).

A number of workers have studied the temperature dependence of the recoil free fraction of Fe^{2+} doped water (100, 180, 425, 447) and methanol (515). Here the Fe^{2+} ions are used as a probe to study the change in frozen solvent properties over a range of temperature. In all cases, the f value drops off sharply, and sometimes approaches zero at a point variously ascribed to a cubic-hexagonal phase change in ice (180, 425), a two-phase model, with the ferrous ions associated with a glassy

or amorphous variety of ice (447), and a transition from a rigid glass to a supercooled state (515). Recent results (100) on Fe^{2+} ions in the cubic phase of ice indicate that the Fe^{2+} ions are unaffected by this phase and that the Fe^{2+} ions are associated with the glassy fraction of the absorber.

IV. Bonding and Structure

A. Sn^{IV} COMPOUNDS

1. *Quadrupole Splittings*

Until very recently, two major problems have hindered any systematic interpretation of Sn^{IV} quadrupole splittings. First, there has been considerable debate as to the origin of the EFG, i.e., whether π -bonding asymmetries, σ -bonding asymmetries, or q_{lat} effects are predominantly responsible for the observed quadrupole splittings. Second, the influence of changing coordination number on the magnitude of the quadrupole splitting was not known, mainly because sufficient structural data was not available. The effect of structure on quadrupole splittings is of particular interest, as many compounds with a four-coordinate stoichiometry do, in fact, possess associated structures in the solid state, involving five- and six-coordinate tin atoms. In this section we shall first deal with the origins of the quadrupole splittings of tin(IV) compounds and then consider in detail the correlation between quadrupole splitting and structure. In the first part of the discussion, it will be necessary to make some structural assumptions, which will be justified later.

In the following discussion we will employ the general symbols R and X to denote an organic group or an electron-withdrawing ligand, respectively. This convention will also be used in Section IV, A, 2.

a. *σ or π Bonding?* Early ^{119}Sn Mössbauer work (5, 6, 8, 9, 84, 138, 279) revealed large quadrupole splittings (in the range 2–4 mm/sec) for a wide variety of substituted organotin compounds of the type $\text{R}_n\text{SnX}_{4-n}$ ($n = 1-3$) with $\text{X} = \text{F}, \text{Cl}, \text{Br}, \text{I}, \text{O}$, and S . It was suggested (6, 138) that the EFG's in these compounds were produced by differences in the polarities of the tin–ligand σ bonds, which could give rise to both a q_{lat} and a q_{val} contribution to the EFG [Eqs. (7) and (9)]. Later work revealed that the compounds $(\text{Ph}_3\text{Sn})_2$ (269), $(\text{Ph}_3\text{Sn})_4\text{M}$ ($\text{M} = \text{Sn}, \text{Ge}, \text{Pb}$) (269), Ph_3SnX ($\text{X} = \text{H}, \text{Li}$) (9), $\text{R}_n\text{SnH}_{4-n}$ ($n = 1-3$, $\text{R} = \text{Me}, \text{Bu}, \text{Ph}$) (9, 334), and Me_3SnNa (141) showed no resolvable quadrupole splitting. If the difference in electronegativity between the donor atoms of the ligands ($\Delta\chi$) is used as a criterion of differences in bond polarity (138, 269), then from Table XVI it is clear that $\Delta\chi$ values for compounds which show quadrupole splitting are in the same range as those for which single-line

spectra are observed (269). From this observation it was suggested (269) that EFG's produced by inequalities in the tin-ligand σ bonds were too small to result in resolvable quadrupole splitting and that some other factor was responsible for the observed quadrupole splittings for organotin halides and chalcogenides.

Gibb and Greenwood noted (269) that quadrupole splitting seemed to be confined to those organotin compounds in which the X ligand contained nonbonding lone-pair electrons. This observation led to the

TABLE XVI
ELECTRONEGATIVITY DIFFERENCES, $\Delta\Psi$, BETWEEN CARBON
AND OTHER ELEMENTS^a

No quadrupole splitting		Quadrupole splitting	
Element	$\Delta\Psi_L^b$	Element	$\Delta\Psi_L^b$
H	-0.30	F	+1.60
Li	-1.53	Cl	+0.33
Ge	-0.48	Br	+0.24
Sn	-0.78	I	-0.29
Pb	-0.95	O	+1.00
		S	-0.06
		N	+0.57

^a Allred Rochow values from F. A. Cotton and G. Wilkinson, "Advanced Inorganic Chemistry," 2nd ed., p. 103. Wiley (Interscience), New York, 1966.

^b $\Delta\Psi_L = \Psi_L - \Psi_C$.

suggestion that these lone-pair electrons formed dative $p_\pi \rightarrow d_\pi$ (269) or $p_\pi \rightarrow p_\pi$ (334) bonds with the empty $5d$ and $6p$ orbitals of the tin atom and that this asymmetric introduction of π -electron density was responsible for the observed quadrupole splittings. A similar explanation was proposed to account for the quadrupole splitting trends of a range of six-coordinate tin species (300). The data available for these compounds at that time are summarized in Table XVII, and it can be seen that although organotin complexes show large quadrupole splittings, in the absence of a tin-carbon bond, no quadrupole splittings could be observed, even when there is a noncubic arrangement of the ligands. It was proposed (300) that for compounds in which all six atoms directly bonded to the Sn atom have filled nonbonding shells available for π bonding, the σ -bonding asymmetries are insufficient to give quadrupole splitting.

However, for organotin derivatives, the lack of π bonding in the Sn-R bond results in a large degree of π -electron asymmetry and, hence, in large quadrupole splitting.

Parish and Platt (440) have presented data for a series of substituted four-coordinate organotin compounds of the type R_3SnX (in which $R=Me$ or Ph and $X = C_6F_5$, C_6Cl_5 , $C\equiv CPh$, $CH=CH_2$, and $CCl=CCl_2$) for which the observed quadrupole splitting trends are incompatible with

TABLE XVII

SELECTION OF EARLY MÖSSBAUER DATA FOR SIX-COORDINATE Sn^{IV} COMPLEXES^a

Code No. ^b	Compound	C.S. ^{c,d}	Q.S. ^c	I^e	Refs.
1	$SnCl_4bipy$	0.42	—	1.31	(300)
2	$SnBr_4bipy$	0.66	—	1.17	(300)
3	SnI_4bipy	0.95	—	1.42	(300)
4	$SnCl_4(en)_2$	0.50	—	—	(278)
5	$SnBr_4(en)_2$	0.43	—	—	(278)
6	$SnCl_4(py)_2$	0.00	—	—	(278)
7	$SnCl_4(oxH)_2$	0.45	—	1.22	(300)
8	$SnCl_4[(NH_2)_2CS]_2$	0.95	—	—	(278)
9	$SnBr_4[(NH_2)_2CS]_2$	0.80	—	—	(278)
10	$SnCl_2(ox)_2$	0.30	—	1.50	(300)
11	$SnCl_2(acac)_2$	0.25	—	1.15	(300)
12	$Me_2Sn(ox)_2$	0.85	1.93	1.05, 1.21	(300)
13	$Me_2Sn(H_2O)_nOH^+$	1.37	3.90	1.31, 1.50	(300)

^a More data for similar compounds may be found in Refs. (300) and (278)

^b Code number will be preceded by table number in text.

^c Data in mm/sec at liquid N_2 temperature.

^d Relative to SnO_2 , values from Ref. (278) converted assuming the center shift of Sn = 2.70.

^e Full width at half height; data taken with SnO_2 source.

the π -bonding theory of quadrupole splitting, but which are fully consistent with a σ -bonding interpretation. Sams *et al.* (114, 115, 150) have reported further data for halogen-substituted organotin phenyl, vinyl, and acetylene derivatives which confirm and further clarify the dependence of quadrupole splitting on σ -bond polarities. Data for these types of compounds are collected in Table XVIII.

The compounds $Me_3SnC_nF_{2n+1}$ ($n = 1-3$) (Table XVIII, compounds 5-7) contain no lone-pair electrons suitable for π bonding and, hence, the only type of π interaction which is possible is hyperconjugation. In contrast, the polarity of the tin-fluorocarbon bond is expected to be

TABLE XVIII

MÖSSBAUER DATA FOR SOME TETRAHEDRAL ORGANOTIN (IV) COMPOUNDS

Code No. ^a	Compound	C.S. ^{a,b}	Q.S. ^a	Ref.
1	Me ₄ Sn	1.31	—	(516)
2	Et ₃ SnCH ₂ X ^c	1.29–1.43	—	(368)
3	Me ₃ SnCH ₂ X ^d	1.32–1.38	—	(368)
4	Me ₃ SnCHF ₂	1.28	0.94	(150)
5	Me ₃ SnCF ₃	1.31	1.48	(150, 440)
6	Me ₃ SnCF ₂ CF ₃	1.30	1.63	(150)
7	Me ₃ SnCF(CF ₃) ₂	1.32	1.89	(150)
8	Me ₃ SnCH(CF ₃) ₂	1.30	1.57	(150)
9	Me ₃ SnCH=CH ₂	1.30	—	(9)
10	Me ₃ SnCCl=CCl ₂	1.31	1.24	(440)
11	Me ₃ SnCF=CF ₂	1.30	1.41	(150)
12	Ph ₃ SnCH=CH ₂	1.28	—	(440)
13	PhSn(CH=CH ₂) ₃	1.25	—	(440)
14	Me ₃ SnC≡C·CHMe ₂	1.15	1.06	(494)
15	Me ₃ SnC≡CPh	1.22	1.29	(65, 440, 494)
16	Me ₃ SnC≡C·C=CEt	1.20	1.80	(494)
17	Me ₃ SnC≡CCF ₃	1.25	1.77	(150)
18	Me ₂ Sn(C≡CCF ₃) ₂	1.19	1.95	(150)
19	Et ₃ SnC≡CH	1.44	1.42	(456, 494)
20	Et ₃ SnC≡CMe	1.37	1.22	(456, 494)
21	Et ₃ SnC≡CEt	1.35	1.05	(456, 494)
22	Et ₃ SnC≡C·CHMe ₂	1.36	1.09	(494)
23	Et ₃ SnC≡C $\left(\begin{array}{c} \text{CH}-\text{CH}_2 \\ \diagdown \quad \diagup \\ \text{CH}_2 \end{array} \right)$	1.38	1.25	(494)
24	Et ₃ SnC≡CPh	1.38	1.48	(456, 494)
25	Et ₃ SnC≡CCl	1.39	1.75	(456, 494)
26	Et ₃ SnC≡CBr	1.40	1.70	(494)
27	Et ₃ SnC≡C·P(O)(OEt) ₂	1.42	2.40	(456, 494)
28	Et ₃ SnC≡C·SnEt ₃	1.38	1.18	(494)
29	Pr ₃ SnC≡CH	1.42	1.37	(494)
30	Pr ₂ Sn(C≡CPr) ₂	1.27	1.60	(494)
31	Bu ₃ SnC≡CH	1.40	1.42	(456, 494)
32	BuSn(C≡CPh) ₃	0.81	1.72	(440)
33	Me ₃ SnPh	1.21	—	(9, 141)
34	MeSnPh ₃	1.19	—	(367)
35	1-R ₃ Sn·C ₆ H ₄ ·X·4 ^e	1.16–1.43	0–0.48	(115, 141, 554)
36	1-Me ₃ Sn·C ₆ H ₄ ·R·x ^f	1.18–1.24	—	(115)
37	1,2-(Me ₃ Sn) ₂ C ₆ Ph ₄	1.25	—	(115)

TABLE XVIII—*continued*

Code No. ^a	Compound	C.S. ^{a,b}	Q.S. ^a	Ref.
38	1-Me ₃ Sn·C ₆ H ₄ ·I·2	1.18	—	(115)
39	1-Me ₃ Sn·C ₆ Ph ₄ ·I·2	1.21	0.74	(115)
40	1-Me ₃ Sn·C ₆ H ₄ ·CF ₃ ·2	1.21	0.66	(115)
41	1- <i>n</i> -Bu ₃ SnC ₆ H ₄ ·CF ₃ ·2	1.37	0.77	(115)
42	Me ₃ SnC ₆ Cl ₅	1.32	1.09	(440)
43	1-Me ₃ SnC ₆ Cl ₄ ·H·2	1.24	0.83	(115)
44	1,2-(Me ₃ Sn) ₂ C ₆ Cl ₄	1.25	0.78	(115)
45	1,4-(Me ₃ Sn) ₂ C ₆ Cl ₄	1.26	1.10	(115)
46	Me ₃ SnC ₆ F ₅	1.27	1.31	(440)
47	1,2-(Me ₃ Sn) ₂ C ₆ F ₄	1.26	0.85	(115)
48	1,4-(Me ₃ Sn) ₂ C ₆ F ₄	1.20	1.20	(115)
49	1-Me ₃ Sn·C ₆ F ₄ ·H·4	1.24	1.08	(115)
50	Me ₂ Sn(C ₆ F ₅) ₂	1.25	1.51	(115, 440, 528)
51	1-Me ₂ Sn(C ₆ F ₅ ·Br·2) ₂	1.25	1.41	(115)
52	MeSn(C ₆ F ₅) ₃	1.19	1.14	(528)
53	1-Ph ₃ Sn·C ₆ H ₄ ·X·4 ^g	1.30	—	(368)
54	1-Ph ₃ Sn·C ₆ H ₄ ·Me·2	1.30	—	(368)
55	Ph ₃ SnC ₆ Cl ₅	1.27	0.84	(440)
56	Ph ₂ Sn(C ₆ Cl ₅) ₂	1.43	1.14	(140, 440)
57	PhSn(C ₆ Cl ₅) ₃	1.11	0.80	(140)
58	Ph ₃ SnC ₆ F ₅	1.28	0.99	(138, 440, 528)
59	Ph ₂ Sn(C ₆ F ₅) ₂	1.22	1.11	(528)
60	PhSn(C ₆ F ₅) ₃	1.16	0.92	(528)
61	(4-Me·C ₆ H ₄) ₂ Sn(C ₆ F ₅) ₂	1.22	1.18	(528)
62	(4-Me·C ₆ H ₄)Sn(C ₆ F ₅) ₃	1.18	1.02	(528)
63	Me ₃ SnC ₅ H ₅	1.05	1.20	(317)
64	Me ₃ SnCH ₂ C ₆ H ₅ [Cr(CO) ₃]	1.67	0.59	(460)
65	Me ₂ (Ph)SnPh[Cr(CO) ₃]	1.74	0.64	(460)
66	(4-Me ₃ Sn) ₂ C ₆ H ₄ Cr(CO) ₃	1.69	0.72	(460)
67	Me ₃ SnPhCr(CO) ₃	1.67	0.72	(460)
68	Me ₃ SnPhMo(CO) ₃	1.43	0.84	(460)
69	Me ₂ Sn[C ₆ H ₅ Cr(CO) ₃] ₂	1.75	0.89	(460)

^a Code number will be preceded by table number in text. Data given in mm/sec at liquid nitrogen temperature; when appropriate an unweighted average has been taken.

^b Relative to SnO₂, assuming an identical shift for BaSnO₃, and a shift of 2.1 mm/sec for α-tin.

^c Range of data for X = Cl, OMe, NMe₂, CN, or pyridine.

^d Range of data for X = F, Cl, OMe, NMe₂, or pyridine.

^e Range of data for R = Me or Et, X = F, Cl, OMe, NMe₂, *t*-Bu, Me.

^f R = Me, Ph, *x* = 2, 3.

^g X = Me, Cl, Br.

much greater than the tin-methyl bond. For example, the Taft σ^* constants (535) of substituents (X), which give a measure of the polarities of the C-X bonds, should provide a reasonable guide to the relative polarities of the Sn-X bonds. The Taft σ^* constants of CF_3 (2.58) and Me (0.00) indicate considerable inequalities in the polarities of the tin σ bonds in Me_3SnCF_3 . The compounds $\text{Me}_3\text{SnCH}_2\text{F}$, $\text{Me}_3\text{SnCHF}_2$, and Me_3SnCF_3 show (150) a trend toward increasing quadrupole splitting with successive fluorine substitution as expected from a σ -bonding interpretation. Further, the order of quadrupole splittings $\text{Me}_3\text{SnCF}(\text{CF}_3)_2 > \text{Me}_3\text{SnC}_2\text{F}_5 > \text{Me}_3\text{SnCF}_3$ parallels the effective electronegativities of the fluorocarbon groups (150) as calculated from NMR data (151), although it is surprising that the compound $\text{Me}_3\text{SnCH}(\text{CF}_3)_2$ has such a large quadrupole splitting.

Of the compounds $\text{Me}_n\text{SnPh}_{4-n}$ ($n = 1, 3$; Table XVIII, compounds 33 and 34) $\text{R}_n\text{Sn}(\text{CH}=\text{CH}_2)_{4-n}$ ($n = 1, 3$; Table XVIII, compounds 9, 12, 13) and $\text{R}_n\text{Sn}(\text{C}\equiv\text{C}-\text{R}')_{4-n}$ ($n = 1-3$; Table XVIII, compounds 14-16, 19-24, etc.), only the acetylene derivatives show quadrupole splitting even though phenyl, vinyl, and acetylene groups have $p\pi$ electrons suitable for π bonding. The evidence for the existence of π bonding in these systems is not conclusive (18), and there is certainly no indication that tin-alkynyl bonds have a greater π -bond order than tin-phenyl or tin-vinyl bonds. However, it is generally recognized that sp hybridized carbon atoms are considerably more electron-withdrawing than sp^2 hybridized carbon atoms as shown, for example, by the Taft σ^* constants of 1.35 for a $\text{C}\equiv\text{CR}$ group compared with 0.36 and 0.6 for vinyl and phenyl groups, respectively. These data strongly indicate that the quadrupole splitting in the alkynyl derivatives is produced by the polarity of the tin-alkynyl bond. Similarly, the acidic cyclopentadienyl group produces a small quadrupole splitting in $\text{Me}_3\text{SnC}_5\text{H}_5$ (Table XVIII, compound 63).

The substitution of fluorine or chlorine atoms into the phenyl or vinyl group produces quadrupole splitting. It would be anticipated that the electron-withdrawing fluorine and chlorine atoms would increase the electron-withdrawing power of the phenyl or vinyl group and, thus, increase the polarity of the tin-phenyl and tin-vinyl bond. This expectation is confirmed by dipole moment data (346), which show that for the compounds $\text{Me}_3\text{Sn}\cdot\text{C}_6\text{H}_4\cdot p\text{-X}$ ($\text{X} = \text{F}, \text{Cl}, \text{Br}$), the Me_3Sn group is electron-releasing with respect to the ring. These data, therefore, provide further strong evidence for a σ -orbital imbalance interpretation of quadrupole splitting which is also supported by the observation (114, 115, 440) that the quadrupole splittings of chlorocarbon compounds are invariably lower than those of their fluorocarbon analogs; for example,

compare the pairs of compounds in Table XVIII: 42 and 46, 44 and 47, 45 and 48, 55 and 58, 56 and 59, 57 and 60, 10 and 11. A suggestion (528) that the quadrupole splittings of fluorocarbon derivatives may arise from π -bonding effects is not consistent with NMR evidence (342) which shows no donation of π electrons to the tin atom in $\text{Me}_3\text{SnC}_6\text{F}_5$. It is also interesting that the coordination of a $\text{Cr}(\text{CO})_3$ or $\text{Mo}(\text{CO})_3$ group to the phenyl ring of the species $\text{Me}_3\text{SnCH}_2\text{Ph}$, Me_2SnPh_2 , $(1,4\text{-Me}_3\text{Sn})_2\text{C}_6\text{H}_4$, or Me_3SnPh (Table XVIII, compounds 64–67) results in a small quadrupole splitting, probably owing to the increased polarity of the tin–phenyl bond (460).

In the series of acetylene derivatives $\text{R}_3\text{SnC}\equiv\text{C-X}$ (Table XVIII, compounds 14–26 and 28–31), the largest quadrupole splittings are found for those compounds in which X is an electron-withdrawing halogen atom or CF_3 group. The series of triethyltin derivatives (Table XVIII, compounds 19–26 and 28) also show (494) good correlations with dipole moment and the inductive, σ^* , (576) and inductive plus mesomeric, σ_n , (576) constants of the X group.

The data discussed above are clearly fully consistent with a σ -bonding interpretation of quadrupole splitting, but provide no indication of π -bonding effects. It was, therefore, suggested (440) that the quadrupole splittings of tin(IV) compounds *in general* arise from a σ -orbital imbalance owing to inequalities in bond polarities. A similar conclusion was reached by Drago *et al.* (338).

In attempting to make a general assessment of the dependence of quadrupole splitting on the nature of the tin–ligand bonds, it is important to realize that the major variations of quadrupole splitting which are observed arise from structural rather than bonding changes (*vide infra*) (Table XIX). Variations in quadrupole splittings which can be attributed to differences in bond character will only be revealed in the quadrupole splittings of isostructural series, such as the tetrahedral compounds discussed above. For example, it has been shown (*vide infra*) that triethyl- and trimethyltin halides are probably isostructural with associated five-coordinate structures, whereas the triphenyl- and trineophyltin halides (with the exception of Ph_3SnF) have monomeric structures with tetrahedral coordination of the tin atom. Data for these compounds are contained in Table XX. Although the four- and five-coordinate species have very different quadrupole splittings due to the structural differences, both series of compounds show a small variation of quadrupole splitting with bond polarity as illustrated by the straight-line relationship between quadrupole splitting and Taft σ^* (400, 440). Further, the lowering of the quadrupole splittings of the triphenyl compared with the trineophyl derivatives is consistent with the greater

polarity of the tin-phenyl bond. For other series of five- or six-coordinate compounds, quadrupole splitting changes are small. For example in the series of five-coordinate compounds in Table XXXVI, variations are difficult to interpret in terms of bond polarities. In cases when significant variations are observed, for example, the five-coordinate carboxylate species $\text{Me}_3\text{SnO}_2\text{CR}'$ ($\text{R}' = \text{CH}_2\text{X}$, CX_3 , $\text{X} = \text{F}$, Cl , Br , I) (170, 459) and the six-coordinate complexes $\text{Ph}_2\text{SnX}_2\text{bipy}$ (465) and $\text{Bu}_2\text{SnX}_2 \cdot \text{phen}$ ($\text{X} = \text{Cl}$, Br , I) (417), the trends are usually those expected from a σ -bonding interpretation.

TABLE XIX
RANGES OF QUADRUPOLE SPLITTINGS FOR COMPOUNDS WITH
DIFFERING STRUCTURES^a

Structural type	Range of quadrupole splitting ^b
Tetrahedral $\text{R}_n\text{SnX}_{4-n}$ ($n = 1-3$)	0.00-2.31
Octahedral R_5SnX_5	1.92
Octahedral <i>cis</i> - R_2SnX_4	1.63-2.34
Trigonal-bipyramidal R_3SnX_2 (X axial)	2.76-3.86
Octahedral <i>trans</i> - R_2SnX_4	3.37-4.32

^a Summary of data considered in Refs. (234) and (440), in which papers full details of data with references are given.

^b Data given in mm/sec at liquid nitrogen temperature.

From the above discussion, it is clear that although there is much positive evidence that quadrupole splittings are produced by σ -bonding inequalities, there is little or no evidence for a significant contribution from π -bonding effects. This is not unexpected as, from the dependence of q_{val} on $\langle r^{-3} \rangle$ (Section II, D), asymmetries in the population of the $5d$ orbitals will make a much smaller contribution to q_{val} than an equivalent asymmetry in the $5p$ electron density (122, 141). Calculations of the relative $\langle r^{-3} \rangle$ values of $5p$ and $5d$ orbitals show that the ratio $\langle r^{-3} \rangle_{5d} : \langle r^{-3} \rangle_{5p}$ is of the order 0.01, and this has been confirmed by comparison of the relative quadrupole splittings of octahedral and tetrahedral compounds (*vide infra*). Hence, even if a significant degree of π bonding is present in the tin-ligand bonds, this will be expected to have a minimal effect on the quadrupole splitting.

It is now worthwhile to reexamine the data which led to the postulation of π -bonding effects, i.e., the lack of quadrupole splitting in the

TABLE XX
MÖSSBAUER DATA FOR TRIALKYL- AND TRIPHENYLTIN HALIDES^a

R	R ₃ SnF		R ₃ SnCl		R ₃ SnBr		R ₃ SnI		M[R ₃ SnCl ₂]		M[R ₃ SnBr ₂]	
	C.S. ^{b,c}	Q.S. ^b	C.S. ^{b,c}	Q.S. ^b	C.S. ^{b,c}	Q.S. ^b	C.S. ^{b,c}	Q.S. ^b	C.S. ^{b,c}	Q.S. ^b	C.S. ^{b,c}	Q.S. ^b
Me	1.26 ^d	3.82 ^d	1.42 ^d	3.44 ^d	1.45 ^d	3.40 ^d	1.49 ^d	3.10 ^d	1.33 ^{j,k}	3.28 ^{j,k}	1.43 ^{j,l}	3.45 ^{j,l}
Et	1.48 ^e	3.94 ^e	1.60 ^e	3.70 ^e	1.61 ^e	3.29 ^e	1.56 ^e	3.05 ^e	1.50 ^{l,m}	3.44 ^{l,m}	—	—
<i>n</i> -Pr	1.46 ^f	4.01 ^f	1.62 ^f	3.66 ^f	1.66 ^f	3.52 ^f	1.59 ^f	2.90 ^f	—	—	—	—
<i>n</i> -Bu	1.34 ^f	3.73 ^f	1.46 ^f	3.48 ^f	1.44 ^f	3.29 ^f	1.43 ^f	2.63 ^f	—	—	—	—
<i>i</i> -Bu	1.47 ^f	3.82 ^f	1.61 ^f	3.36 ^f	1.60 ^f	3.20 ^f	1.63 ^f	2.73 ^f	—	—	—	—
Neo ^h	1.33 ^g	2.79 ^g	1.39 ^g	2.65 ^g	1.42 ^g	2.65 ^g	1.41 ^g	2.40 ^g	—	—	—	—
Ph	1.22 ⁱ	3.58 ⁱ	1.34 ⁱ	2.54 ⁱ	1.29 ⁱ	2.50 ⁱ	1.20 ⁱ	2.15 ⁱ	1.32 ^{l,n} 1.23 ^o	3.00 ^{l,n} 2.87 ^o	1.29 ^o	2.88 ^o

^a Data have been selected from references reporting full series of compounds. Other data for these and related compounds may be found in Ref. (516).

^b Data in mm/sec at liquid nitrogen temperature assuming a shift of 2.1 mm/sec for α -tin.

^c Relative to SnO₂.

^d An average of data from Refs. (141), (258).

^e An average of data from Refs. (176, 258, 442).

^f An average of data from Refs. (176, 258).

^g Reference (336).

^h Neo = Me₂(Ph)CCH₂-.

ⁱ An average of data from Refs. (258, 442).

^j M = (Et₄N)⁺.

^k An average of data from Refs. (440, 442).

^l Reference (442).

^m M = (Ph₃CCH₂Ph)⁺.

ⁿ M = (Me₄N)⁺.

^o Reference (207). M = (Ph₃PC₁₀H₂₁)⁺.

compounds $(\text{Ph}_3\text{Sn})_2$, $(\text{Ph}_3\text{Sn})_4\text{M}$ ($\text{M} = \text{Sn}, \text{Ge}, \text{Pb}$), Ph_3SnX ($\text{X} = \text{H}, \text{Li}$), $\text{R}_n\text{SnH}_{4-n}$ ($n = 1-3$, $\text{R} = \text{Me}, \text{Bu}, \text{Ph}$), Me_3SnNa , SnX_4Y_2 , and SnX_2Y_4 . The original observation (278, 300) of zero quadrupole splittings for all SnX_4Y_2 and SnX_2Y_4 species, in which X is a halogen atom and Y is an electronegative donor ligand, has been superseded by more recent data. Quadrupole splittings have been reported for many SnX_4Y_2 compounds in which both X and Y have π -donor electrons (see data in Table XXXVII) and it has also been observed that some compounds in which the Y group has no suitable π electrons [e.g. $\text{SnCl}_4 \cdot \text{en}$ (457) and $\text{SnCl}_4 \cdot [\text{Ph}_2\text{P} \cdot (\text{CH}_2)_2 \cdot \text{PPh}_2]$ (103)] give only small or zero quadrupole splitting. The differences in the bond polarity for organotin hydrides are not expected to be large, as illustrated by the Taft σ^* constants of Me(0.00) and H(0.49) and molecular orbital calculations for Me_3SnH (299); the lack of quadrupole splitting for the compounds is, therefore, not unexpected. Similarly, large variations in bond polarity could not be expected for the $\text{Sn}-\text{M}$ ($\text{M} = \text{C}, \text{Si}, \text{Ge}, \text{Sn}, \text{Pb}$) bonds and recent work (65) has shown some evidence of unresolved quadrupole splitting in the species $\text{R}_3\text{Sn}-\text{MR}_3$ ($\text{R} = \text{Me}$ or Ph , $\text{M} = \text{C}, \text{Si}, \text{Ge}$, or Sn), which is at a maximum for $\text{M} = \text{Sn}$. Finally it is difficult to evaluate the significance of the reported data for Ph_3SnLi and Me_3SnNa , as these compounds do not exist in the solid state (558), and Goldanskii (57) has shown that frozen solution spectra vary markedly with solvent.

b. Influence of Coordination Number and Structural Determination.

Tin(IV) compounds are found with a wide variety of structures including four-, five-, and six-coordinate tin atoms. Many compounds with a nominally tetrahedral stoichiometry have associated solid state structures involving five- or six-coordinate tin atoms. For example, X-ray diffraction studies of Me_3SnX [$\text{X} = \text{F}$ (122), CN (506), OH (366), or NCS (243)] show polymeric structures with five-coordination of the tin atom, whereas Me_2SnF_2 (507) has a polymeric structure with trans-octahedral coordination of the tin atom. The quadrupole splitting observed in the Mössbauer spectra of tin(IV) compounds provide a very powerful means of studying these structural variations.

The first attempt to correlate quadrupole splitting with structure was made by Herber *et al.* (336), who noted that R_3SnX and R_2SnX_2 compounds which probably have associated structures (e.g., Me_2SnF_2 , Me_3SnOH , $\text{Me}_3\text{Sn-imidazole}$) appeared to give larger quadrupole splitting than other R_3SnX and R_2SnX_2 species. A parameter ρ (defined as the quadrupole splitting divided by the center shift relative to SnO_2) was introduced, and it was postulated that R_3SnX and R_2SnX_2 compounds for which ρ was greater than 2.1 had associated structures.

Later the additivity model, using a point charge formalism, was used

TABLE XXI

QUADRUPOLE SPLITTING DATA FOR SOME ORGANOTIN HALIDES
AND HALIDE ANIONS

Compound	V_{zz}/e^a	Q.S.(obs.) ^b	Ref.	Q.S.(cal.) ^{b,c}
$K_2[R_2SnF_4]^d$	$4[R]^{oct} - 4[F]^{oct}$	4.28 ^d	(442)	4.16
$M_2[R_2SnCl_4]^e$	$4[R]^{oct} - 4[Cl]^{oct}$	4.21 ^e	(234, 442)	3.76
$Cs_2[Me_2SnBr_4]$	$4[R]^{oct} - 4[Br]^{oct}$	4.22	(442)	3.64
$(pyH)_2[Ph_2SnCl_4]^f$	$4[Ph]^{oct} - 4[Cl]^{oct}$	3.80	(234)	3.32
$M_2[R_2SnCl_5]^f$	$2[R]^{oct} - 2[Cl]^{oct}$	1.90 ^f	<i>f</i>	1.88
$(pyH)_2[PhSnCl_5]$	$2[Ph]^{oct} - 2[Cl]^{oct}$	1.92	(234)	1.66
$(R_3SnF)_n^g$	$4[F]^{tba} - 3[R]^{tbe}$	3.88 ^g	<i>g</i>	<i>h</i>
$(R_3SnCl)_n^g$	$4[Cl]^{tba} - 3[R]^{tbe}$	3.57 ^g	<i>g</i>	<i>h</i>
$(R_3SnBr)_n^g$	$4[Br]^{tba} - 3[R]^{tbe}$	3.35 ^g	<i>g</i>	<i>h</i>
$(R_3SnI)_n^g$	$4[I]^{tba} - 3[R]^{tbe}$	3.08 ^g	<i>g</i>	<i>h</i>
NeO_3SnF^j	$2[F]^{tet} - 2[R]^{tet}$	2.79	(336)	2.08
NeO_3SnCl	$2[Cl]^{tet} - 2[R]^{tet}$	2.65	(336)	1.88
NeO_3SnBr	$2[Br]^{tet} - 2[R]^{tet}$	2.65	(336)	1.82
NeO_3SnI	$2[I]^{tet} - 2[R]^{tet}$	2.40	(336)	1.68
Ph_3SnCl	$2[Cl]^{tet} - 2[Ph]^{tet}$	2.54 ⁱ	<i>i</i>	1.66
Ph_3SnBr	$2[Br]^{tet} - 2[Ph]^{tet}$	2.50 ⁱ	<i>i</i>	1.60
Ph_3SnI	$2[I]^{tet} - 2[Ph]^{tet}$	2.15 ⁱ	<i>i</i>	1.46

^a Taken from Table IV.^b Data given in mm/sec.^c Calculated using the point charge parameters from Ref. (442).^d Average of R = Me, Et.^e Average of R = Me, Et, M = Cs and R = Me, M = pyH.^f Average of R = Et, M = Me₄N (442) and R = Bu, M = Et₄N (171).^g Average of R = Me, Et; data taken from Table XX.^h Data used in calculation of point charge parameters.ⁱ Data taken from Table XX.^j PyH = pyridinium, Neo = Me₂CPhCH₂.

to assess the expected variation of quadrupole splitting with structure (234, 440). From Table XXI it can be seen that the relative quadrupole splittings calculated for organotin compounds fall into two main groups. Compounds with tetrahedral R_nSnX_{4-n} ($n = 1-3$) and octahedral R_2SnX_4 and *cis*- R_2SnX_4 structures should all have comparable quadrupole splittings, whereas compounds with *trans*- R_2SnX_4 and trigonal-bipyramidal R_3SnX_2 (X axial) coordination should have quadrupole splittings which are roughly twice as large. The data available at the time (Table XIX) for compounds whose structures are reasonably well established appeared to be in general agreement with this conclusion

as noted by Fitzsimmons *et al.* (234) for octahedral compounds and by Parish and Platt (440) for a more general range of compounds.

One important conclusion from these original additivity model calculations concerns the effect of intermolecular association on quadrupole splitting. Thus, the formation of associated structures for tri- and dialkyltin species involving trigonal-pyramidal R_3SnX_2 (X axial) and octahedral *trans*- R_2SnX_4 coordination of the tin atom, respectively, should result in a significant increase in quadrupole splitting compared with the unassociated forms. As center shifts of tri- and dialkyltin species generally fall into a rather narrow range, this increase in quadrupole splitting forms the basis of the correlation of ρ with structure. In contrast, an associated six-coordinate $RSnX_5$ structure for a monoalkyltin compound would be expected to show approximately the same quadrupole splitting as a monomeric tetrahedral species.

Although the data in Table XIX show that, at least in a general way, the additivity model provides a realistic description of quadrupole splitting trends, it has recently been shown (122) (see Section II, D) that strict adherence to the simple additivity model would not be expected for compounds with differing coordination numbers. However, before more detailed consideration can be given to the degree of precision with which the additivity model allows a prediction of quadrupole splitting values, it is necessary to describe some structural conclusions for trialkyltin halides, which have been reached with the aid of Mössbauer data.

Organotin fluorides are generally involatile insoluble solids in keeping with polymeric structures, observed crystallographically for Me_3SnF (118) and Me_2SnF_2 (507). In contrast, other organotin halides are low-melting solids or liquids and the observation (51, 123, 428) of two Sn-C stretching frequencies in both solid and solution has often been taken as evidence for monomeric tetrahedral structures. However, IR evidence is not unambiguous in that changes in the Sn-X stretching frequency for Me_3SnX (X = Cl, Br) in the solid melt and carbon disulfide solution indicate some degree of intermolecular association (379). By the same criterion, the triphenyltin halides Ph_3SnX (X = Cl, Br, I) do not seem to be associated (378). Mössbauer data for some trialkyl- and triaryl tin halides and some halide complexes are summarized in Table XX. Infrared data suggests that the complexes have trigonal-bipyramidal R_3SnX_2 structures (442).

The quadrupole splitting observed for Me_3SnF is large as expected from the trigonal-bipyramidal coordination of the tin atom. The quadrupole splittings of other trimethyltin halides are also large and show a regular decrease in quadrupole splitting with increasing size of

the halogen atom. Further, there is a close similarity in the quadrupole splittings of Me_3SnX ($\text{X} = \text{Cl}, \text{Br}$) and the corresponding halide anions $[\text{Me}_3\text{SnX}_2]^-$ ($\text{X} = \text{Cl}, \text{Br}$). As monomeric tetrahedral structures would be anticipated to give much lower quadrupole splittings, the data provide strong evidence that, like Me_3SnF , the compounds Me_3SnX ($\text{X} = \text{Cl}, \text{Br}, \text{I}$) are strongly associated with five-coordinate tin atoms (442). This has been confirmed in the case of Me_3SnCl , by an X-ray diffraction study (164). Quadrupole splittings for trialkyltin halides R_3SnX ($\text{R} = \text{Et}, n\text{-Pr}, n\text{-Bu}, i\text{-Bu}$; $\text{X} = \text{F}, \text{Cl}, \text{Br}, \text{I}$) are similar to those of their trimethyltin analogs indicative of similar polymeric structures. There is, however, a trend (128) to lower quadrupole splitting for R_3SnBr and R_3SnI species as the size of the alkyl group is increased from Et to $i\text{-Bu}$. This may be reflection of a weakening of the intermolecular association due to steric hindrance of the alkyl group.

The quadrupole splitting of triphenyltin fluoride is slightly lower than that of trimethyltin fluoride, consistent with a fully associated polymeric structure (442). The lowering of quadrupole splitting is probably due to the greater polarity of the tin-phenyl bond as illustrated by the relative quadrupole splittings of the anions $[\text{R}_3\text{SnCl}_2]^-$ ($\text{R} = \text{Me}, \text{Ph}$). In contrast, the quadrupole splittings of the triphenyltin halides Ph_3SnX ($\text{X} = \text{Cl}, \text{Br}, \text{I}$) are considerably lower than those of the fluoride and also less than that of the $[\text{Ph}_3\text{SnCl}_2]^-$ ion, indicating a reduction in the degree of intermolecular association (442). The trineophyltin halides also show much lower quadrupole splittings than the trimethyltin halides. In order to assign structures unambiguously to the compounds Ph_3SnX ($\text{X} = \text{Cl}, \text{Br}, \text{I}$) and Neo_3SnX ($\text{X} = \text{F}, \text{Cl}, \text{Br}, \text{I}$) it is necessary to compare the quadrupole splittings with that of a known tetrahedral organotin halide.

The crystal structure (131) of the compound $\text{Ph}_2\text{Sn(I)} \cdot [\text{CH}_2]_4 \cdot \text{Sn(I)Ph}_2$ shows a slightly distorted tetrahedral environment of the tin atoms with no close intermolecular Sn-I distances, and this compound can be regarded as a model tetrahedral compound. The quadrupole splitting of 2.37 mm/sec (400) observed for $\text{Ph}_2\text{Sn(I)} \cdot [\text{CH}_2]_4 \cdot \text{Sn(I)Ph}_2$ is closely similar to those found for Neo_3SnI and Ph_3SnI , and the relative quadrupole splittings of the three compounds are consistent with the differing number of tin-phenyl bonds. This observation, together with the good correlation observed between quadrupole splitting and Taft σ^* constant of the halogen atom, strongly suggests that the compounds R_3SnX ($\text{R} = \text{Neo}, \text{X} = \text{F}, \text{Cl}, \text{Br}, \text{I}$; $\text{R} = \text{Ph}, \text{X} = \text{Cl}, \text{Br}, \text{I}$) are isostructural with tetrahedral coordination of the tin atom. The lack of intermolecular association is probably due to the steric hindrance of the bulky neophyl and phenyl groups.

Ensling *et al.* (207) have recently suggested that the large difference in quadrupole splitting between Ph_3SnX ($\text{X} = \text{Cl}, \text{Br}$) and the four-coordinate species $\text{Ph}_3\text{Sn}(\text{S}_2\text{CNEt}_2)$ [$\Delta = 1.85 \text{ mm/sec}$ (207)] argues against a monomeric structure for the triphenyltin halides. However, this difference in quadrupole splitting is more probably due to the difference in bond polarity between the tin-halide and tin-sulfur bonds, as illustrated by the large difference in quadrupole splitting between the trans-octahedral species $[\text{Me}_2\text{SnX}_4]^{2-}$ [$\text{X} = \text{Cl}, \text{Br}, \Delta = \text{ca. } 4.1\text{--}4.2 \text{ mm/sec}$ (Table XXIV)] and $\text{Me}_2\text{Sn}(\text{S}_2\text{CNEt}_2)_2$ ($\Delta = 3.14 \text{ mm/sec}$) (Table XXIV). Indeed the relative quadrupole splittings of Ph_3SnX ($\text{X} = \text{Cl}, \text{Br}$) and $\text{Ph}_3\text{Sn}(\text{S}_2\text{CNEt})$ are in excellent agreement with the additivity model calculations (see Table XXIII), and a recent crystal structure determination of triphenyltin chloride has shown monomeric tetrahedral coordination of the tin atom (70).

The assignment of structures to the trialkyl- and triphenyltin halides makes possible a more rigorous investigation of the additivity description of quadrupole splitting. The compounds contained in Table XXI form a series of four-, five-, and six-coordinate tin species with closely similar ligands, and the appropriate additivity expressions for V_{zz} , written in terms of the $L^{\text{superscript}}$ parameters defined in Eqs. (29.1)–(29.4) are also included in Table XXI.

In the point charge formulation of the additivity model (440, 442), it is assumed that the parameters $[\text{L}]^{\text{oct}}$, $[\text{L}]^{\text{tet}}$, $[\text{L}]^{\text{tba}}$, and $[\text{L}]^{\text{tbe}}$ are identical. On this basis a series of partial quadrupole splitting parameters $(\text{p.q.s.})_{\text{L}}$, where $(\text{p.q.s.})_{\text{L}} = \frac{1}{2}e^2|Q|[\text{L}]$, has been calculated (442).^{*} The quadrupole splittings of the anions $[\text{SnCl}_5]^-$ (Δ in the range $0.46\text{--}0.77 \text{ mm/sec}$ (316, 442)) were used to obtain a value of $(\text{p.q.s.})_{\text{Cl}}$, while $(\text{p.q.s.})_{\text{R}}$ was calculated from the quadrupole splittings of the five-coordinate $(\text{R}_3\text{SnCl}_2)_n$ and $[\text{R}_3\text{SnCl}_2]^-$ ($\text{R} = \text{Me}, \text{Et}$) species. Values of $(\text{p.q.s.})_{\text{L}}$ for other ligands were obtained in a similar manner. Calculated quadrupole splittings obtained using these $(\text{p.q.s.})_{\text{L}}$ values are included in Table XXI. Clearly, although the overall trends of the quadrupole splitting patterns are reproduced, detailed numerical agreement is not obtained.

In Section II, D, it was shown using a simple molecular orbital model (122), that it is not a good approximation to describe octahedral, tetrahedral, trigonal-bipyramidal axial, and trigonal-bipyramidal equatorial bonds with the same $[\text{L}]$ values. It is probably the inadequacy of this approximation which gives rise to the discrepancies between the observed and calculated quadrupole splittings in Table XXI.

A more realistic application of the additivity model involves the

^{*} In Parish and Platt (442), the $(\text{p.q.s.})_{\text{L}}$ of a ligand L is given the symbol $[\text{L}]$.

calculation of separate partial quadrupole splitting parameters for each type of bond. Calculations of partial quadrupole splitting for octahedral and tetrahedral compounds have been described and these will be discussed below. Some discussion of the quadrupole splittings of five-coordinate compounds will also be given.

Before describing the derivation of $(p.q.s.)_L^{oct}$ and $(p.q.s.)_L^{tet}$ values, it is necessary to pay some attention to the signs of the quadrupole splittings. Using the additivity model, assuming a dominance of the valence contribution to the EFG, the sign of V_{zz} expected for any particular structure may be predicted. For example, consider a *trans*- R_2SnX_4 compound. Substitution of $[R]^{oct}$ and $[L]^{oct}$ into the appropriate equation in Table IV yields the expression

$$V_{zz} = \{4[R]^{oct} - 4[X]^{oct}\} e \quad (39)$$

Clearly, if X is more electron-withdrawing than R, then $\sigma_R^{oct} > \sigma_L^{oct}$, $-[R]^{oct} > -[X]^{oct}$ and, hence, V_{zz} is negative. In pictorial terms, the greater electron-withdrawing power of the X ligand produces a deficiency of negative charge in the XY plane and, hence, a negative value of V_{zz} . It is probable that the sign of the quadrupole moment for ^{119}Sn is negative (see Section IV, E) and, hence, the sign of $\frac{1}{2}e^2qQ$ ($\frac{1}{2}eQV_{zz}$) for a *trans*- R_2SnX_4 species is expected to be positive. In a similar manner, positive values of $\frac{1}{2}e^2qQ$ are predicted for R_5SnX and R_3SnX_3 species, while *cis*- R_2SnX_4 , R_3SnX_2 (X axial), and R_3SnX compounds would be expected to have negative signs (439).

The sign of $\frac{1}{2}e^2qQ$ may be determined by application of an external magnetic field, and the analysis of this type of spectra has been discussed by Gibb (265). The signs which have been reported (64, 217, 232, 288-291, 402, 439) are summarized in Table XXII. With the exception of *cis*- R_2SnX_4 species, which will be discussed in detail later, all the signs are in agreement with those expected from the additivity model, as noted by Parish and Johnson (439) for a general range of structures and by other groups (217, 232, 288, 290, 291) for more limited data. Goodman and Greenwood (290) have suggested that the negative sign observed for Ph_3SnCl indicates a polymeric five-coordinate structure rather than a monomeric tetrahedral configuration (400). In contrast, additivity calculations do not predict a change of sign of $\frac{1}{2}e^2qQ$ for R_3SnX and R_3SnX_2 (X axial) species, and this is confirmed by the experimental data in Table XXII and the recent crystal structure (70).

The positive signs of $\frac{1}{2}e^2qQ$ observed (288) for the compounds $[\pi\text{-cpFe(CO)}_2]_2SnX_2$ (X = Cl, NCS) are interesting as an idealized SnA_2B_2 system would be expected to have $\eta = 1$. However, η is very sensitive to small distortions (122) and the crystal structure of $[\pi\text{-cpFe(CO)}_2]_2SnCl_2$

TABLE XXII

SIGN $\frac{1}{2}e^2qQ$ OBSERVED FOR SOME TIN(IV) COMPOUNDS

Compound	Q.S. = $\frac{1}{2}e^2qQ^a$	Ref.
<i>trans</i> -R ₂ SnX ₄		
Me ₂ SnF ₂	+4.65	<i>b</i>
Me ₂ SnCl ₂ (pyo) ₂	+4.10	(232)
Cs ₂ [Me ₂ SnCl ₄]	+4.28	(439)
K ₂ [Me ₂ SnF ₄]	+4.12	(439)
Bu ₂ Sn maleate	+3.74	(439)
Me ₂ SnMoO ₄	+4.20 ^c	(289)
Me ₂ Sn(acac) ₂	+3.93 ^d	(217)
<i>n</i> -Pr ₂ SnCl ₂ 2β-pic ^e	+3.99	(291)
<i>n</i> -Pr ₂ SnCl ₂ 4-pic ^e	+3.42	(291)
<i>cis</i> -R ₂ SnX ₄		
Me ₂ Sn(oxin) ₂	+2.06	(439)
Ph ₂ Sn(oxin) ₂	+1.67	(439)
Ph ₂ Sn(S ₂ CNEt ₂) ₂	+1.72	(439)
Ph ₂ Sn(NCS) ₂ phen	+2.36	(439)
Ph ₂ SnCl ₂ (morph) ₄ ^f	+1.92	(291)
<i>n</i> -Pr ₂ SnCl ₂ (morph) ₂ ^f	+2.41	(291)
RSnX ₅		
<i>n</i> -PrSnCl ₃ (pip) ₂ ^g	+1.99	(291)
(Me ₄ N) ₂ [EtSnCl ₅]	+1.94	(439)
R ₃ SnX		
Me ₃ SnC ₆ F ₅	-1.39	(439)
Ph ₃ SnC ₆ F ₅	-0.97	(439)
Ph ₃ SnCl	-2.51 ^h	(290)
Ph ₂ Sn(I) · (CH ₂) ₄ · (I)SnPh ₂	-2.37 ⁱ	(400)
Bu ₃ Sn(π-cp)Fe(CO) ₂	-0.59	(288)
R ₂ SnX ₂ ^j		
[Mn(CO) ₅]MeSnCl ₂	+2.56	(288)
(π-cp)Fe(CO) ₂ SnCl ₂	+2.35	(288)
(π-cp)Fe(CO) ₂ Sn(NCS) ₂	+2.57	(288)
RSnX ₃ ^j		
Mn(CO) ₅ SnCl ₃	+1.58	(288)
(π-cp)Fe(CO) ₂ SnCl ₃	+1.77, 1.82	(288, 364)
R ₃ SnX ₂ (X axial) ^k		
(Me ₄ N)[Me ₃ SnCl ₂]	-3.31	(439)
(Ph ₃ PCH ₂ Ph)[Et ₃ SnCl ₂]	-3.49	(439)
(Me ₄ N)[Ph ₃ SnCl ₂]	-3.02	(439)

TABLE XXII—*continued*

Compound	Q.S. = $\frac{1}{2}e^2qQ^a$	Ref.
$R_3SnX_2(X \text{ axial})^k$ (<i>continued</i>)		
$(Et_3SnCN)_n$	-3.17	(439)
$(Me_3SnNCS)_n$	-3.77 ^h	(290)
Me_3SnOH	-2.91 ⁱ	(290)
Ph_3SnF	-3.62	(290)
$Ph_3SnCl \cdot \text{pip}^g$	-2.95	(291)
$Ph_3SnCl \cdot 2\beta\text{-pic}^e$	-2.97	(291)
$R_2SnX_3(R \text{ equatorial})^h$		
$Et_4N[Me_2SnBr_3]$	+3.39	(439)
Me_2SnCl_2	+3.4 ^c	(289)
Bu_2SnO	+2.13	(439)
Me_2SnO	+2.09 ^m	(290)

^a Data given in mm/sec.^b References (217, 290); magnitude of Q.S. from Ref. (327).^c Original data in Ref. (289); reinterpretation as described in Refs. (217, 438).^d Magnitude of Q.S. taken from Ref. (323).^e $\beta\text{-pic}$ = β -picoline.^f morph = Morpholine.^g pip = Piperidine.^h Magnitude of Q.S. taken from Ref. (439).ⁱ Magnitude of Q.S. taken from Ref. (400).^j Definition of R extended to include $Mn(CO)_5$ and $\pi\text{-cpFe(CO)}_2$.^k Trigonal-bipyramidal structure.^l Magnitude of Q.S. taken from Ref. (141).^m Magnitude of Q.S. taken from Ref. (440).

(426) shows a distorted tetrahedral coordination with an enlarged Fe-Sn-Fe angle and reduced X-Sn-X angle. Both the point charge (288) and molecular orbital (122) treatments of this type of distortion predict a positive sign for $\frac{1}{2}e^2qQ$.

The crystal structure of $Me_2Sn(ox)_2$ (505) shows a distorted *cis*- R_2SnX_4 configuration and the magnitudes of the quadrupole splittings of this compound and the species $Ph_2Sn(ox)_2$, $Ph_2Sn(S_2CNEt)_2$, $Ph_2Sn(NCS)_2phen$, $Ph_2SnCl_2 \cdot 4morph$ and $N\text{-Pr}_2SnCl_2 \cdot 2morph$ are those expected for *cis*-octahedral structures (*vide infra*). It is rather surprising therefore that the predicted negative values of $\frac{1}{2}e^2qQ$ are not observed. The origins of this inconsistency probably lie in deviations of the structure from a regular geometry (291, 439). For example, Parish and Johnson (439) have calculated, using the point charge model, the

contribution of one pair of ligands to the EFG as a function of L-Sn-L bond angle (α) (Fig. 9). Only when α lies between 70.5° and 109.5° does V_{zz} lie perpendicular to the L-Sn-L plane. For other values of α , V_{zz} lies in the L-Sn-L plane and, hence, has opposite sign to that expected for a regular cis geometry with $\alpha = 90^\circ$. The positive sign of $\frac{1}{2}e^2qQ$ observed for cis compounds may, therefore, be associated with an enlargement of the R-Sn-R angle as observed for $\text{Me}_2\text{Sn}(\text{ox})_2$, in which the Me-Sn-Me angle is 111° . Such distortions probably have only a marginal effect on the magnitude of the quadrupole splitting (439). The positive

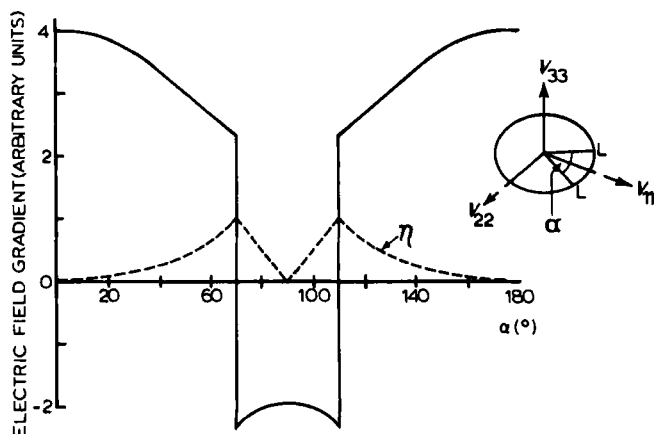


FIG. 9. Relative magnitude of the electric field gradient for an L-Sn-L system as a function of the bond angle (α). The principal component (V_{zz}) coincides with V_{11} for $0^\circ < \alpha < 70.5^\circ$, with V_{33} for $70.5^\circ < \alpha < 109.5^\circ$, and with V_{22} for $109.5^\circ < \alpha < 180^\circ$ (439).

signs observed for Me_2SnCl_2 and $(\text{Et}_4\text{N})(\text{Me}_2\text{SnBr}_3)$ are also consistent (439) with distorted structures as observed for Me_2SnCl_2 (167) and suggested for $(\text{Et}_4\text{N})(\text{Me}_2\text{SnBr}_3)$ (442).

The information used in determining partial quadrupole splittings is collected in Table XXIII for tetrahedral compounds and Table XXIV for octahedral species. The first twenty-four compounds in Table XXIII and the first thirty-six compounds in Table XXIV have been used to derive partial quadrupole splitting values, while the remaining compounds serve as cross-checks. Most of the information is considered in Clark *et al.* (122), although several additions have been made.

The structures of the compounds used in calculating partial quadrupole splitting values are reasonably well established. Crystal structures of a wide range of tin-transition metal species have been reported [see

references contained in Goodman *et al.* (288)] and all are tetrahedral, although severe distortions are sometimes found. Structural assignments for the triphenyl- and trineophyltin halides have been discussed above, and a tetrahedral structure of $\text{NeO}_3\text{SnO}_2\text{CMe}$ has been deduced by Herber *et al.* (336) and Ford and Sams (241). Crystal structures of $\text{Me}_2\text{SnCl}_2\text{L}_2$ [L = dimethyl sulfoxide (353) and pyridine N-oxide (69)] show trans-octahedral structures and the large quadrupole splittings found for the compounds in Table XXIV (compounds 1–14 and 16–35) also indicate trans structures as noted by the authors referred to in Table XXIV. Poller *et al.* (463) have assigned structures on the basis of quadrupole splitting data, to a range of $\text{Sn}(\text{S}_2\text{R})_2\text{L}_2$ species (where S_2R is 1,2-ethane dithiol, 1,3-propane dithiol, or 1,2-propane dithiol, and L is a nitrogen or oxygen donor) and the ethane dithiol species are included as representative examples. The sign of $\frac{1}{2}e^2qQ$ has been included in Tables XXIII and XXIV when available. In some other cases a sign has been assigned by consideration of structural type, and these are given in parentheses.

A survey of the compounds in Tables XXIII and XXIV reveals that phenyl, alkyl, and halogen are relatively more common than most others. Further, it is found that the differences between different alkyl ligands are not significant in relation to the overall accuracy of the additivity model. All alkyl ligands may, therefore, be assigned a single octahedral or tetrahedral partial quadrupole splitting value. By the same criterion, F, Cl, or Br may also be assigned a single parameter, and we arbitrarily assign $(\text{p.q.s.})_{\text{X}} = 0$.^{*} In view of these observations it was decided to concentrate (122) on careful determinations of $(\text{p.q.s.})_{\text{R}}^{\text{tet}} - (\text{p.q.s.})_{\text{X}}^{\text{tet}}$, $(\text{p.q.s.})_{\text{Ph}}^{\text{tet}} - (\text{p.q.s.})_{\text{X}}^{\text{tet}}$, and $(\text{p.q.s.})_{\text{R}}^{\text{oct}} - (\text{p.q.s.})_{\text{X}}^{\text{oct}}$ where X = F, Cl, Br and $(\text{p.q.s.})_{\text{L}}$ is the partial quadrupole splitting for ligand L. Values of these parameters were calculated by taking unweighted averages of statistically independent estimates from several different sets of compounds, using the appropriate additivity expressions from Table IV. The calculations are summarized in Table XXV.

For the remaining ligands the partial quadrupole splitting values were obtained by the rather more subjective procedure of calculating values from data on compounds believed to be relatively close to idealized geometry. The values obtained are summarized in Table XXVI. For *trans*- $\text{R}_2\text{SnCl}_2\text{L}_2$ systems, in which L is monodentate, the calculated values are independent of the arrangement of the Cl and L ligands as $(\text{p.q.s.})_{\text{L}}^{\text{oct}} - (\text{p.q.s.})_{\text{Cl}}^{\text{oct}}$ is small in all cases. For the bidentate ligands pic

^{*} It should be emphasized that we do not consider this to be an accurate value; $(\text{p.q.s.})_{\text{X}}$ almost certainly is *not* zero. Relative p.q.s. values and calculated Q.S. values are *independent* of what we choose as a reference value.

TABLE XXIII
OBSERVED AND CALCULATED QUADRUPOLE SPLITTINGS
FOR SOME TETRAHEDRAL COMPOUNDS

Code No. ^a	Compound ^b	Ref.	Quadrupole splitting ^c	
			Obs.	Calc.
1	NeO ₃ SnF	(336)	(-)2.79	—
2	NeO ₃ SnCl	(336)	(-)2.65	—
3	NeO ₃ SnBr	(336)	(-)2.65	—
4	NeO ₃ SnI	(336)	(-)2.40	—
5	NeO ₃ Sn(O ₂ C·Me)	(336)	(-)2.45	—
6	Me ₃ SnC ₆ F ₅	(439, 440)	-1.35	—
7	Me ₃ SnC ₆ Cl ₅	(440)	(-)1.09	—
8	Me ₃ SnCF ₃	(150, 440)	(-)1.48	—
9	Me ₃ Sn(<i>o</i> -CF ₃ ·C ₆ H ₄)	(115)	(-)0.66	—
10	(<i>p</i> -F·C ₆ H ₄) ₃ SnI	(336)	(-)1.91	—
11	Ph ₃ SnCo(CO) ₄	(364)	(-)1.00	—
12	Cl ₃ SnMn(CO) ₅	(29, 288, 364, 431, 569)	+1.59	—
13	ClSn[Re(CO) ₅] ₃	(364)	(-)1.60	—
14	Ph ₃ SnCl	(258, 290, 442)	-2.54	—
15	Ph ₃ SnBr	(258, 442)	(-)2.50	—
16	MeSn(C ₆ F ₅) ₃	(528)	(+)1.14	—
17	Ph ₃ SnC ₆ F ₅	(439, 440, 528)	-0.95	—
18	[cpFe(CO) ₂] ₂ SnCl ₃	(29, 64, 288, 331)	+1.81	—
19	(C ₆ F ₅) ₃ SnCl	(138)	(-)1.55	—
20	(C ₆ F ₅) ₃ SnBr	(138)	(-)1.60	—
21	Cl ₃ SnRh(PPh ₃) ₃	(227)	+1.73	—
22	Cl ₃ SnIr(C ₈ H ₁₂) ₂	(227)	(+)1.64	—
23	[cpFe(CO) ₂] ₂ Sn(NCS) ₃	(64)	(+)2.24	—
24	[cpFe(CO) ₂] ₂ Sn(HCO ₂) ₃	(64)	(+)1.45	—
25	Ph ₃ SnI	(258, 442)	2.15	-2.18
26	Ph ₂ SnI(CH ₂) ₄ SnIPh ₂	(400, 402)	-2.37	-2.26
27	Me ₂ Sn(C ₆ F ₅) ₂	(114, 440, 528)	1.51	1.55 ^d
28	Ph ₃ SnC ₆ Cl ₅	(440)	0.84	-0.86
29	Ph ₂ Sn(C ₆ Cl ₅) ₂	(140, 440)	1.14	0.99 ^d
30	PhSn(C ₆ Cl ₅) ₃	(140)	0.80	+0.86
31	Ph ₂ Sn(C ₆ F ₅) ₂	(528)	1.11	1.29 ^{d,e}
32	PhSn(C ₆ F ₅) ₃	(528)	0.92	+1.12
33	(4-MePh)Sn(C ₆ F ₅) ₃	(528)	1.02	+1.12 ^e
34	(4-MePh) ₂ Sn(C ₆ F ₅) ₂	(528)	1.18	1.29 ^{d,e}
35	(<i>m</i> -CF ₃ ·C ₆ H ₄) ₃ SnBr	(336)	1.94	-2.08 ^f
36	(PhCH ₂) ₃ SnCl	(367)	2.80	-2.74 ^g
37	PhSn[Co(CO) ₄] ₃	(226)	1.28	+1.00
38	Ph ₂ Sn[Co(CO) ₄] ₂	(226, 364)	1.29	1.15 ^d
39	Br ₃ SnMn(CO) ₅	(364, 431, 569)	1.54	+1.60

TABLE XXIII—continued

Code No. ^a	Compound ^b	Ref.	Quadrupole splitting ^c	
			Obs.	Calc.
40	BrSn[Re(CO) ₅] ₃	(364)	1.60	-1.60
41	ClSn[Mn(CO) ₅] ₃	(364)	1.55	-1.60
42	Me ₃ SnMn(CO) ₅	(29, 431, 569)	0.75	-1.14
43	Me ₂ Sn[Mn(CO) ₅] ₂	(569)	0.92	1.32 ^d
44	MeSn[Mn(CO) ₅] ₃	(569)	0.95	+1.14
45	Me ₂ ClSnMn(CO) ₅	(29, 431)	2.63	-2.59 ^h
46	MeCl ₂ SnMn(CO) ₅	(234, 288, 431)	+2.59	+2.67 ^h
47	Me ₂ BrSnMn(CO) ₅	(431)	2.54	-2.59
48	MeBr ₂ SnMn(CO) ₅	(431)	2.51	+2.67
49	Ph ₂ ClSnMn(CO) ₅	(364, 431)	2.55	-2.38
50	PhCl ₂ SnMn(CO) ₅	(431)	2.36	+2.50
51	Ph ₂ BrSnMn(CO) ₅	(431)	2.28	-2.38
52	PhBr ₂ SnMn(CO) ₅	(431)	2.63	+2.50
53	Ph ₂ ClSn[cpFe(CO) ₂]	(29)	2.54	-2.38 ^h
54	PhCl ₂ Sn[cpFe(CO) ₂]	(29)	2.84	+2.57 ^h
55	Ph ₂ Sn[Mn(CO) ₅][Co(CO) ₄]	(364)	1.15	-1.11
56	Ph ₂ SnCl[Co(CO) ₄]	(364)	2.22	-2.38
57	ClSn[Mn(CO) ₅][cpFe(CO) ₂] ₂	(275)	2.02	-1.76
58	[cpFe(CO) ₂] ₂ SnCl ₂	(64, 288, 331)	+2.38	2.10 ^d
59	[cpFe(CO) ₂] ₂ SnBr ₂	(64)	2.42	2.10 ^d
60	[cpFe(CO) ₂] ₂ SnI ₂	(64)	2.25	1.71 ^d
61	[cpFe(CO) ₂] ₂ Sn(NCS) ₂	(64, 288)	+2.56	2.59 ^d
62	[cpFe(CO) ₂] ₂ Sn(HCO ₂) ₂	(64)	2.19	1.69 ^d
63	[cpFe(CO) ₂] ₂ SnBr ₃	(64)	1.60	+1.82
64	[cpFe(CO) ₂] ₂ SnI ₃	(64)	1.50	+1.48
65	[cpFe(CO) ₂] ₂ Sn(O ₂ CMe) ₃	(64)	1.87	+1.52
66	[cpFe(CO) ₂] ₂ Sn(O ₂ CMe) ₂	(64)	2.60	1.75 ^d
67	[Re(CO) ₅][Mn(CO) ₅]SnCl ₂	(364)	2.48	1.85 ^d
68	Ph ₃ Sn(S·CS·NEt ₂)	(207)	1.85	-1.86 ⁱ

^a Code number will be preceded by table number in text.^b Neo = 2-methyl-2-phenylpropyl, cp = π -cyclopentadienyl.^c Data given in mm/sec. Observed values are unweighted averages; all measurements at liquid nitrogen or below.^d Denotes $\eta = 1$.^e Calculated using (p.q.s.)_{Ph}^{tet}.^f Assuming (p.q.s.)_{o-CF₃Ph}^{tet} = (p.q.s.)_{m-CF₃Ph}^{tet}.^g Assuming (p.q.s.)_R^{tet} = (p.q.s.)_{PhCH₃}^{tet}.^h Values obtained in Ref. (29); compound 45, $\Delta = -2.28$; compound 46, $\Delta = +2.42$; compound 53, $\Delta = -2.06$; compound 54, $\Delta = +2.30$ (2.79 with distortion).ⁱ Calculated assuming (p.q.s.)_L^{tet} : (p.q.s.)_L^{oct} is 1 : 0.75 for the ligand S₂CNMe₂.

TABLE XXIV

OBSERVED AND CALCULATED QUADRUPOLE SPLITTINGS FOR SOME OCTAHEDRAL COMPOUNDS

Code No. ^a	Compound ^b	Ref.	Quadrupole splitting ^c	
			Obs.	Calc.
1	K ₂ [Me ₂ SnF ₄]	(439, 442)	+4.12	—
1a	K ₂ [Et ₂ SnF ₄]	(442)	(+)4.44	—
2	Cs ₂ [Me ₂ SnCl ₄]	(439, 442)	+4.30	—
3	(pyH) ₂ [Me ₂ SnCl ₄]	(234)	(+)4.32	—
4	(Me ₄ N) ₂ [Et ₂ SnCl ₄]	(442)	(+)3.99	—
5	Cs ₂ [Me ₂ SnBr ₄]	(442)	(+)4.22	—
6	(pyH) ₂ [Ph ₂ SnCl ₄]	(442)	(+)3.80	—
7	Bu ₂ SnCl ₂ phen	(417)	(+)4.07	—
8	Me ₂ SnCl ₂ phen	(323)	(+)4.03	—
9	Me ₂ SnCl ₂ bipy	(323)	(+)4.09	—
10	Bu ₂ SnCl ₂ bipy	(417)	(+)3.83	—
11	Bu ₂ SnI ₂ phen	(417)	(+)3.75	—
12	Me ₂ SnCl ₂ (dmso) ₂	(168, 464)	(+)4.13	—
13	Me ₂ SnCl ₂ (pyO) ₂	(168, 232)	+4.03	—
14	Me ₂ SnCl ₂ (py) ₂	(10, 141)	(+)3.92	—
15	(edt) ₂ Snphen	(210, 463)	(+)1.03	—
16	(Me ₄ N) ₂ [(CH ₂ =CH) ₂ SnCl ₄]	(400)	(+)3.84	—
17	Bu ₂ Sn(NCS) ₂ phen	(418)	(+)4.18	—
18	Et ₂ SnCl ₂ dipyam	(465)	(+)3.78	—
19	(Me ₄ N) ₂ [EtSnCl ₅]	(439, 442)	+1.94	—
20	(Et ₄ N) ₂ [BuSnCl ₅]	(168, 171)	(+)1.86	—
21	Bu ₂ Sn(2-SpyO) ₂	(455)	(+)3.20	—
22	Bu ₂ Sn(pic) ₂	(421)	(+)4.35	—
23	<i>n</i> -Pr ₂ SnCl ₂ 2pip	(291)	(+)4.10	—
24	<i>n</i> -Pr ₂ SnCl ₂ 2β-pic	(291)	+3.99	—
25	Bu ₂ Sn(trop) ₂	(420)	(+)3.68	—
26	Bu ₂ Sn(koj) ₂	(420)	(+)3.60	—
27	Bu ₂ SnCl ₂ (Bu ₃ PO) ₂	(416)	(+)4.13	—
28	Bu ₂ SnCl ₂ (Ph ₃ AsO) ₂	(416)	(+)4.04	—
29	Bu ₂ SnCl ₂ (Ph ₃ PO) ₂	(416)	(+)4.11	—
30	Me ₂ Sn(S ₂ CNEt ₂) ₂	(416)	(+)3.14	—
31	Me ₂ Sn(S ₂ CNPh ₂) ₂	(233)	(+)3.20	—
32	Bu ₂ Sn(S ₂ CNPh ₂) ₂	(233)	(+)3.21	—
33	Me ₂ Sn[S ₂ CN(CH ₂) ₄] ₂	(233)	(+)2.85	—
34	Bu ₂ Sn[S ₂ CN(CH ₂) ₄] ₂	(233)	(+)3.06	—
35	Bu ₂ Sn[S ₂ CN(CH ₂ Ph) ₂] ₂	(233)	(+)3.38	—
36	Bu ₂ SnBr ₂ phen	(417)	3.94	+4.04 ^m
37	Bu ₂ SnBr ₂ bipy	(417)	3.95	+3.96 ^m
38	Bu ₂ Sn(NCS) ₂ bipy	(418)	4.04	+4.10 ^m
39	Ph ₂ Sn(NCS) ₂ phen	(418, 439)	+2.35	-2.26 ^d

TABLE XXIV—*continued*

Code No. ^a	Compound ^b	Ref.	Quadrupole splitting ^c	
			Obs.	Calc.
40	Ph ₂ Sn(NCS) ₂ bipy	(418)	2.13	See text
41	Ph ₂ SnCl ₂ bipy	(418, 465)	3.45	+3.64 ^e
42	Ph ₂ SnCl ₂ phen	(418)	3.37	+3.72 ^e
43	Me ₂ SnF ₂	(168, 217, 327)	+4.38	+4.12 ^f
44	Ph ₂ SnCl ₂ (py) ₂	(465)	3.39	+3.60 ^e
45	Ph ₂ SnCl ₂ dipyam	(465)	3.58	+3.46 ^e
46	Ph ₂ SnCl ₂ (dmsO) ₂	(465)	3.54	+3.82 ^e
47	Ph ₂ SnCl ₂ 4β-pic	(291)	+3.42	+3.66 ^e
48	Ph ₂ SnCl ₂ 4pip	(291)	3.49	+3.78 ^e
49	Ph ₂ SnBr ₂ bipy	(465)	3.52	+3.64 ^e
50	Ph ₂ SnBr ₂ (py) ₂	(465)	3.49	+3.60 ^e
51	Ph ₂ SnI ₂ bipy	(465)	3.35	+3.36 ^e
52	Ph ₂ SnCl ₂ dipyam	(465)	3.58	+3.46 ^e
53	Ph ₂ SnBr ₂ dipyam	(465)	3.45	+3.46 ^e
54	Et ₂ SnBr ₂ dipyam	(465)	3.64	+3.78 ^e
55	(edt) ₂ Sn(py) ₂	(210, 463)	1.85	-1.84 ^g
56	(edt) ₂ Snbipy	(336)	1.17	+0.96
57	Ph ₂ Sn(2-SpyO) ₂	(455)	1.45	-1.44 ^h
58	BuSnCl(2-SpyO) ₂	(415)	1.72	+1.87 ⁱ
59	PhSnCl(2-SpyO) ₂	(415)	1.52	+1.71 ⁱ
60	Bu ₂ SnI ₂ bipy	(417)	3.82	+3.68 ^m
61	Ph ₂ Sn(pic) ₂	(421)	1.94	-2.02 ^h
62	(pyH) ₂ [PhSnCl ₅]	(234)	1.92	+1.90
63	(CH ₂ =CH) ₂ SnCl ₂ (dmsO) ₂	(420)	3.80	+3.86 ^j
64	(CH ₂ =CH) ₂ SnCl ₂ (py) ₂	(420)	3.63	+3.64 ^j
65	(CH ₂ =CH) ₂ SnCl ₂ (pyO) ₂	(420)	3.74	+3.82 ^j
66	(CH ₂ =CH) ₂ SnCl ₂ phen	(420)	3.71	+3.76 ^j
67	(CH ₂ =CH) ₂ SnCl ₂ bipy	(420)	3.73	+3.68 ^j
68	(CH ₂ =CH) ₂ Sn(pic) ₂	(420)	4.02	+4.08 ^j
69	Ph ₂ Sn(trop) ₂	(420)	1.88	-1.68 ^h
70	(CH ₂ =CH) ₂ Sn(trop) ₂	(420)	1.92	-1.70 ^k
71	(CH ₂ =CH) ₂ Sn(NCS) ₂	(420)	4.28	+4.12 ^j
72	(CH ₂ =CH) ₂ Sn(NCS) ₂ (py) ₂	(420)	3.81	+3.78 ^j
73	(CH ₂ =CH) ₂ Sn(NCS) ₂ (pyO) ₂	(420)	3.88	+3.88 ^j
74	(CH ₂ =CH) ₂ Sn(NCS) ₂ phen	(420)	2.62	+2.28 ^l
75	(CH ₂ =CH) ₂ Sn(NCS) ₂ bipy	(420)	2.27	See text
76	(Et ₄ N) ₂ [(CH ₂ =CH) ₂ Sn(NCS) ₄]	(420)	3.94	+4.12 ^j
77	(Et ₄ N) ₂ [Bu ₂ Sn(NCS) ₄]	(420)	4.35	+4.40 ^m
78	(Et ₄ N) ₂ [Ph ₂ Sn(NCS) ₄]	(420)	3.82	+4.08 ^e
79	(CH ₂ =CH) ₂ Sn(2-SpyO) ₂	(420)	1.76	-1.46 ^k
80	Ph ₂ Sn(koj) ₂	(420)	1.98	-1.64 ^h
81	(CH ₂ =CH) ₂ Sn(S ₂ CNEt ₂) ₂	(420)	2.67	+2.84 ^j
82	Ph ₂ SnCl ₂ (Bu ₃ PO) ₂	(416)	3.81	+3.80 ^e

continued

TABLE XXIV—*continued*
OBSERVED AND CALCULATED QUADRUPOLE SPLITTINGS FOR SOME OCTAHEDRAL COMPOUNDS

Code No. ^a	Compound ^b	Ref.	Quadrupole splitting ^c	
			Obs.	Calc.
83	Ph ₂ Sn[S ₂ CNPh ₂] ₂	(233)	1.69	-1.44 ^e
84	Ph ₂ Sn[S ₂ CNEt ₂] ₂	(233)	1.76	-1.40 ^h
85	Ph ₂ Sn[S ₂ CN(CH ₂ Ph) ₂] ₂	(233)	1.66	-1.52 ^h
86	Ph ₂ Sn[S ₂ CN(CH ₂) ₄] ₂	(233)	1.68	-1.32 ^h

^a Code number will be preceded by table number in text.

^b phen = 1,10-Phenanthroline; bipy = 2,2'-bipyridyl; dmsO = dimethyl-sulf-oxide; pyO = pyridine oxide; py = pyridine; edtH = ethanedithiol; dipyam = di-(2-pyridylamine); 2-HSpyO = 2-pyridinethiol 1-oxide; picH = picolinic acid; pip = piperidine; β -pic = β -picoline; Htrop = tropolone; koj = kojate anion.

^c When appropriate an unweighted average has been taken, mm/sec at liquid N₂ or below. Bracketed signs are assumed.

^d *cis*-Ph₂, *trans*-(NCS)₂.

^e *trans*-Ph₂.

^f *trans*-Me₂.

^g *trans*-py₂.

^h *cis*-Ph₂.

ⁱ See text.

^j *trans*-(CH₂=CH)₂.

^k *cis*-(CH₂=CH).

^l *cis*-(CH₂=CH), *trans*-(NCS)₂.

^m *trans*-Bu₂.

and SpyO, in which the donor atoms are different, it is assumed that, at least in this semiempirical treatment, one (p.q.s.)_L^{oct} value will suffice to represent the average effect of the ligands.

It should be noted that the partial quadrupole splittings are quoted in units of magnitude of quadrupole splitting; in other words, the tabulated quantities are $\frac{1}{2}e^2|Q|([L] - [X])$. Thus, when using these values to calculate quadrupole splittings, the negative sign of the quadrupole moment of ¹¹⁹Sn must be included. It is also important to note that the partial quadrupole splittings have only a *relative* significance and no importance should be placed on the absolute magnitudes.

In the remainder of the section, we will use the term (p.q.s.)_L to describe the partial quadrupole splitting of a ligand L with the implication that

$$(\text{p.q.s.})_L = \frac{1}{2}e^2|Q|([L] - [X]) \quad (X = \text{F, Cl, or Br}) \quad (40)$$

Calculated quadrupole splittings are compared with experimental

TABLE XXV

CALCULATION OF PARTIAL QUADRUPOLE SPLITTING DIFFERENCES FOR KEY LIGANDS (122)

Parameter ^a	Estimator	Estimate ^d	Mean value ^d
[R] ^{tet} - [X] ^{tet}	$+\frac{1}{2}QS(1)^b$	-1.40	-1.37 ± 0.06
	$+\frac{1}{2}QS(2)^b$	-1.33	
	$+\frac{1}{2}QS(3)^b$	-1.32	
	$+\frac{1}{2}[QS(6) + QS(19)]^b$	-1.45	
	$+\frac{1}{2}[-QS(16) + QS(20)]^b$	-1.37	
[Ph] ^{tet} - [X] ^{tet}	$+\frac{1}{2}QS(14)^b$	-1.27	-1.26 ± 0.01
	$+\frac{1}{2}QS(15)^b$	-1.25	
	$+\frac{1}{2}[2QS(17) + QS(19) + QS(20)]^b$	-1.26	
[R] ^{oct} - [X] ^{oct}	$-\frac{1}{2}QS(1)^c$	-1.03	-1.03 ± 0.06
	$-\frac{1}{2}QS(1a)^c$	-1.11	
	$-\frac{1}{2}QS(2)^c$	-1.08	
	$-\frac{1}{2}QS(3)^c$	-1.08	
	$-\frac{1}{2}QS(4)^c$	-1.00	
	$-\frac{1}{2}QS(5)^c$	-1.05	
	$-\frac{1}{2}QS(19)^c$	-0.97	
	$-\frac{1}{2}QS(20)^c$	-0.93	

^a R = alkyl; X = F, Cl, or Br.^b Code numbers refer to Table XXIII.^c Code numbers refer to Table XXIV.^d Quantity tabulated is $\frac{1}{2}e^2|Q| ([L] - [X])$ (X = F, Cl, or Br) in units of mm/sec, i.e., (p.q.s.)_L.

values in Tables XXIII and XXIV. Once again the additivity expressions contained in Table IV have been employed. Calculations for compounds 45, 46, 53, and 54 in Table XXIII were first reported by Bancroft *et al.* (29) using different (p.q.s.)_L values, and these calculations are included as a footnote to Table XXIII.

The additivity approximation is expected to be satisfactory only if terms arising from nonadditivity or distortions contribute no more than 10–20% of the total EFG. It is suggested, therefore (122), that a discrepancy between observed and calculated quadrupole splittings should be considered exceptional if it exceeds approximately 0.4 mm/sec. The vast majority of cross-checks in Tables XXIII and XXIV lie well within this limit, lending greater confidence to the additivity description of quadrupole splittings. It is also interesting to note that the largest discrepancies are observed for compounds of type X₂SnM₂ (M = transition metal, X = electronegative ligand), and in each case the predicted

quadrupole splitting is too low. These discrepancies probably arise from deviations from a regular geometry (29, 64, 288). For example, the crystal structure (426) of $[\text{cpFe}(\text{CO})_2]_2\text{SnCl}_2$ shows a very distorted tetrahedral structure with an Fe–Sn–Fe bond angle of 128.6° . Both the point charge

TABLE XXVI
VALUES OF PARTIAL QUADRUPOLE SPLITTING PARAMETERS (122)

Tetrahedral structures			Octahedral structures		
Ligand ^a	Data used ^b	Value ^c	Ligand ^a	Data used ^d	Value ^e
Alkyl	Table XXV	–1.37	Alkyl	Table XXV	–1.03
Ph	Table XXV	–1.26	Ph	6	–0.95
I	4	–0.17	I	11	–0.14
NCS	23	+0.21	NCS	17	+0.07
MeCO ₂	5	–0.15	$\frac{1}{2}(\text{phen})$	7, 8	–0.04
C ₆ F ₅	6	–0.70	$\frac{1}{2}(\text{bipy})$	9, 10	–0.08
C ₆ Cl ₅	7	–0.83	dmso	12	+0.01
CF ₃	8	–0.63	pyO	13	–0.05 ^f
<i>o</i> -CF ₃ –C ₆ H ₄	9	–1.04	py	14	–0.10
<i>p</i> -F–C ₆ H ₄	10	–1.12	$\frac{1}{2}(\text{edt})$	15	–0.56
Co(CO) ₄	11	–0.76	CH ₂ =CH	16	–0.96
Mn(CO) ₅	12	–0.80 ^f	$\frac{1}{2}(\text{dipyam})$	18	–0.17
Re(CO) ₅	13	–0.80	$\frac{1}{2}(\text{pic})$	22	+0.06
cpFe(CO) ₂	18	–0.91	$\frac{1}{2}(2\text{-SpyO})$	21	–0.23
HCO ₂	24	–0.18	pip	23	–0.01
Rh(PPh ₃) ₃	21	–0.87	β -pic	24	–0.07
Ir(C ₈ H ₁₂) ₂	22	–0.82	$\frac{1}{2}(\text{trop})$	25	–0.11
			$\frac{1}{2}(\text{koj})$	26	–0.13
			Bu ₃ PO	27	0
			Ph ₃ PO	29	0
			Ph ₃ AsO	28	–0.04
			$\frac{1}{2}(\text{S}_2\text{CNEt}_2)$	30	–0.25
			$\frac{1}{2}(\text{S}_2\text{CNPh}_2)$	31, 32	–0.23
			$\frac{1}{2}[\text{S}_2\text{CN}(\text{CH}_2)_4]$	33, 34	–0.29
			$\frac{1}{2}[\text{S}_2\text{CH}(\text{CH}_2\text{Ph})_2]$	35	–0.19

^a See Tables XXIII and XXIV for abbreviations.

^b Code numbers refer to Table XXIII.

^c Quantity tabulated is $(\text{p.q.s.})_{\text{L}}^{\text{tet}} = \frac{1}{2}e^2|Q|q|([L]^{\text{tet}} - [X]^{\text{tet}})$, where X = F, Cl, or Br.

^d Code numbers refer to Table XXIV.

^e Quantity tabulated is $(\text{p.q.s.})_{\text{L}}^{\text{oct}} = \frac{1}{2}e^2q|Q|([L]^{\text{oct}} - [X]^{\text{oct}})$, where X = F, Cl, or Br.

^f Values differ slightly from Ref. (122), owing to the inclusion of additional data.

(64, 288) and molecular orbital (122) treatments of this type of distortion predict an increase in quadrupole splitting. Bancroft *et al.* (29) have also improved the agreement between observed and calculated quadrupole splittings of $\text{PhCl}_2\text{Sn}[\text{cpFe}(\text{CO})_2]$ (Table XXIII, compound 54) by consideration of distortions.

For octahedral compounds which have more than one geometric isomer, the calculated splitting listed is that which gives the best agreement. The structures predicted in this manner are indicated in the footnotes to Table XXIV. For *trans*- $\text{R}_2\text{SnX}_2\text{L}_2$ species (L is a monodentate ligand), the calculated values vary very little with the arrangement of the X and L ligands and the values given in the table are for a *cis* arrangement of L_2 and X_2 . In most cases the structural assignments are those put forward in the references cited in Table XXIV. For example, Curran *et al.* (417, 418, 420, 421, 455) have assigned structures with *trans*-alkyl, phenyl, or vinyl groups in the following species in Table XXIV, compounds 36–38, 60, 63–68, 71–73, 76–78, and 81. They assigned structures with *cis*-phenyl or vinyl groups to these species in Table XXIV, compounds 39, 40, 57, 61, 69, 79, and 80. In many cases, the above assignments were confirmed by dipole moment data. Similarly, the structures assigned to compounds 55 and 56 are those of Poller *et al.* (463), while the structures of compounds 47 and 48, Table XXIV were first deduced by Goodman *et al.* (291). Fitzsimmons *et al.* (233) have argued that the species in Table XXIV, compounds 83–86 have *cis*-phenyl groups.

In some cases, the calculations allow a more detailed appraisal of the structure. For example, the calculated quadrupole splittings of $\text{RSnCl}(\text{2-SpyO})_2$ ($\text{R} = \text{Ph}, \text{Bu}$) for Cl *cis* to R (Table XXIV, compounds 58 and 59) are much closer to the observed values than those obtained for Cl *trans* to R (-1.14 mm/sec, $\text{R} = \text{Bu}$ and -0.98 mm/sec, $\text{R} = \text{Ph}$). A structure with Cl *cis* to R is also indicated by dipole moment data (415). Similarly, Poller *et al.* (465) have suggested that the relatively low quadrupole splittings of the compounds $\text{Ph}_2\text{SnX}_2\text{L}_2$ ($\text{X} = \text{Cl}, \text{Br}, \text{or I}$; $\text{L} = \text{py}, \text{bipy}, \text{dipyam}, \text{or tripyam}$) indicate deviations from a regular geometry, whereas the calculations in Table XXIV show that the lowering is more probably due to the polarity of the tin-phenyl bond.

The additivity model does not always resolve structural ambiguities. For example, Mullins and Curran (418) deduced from dipole moment data that, at least in solution, the NCS groups in $\text{Ph}_2\text{Sn}(\text{NCS})_2\text{L}_2$ ($\text{L} = \text{bipy}$ or *phen*) are *trans* to each other. For $\text{Ph}_2\text{Sn}(\text{NCS})_2\text{phen}$ ($\Delta = 2.34$ mm/sec) the calculated quadrupole splittings for a *cis*- Ph_2 -*trans*-(NCS)₂ isomer (Table XXIV, compound 39) (-2.26 mm/sec) is in much closer numerical agreement with the experimental value than that calculated

for the *cis-cis* isomer (-1.94 mm/sec), confirming the assignment of Mullins and Curran (418). In contrast, the calculated quadrupole splittings for the *cis-trans* and *cis-cis* isomers of $\text{Ph}_2\text{Sn}(\text{NCS})_2\text{bipy}$ (Table XXIV, compound 40) are -2.34 and -1.89 mm/sec. A similar situation is encountered for the species $(\text{CH}_2=\text{CH})_2\text{Sn}(\text{NCS})_2\text{L}$ [$\text{L} = \text{phen}$ (Table XXIV, compound 74); $\text{L} = \text{bipy}$ (Table XXIV, compound 75)], in which cases the calculated quadrupole splittings indicate a *cis*-($\text{CH}_2=\text{CH})_2$ -*trans*-($\text{NCS})_2$ structure for $\text{L} = \text{phen}$, whereas the observed value for $\text{L} = \text{bipy}$ falls between the calculated values for *cis*-($\text{CH}_2=\text{CH})_2$ -*cis*-($\text{NCS})_2$ ($\Delta = 1.91$ mm/sec) and *cis*-($\text{CH}_2=\text{CH})_2$ -*trans*-($\text{NCS})_2$ ($\Delta = 2.36$ mm/sec).

A further example is provided by the complexes of type RSnCl_3L_2 (168, 415), data for which are summarized in Table XXVII, together with the calculated quadrupole splitting values for the various structural isomers. In most cases it is not possible to assign structures confidently in view of the lack of variation in the calculated quadrupole splittings and the relatively poor agreement between observed and calculated values. However, the results for $2\text{L} = \text{phen}$ or *bipy* (Table XXVII, compounds 6–13) do show an indication that a structure with all *cis*-X groups is the most probable, although such a structure is at variance with dipole moment data (415).

The (p.q.s.)_L values listed in Table XXVI, may be used to check the prediction made in Section II, D, that $[\text{L}]^{\text{oct}}$ should be approximately 70% of $[\text{L}]^{\text{tet}}$. From Eqs. (29.1)–(29.4),

$$\frac{(\text{p.q.s.})_{\text{L}}^{\text{oct}} - (\text{p.q.s.})_{\text{X}}^{\text{oct}}}{(\text{p.q.s.})_{\text{L}}^{\text{tet}} - (\text{p.q.s.})_{\text{X}}^{\text{tet}}} = \frac{2}{3} \left(\frac{\sigma_{\text{L}}^{\text{oct}} - \sigma_{\text{X}}^{\text{oct}}}{\sigma_{\text{L}}^{\text{tet}} - \sigma_{\text{X}}^{\text{tet}}} \right) = r[\text{L}]$$

Values of $r[\text{L}]$ for $\text{L} = \text{alkyl}$, *phenyl*, *iodine*, and *NCS* are 0.75 ± 0.06 , 0.75 ± 0.07 , 0.82 ± 0.51 , and 0.33 ± 0.33 , respectively, where the errors quoted are standard deviations calculated on the basis that an effective standard deviation of 0.067 mm/sec can be assigned to all parameters listed in Table XXVI. These values of $r[\text{L}]$ support the prediction, although $r[\text{NCS}]$ seems rather low.

From Eqs. (29.1)–(29.4), the (p.q.s.)_L values may be written in the form

$$(\text{p.q.s.})_{\text{L}}^{\text{tet}} = \frac{3}{8} \Delta_o \sigma_{\text{L}}^{\text{tet}} \quad (41)$$

$$(\text{p.q.s.})_{\text{L}}^{\text{oct}} = \frac{1}{4} \Delta_o \sigma_{\text{L}}^{\text{oct}} \quad (42)$$

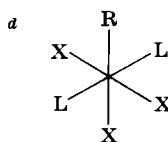
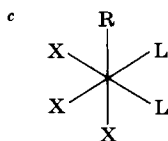
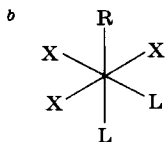
where Δ_o is the quadrupole splitting due to one $5p_z$ electron. As both $\sigma_{\text{L}}^{\text{tet}}$ and $\sigma_{\text{L}}^{\text{oct}}$, in the limit of the additivity approximation, are equal to $2c_1^2[\text{Eq. (25)}]$, (p.q.s.)_L values should be a reflection of the relative

TABLE XXVII

OBSERVED AND CALCULATED QUADRUPOLE SPLITTINGS FOR COMPOUNDS
OF TYPE RSnX_3L_2

Code No. ^a	Compound ^a	Ref.	Quadrupole splitting			
			Obs.	Calc. ^b	Calc. ^c	Calc. ^d
1	$\text{BuSnCl}_3(\text{py})_2$	(168)	1.86	+2.17	+1.86	+1.89
2	$\text{BuSnCl}_3(\text{Ph}_3\text{PO}_4)_2$	^e	2.34	+2.06	+2.06	+2.06
3	$\text{PhSnCl}_3(\text{Ph}_3\text{PO})_2$	(416)	2.01	+1.90	+1.90	+1.90
4	$\text{BuSnCl}_3(\text{Ph}_3\text{AsO})_2$	(416)	1.81	+2.10	+1.98	+2.00
5	$\text{BuSnCl}_3(\text{dmso})_2$	(168)	1.73	+2.05	+2.08	+2.08
6	$\text{BuSnCl}_3\text{phen}$	(168, 415)	1.64	+2.10	+1.98	—
7	$\text{BuSnCl}_3\text{bipy}$	(168, 415)	1.64	+2.14	+1.90	—
8	$\text{PhSnCl}_3\text{phen}$	(415)	1.48	+1.94	+1.82	—
9	$\text{PhSnCl}_3\text{bipy}$	(415)	1.50	+1.98	+1.74	—
10	$\text{BuSn}(\text{NCS})_3\text{phen}$	(415)	1.80	+2.32	+1.98	—
11	$\text{BuSn}(\text{NCS})_3\text{bipy}$	(415)	1.75	+2.37	+1.90	—
12	$\text{PhSn}(\text{NCS})_3\text{phen}$	(415)	1.56	+2.16	+1.82	—
13	$\text{PhSn}(\text{NCS})_3\text{bipy}$	(415)	1.55	+2.21	+1.74	—
14	$n\text{-PrSnCl}_3(\text{piperidine})_2$	(291)	+1.99	+2.07	+2.04	+2.04
15	$n\text{-PrSnCl}_3(\beta\text{-picoline})_2$	(291)	1.87	+2.13	+1.92	+1.94
16	$\text{PhSnCl}_3(\text{piperidine})_2$	(291)	1.70	+1.91	+1.88	+1.88
17	$\text{PhSnCl}_3(\beta\text{-picoline})_2$	(291)	1.40	+1.97	+1.76	+1.78

^a Code number is preceded by table number in text, py = pyridine; dmso = dimethyl sulfoxide; bipy = 2,2'-bipyridyl; phen = 1,10-phenanthroline.



^e Average of Refs. (168, 416).

populations of the tin-ligand bonds. Williams and Kocher (566) have recently reported a method of calculating orbital populations for tetrahedral compounds using Mössbauer data and it is of interest to compare these calculations with the (p.q.s.)_L values.

In their original paper, Williams and Kocher (566) derived a value of $\Delta_o = +5.8$ mm/sec by consideration of Br NQR and ^{119}Sn Mössbauer data for the compound Et_3SnBr . However, in view of the probable trigonal-bipyramidal structure of this compound (442), this value of Δ_o

TABLE XXVIII
CALCULATED ORBITAL POPULATIONS FOR Sn^{IV}
TETRAHEDRAL COMPOUNDS^a

Compound	α_{R}^b	α_{X}^b	$\alpha_{\text{X}}(\text{NQR})^c$
$\text{NeO}_3\text{SnF}^{d,e}$	1.128	0.263	—
$\text{NeO}_3\text{SnCl}^{d,e}$	1.127	0.305	—
$\text{NeO}_3\text{SnBr}^{d,e}$	1.131	0.311	—
$\text{NeO}_3\text{SnI}^{d,e}$	1.111	0.366	—
Ph_3SnCl^f	1.107	0.313	0.307
Ph_3SnBr^f	1.110	0.341	0.365
Ph_3SnI^f	1.065	0.367	0.447

^a From Ref. (401).

^b Orbital populations derived from Mössbauer data, $\Delta_o = 4.3$ mm/sec.

^c Orbital populations derived from halogen NQR data (566).

^d Neo = $\text{CH}_3\text{—CH(Ph)CH}_3\text{—CH}_2$.

^e Mössbauer data from Ref. (336).

^f Mössbauer data from Ref. (442).

is probably inflated (401). An alternative value of $\Delta_o = 4.3$ mm/sec has been reported (401) based on ^{119}Sn Mössbauer and Cl NQR data for Ph_3SnCl . Calculated orbital populations (401) for NeO_3SnX ($\text{X} = \text{F}, \text{Cl}, \text{Br}, \text{or I}$) and Ph_3SnX ($\text{X} = \text{Cl}, \text{Br}, \text{or I}$) are given in Table XXVIII. Recently Williams and Kocher (567) have amended their equations and, using a value of $\Delta_o = 5.5$ mm/sec, obtained a second set of orbital populations for such compounds as Ph_3SnX and Ph_4Sn . It is interesting to note that from Williams's and Kocher's data, with $\Delta_o = 4.3$, values of $(\text{p.q.s.})_{\text{R}}^{\text{tet}} - (\text{p.q.s.})_{\text{X}}^{\text{tet}} = -1.35$ mm/sec and $(\text{p.q.s.})_{\text{Ph}}^{\text{tet}} - (\text{p.q.s.})_{\text{X}}^{\text{tet}} = -1.26$ mm/sec can be calculated and these differences are in excellent agreement with those in Table XXVI obtained directly from Q.S. data.

Perhaps the most interesting (p.q.s.)_L values are those found for the transition metal groups π -cpFe(CO)₂ (−0.91 mm/sec), Rh(PPh₃)₃ (−0.87 mm/sec), Ir(C₈H₁₂)₂ (−0.82 mm/sec), Re(CO)₅ (−0.80 mm/sec), Mn(CO)₅ (−0.80 mm/sec), and Co(CO)₄ (−0.76 mm/sec). These values indicate that these groups are poorer σ donors than alkyl or phenyl. In semiquantitative terms, using $\Delta_o = 4.3$ mm/sec, $\sigma_R^{\text{tet}} - \sigma_M^{\text{tet}}$ values for these compounds are in the approximate range 0.29–0.37 and have the relative ordering Co(CO)₄ > Mn(CO)₅ = Re(CO)₅ > Ir(C₈H₁₂)₂ > Rh(PPh₃)₃ > π -cpFe(CO)₂. These conclusions are supported by the quadrupole splitting observed for Me₃SnMn(CO)₅ ($\Delta = 0.62$ – 0.82 mm/sec) (29, 431, 569) and Me₃Sn[π -cpFe(CO)₂] ($\Delta = 0.46$ mm/sec) (149) compared with the absence of or small quadrupole splittings in their triphenyltin analogs (29, 149, 431), and by the negative sign observed for $\frac{1}{2}e^2qQ$ of the compound Bu₃Sn[π -cpFe(CO)₂] (288). In many ways these (p.q.s.)_L values are rather surprising as Fenton and Zuckerman (226) and Onaka *et al.* (431) have shown that NMR, X-ray diffraction, and center shift data (see Section IV,A,2) all indicate that these transition metal groups are all better σ donors than alkyl or phenyl. In this context the quadrupole splitting trends found for the compounds R₃Sn[π -cpFe(CO)L] (R = Me, Ph; L = Ph₃P, Ph₃As, Ph₃Sb, Ph₂CF₃P, Ph₂AsCF₃, Ph₂PMe, PhPMe₂, or Ph₂AsCF₃) reported by Sams *et al.* (149) are of interest. Thus, the triphenyltin species all have small quadrupole splittings (Δ in the range 0.44–0.78 mm/sec), while the trimethyltin analogs show single-line spectra or, in the case of L = Ph₃P, a very small quadrupole splitting. Although these data strongly suggest that the groups π -cpFe(CO)L, in contrast to π -cpFe(CO)₂, are better σ donors than methyl or phenyl, this is not reflected in the magnitude of the quadrupole splitting of Cl₃Sn[π -cpFe(CO)PPh₃], which is closely similar to that of Cl₃Sn[π -cpFe(CO)₂].

An additivity model treatment of five-coordinate compounds is rather more complicated than that for tetrahedral or octahedral compounds. A literal point charge model interpretation of the relative quadrupole splittings of [R_nSnCl_{5-n}][−] ($n = 0$ – 3) ions has been reported (442), and this type of treatment has been extended to other systems (152, 207). In the point charge model, differences between equatorial and axial bonds were ignored and the quadrupole splittings of the [SnCl₅][−] ions were taken as an absolute value of (p.q.s.)_{Cl}. It is probable that both these assumptions are incorrect.

An SnA₅ system will have an axially symmetric EFG with principal component:

$$V_{zz} = (4[A]^{\text{tba}} - 3[A]^{\text{tbe}})e \quad (43)$$

substitution for $[A]^{tba}$ and $[A]^{tbe}$ from Eqs. (29.1)–(29.4) yields

$$V_{ZZ} = \frac{4}{5} \langle r^{-3} \rangle_p e (\sigma_A^{tbe} - \sigma_A^{tba}) \quad (44)$$

and the corresponding quadrupole splitting is given by

$$\Delta = \frac{1}{2} e Q V_{ZZ} = \Delta_o (\sigma_A^{tbe} - \sigma_A^{tba}) \quad (45)$$

From Eq. (45), if axial and equatorial bonds are identical in $[\text{SnCl}_5]^-$, i.e., $\sigma_{\text{Cl}}^{tbe} = \sigma_{\text{Cl}}^{tba}$, then zero quadrupole splitting is expected. The small quadrupole splittings which are observed show that σ_{Cl}^{tbe} does not equal σ_{Cl}^{tba} . Further, from Eq. (45), it can be seen that the quadrupole splittings of $[\text{SnCl}_5]^-$ ions give a measure of $(\text{p.q.s.})_{\text{Cl}}^{tba} - \frac{3}{4}(\text{p.q.s.})_{\text{Cl}}^{tbe}$ and not the absolute value of $(\text{p.q.s.})_{\text{Cl}}$. Indeed, as explained in Section II, D, it is not possible to calculate absolute $(\text{p.q.s.})_{\text{L}}$ values direct from quadrupole splitting data (122).

At this stage, it does not seem worthwhile to pursue the detailed calculations of five-coordinate additivity parameters for two reasons. First, although the quadrupole splittings of $[\text{SnCl}_5]^-$ ions can be used to calculate a value of $(\text{p.q.s.})_{\text{Cl}}^{tba} - \frac{3}{4}(\text{p.q.s.})_{\text{Cl}}^{tbe}$, the sign of $\frac{1}{2}e^2qQ$ for these species has not yet been reported. Second, as most five-coordinate tin compounds, for which both Mössbauer and structural data are available, are of type R_3SnX_2 (X axial), calculation of additivity parameters would amount merely to a parameterization of the data. The best course of action, at present, seems to be to use quadrupole splitting data for five-coordinate compounds in a purely empirical manner.

The relationship of the quadrupole splittings of five-coordinate R_3SnX_2 (X axial) species to those of tetrahedral R_3SnX compounds is of interest in the study of intermolecular association. From Eqs. (29.1)–(29.4),

$$\Delta(\text{R}_3\text{SnX}) = -\frac{3}{5} \langle r^{-3} \rangle_p (\sigma_{\text{X}}^{\text{tet}} - \sigma_{\text{R}}^{\text{tet}}) \frac{e^2 Q}{2}$$

$$\Delta(\text{R}_3\text{SnX}_2) = -\frac{4}{5} \langle r^{-3} \rangle_p (\sigma_{\text{X}}^{tba} - \sigma_{\text{R}}^{tbe}) \frac{e^2 Q}{2}$$

and, hence,

$$\frac{\Delta(\text{R}_3\text{SnX})}{\Delta(\text{R}_3\text{SnX}_2)} = \frac{3}{4} \frac{(\sigma_{\text{X}}^{\text{tet}} - \sigma_{\text{R}}^{\text{tet}})}{(\sigma_{\text{X}}^{tba} - \sigma_{\text{R}}^{tbe})} \quad (46)$$

It may be anticipated, therefore, that for a compound of stoichiometry R_3SnX , the formation of an associated structure would result in a quadrupole splitting approximately 1.33 times that expected for a monomeric tetrahedral structure. The quadrupole splittings observed for the five-coordinate species Me_3SnX (X = F, Cl, Br, or I) and the four

coordinate species Neos_3SnX ($\text{X} = \text{F}, \text{Cl}, \text{Br}, \text{or I}$) show an average ratio of 1.28, in good agreement with the predicted value.

c. Organometallic Compounds and Halogen Complexes. The variation of quadrupole splitting with structure discussed in the preceding section makes ^{119}Sn Mössbauer spectroscopy a very powerful means of studying the structures of organotin compounds. In particular, it has greatly helped in the study of intermolecular association.

One of the best examples of this approach is provided by the trialkyltin carboxylates, data for which are summarized in Table XXIX. Infrared evidence (355) strongly suggests that the compounds $\text{R}_3\text{SnO}_2\text{CMe}$ ($\text{R} = \text{Me}, \text{Et}, \text{Bu}$) have polymeric structures with trigonal-bipyramidal R_3SnX_2 (X axial) coordination of the tin atom. The quadrupole splittings observed for these compounds are high (Table XXIX, compounds 2, 12, 14) as expected for R_3SnX_2 (X axial) species (440). In contrast, monomeric tetrahedral structures would be expected to result in much smaller quadrupole splittings (440). Using these considerations Sams *et al.* (240, 241, 459) have assigned polymeric five-coordinate structures to the following species in Table XXIX, compounds 3–5, 7, 9–11, and 23–30, and monomeric four-coordinate structures to Table XXIX, compounds 31–33. In a similar manner Debye *et al.* (170) have assigned polymeric structures to compounds 6, 8, and 17–22 in Table XXIX, and this assignment may be extended to the remaining compounds in Table XXIX. In some cases, infrared evidence provides further confirmation of the assignments in that the OCO bands are shifted further from the normal ester frequencies in the five-coordinate compounds as compared with the four-coordinate species (240, 241, 459).

The most probable reason for the lack of association in the species 31–33 in Table XXIX are steric effects. Sams *et al.* (240, 241) have suggested that the major factor in producing monomeric structures is the presence of bulky groups bonded to the α -carbon atom of the carboxylate group. However, the steric effects of the phenyl groups are also important (400), as evidenced by the associated structures found for $\text{R}_3\text{SnO}_2\text{CCMe}=\text{CH}_2$ ($\text{R} = \text{Et}, \text{Bu}$). Tricyclohexyltin acetate provides an interesting example as the crystal structure (4) shows essentially monomeric coordination with an intermolecular Sn–O distance of 3.84 Å. The observed quadrupole splitting [$\Delta = 3.27$ mm/sec (400)], however, is between the values expected for tetrahedral and five-coordinate structures. At present, no obvious explanation of this anomaly is apparent, although intramolecular interaction with the carbonyl oxygen is possible, as this Sn–O distance is only 2.95 Å.

TABLE XXIX

MÖSSBAUER PARAMETERS FOR SOME COMPOUNDS OF TYPE $R_3SnO_2CR^1$

Code No. ^a	R ¹	C.S. ^{b,c}	Q.S. ^b	Ref.
R = Me				
1	H	1.31	3.55	(170, 323, 516)
2	Me	1.34	3.53	(240, 323, 336, 516)
3	CH ₂ I	1.37	3.83	(459)
4	CH ₂ Br	1.34	3.90	(459)
5	CH ₂ Cl	1.41	3.89	(459)
6	CH ₂ F	1.37	3.86	(170)
7	CHCl ₂	1.37	4.08	(459)
8	CHF ₂	1.40	4.02	(459)
9	CBr ₃	1.43	4.13	(459)
10	CCl ₃	1.44	4.15	(459)
11	CF ₃	1.40	4.20	(170, 459)
R = Et				
12	Me	1.49	3.35	(84, 367)
13	C(Me)=CH ₂	1.35	3.00	(83)
R = Bu				
14	Me	1.40	3.61	(170, 240, 323, 367)
15	C(Me)=CH ₂	1.45	3.70	(8)
16	(CH ₂) ₁₁ Me	1.40	3.62	(516)
17	CH ₂ Cl	1.40	3.94	(170)
18	CHCl ₂	1.47	4.00	(170)
19	CCl ₃	1.57	3.96	(170)
20	CH ₂ F	1.42	3.96	(170)
21	CHF ₂	1.59	3.92	(170)
22	CF ₃	1.62	4.04	(170)
R = Ph				
23	H	1.37	3.58	(240)
24	Me	1.24	3.30	(240, 323, 464)
25	(CH ₂) _n Me ^d	1.24–1.33	3.31–3.46	(240, 464)
26	(CH ₂) _n CHMe ₂ ^e	1.25–1.27	3.21–3.39	(84, 240, 367)
27	(CH ₂) ₇ CH=CH-			
	(CH ₂) ₇ -Me	1.27	3.38	(240)
28	CH ₂ CHMeEt	1.29	3.39	(241)
29	CHMePr	1.26	3.34	(241)
30	CH=CH ₂	1.28	3.41	(241)
31	CMe=CH ₂	1.15	2.18	(84, 240, 367)
32	CHEtBu	1.21	2.26	(241)
33	CMe ₃	1.22	2.35	(240, 464)
34	CH ₂ Cl	1.30	3.46	(464)
35	CHCl ₂	1.35	3.72	(516)

^a Code number will be preceded by table number in text.^b Units are mm/sec at liquid nitrogen temperature; when appropriate an unweighted average has been taken.^c Relative to SnO₂, assuming center shift of BaSnO₃ is zero.^d Range of data for $n = 1, 2, 4, 6, 7, 8, 10, 14$, or 16 .^e Range of data for $n = 0, 1, 2$.

The quadrupole splitting and center shift patterns observed for the halogeno-substituted trimethyl- and tributyltin carboxylates are of interest. Poder and Sams (459) could detect little variation in center shift for the compounds 2-5, 7, and 9-11 in Table XXIX, whereas the quadrupole splitting increases uniformly with increasing Taft σ^* of the substituent and decreasing pK_a of the acid. These data were interpreted in terms of a progressive weakening and, hence, lengthening of the intermolecular Sn-O bond with increasing inductive power of the halogen substituent. Infrared data (459) are also in agreement with this interpretation, as increasing quadrupole splitting is reflected in a shift of the carbonyl and carboxyl bands to higher and lower frequency, respectively. Substantially similar quadrupole splitting trends were found by Debye *et al.* (170) for the compounds 6, 8, 9, and 22 in Table XXIX, although there is a marked saturation effect in the variation of quadrupole splitting with halogen substitution for the tributyltin species.

Debye *et al.* (170) also observed a regular increase in center shift with inductive power of the halogen group, which was attributed to shielding effects. Both Debye *et al.* (170) and Poder and Sams (459) use the $J_{119\text{Sn-CH}_3}$ coupling constants observed in NMR spectra of the trimethyltin derivatives in discussing their Mössbauer data. Poder and Sams (459) take the data as evidence for a constant electron density in the tin-methyl bonds, while Debye *et al.* (170) find an increase in $J_{119\text{Sn-CH}_3}$ with both center shift and quadrupole splitting. It should, however, be remembered that as NMR measurements are made on dilute solutions, the correlation with Mössbauer results obtained on the solid compounds may be rather tenuous.

Mössbauer data for compounds of type $R_3\text{SnX}$ ($X = \text{NCS}, \text{NCO}, \text{N}_3, \text{CN}, \text{OH}, \text{and } \text{ON}=\text{C}_6\text{H}_{10}$) are collected in Table XXX. All the compounds of type $R_3\text{SnX}$ ($X = \text{OH}, \text{CN}, \text{NCS}$) show relatively large quadrupole splittings allowing the assignment (258) of polymeric five-coordinate structures as found crystallographically for Me_3SnCN (506), Me_3SnOH (366), and Me_3SnNCS (243). Cheng and Herber (112) have shown that both quadrupole splitting data and the temperature dependence of the recoil free fraction (see Section IV, A, 2) of Me_3SnN_3 are consistent with an associated structure and similar structures seem probable for the higher alkyl analogs. The relatively small quadrupole splittings found for $(\text{PhCH}_2)_3\text{SnNCO}$ and Ph_3SnNCO argue against any appreciable degree of association (383). However, some form of intermolecular interaction seems probable for the species $R_3\text{SnNCO}$ ($R = \text{Me}, \text{Et}, \text{Pr}, \text{and Bu}$), confirmed in the case of Me_3SnNCO by the temperature dependence of the recoil free fraction. Harrison and Zuckerman (318) have demonstrated that the quadrupole splittings of

TABLE XXX
MÖSSBAUER DATA FOR SOME R_3SnX SPECIES*

X R	=	CN			NCS			OH			N ₃			NCO			ON = C ₆ H ₁₀		
		C.S.‡	Q.S.	Ref.	C.S.‡	Q.S.	Ref.	C.S.‡	Q.S.	Ref.	C.S.‡	Q.S.	Ref.	C.S.‡	Q.S.	Ref.	C.S.‡	Q.S.	Ref.
Me		1.35	3.10	<i>a</i>	1.40	-3.77	<i>b</i>	1.11	-2.86	<i>c</i>	1.34	3.45	<i>d</i>	1.36	3.31	<i>e</i>	1.43‡	2.96‡	<i>f</i>
Et		1.37	-3.11	<i>g</i>	1.57	3.80	<i>h</i>	1.35	3.00	<i>h</i>	1.24	3.04	<i>i</i>	1.46	3.29	<i>e</i>	1.58	1.96	<i>f</i>
<i>n</i> -Pr		—	—		—	—		—	—		1.21	2.96	<i>i</i>	1.48	3.33	<i>e</i>	1.42	2.03	<i>f</i>
<i>n</i> -Bu		1.37	3.27	<i>h</i>	1.60	3.69	<i>h</i>	1.46	3.21	<i>h</i>	1.26	3.17	<i>i</i>	1.36	3.19	<i>e</i>	1.48	1.76	<i>f</i>
<i>n</i> -Ph		—	—		1.35	3.50	<i>h</i>	1.23	2.73	<i>j</i>	1.40	3.19	<i>k</i>	1.30	2.47	<i>e</i>	1.38	1.44	<i>f</i>
Cyclo-C ₆ H ₁₁		—	—		1.68	3.82	<i>l</i>	1.40	2.99	<i>l</i>	—	—		—	—		—	—	
PhCH ₂		—	—		—	—		—	—		—	—		1.51	2.85	<i>e</i>	—	—	
Neo		—	—		—	—		1.13	1.08	<i>k</i>	1.33	2.48	<i>k</i>	—	—		—	—	

* When appropriate data is an average of the references quoted. Data in mm/sec at liquid nitrogen temperature.

‡ Relative to SnO₂ assuming that the center shifts of SnO₂ and BaSnO₃ are identical.

† X=ON=CMe₂, C.S. = 1.40 mm/sec, Q.S. = 2.93 mm/sec.

Key to references:

^a(258, 367, 525) ^b(258, 290) ^c(141, 258, 290, 516) ^d(131, 336) ^e(383) ^f(318) ^g(258, 367, 439) ^h(258) ⁱ(131) ^j(258, 279, 336, 525) ^k(336) ^l(400).

TABLE XXXI

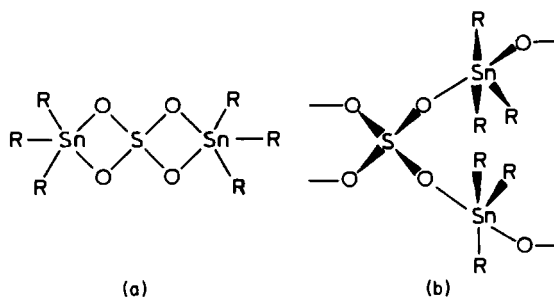
MÖSSBAUER DATA FOR COMPOUNDS OF TYPE $(R_3Sn)_2XO_4$

Compound	Temp.(°K)	C.S. ^{a,b}	Q.S. ^a	Ref.
(Me ₃ Sn) ₂ SO ₄	80	1.37	4.06	(242)
	295	No effect		
(Me ₃ Sn) ₂ SeO ₄	80	1.39	4.09	(242)
	295	1.33	4.14	
(Me ₃ Sn) ₂ CrO ₄	80	1.36	3.77	(242)
	295	1.35	3.73	
(Bu ₃ Sn) ₂ SO ₄	80	1.56	4.01	(520)
	295	No effect		
Me ₃ SnNO ₃	80	1.44	4.14	(141)

^a Data given in mm/sec.^b Relative to SnO_2 , assuming a shift of 2.1 mm/sec for α -tin.

$R_3SnON=C_6H_{10}$ ($R = Me, Et, Pr, Bu,$ and Ph) and $Me_3SnON=CMe_2$, together with infrared and mass spectra, indicate that only the trimethyltin derivatives are appreciably polymeric.

Data for compounds of type $(R_3Sn)_2XO_4$ ($X = S, Se, Cr$) are given in Table XXXI. Ford *et al.* (242) have shown that both Mössbauer and infrared data for $(Me_3Sn)_2XO_4$ ($X = S, Se,$ and Cr) are consistent with a polymeric structure as illustrated in Fig. 10b. The structure of $(Bu_3Sn)_2SO_4$, however, has been the subject of some controversy. Stapfer *et al.* (326, 335, 520) have suggested a monomeric structure (Fig. 10a) based on consideration of frozen solution data, IR spectra, and the temperature dependence of the recoil free fraction (326), whereas Garrod *et al.* (257) have pointed out that the similarity of the spectra of $(Me_3Sn)_2SO_4$ and $(Bu_3Sn)_2SO_4$ argues against a change in structure.

Fig. 10. Two possible structures for $[R_3Sn]_2SO_4$ compounds (257).

It is also interesting to note that adducts formed between $(\text{Me}_3\text{Sn})_2(\text{XO}_4)$ and water, methanol, dimethylformamide, or pyridine show only slight changes compared with the parent compound (242).

In Table XXXII are collected the Mössbauer parameters for the compounds R_2SnX_2 ($\text{X} = \text{F}, \text{Cl}, \text{Br}, \text{I}, \text{NCS}, \text{N}_3, \text{or NCO}$), while in Table XXXIII are given data for dialkyltin dicarboxylates and related species. The high quadrupole splittings observed for the compounds R_2SnF_2 ($\text{R} = \text{Me}, \text{Et}, \text{Pr}, \text{Bu}, \text{Ph}, \text{Oct}$), $\text{R}_2\text{Sn}(\text{NCS})_2$ ($\text{R} = \text{Me}, \text{Et}, \text{Bu}, \text{Ph}$), Me_2SnXO_4 ($\text{X} = \text{S}, \text{Se}, \text{Mo}, \text{W}$), Bu_2SnSO_4 , $\text{Me}_2\text{Sn}(\text{NO}_3)_2$, $\text{Me}_2\text{Sn}(\text{acac})_2$, and $\text{Me}_2\text{SnSO}_3\text{X}$ ($\text{X} = \text{F}, \text{Cl}, \text{CF}_3, \text{Me}, \text{Et}$) indicate (167, 234, 242, 258, 300, 418, 572) polymeric structures with trans-octahedral coordination of the tin atom as found crystallographically for Me_2SnF_2 (507) and $\text{Me}_2\text{Sn}(\text{NCS})_2$ (116, 244). The crystal structure of $\text{Me}_2\text{Sn}(\text{NCS})_2$ does, in fact, show a considerable distortion with a Me-Sn-Me angle of 148.9° , and this may be reflected in the quadrupole splittings of the $\text{R}_2\text{Sn}(\text{NCS})_2$ ($\text{R} = \text{Me}, \text{Et}, \text{Bu}$) species, which are considerably lower than the calculated value for a *trans*- $\text{R}_2\text{Sn}(\text{NCS})_4$ species ($\Delta = 4.40$ mm/sec). Ford *et al.* (242, 572) have shown that infrared data support the quadrupole splittings in indicating trans-octahedral structures for Me_2SnXO_4 ($\text{X} = \text{S}, \text{Se}$) and $\text{Me}_2\text{Sn}(\text{SO}_3\text{X})_2$ ($\text{X} = \text{F}, \text{Cl}, \text{CF}_3, \text{Me}, \text{Et}$). It is also interesting to note that, unlike $(\text{Me}_3\text{Sn})_2\text{XO}_4$ ($\text{X} = \text{S}, \text{Se}, \text{Cr}$), adduct formation of pyridine, dimethyl sulfoxide or dimethylformamide with Me_2SnXO_4 ($\text{X} = \text{S}, \text{Se}$) produces a marked lowering of quadrupole splitting (242). The low quadrupole splitting observed for Me_2SnWO_4 is rather curious, and ^{182}W Mössbauer shows a marked asymmetry around the tungsten atom in this compound (254).

Using the rather crude assumption that the $(\text{p.q.s.})^{\text{oct}}$ value for half of a bidentate carboxylate group is approximately 75% of $(\text{p.q.s.})_{\text{O}_2\text{CMe}}^{\text{tet}}$, an estimate of ca. 3.7 mm/sec can be obtained for the quadrupole splittings expected for a trans-octahedral structure for the dialkyltin dicarboxylates. Such structures could arise from either inter- or intramolecular bidentate coordination of the carboxylate groups. The data for the dialkyltin dicarboxylates in Table XXXIII are in reasonable agreement with this prediction, although the quadrupole splittings for the dimethyltin species appear to be rather high.

The quadrupole splittings of the dialkyltin dihalides R_2SnX_2 ($\text{X} = \text{Cl}, \text{Br}, \text{I}$) fall between the values calculated for monomeric tetrahedral structures ($\text{X} = \text{Cl}, \text{Br}, \Delta = 3.16$ mm/sec; $\text{X} = \text{I}, \Delta = 2.77$ mm/sec) and associated trans-octahedral structures ($\text{X} = \text{Cl}, \text{Br}, \Delta = 4.12$ mm/sec; $\text{X} = \text{I}, \Delta = 3.56$ mm/sec), consistent with highly distorted octahedral structure as observed for Me_2SnCl_2 (167). In contrast, the quadrupole splittings of Ph_2SnX_2 ($\text{X} = \text{Cl}, \text{Br}, \text{I}$) are those expected for

TABLE XXXII
MÖSSBAUER DATA FOR SOME R_2SnX_2 SPECIES^{a,b}

X R	F*			Cl†			Br			I			NCS			NCO§			N ₃		
	C.S. ^c	Q.S.	Ref.	C.S. ^c	Q.S.	Ref.	C.S. ^c	Q.S.	Ref.	C.S. ^c	Q.S.	Ref.	C.S. ^c	Q.S.	Ref.	C.S. ^c	Q.S.	Ref.	C.S. ^c	Q.S.	Ref.
Me	1.33	+4.38	<i>d</i>	1.56	+3.55	<i>e</i>	1.60	3.36	<i>f</i>	—	—	—	1.48	3.87	<i>g</i>	1.29	2.84	<i>h</i>	1.06	2.61	<i>i</i>
Et	1.42	4.27	<i>j</i>	1.64	3.64	<i>k</i>	1.70	3.27	<i>l</i>	1.75	3.09	<i>m</i>	1.56	3.96	<i>g</i>	—	—	—	1.23	2.94	<i>i</i>
<i>n</i> -Pr	1.45	4.36	<i>j</i>	1.70	3.60	<i>n</i>	—	—	—	—	—	—	—	—	—	—	—	—	1.15	2.74	<i>i</i>
<i>n</i> -Bu	1.42	4.07	<i>o</i>	1.62	3.40	<i>p</i>	1.65	3.28	<i>q</i>	1.80	2.65	<i>r</i>	1.56	3.90	<i>s</i>	1.31	3.15	<i>h</i>	1.29	2.99	<i>i</i>
Ph	1.28	3.43	<i>j</i>	1.38	2.82	<i>t</i>	1.43	2.54	<i>l</i>	1.51	2.38	<i>l</i>	1.45	3.96	<i>u</i>	—	—	—	—	—	—
*R = Oct			†R = CH ₂ =CH												§R = <i>i</i> -Bu						
1.45 4.31 <i>j</i>			1.45 3.34 <i>l</i>												1.45 3.51 <i>h</i>						
			R = Cyclo-C ₆ H ₁₁												R = Ph·CH ₂						
			1.68 3.44 <i>v</i>												1.12 2.21 <i>h</i>						

^a Where appropriate an average of the data has been taken.

^b Data given in mm/sec at liquid nitrogen temperature.

^c Relative to SnO₂ assuming center shifts of SnO₂ and BaSnO₃ are identical.

Key to references :

^a(167, 217, 290, 327) ^e(138, 141, 167, 171, 289, 336, 367, 442, 528) ^f(442, 528) ^g(258) ^h(383) ⁱ(112) ^j(167) ^k(167, 442) ^l(442) ^m(81, 442)
ⁿ(84) ^o(6, 167, 367) ^p(6, 84, 167, 516) ^q(6, 7, 367, 516) ^r(6, 367) ^s(258, 418, 516) ^t(84, 141, 167, 171, 338, 418, 442, 531) ^u(418) ^v(336, 400)

TABLE XXXIII

MÖSSBAUER DATA FOR SOME FURTHER R_2SnX_2 SPECIES

Compound	C.S. ^{a,b}	Q.S. ^a	Ref.
$Me_2Sn(acac)_2$	1.18	3.93	(323)
$Me_2Sn(O_2CH)_2$	1.30	4.60	(323, 531)
$Me_2Sn(O_2CPH)_2$	1.40	3.96	(323)
$Me_2Sn(O_2CC_5H_4N)_2$	1.28	4.43	(323)
$Me_2SnC_2O_4H_2O$	1.55	4.65	(551)
Me_2SnSO_4	1.61	5.00	(242)
Me_2SnSeO_4	1.52	4.82	(242)
Me_2SnMoO_4	1.42	4.10	(551)
Me_2SnWO_4	1.39	3.53	(551)
$Me_2Sn(NO_3)_2$	1.62	4.13	(516)
$Me_2Sn(SO_3F)_2$	1.82	5.54	(572)
$Me_2Sn(SO_3CF_3)_2$	1.79	5.51	(572)
$Me_2Sn(SO_3Cl)_2$	1.75	5.20	(572)
$Me_2Sn(SO_3Me)_2$	1.52	5.05	(572)
$Me_2Sn(SO_3Et)_2$	1.52	4.91	(572)
$Bu_2Sn[O_2C(CH_2)_nMe]_2^c$	1.34–1.49 ^c	3.23–3.70 ^c	(5, 279, 380)
$Bu_2Sn[O_2C(CH_2)_nCH_2Cl]_2^d$	1.30–1.60 ^d	2.89–3.65 ^d	(5, 367, 380)
$Bu_2Sn(O_2CHCl_2)_2$	1.54	3.73	(367)
$Bu_2Sn(O_2CCl_3)_2$	1.58	3.93	(5, 7, 367)
$Bu_2Sn(O_2CMe=CH_2)_2$	1.43	3.70	(5, 9)
Bu_2Sn maleate	1.44	3.58	(5, 367, 400)
$Bu_2Sn(O_2CPh)_2$	1.60	3.50	(323, 367)
Bu_2SnSO_4	1.66	4.78	(6, 367)
$Ph_2Sn(acac)_2$	0.74	2.14	(234)

^a Data given in mm/sec at liquid nitrogen temperature.^b Relative to SnO_2 assuming that the center shifts of SnO_2 and $BaSnO_3$ are identical.^c Range of data observed for $n = 0, 1, 3, 5, 6, 8, 10$, or 16 .^d Range of data observed for $n = 0, 3, 5$, or 13 ; when appropriate an average of the data has been taken.

tetrahedral structures (400).^{*} Using a similar criterion, Herber *et al.* (112, 383) have assigned tetrahedral structures to the compounds R_2SnX_2 ($X = N_3$, $R = Me, Et, Pr$, or Bu ; $X = NCO$, $R = Me, Bu, i-Bu$, or $PhCH_2$).

In Table XXXIV are given quadrupole splitting data for some organotin trihalides and $BuSn(SCN)_3$, together with calculated quadrupole splittings for monomeric and associated structures. These data are

^{*} A very recent crystal structure of Ph_2SnCl_2 (296) confirms the tetrahedral structure.

clearly consistent with some degree of association, although the quadrupole splitting of $\text{BuSn}(\text{SCN})_3$ appears rather anomalous.

The organotin oxinates (Table XXXV) form an interesting series of compounds. The quadrupole splittings of all dialkyltin dioxinates fall in a very narrow range, while, as expected, that of diphenyltin dioxinate is rather lower, indicative (10, 234, 418, 462) of common *cis*-octahedral structures as found crystallographically for $\text{Me}_2\text{Sn}(\text{ox})_2$ (505). From the

TABLE XXXIV
OBSERVED AND CALCULATED QUADRUPOLE SPLITTINGS
FOR SOME RSnX_3 SPECIES

Compound	Quadrupole splitting ^a			
	Obs.	Ref.	Calculated ^b octahedral	Calculated ^b tetrahedral
MeSnBr_3	1.91	(528)	+2.06	+2.74
EtSnCl_3	1.97	(442)	+2.06	+2.74
EtSnBr_3	1.85	(442)	+2.06	+2.74
$(\text{CH}_2=\text{CH})\text{SnCl}_3$	1.86	(442)	+1.92	+2.56
BuSnCl_3	1.88	<i>c</i>	+2.06	+2.74
PhSnCl_3	1.79	<i>d</i>	+1.90	+2.52
PhSnBr_3	1.62	(442)	+1.90	+2.52
$\text{BuSn}(\text{NCS})_3$	1.46	(258)	+2.20	+3.16

^a Data given in mm/sec at liquid nitrogen temperature.

^b Using $(\text{p.q.s.})_{\text{L}}$ values from Table XXVI, assuming $(\text{p.q.s.})_{\text{CH}_2=\text{CH}}^{\text{oct}} = 0.75 (\text{p.q.s.})_{\text{CH}_2=\text{CH}}^{\text{tet}}$.

^c Average of Refs. (168, 171, 415).

^d Average of Refs. (84, 275, 415, 442, 528).

magnitude of the quadrupole splittings of $\text{R}_2\text{Sn}(\text{ox})_2$ species, it is apparent that $\frac{1}{2}\text{ox}$ has a similar $(\text{p.q.s.})^{\text{oct}}$ value to that of Cl.

Monomeric five-coordinate structures seem probable for the species $\text{R}_2\text{Sn}(\text{ox})\text{X}$ (Table XXV, compounds 4–10) as the observed quadrupole splittings are midway between the values expected for associated structures with either *cis* or *trans* R groups (418, 462). Unfortunately, the additivity description of the quadrupole splittings for the five-coordinate compounds is not sufficiently advanced to speculate on the geometric isomerism of these species or of the compound $\text{Ph}_3\text{Sn}(\text{ox})$. Mullins and Curran (418) have concluded from dipole moment data that the most probable structure for $\text{Ph}_2\text{Sn}(\text{ox})\text{NCS}$ is one with a phenyl

group and nitrogen atom in the axial position. These authors (418) also find some evidence for association in $\text{Bu}_2\text{Sn}(\text{ox})\text{NCS}$, but this does not seem to be reflected in the quadrupole splitting.

Six-coordinate structures have been assigned (415, 462) to the species $\text{R}_2\text{Sn}(\text{ox})_2\text{X}$ (Table XXXV, compounds 11–14), although the

TABLE XXXV
MÖSSBAUER DATA FOR SOME ORGANOTIN OXINATES

Code No. ^a	Compound ^b	C.S. ^{c,d}	Q.S. ^c	Ref.
1	$\text{Ph}_3\text{Sn}(\text{ox})$	1.07	1.75	(462)
2	$\text{R}_2\text{Sn}(\text{ox})_2^e$	0.77–1.13	1.81–2.21	(10, 141, 234, 300, 323, 367, 418, 439, 462)
3	$\text{Ph}_2\text{Sn}(\text{ox})_2$	0.73	1.65	(10, 234, 323, 418, 439, 462)
4	$\text{R}_2\text{Sn}(\text{ox})\text{Cl}^f$	1.26–1.56	2.78–3.36	(462)
5	$\text{Et}_2\text{Sn}(\text{ox})\text{Br}$	1.39	3.08	(462)
6	$\text{Et}_2\text{Sn}(\text{ox})\text{I}$	1.43	2.85	(462)
7	$\text{Et}_2\text{Sn}(\text{ox})\text{NCS}$	1.31	3.07	(462)
8	$\text{Bu}_2\text{Sn}(\text{ox})\text{NCS}$	1.33	3.25	(418)
9	$\text{Ph}_2\text{Sn}(\text{ox})\text{Cl}$	1.10	2.40	(418, 462)
10	$\text{Ph}_2\text{Sn}(\text{ox})\text{NCS}$	0.98	2.48	(418)
11	$\text{BuSn}(\text{ox})_2\text{Cl}$	0.82	1.68	(168, 415, 462)
12	$\text{BuSn}(\text{ox})_2\text{NCS}$	0.76	1.73	(415)
13	$\text{PhSn}(\text{ox})_2\text{Cl}$	0.67	1.48	(415, 462)
14	$\text{PhSn}(\text{ox})_2\text{NCS}$	0.58	1.57	(415)
15	$\text{BuSn}(\text{ox})_3$	0.69	1.76	(168, 462)

^a Code number will be preceded by table number in text.

^b ox = 8-hydroxyquinoline anion.

^c Data given in mm/sec at liquid nitrogen temperature; when appropriate an average has been taken.

^d Relative to SnO_2 , assuming identical center shift for SnO_2 and BaSnO_3 .

^e Range of data for R = Me, Et, Pr, Bu, *i*-Bu, or Oct.

^f Range of data for R = Me, Et, Pr, Bu, or Oct.

quadrupole splittings are rather lower than expected. This seems to be a general phenomenon of six-coordinate monoalkyl- or monophenyltin compounds as shown by the data in Table XXVII. For the compound $\text{BuSn}(\text{ox})_3$ a seven-coordinate structure seems the most probable (168, 462).

Mössbauer data for a wide range of organotin oxygen and sulfur derivatives of general type $\text{R}_3\text{SnXR}'$, $(\text{R}_2\text{SnX})_n$, and $\text{R}_2\text{Sn}(\text{XR}')_2$ (X = O, S) have been reported. Most of the compounds give quadrupole

splittings in the general range 1–3 mm/sec and convenient tabulations of the data are available in Refs. (167, 577). At the present time, the relationship between quadrupole splitting and structure, and especially the degree of association, for these species has not been fully elucidated (167). As mentioned in Section II, E, Goldanskii and his co-workers (424) have exploited frozen solution data to study intermolecular association in the species of type $R_3Sn-S-R'$ and $Et_3Sn-O-C_6H_4 \cdot X \cdot p$, while Davies *et al.* (169) have concluded that compounds of the type $XBu_2SnOSnBu_2X$ [$X = F, Cl, Br, NCS, OSiMe_3, O_2CMe, OC_6H_4 \cdot X' \cdot 4$ ($X' = H, Me, OMe, Cl$)], which show quadrupole splittings in the range 2.74–3.36 mm/sec, have a ladder-type dimeric structure with five-coordinate tin atoms (169). Ford *et al.* (240) from correlation of Mössbauer, IR, and chromatographic studies of compounds $Ph(OCOR')O$ [$R' = (CH_2)_8CH=CH_2, (CH_2)_{16}Me$] have assigned trimeric structures, whereas for the analogous compounds with $R' = CMe_3, CCl_3$, and CF_3 , Poller *et al.* (464) prefer a polymeric structure.

Organotin nitrogen derivatives of type $(R_3Sn)_{3-n}NR_n$ ($n = 0-2$) show relatively small quadrupole splittings (Δ in the range 0–1.84 mm/sec), in keeping with tetrahedral coordination (159). It is interesting that there is a trend to decreasing quadrupole splitting as n varies from 2 \rightarrow 0. In contrast, trialkyl and triphenyl derivatives of the bidentate ligands imadazole, 1,2,4-triazole, benzimidazole, and 1,2,3-benzitriazole show large splittings [Δ in the range 2.59–3.18 mm/sec (336, 440)], consistent with five-coordinate associated structures (336).

Data for a series of five-coordinate complexes of type R_3SnXL are summarized in Table XXXVI. As expected, the coordination of a further ligand to Me_3SnCl produces relatively little variation in quadrupole splitting reflecting the common five-coordinate structure. In contrast, the coordination of a ligand to Ph_3SnX ($X = Cl, Br$) gives rise to a marked increase in quadrupole splitting, probably arising mainly from a change in structure from tetrahedral to trigonal-bipyramidal (556).

Mössbauer data for a great many halide complexes have been reported and a selection of the available data is given in Table XXXVII. The majority of the center shifts show a decrease compared with SnX_4 (10, 103, 457, 574) and show some variation with the nature of the donor atom (103, 457). For example, phosphine derivatives tend to give the most negative shifts, and Carty *et al.* (103) have interpreted this trend in terms of a concentration of $5s$ density in the $Sn-P$ bonds. A more detailed discussion of center shifts is given in Section IV, A, 2.

The small or zero quadrupole splittings observed are expected in view of the very similar (p.q.s.)^{oct} values of ligands such as $dmso, Ph_3XO$ ($X = As, P$), Bu_3PO , py and $\frac{1}{2}(bipy)$ to those of the halogens

(Table XXVI). Yeats *et al.* (574) have suggested that the observation of quadrupole splittings for SnX_4L_2 species in which L is an oxygen donor reflects a weaker donor interaction for the $\text{L} \rightarrow \text{Sn}$ as opposed to the $\text{X} \rightarrow \text{Sn}$ bond. This suggestion is supported by the following observations.

(1) For ligands of type R_2SO , R_2SO_2 , and R_3PO , the shift of $\text{M}-\text{O}$ ($\text{M} = \text{S}, \text{P}$) stretching frequency on complexation, which gives some guide to the strength of the donor bond, tends to be largest for compounds which give single-line spectra.

TABLE XXXVI
MÖSSBAUER DATA FOR SOME FIVE-COORDINATE COMPLEXES^a

Compound ^b	C.S. ^{c,d}	Q.S. ^c	Ref.
Me_3SnCl	1.39	3.30	<i>e</i>
$(\text{Et}_4\text{N})\text{Me}_3\text{SnCl}_2$	1.33	3.28	<i>f</i>
Me_3SnClpy	1.43	3.44	<i>e</i>
$\text{Me}_3\text{SnClPh}_3\text{PO}$	1.45	3.49	(338)
$\text{Me}_3\text{SnClMeCONMe}_2$	1.50	3.69	(338)
$\text{Me}_3\text{SnCl}(\text{C}_5\text{H}_4\text{NOMe-4})$	1.44	3.45	(338)
$\text{Me}_3\text{SnClHMPA}$	1.44	3.52	(338)
Ph_3SnCl	1.35	2.49	<i>g</i>
$(\text{Me}_4\text{N})[\text{Ph}_3\text{SnCl}_2]$	1.32	3.00	(442)
$(\text{Ph}_3\text{PC}_{10}\text{H}_{21})[\text{Ph}_3\text{SnCl}_2]$	1.23	2.87	(207)
$\text{Ph}_3\text{SnClR}_2\text{SO}$	1.26–1.30	3.08–3.25	<i>h</i>
$\text{Ph}_3\text{SnCl}(\text{RO})_3\text{PO}$	1.30–1.31	3.07–3.18	<i>i</i>
$\text{Ph}_3\text{SnClPh}_3\text{PO}$	1.29	3.19	<i>j</i>
$\text{Ph}_3\text{SnClPh}_3\text{AsO}$	1.29	3.09	(556)
$\text{Ph}_3\text{SnClpyO}$	1.30	3.03	(556)
$\text{Ph}_3\text{SnCl}(\text{Me}_2\text{NCHO})$	1.31	2.84	(556)
Ph_3SnBr	1.32	2.48	<i>g</i>
$(\text{Ph}_3\text{PC}_{10}\text{H}_{21})[\text{Ph}_3\text{SnBr}_2]$	1.29	2.87	(207)
$\text{Ph}_3\text{SnBrpyO}$	1.28	3.03	(207)
$\text{Ph}_3\text{SnBrPh}_3\text{PO}$	1.29	3.20	(207)
$\text{Ph}_3\text{SnBrMe}_2\text{SO}$	1.31	3.22	(207)

^a Only a selection of the available data is given; note that Ph_3SnCl and Ph_3SnBr are four-coordinate.

^b HMPA = hexamethylphosphoramide, pyO = pyridine *N*-oxide.

^c Data given in mm/sec at liquid nitrogen temperature.

^d relative to SnO_2 , assuming zero shift for BaSnO_3 .

^e Average of data quoted in Ref. (516).

^f Average of data from Refs. (171, 442).

^g Average of data from Refs. (207, 516).

^h Range of data for $\text{R} = \text{Me}, \text{Pr}, \text{Bu}, \frac{1}{2}(\text{CH}_2)_4$ (207, 556).

ⁱ Range of data for $\text{R} = \text{Me}, \text{Et}, \text{Ph}$ (556).

^j Average of data from Refs. (207, 556).

(2) Larger quadrupole splittings are observed for derivatives of the weaker acceptor SnBr_4 (457).

(3) The Sn—O bond distances in $\text{SnCl}_4 \cdot 2\text{POCl}_3$ [2.30 and 2.25 Å (77)], which shows a quadrupole splitting of 1.12 mm/sec (574), are larger than those of $\text{SnCl}_4 \cdot 2\text{MeSO}$ [2.17 and 2.10 Å (315)] or $\text{SnCl}_4 \cdot 2\text{SeOCl}_2$ [2.12 Å (337)] for which no quadrupole splittings are observed.

(4) Most complexes with nitrogen donor ligands, which are thought to be better donors than analogous oxygen derivatives, do not give quadrupole splittings. Of particular interest in this context are the complexes of the bidentate ligand pyrazine. Thus, the 1:2 derivative, $\text{SnCl}_4 \cdot 2\text{pyz}$ does not show quadrupole splitting, whereas the 1:1 derivatives, $\text{SnX}_4 \cdot \text{pyz}$ ($\text{X} = \text{Cl}, \text{Br}, \text{I}$) (Table XXXVII, compounds 65–67), which probably have bridging pyz groups and, hence, a weaker interaction, show quadrupole splitting which increase in the order $\text{Cl} > \text{Br} > \text{I}$ (286). Similar quadrupole splittings are observed for RCN adducts (Table XXXVII, compounds 25, 26) in which the *sp* hybridization of the nitrogen atom will also be expected to result in a weaker interaction.

Yeats *et al.* (574) also note that the trend of quadrupole splitting for the species $\text{SnCl}_4 \cdot \text{R}_2\text{SO}$ (Table XXXVII, compounds 1–4) suggest that steric effects may be important.

In contrast to oxygen and nitrogen donor adducts, the data for phosphine and arsine complexes indicate that the quadrupole splittings arise from an increased donor interaction in the Sn—P as compared with the Sn—Cl bond. Thus, Cunningham *et al.* (152) and Carty *et al.* (103) have

TABLE XXXVII

MÖSSBAUER PARAMETERS FOR SOME HALIDE COMPLEXES OF Sn^{IVa}

Code No.	Compound ^b	C.S. ^{c,d}	Q.S. ^c	Ref.
	$\text{SnCl}_4 \cdot 2\text{L}$ (L)			
1	Me_2SO	0.38	—	<i>e</i>
2	Et_2SO	0.36	Small	(574)
3	<i>n</i> - Pr_2SO	0.38	0.59	(574)
4	<i>n</i> - Bu_2SO	0.37	0.67	(574)
5	$(\text{Me}_2\text{O})_2\text{SO}$	0.34	—	(574)
6	$\frac{1}{2}(\text{R}_2\text{SO}_2)^f$	0.38–0.51	0.83–1.57	(574)
7	$\text{Ph}_n\text{CCl}_{3-n}\text{PO}^g$	0.27–0.51	0.50–1.61	<i>e</i>
8	<i>n</i> - Bu_3PO	0.24	—	(574)
9	$\text{Cl}_n(\text{PhO})_{3-n}\text{PO}^h$	0.34–0.42	0.71–1.13	(574)
10	Ph_3AsO	0.44	0.70	(574)

continued

TABLE XXXVII—*continued*
 MÖSSBAUER PARAMETERS FOR SOME HALIDE COMPLEXES OF Sn^{IVa}

Code No. ^a	Compound ^b	C.S. ^c		Ref.
11	pyO	0.42	—	(574)
12	Cl_2SeO	0.37	—	(574)
13	$(\text{Me}_2\text{N})_3\text{PO}$	0.31	0.70	(457)
14	$(\text{Me}_2\text{N})_2\text{CO}$	0.35	0.75	(457)
15	$\frac{1}{2}[\text{MeO}(\text{CH}_2)_3\text{OMe}]$	0.51	0.80	(457)
16	oxH	0.45	—	<i>i</i>
17	SalH	0.43	1.10	(10)
18	ROH ^j	0.33–0.43	0.50–0.70	(349)
19	$(\text{Me}_2\text{N})_2\text{CS}$	0.70	—	(457)
20	$\frac{1}{2}[\text{MeS}(\text{CH}_2)_2\text{SMe}]$	0.70	—	(457)
21	$\frac{1}{2}(\text{bipy})$	0.45	—	<i>k</i>
22	py	0.51	—	(457)
23	$\frac{1}{2}(\text{en})$	0.61	—	(457)
24	NMe_2	0.59	—	(152)
25	MeCN	0.41	0.81	(152, 349)
26	PhCN	0.41	0.77	(152)
27	$\text{F}^-, \text{Cl}^-, \text{Br}^-, \text{I}^-$	0.29–0.78	—	<i>l</i>
28	Ph_3P	0.77	—	(103, 152)
29	RPh_2P^m	0.63–0.81	0.45–0.58	(103, 152)
30	R_2PhP^n	0.85–0.88	0.97–1.04	(103, 152)
31	R_3P^o	0.85–0.89	0.95–1.15	(103, 152, 457)
32	$\frac{1}{2}(\text{Ph}_2\text{P} \cdot \text{CH}_2 \cdot \text{PPh}_2)$	0.69	—	(152)
33	$\frac{1}{2}[\text{Ph}_2\text{P}(\text{CH}_2)_2\text{PPh}_2]$	0.72	—	(103)
34	AsPh_3	0.81	—	(152)
35	AsEt_3	0.87	0.90	(152)
	$\text{SnBr}_4 \cdot 2\text{L}$ (L)			
36	Me_2SO	0.66	—	(457)
37	$(\text{Me}_2\text{N})_2\text{CO}$	0.70	—	(457)
38	$(\text{Me}_2\text{N})_3\text{PO}$	0.56	0.76	(457)
39	Ph_3PO	0.63	0.61	(457)
40	$\frac{1}{2}[\text{MeO}(\text{CH}_2)_2\text{OMe}]$	0.81	—	(457)
41	oxH	0.65	—	(10)
42	SalH	0.73	1.22	(10)
43	$\text{C}_4\text{H}_8\text{S}$	0.99	—	(457)
44	$(\text{Me}_2\text{N})_2\text{CS}$	0.94	—	(457)
45	$\text{MeS}(\text{CH}_2)_2\text{SMe}$	0.97	—	(457)
46	NH_2CS	0.80	—	(278)
47	$\frac{1}{2}(\text{bipy})$	0.70	—	<i>k</i>
48	py	0.74	—	(457)
49	NMe_2	0.90	—	(152)
50	$\text{F}^-, \text{Cl}^-, \text{Br}^-, \text{I}^-$	0.53–1.01	—	<i>l</i>
51	Ph_3P	0.63	0.66	(457)
52	<i>n</i> - Bu_3P	1.03	1.01	(152)

TABLE XXXVII—*continued*

Code No.	Compound ^b	C.S. ^{c,d}	Q.S. ^c	Ref.
53	AsPh ₃	1.06	—	(152)
54	AsEt ₃	1.02	0.83	(152)
	SnI ₄ ·2L (L)			
55	oxH	0.91	—	(10)
56	$\frac{1}{2}$ (bipy)	0.95	—	(300)
57	NMe ₃	1.30	—	(152)
58	Cl ⁻ , Br ⁻ , I ⁻	0.98–1.60	—	<i>l</i>
59	Sn(SpyO) ₂ X ₂ ^p	0.32–0.90	0.60–0.82	(455)
60	PcSnX ₂ ^q	0.03–0.45	0 –1.13	(433, 530)
61	Sn(porph)X ₂ ^r	(–)0.06–0.24	<i>r</i>	(433)
62	Sn(ox) ₂ X ₂ ^s	0.30–0.61	—	<i>s</i>
63	Sn(Sal) ₂ X ₂ ^t	0.23–0.41	—	<i>t</i>
64	SnCl ₄ (pyz) ₂	0.43	—	(286)
65	SnCl ₄ pyz	0.38	0.60	(286)
66	SnBr ₄ pyz	0.85	0.92	(286)
67	SnI ₄ pyz	1.48	0.96	(286)

^a Only a selection of data is given. Further data may be found in the references quoted in Table XXXVIII and in Ref. (577). In text code number will be preceded by table number.

^b oxH = 8 oxiquinoline; SalH = salicylaldehyde; en = Me₂N·(CH₂)₂NMe₂; bipy = 2,2'-bipyridyl; py = pyridine; HSpyO = 2-pyridinethiol-1-oxide; Pc = phthalocyanine; pyz = pyrazine.

^c Data given in mm/sec.

^d Relative to SnO₂, assuming center shift of BaSnO₃ is zero and Pd(Sn) is 1.52 mm/sec.

^e Average of data from Refs. (457, 574).

^f Range of data for R = Me, Et, *n*-Pr, *n*-Bu, Ph, and $\frac{1}{2}$ (CH₂)₄.

^g Range of data for *n* = 0, 1, 3.

^h Range of data for *n* = 0, 1, 2.

ⁱ Average of data from Refs. (10, 300).

^j Range of data for R = Me, Et, *n*-Pr, *i*-Pr.

^k Average of data from Refs. (300, 457).

^l Range of data from Table XXXVIII.

^m Range of data for R = Me, Et, MeO.

ⁿ Range of data for R = Et, Me.

^o Range of data for R = Et, *n*-Pr, *n*-Bu.

^p Range of data for X = F, Cl, Br, I.

^q Range of data for X = F, Cl, Br, I, OH.

^r X = F, Cl, OH; porph = tetra(4-X'-C₆H₄)porphine (X' = MeOH, Me, Cl, H); only X = OH, X' = Cl show a quadrupole splitting (0.76 mm/sec).

^s Range of data for X = Cl, Br, I from Table XXXVIII.

^t Range of data for X = Cl, Br, I from Table XXXVIII.

noted that while the complexes $\text{SnCl}_4 \cdot 2\text{LPh}_3$ ($\text{L} = \text{As}, \text{P}$) do not show quadrupole splittings, the substitution of alkyl for phenyl, which will increase the donor ability of the LR_3 group, gives rise to quadrupole splitting. The overall quadrupole splitting trends are consistent with the order of donor ability of the ligands $\text{R}_3\text{P} \sim \text{R}_3\text{As} > \text{Ph}_3\text{P} \sim \text{Ph}_3\text{As} \geq \text{N}(sp^2) \sim \text{N}(sp^3) \sim \text{Cl} > \text{N}(sp)$.

The quadrupole splittings observed for the species $\text{Sn}(\text{SpyO})_2\text{X}_2$ (455) are of interest as from (p.q.s.)_L^{oct} values, these may be attributed to the greater donor power of SpyO as opposed to halogen. The PcSnX_2 derivatives (433) form the only series of sp^2 nitrogen donors to give quadrupole splittings and it is curious that analogous tetraarylporphyrin derivatives [with the exception of dihydroxytetra(*p*-tolyl)porphyrinotin-(IV)] give single-line spectra (433).

Very little correlation between quadrupole splitting and ligand geometry has been found for the halide complexes. One example is provided by species $\text{SnCl}_4(\text{Ph}_2\text{P}(\text{CH}_2)_n\text{PPh}_2)$ ($n = 1, 2$), for which the lack of quadrupole splitting may be associated with *cis* geometry, as opposed to $\text{SnCl}_4 \cdot 2\text{PRPh}_2$ species, which are probably *trans* and which give quadrupole splittings in the range 0.45–0.58 mm/sec (103, 152). However, the quadrupole splittings of the species $\text{Sn}(\text{SpyO})_2\text{X}_2$ ($\text{X} = \text{F}, \text{Cl}, \text{Br}$) fall between the values calculated for *trans* (ca. 0.92 mm/sec) and *cis* (ca. 0.46 mm/sec) geometries. Clausen and Good (127) have attributed the large line-width found for the species SnX_4F_2 ($\text{X} = \text{Cl}, \text{Br}$) ($\Gamma = 1.09, 1.43$ mm/sec) compared with the other halide anions ($\Gamma = 0.94$ – 1.19 mm/sec) to *trans* structures, whereas Yeats *et al.* (574) have isolated two forms of $\text{SnCl}_2 \cdot 2(n\text{-Pr}_2\text{SO}_2)$ with quadrupole splittings approximating to a 2 : 1 ratio as expected for a *cis-trans* pair.

2. Center Shifts

The center shifts of tin(IV) compounds are smaller than those of gray tin, reflecting the transition from the $5sp^3$ configuration of gray tin to the $4d^{10}$ configuration anticipated for a "perfect" Sn^{4+} ion. Increasing polarity of the tin–ligand bonds would be expected to result in a decrease in center shift with a limiting value corresponding to that of a perfect Sn^{4+} ion.

Some evidence for such trends has been found for compounds in which all the tin–ligand bonds are reasonably polar; a selection of data for these types of compounds is given in Table XXXVIII. The center shifts of the series of halide anions (Table XXXVIII, compounds 9–20) correlate (127, 168, 330) well with the average electronegativity of the ligands, and similar correlations have been found (273) for the tetrahalides [excluding SnF_4 which has a different structure (374) to the other

halides]. These trends are illustrated in Fig. 11. The center shifts of these compounds have also been correlated with S.C.F.M.O. calculations (299).

Further evidence of a general trend to lower center shifts with decreasing size of the halogen atom is provided by the series PcSnX_2 (Table XXXVIII, compounds 23–26) (433); $\text{Sn}(\text{SpyO})_2\text{X}_2$ (compounds 28–31) (455); $\text{SnX}_4 \cdot 2\text{oxH}$ (compounds 38–40) (10); $\text{Sn}(\text{sal})_2\text{X}_2$ (compounds 41–43) (10); $\text{Sn}(\text{ox})_2\text{X}_2$ (compounds 35–37) (10); $\text{SnX}_4 \cdot 2\text{NR}_3$ ($\text{R} = \text{Me}$ or Et) (compounds 49–52) (152), and $(\text{SnCl}_4 \cdot \text{pyz})_n$ (compounds 53–55) (286), while there is also a gradual decrease in center shift as chlorine is replaced by ligand in the series SnCl_6^{2-} , SnCl_4 (2oxH),

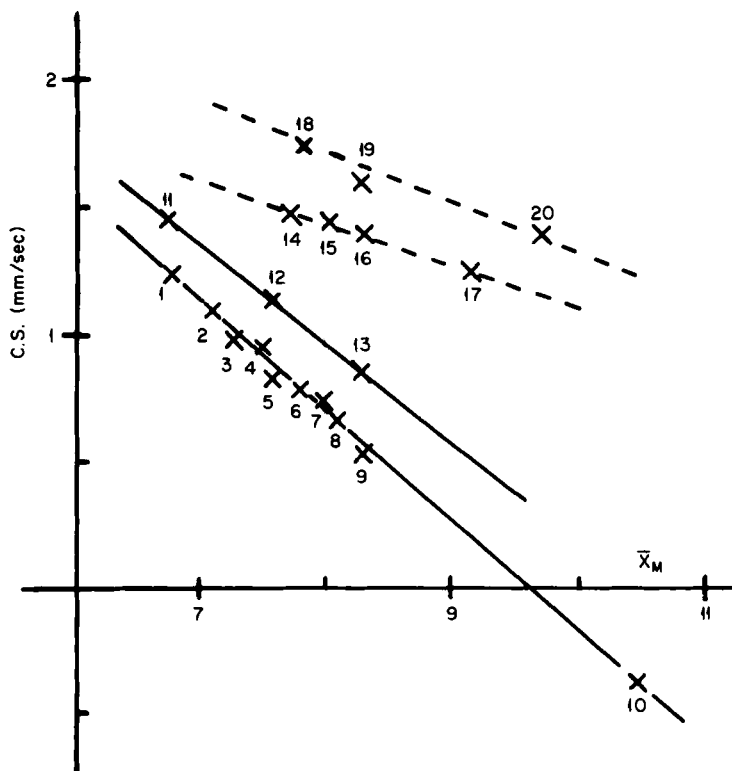


FIG. 11. Center shift versus average electronegativity (441). Data from (330) (points 1–9), Pauling scale, 2.2 assumed for methyl group (14–20). Data from (127) (points 1–10), Mulliken scale, 8.3 assumed for methyl group (points 14–20). Key: (1) SnI_6^{2-} , (2) $\text{SnBr}_2\text{I}_4^{2-}$, (3) $\text{SnCl}_2\text{I}_4^{2-}$, (4) $\text{SnBr}_4\text{I}_2^{2-}$, (5) SnBr_6^{2-} , (6) $\text{SnCl}_4\text{I}_2^{2-}$, (7) $\text{SnCl}_2\text{Br}_4^{2-}$, (8) $\text{SnCl}_4\text{Br}_2^{2-}$, (9) SnCl_6^{2-} , (10) SnF_6^{2-} , (11) SnI_4 , (12) SnBr_4 , (13) SnCl_4 , (14) Me_3SnI , (15) Me_3SnBr , (16) Me_3SnCl , (17) Me_3SnF , (18) $\text{Me}_2\text{SnBr}_4^{2-}$, (19) $\text{Me}_2\text{SnCl}_4^{2-}$, (20) $\text{Me}_2\text{SnF}_4^{2-}$.

$\text{SnCl}_3\text{ox} \cdot \text{oxH}$, and SnCl_2ox_2 (10). These types of correlations have been used by Herber *et al.* (112, 383) to assign Mulliken group electronegativities to N_3^- [8.54 (112)] and NCO^- [9.68 (383)]. Unexpectedly, the compounds SnOX_2 (Table XXXVIII, compounds 56–58) show a gradual decrease in center shift with increasing size of the halogen atom (113), and this trend has been explained in terms of the probable bonding (113).

Correlations have also been found between center shift and coordination number (10, 103, 316, 440, 457, 513, 574). Thus, the series SnCl_4 , $[\text{SnCl}_5]^-$, and $[\text{SnCl}_6]^{2-}$ show a decrease in center shift, and a further decrease is found for the seven-coordinate compounds $(\text{SnX}(\text{pic})_3)$ ($\text{X} = \text{Cl}, \text{Br}$) (Table XXXVIII, compounds 60, 61) (421) and the eight-coordinate species $\text{Sn}(\text{ox})_4$ and Pc_2Sn (Table XXXVIII, compounds 48, 59) (10, 421). It is, in fact, a general observation, exemplified by the data in Table XXXVIII, that coordination of donor ligands to SnCl_4 results in a decrease in center shift.

The effect of coordination number on center shift has been attributed (440) to a lengthening of the tin–ligand bonds with increasing coordination number, as illustrated by the bond lengths of SnCl_4 (2.32 Å), SnCl_5^- (2.37 Å), and SnCl_6^{2-} (2.42 Å) (79, 111). An alternative explanation (513) is that the participation of $5d$ orbitals in the bonding produces a greater shielding of the $5s$ electrons. Both effects are, in fact, complementary, as increased d orbital participation will produce bond lengthening owing to the larger radial functions.

The dependence of center shift on coordination number for these types of compounds has enabled structural assignments to be made. For example, Ali *et al.* (10) have used the similarity of the center shifts of SnCl_3ox (Table XXXVIII, compound 44), SnCl_2ox_2 (compound 35), and $\text{SnCl}_3\text{ox} \cdot \text{oxH}$ (compound 45) to assign a polymeric structure to SnCl_3ox . In a similar manner, the center shifts of the pairs of compounds SnCl_3ox_3 , Snox_4 (Table XXXVIII, compounds 47, 48) and $\text{SnCl}_4 \cdot \text{oxH}$, $\text{SnCl}_4 \cdot 2\text{oxH}$ (Table XXXVIII, compounds 46, 47) indicate polymeric structures for SnCl_3ox_3 and $\text{SnCl}_4 \cdot \text{oxH}$ containing eight- and six-coordinate tin atoms, respectively (10). These assignments have been confirmed (10) by the observation of room temperature Mössbauer effects for SnCl_3ox , SnCl_3ox_3 , and $\text{SnCl}_4 \cdot \text{oxH}$.

Attempts have been made to estimate the center shift of a “perfect” Sn^{4+} ion. Some authors have suggested that the $[\text{SnF}_6]^{2-}$ ion, which gives the lowest observed center shift, is essentially ionic and that the center shifts of these compounds may be taken as representative of that of an Sn^{4+} ion (381). An alternative approach has been suggested by Goldanskii *et al.*, who compared the relative center shifts of the tin tetrahalides with estimates of the ionic characters of the tin–halogen bonds from

electro-negativity, NQR, and dielectric permittivity data (273, 276). Extrapolation to 100% ionic character yielded a center shift of 2.9 mm/sec relative to SnO_2 for the Sn^{4+} ion. This value is much lower than the center shift of $[\text{SnF}_6]^{2-}$ ions and, if correct, indicates that the $[\text{SnF}_6]^{2-}$ ion has a substantial degree of covalent character. Such a conclusion is supported by S.C.F.M.O. calculations (299), which show a significant $5s$ and $5p$ population for $[\text{SnF}_6]^{2-}$. It is also interesting that the calculated center shifts of Sn^{4+} (-5.0 mm/sec) and Sn^{2+} (5.6 mm/sec; see Section IV, E) ions from gray tin, which correspond to a loss and a gain of $5s$ electrons, respectively, are remarkably similar in magnitude.

The straightforward correlation of center shift with bond polarity and coordination number does not extend to organotin compounds. From the trends outlined above, it might be anticipated that the substitution of an electronegative ligand, X, into R_4Sn would produce a reduction in center shift, which is proportional to the electron-withdrawing ability of X. Further, it would be expected that an increase in coordination number would result in a further lowering of center shift and that for isostructural compounds the center shift would increase with the number of Sn-R bonds and vary with the nature of the ligands. An appraisal of the available center shift data reveals that many of these expected trends are absent.

Let us first consider the variation of center shift with bond polarity. The center shift data for the tetrahedral R_3SnX species in Table XVIII, the tetrahedral halides Neo_3SnX ($\text{X} = \text{F}, \text{Cl}, \text{Br}, \text{I}$) and Ph_3SnX ($\text{X} = \text{Cl}, \text{Br}, \text{I}$) in Table XX, and the tetrahedral acetates $\text{Ph}_3\text{SnO}_2\text{CR}'$ ($\text{R}' = \text{CMe}=\text{CH}_2, \text{CHEtBu}, \text{CMe}_3$) in Table XXIX show a remarkable consistency and give no evidence of trend to decreasing center shift with increasing bond polarity (114, 115, 440). On the other hand, some evidence for such a trend may be found for five- and six-coordinate compounds as illustrated by the series of compounds $\text{Et}_2\text{Sn}(\text{ox})\text{X}$ ($\text{X} = \text{Cl}, \text{Br}, \text{I}$), $\text{Ph}_2\text{SnX}_2\text{phen}$ ($\text{X} = \text{Cl}, \text{Br}, \text{I}$), and $\text{R}_2\text{SnX}_2\text{bipy}$ ($\text{R} = \text{Bu}, \text{Ph}, \text{X} = \text{Cl}, \text{Br}, \text{I}$) (Table XXXIX), which show a decrease in center shift with decreasing halogen size (417, 462, 465). Similarly, linear relationships have been found (Fig. 11) between center shift and Mulliken electronegativity of the X ligand for the series Me_3SnX ($\text{X} = \text{F}, \text{Cl}, \text{Br}, \text{I}, \text{OH}$) (383) and $[\text{Me}_2\text{SnX}_4]^{2-}$ ($\text{X} = \text{Cl}, \text{Br}, \text{I}$) (441). However, these types of correlations are not general for five- and six-coordinate compounds as illustrated by the trimethyl- and triethyltin haloacetates (Table XXIX).

The effects of varying the number of R groups are also rather unexpected; for example, consider the series of compounds in Table XL. The expected increase in center shift with alkyl or aryl substitution is

TABLE XXXVIII
 SOME CENTER SHIFT DATA FOR Sn^{IV} COMPOUNDS

Code No. ^a	Compound ^b	C.S. ^c	Ref.
1	SnF_4	-0.25	(139)
2	SnCl_4	0.85	(139)
3	SnBr_4	1.14	(139)
4	SnI_4	1.45	(139)
5	SnS_2	1.20	(139)
6	SnO_2	0.00	(139)
7	SnCl_5^-	0.47-0.63 ^d	d
8	SnBr_5^-	0.93-0.99 ^e	(316)
9	SnF_6^{2-}	(-)0.26-(-)0.50 ^f	f
10	$\text{SnCl}_4\text{F}_2^{2-}$	0.29 ^g	(127)
11	SnCl_6^{2-}	0.48-0.52 ^g	g
12	$\text{SnCl}_4\text{Br}_2^{2-}$	0.62-0.67 ^h	h
13	$\text{SnCl}_4\text{I}_2^{2-}$	0.53-0.78 ^j	j
14	$\text{SnBr}_4\text{F}_2^{2-}$	0.53 ⁱ	(127)
15	$\text{SnBr}_4\text{Cl}_2^{2-}$	0.65-0.77 ^j	j
16	SnBr_6^{2-}	0.84-0.90 ^k	k
17	$\text{SnBr}_4\text{I}_2^{2-}$	0.89-1.01 ^p	p
18	$\text{SnI}_4\text{Cl}_2^{2-}$	0.98-1.17 ^j	j
19	$\text{SnI}_4\text{Br}_2^{2-}$	1.09-1.35 ^j	j
20	SnI_6^{2-}	1.23-1.60 ^l	l
21	$\text{Sn}(\text{NCO})_6^{2-}$	(-)0.05-(-)0.10 ^m	(383)
22	$\text{Sn}(\text{N}_3)_6^{2-}$	0.48 ⁿ	(112)
23	PcSnF_2	0.03 ^o	(433)
24	PcSnCl_2	0.28 ^o	(433)
25	PcSnBr_2	0.34 ^o	(433)
26	PcSnI_2	0.45 ^o	(433)
27	$\text{PcSn}(\text{OH})_2$	0.09 ^o	(433)
28	$\text{Sn}(\text{SpyO})_2\text{F}_2$	0.32	(455)
29	$\text{Sn}(\text{SpyO})_2\text{Cl}_2$	0.59	(455)
30	$\text{Sn}(\text{SpyO})_2\text{Br}_2$	0.69	(455)
31	$\text{Sn}(\text{SpyO})_2\text{I}_2$	0.90	(455)
32	$\text{Sn}(\text{pic})_2\text{Cl}_2$	0.31	(421)
33	$\text{Sn}(\text{pic})_2\text{Br}_2$	0.44	(421)
34	$\text{Sn}(\text{pic})_2\text{I}_2$	0.64	(421)
35	$\text{Sn}(\text{ox})_2\text{Cl}_2$	0.30, 0.32	(10, 300)
36	$\text{Sn}(\text{ox})_2\text{Br}_2$	0.44	(10)
37	$\text{Sn}(\text{ox})_2\text{I}_2$	0.61	(10)
38	$\text{SnCl}_4(\text{oxH})_2$	0.45	(10, 300)
39	$\text{SnBr}_4(\text{oxH})_2$	0.65	(10)
40	$\text{SnI}_4(\text{oxH})_2$	0.91	(10)
41	$\text{Sn}(\text{sal})_2\text{Cl}_2$	0.23	(10)
42	$\text{Sn}(\text{sal})_2\text{Br}_2$	0.28	(10)
43	$\text{Sn}(\text{sal})_2\text{I}_2$	0.41	(10)

TABLE XXXVIII—continued

Code No. ^a	Compound ^b	C.S. ^c	Ref.
44	Sn(ox)Cl ₃	0.34	(10)
45	Sn(ox)Cl ₃ oxH	0.37	(10)
46	SnCl ₄ oxH	0.42, 0.43	(10, 300)
47	Sn(ox) ₃ Cl	0.11	(10)
48	Sn(ox) ₄	0.03	(10)
49	SnF ₄ (NEt ₃) ₂	-0.22	(152)
50	SnCl ₄ (NMe ₃) ₂	0.59	(152)
51	SnBr ₄ (NMe ₃) ₂	0.90	(152)
52	SnI ₄ (NMe ₃) ₂	1.30	(152)
53	(SnCl ₄ pyz) _n	0.38	(286)
54	(SnBr ₄ pyz) _n	0.85	(286)
55	(SnI ₄ pyz) _n	1.48	(286)
56	SnOCl ₂	0.25	(113)
57	SnOBr ₂	0.22	(113)
58	SnOI ₂	0.16	(113)
59	Pc ₂ Sn	0.11	(433)
60	Sn(pic) ₃ Cl ₂	0.15	(421)
61	Sn(pic) ₃ Br ₂	0.18	(421)

^a In the text, the code number will be preceded by the table number.

^b oxH = 8-hydroxyquinoline; Pc = phthalocyanine; HSPyO = 2-pyridinethiol 1-oxide; picH = picolinic acid; salH = salicylaldehyde.

^c Data given in mm/sec relative to SnO₂, assuming identical center shifts for SnO₂ and BaSnO₃; only a selection of the available data has been included.

^d Range of values for the cations Et₄N⁺ (442), Ph₃C⁺ (316), Ph₂(4-Me-C₆H₄)C⁺ (316), Ph(4-Me-C₆H₄)₂C⁺ (316), and (4-Me-C₆H₄)₃C⁺ (316).

^e Range of values for the cations Ph₃C⁺ (316), Ph₂(4-Me-C₆H₄)C⁺ (316), Ph(4-Me-C₆H₄)C⁺ (316).

^f Range of values for the cations Li⁺ (534), K⁺ (127, 168, 278, 534), Rb⁺ (534), Cu²⁺ (534), Sr²⁺ (534), Be²⁺ (534), and Cs⁺ (137, 278).

^g Range of values for the cations K⁺ (316, 330), NH₄⁺ (316), Me₄N⁺ (316, 330), Et₄N⁺ (127, 168), MeNH₃⁺ (300, 457), tropanylium (316), Ph(4-Me-C₆H₄)₂C⁺ (316), and (4-Me-C₆H₄)₃C⁺ (316).

^h Range of data for the cations Me₄N⁺ (330), and Et₄N⁺ (127, 168).

ⁱ Cation = Et₄N⁺.

^j Range of data for the cations Me₄N⁺ (330), and Et₄N⁺ (127, 168).

^k Range of data for the cations Et₄N⁺ (127, 168, 457), Me₄N⁺ (316, 330), K⁺ (330), NH₄⁺ (300), tropanylium (316), Ph(4-Me-C₆H₄)₂C⁺ (316), and (4-Me-C₆H₄)₃C⁺ (316).

^l Range of data for the cations Et₄N⁺ (127, 168, 330), Me₄N⁺ (300, 330), and K⁺ (330).

^m Values for the cations Me₄N⁺ and Et₄N⁺, respectively.

ⁿ Cation is Me₄N⁺.

^o For an alternative set of data, see Ref. (530).

^p Range of data for the cations Me₄N⁺ (330), Et₄N⁺ (127, 168), and NH₄⁺ (330).

TABLE XXXIX
SOME CENTER SHIFT DATA FOR FIVE- AND SIX-COORDINATE
Sn^{IV} COMPOUNDS

Compound ^a	C.S. ^b	Ref.
Bu ₂ SnCl ₂ phen	1.59	(417)
Bu ₂ SnBr ₂ phen	1.63	(417)
Bu ₂ SnI ₂ phen	1.69	(417)
Bu ₂ SnCl ₂ bipy	1.56	(417)
Bu ₂ SnBr ₂ bipy	1.62	(417)
Bu ₂ SnI ₂ bipy	1.70	(417)
Ph ₂ SnCl ₂ bipy	1.26, 1.22	(418, 465)
Ph ₂ SnBr ₂ bipy	1.33	(465)
Ph ₂ SnI ₂ bipy	1.41	(465)
Et ₂ Sn(ox)Cl	1.34	(462)
Et ₂ Sn(ox)Br	1.39	(462)
Et ₂ Sn(ox)I	1.43	(462)
K ₂ [Me ₂ SnF ₄]	1.38	(442)
[Me ₂ SnCl ₄] ²⁻	1.59 ^c , 1.63 ^d	(234, 442)
Cs ₂ [Me ₂ SnBr ₄]	1.76	(442)

^a phen = 1,10-Phenanthroline; bipy = 2,2'-bipyridyl;
ox = 8-oxyquinoline.

^b Data given in mm/sec assuming identical center shifts
for SnO₂ and BaSnO₃; data from Refs. (417), (418) have
been converted assuming a center shift of 1.52 for Pd(Sn).

^c Cation is pyridinium.

^d Cation is Cs⁺.

TABLE XL
CENTER SHIFT^a AS A FUNCTION OF THE NUMBER OF Sn-R BONDS

Compound	n =				
	0	1	2	3	4
Et _n SnCl _{6-n} ²⁻	0.52 ^b	1.10 ^b	1.64 ^b	—	—
Et _n SnCl _{5-n} ⁻	0.59 ^b	1.18 ^b	1.54 ^b	1.50 ^b	—
Me _n Sn(C ₆ F ₅) _{4-n}	1.04 ^c	1.19 ^c	1.25 ^c	1.27 ^d	1.21 ^c
Ph _n Sn(C ₆ F ₅) _{4-n}	1.04 ^c	1.16 ^c	1.22 ^c	1.25 ^c	1.22 ^c

^a Data given in mm/sec relative to SnO₂ at liquid nitrogen temperature.

^b Ref. (442).

^c Ref. (528).

^d Ref. (440).

observed in early stages of the series, i.e., $[\text{SnCl}_6]^{2-} < [\text{EtSnCl}_5]^{2-} < [\text{Et}_2\text{SnCl}_4]^{2-}$; $[\text{SnCl}_5]^- < [\text{EtSnCl}_4]^- < [\text{Et}_2\text{SnCl}_3]^-$, and $\text{Sn}(\text{C}_6\text{F}_5)_4 < \text{RSn}(\text{C}_6\text{F}_5)_3 < \text{R}_2\text{Sn}(\text{C}_6\text{F}_5)_2$ ($\text{R} = \text{Me}, \text{Ph}$). Further substitution may arrest the decrease $[\text{R}_n\text{Sn}(\text{C}_6\text{F}_5)_{4-n}]$ ($n = 2, 3, 4$; $\text{R} = \text{Me}, \text{Ph}$) or even reverse it $[\text{EtSnX}_{5-n}]$ ($n = 2, 3$). There is also strong evidence that octahedral *cis*- R_2SnX_4 species have lower center shifts than octahedral *trans*- R_2SnX_4 compounds (421, 441). Thus, Table XLI contains center shifts for pairs of R_2SnX_4 compounds with similar X ligands but with

TABLE XLI

CENTER SHIFT DATA FOR SOME COMPOUNDS OF TYPE *cis*- AND *trans*- R_2SnX_4

Code No. ^a	Compound (cis) ^c	C.S. ^b	Ref.	Compound (trans)	C.S. ^b	Ref.
1	$\text{Ph}_2\text{Sn}(\text{S}_2\text{CNPh}_2)_2$	1.19	(233)	$\text{R}_2\text{Sn}(\text{S}_2\text{CNPh}_2)_2^d$	1.54–1.72	(233)
2	$\text{Ph}_2\text{Sn}(\text{S}_2\text{CNEt}_2)_2$	1.17	(233)	$\text{Me}_2\text{Sn}(\text{S}_2\text{CNEt}_2)_2$	1.57	(233)
3	$\text{Ph}_2\text{Sn}[\text{S}_2\text{CN}(\text{CH}_2)_4]_2$	1.17	(233)	$\text{R}_2\text{Sn}[\text{S}_2\text{CN}(\text{CH}_2)_4]_2^d$	1.53–1.59	(233)
4	$\text{Ph}_2\text{Sn}(\text{S}_2\text{CNCH}_2\text{Ph})_2$	1.08	(233)	$\text{Bu}_2\text{Sn}(\text{S}_2\text{CNCH}_2\text{Ph})_2$	1.69	(233)
5	$\text{Bu}_2\text{Sn}(\text{ox})_2$	0.92	(421)	$\text{Bu}_2\text{Sn}(\text{pic})_2$	1.45	(421)
6	$\text{Ph}_2\text{Sn}(\text{acac})_2$	0.74	(234)	$\text{Me}_2\text{Sn}(\text{acac})_2$	1.18	(233)
7	$\text{Ph}_2\text{Sn}(\text{NCS})_2\text{bipy}$	0.82	(418)	$\text{Bu}_2\text{Sn}(\text{NCS})_2\text{bipy}$	1.43	(418)
8	$\text{Ph}_2\text{Sn}(\text{NCS})_2\text{phen}$	0.81	(418)	$\text{Bu}_2\text{Sn}(\text{NCS})_2\text{phen}$	1.42	(418)
9	$\text{Ph}_2\text{SnCl}_2 \cdot 4\text{morph}$	0.94	(291)	$\text{Ph}_2\text{SnCl}_2 \cdot 4\text{pip}$	1.33	(291)
10	$n\text{-Pr}_2\text{SnCl}_2 \cdot 2\text{morph}$	0.98	(291)	$n\text{-Pr}_2\text{SnCl}_2 \cdot 2\text{pip}$	1.63	(291)

^a In the text code number will be preceded by table number.

^b Data given in mm/sec relative to SnO_2 at liquid nitrogen temperature, assuming identical center shifts for SnO_2 and BaSnO_3 . Data from Ref. (418) have been converted assuming a center shift of 1.52 for $\text{Pd}(\text{Sn})$.

^c bipy = 2,2'-Bipyridyl; oxH = 8-hydroxyquinoline; acac = acetylacetonate; phen = 1,10-phenanthroline; picH = picolinic acid; pip = piperidine; morph = morpholine.

^d Range of values for $\text{R} = \text{Me}, \text{Bu}$.

cis and *trans* arrangement of the R groups. Clearly, there is a marked trend to lower shifts for the *cis* species. For the pairs of compounds 1–4 and 6–8 in Table XLI, some of the difference may be due to the differing polarities of the tin–phenyl and tin–alkyl bonds, but this effect is not large enough to account for the whole of the change.

Unlike the complexes in Table XXXVIII, organotin compounds do not seem to show a dependence of center shift on coordination number, except perhaps for the small differences in center shift between the species $[\text{EtSnCl}_4]^-$ and $[\text{EtSnCl}_5]^{2-}$ and the low center shifts found for the seven-coordinate compound $\text{BuSn}(\text{ox})_3$ (168, 462). Thus, for example, the data in Tables XX and XXIX show that the center shifts of tri-alkyltin halides and carboxylates with associated five-coordinate

structures are very similar to those for analogous monomeric tetrahedral species. Similarly, the coordination of an extra ligand to Ph_3SnCl to form a five-coordinate complex, Ph_3SnClX , produces no significant change in center shift either for $\text{X} = \text{Cl}^-$ (207, 442) or an oxygen donor such as R_2SO [$\text{R} = \text{Me, Et, Bu, } \frac{1}{2}(\text{CH}_2)_4$] or R_3PO ($\text{R} = \text{MeO, EtO, PhO}$) (207, 556) (Table XXXVI). Six coordinate *trans*- R_2SnX_4 species have some of the highest center shifts, as exemplified by the data for the $[\text{Me}_2\text{SnX}_4]^{2-}$ ions (Table XXXIX), despite the high coordination number and the presence of four Sn-X bonds.

At present, no complete interpretation of the center shifts found for organotin compounds has appeared. Two explanations have been proposed to account for the constant center shifts of tetrahedral R_3SnX species. Chivers and Sams (114, 115) have suggested that the substitution of an electronegative ligand causes a rehybridization of the bonding orbitals of the tin atom, which results in an asymmetric distribution of $5p$ electrons (and, hence an EFG), a reduction in s character of the Sn-X bond, but no net loss of charge. Although the distortions of bond angles observed (131) for the compound $\text{Ph}_2\text{Sn(I)} \cdot (\text{CH}_2)_4 \cdot (\text{I})\text{SnPh}_2$ indicate some degree of rehybridization, halogen NQR data provide strong evidence (566) for loss of charge from the tin orbital of the Sn-X bond. Alternatively, it was suggested (441) that an electronegative substituent removes charge from the valence shell, but that the resultant residual positive charge provides a deshielding and contraction of the $5s$ orbitals, i.e., an increase in the effective nuclear charge. Such an effect would compensate for the loss of $5s$ electron density to the ligand. Any rehybridization which does occur can then be seen as a complementary effect which increases the s character of the R-Sn bond and, hence, accentuates the deshielding effect. Similar explanations (459) have been proposed to account for the relative insensitivity of the center shifts of five- and six-coordinate compounds.

It has been argued (421, 441) that the difference in the center shifts of *cis*- and *trans*- R_2SnX_4 isomers reflects a variation in the $5s$ character of the Sn-R bonds, and this suggestion is supported by the higher $J_{\text{H-Sn-CH}_3}$ NMR coupling constant observed for $\text{Me}_2\text{Sn(pic)}_2$ [$J_{\text{H-Sn-CH}_3} = 77.6 \text{ Hz}$ (395)] compared with $\text{Me}_2\text{Sn(ox)}_2$ [$J_{\text{H-Sn-CH}_3} = 71.2 \text{ Hz}$ (395)] and by simple molecular orbital considerations (441). In fact, there may be a general correlation between the stereochemistry of Sn-R bonds and center shifts (441). Gassenheimer and Herber (258) have proposed an electron delocalization effect (i.e., deshielding) associated with a change in hybridization to explain the high center shifts of five-coordinate species relative to four-coordinate compounds.

In summary, it is evident from the above discussion that the factors

controlling the center shifts of organotin compounds are poorly understood. In contrast, complexes without Sn-R bonds seem to conform reasonably accurately to an interpretation based on bond polarity charges and it may, in fact, be possible to calculate partial center shift values for these species in an analogous manner to low-spin Fe^{II} (44).

The center shifts of tin-transition metal species are of interest, and some of the available data are summarized in Table XLII. These data show a consistent general trend to increased center shift with increasing number of Sn-M bonds (64, 226, 275, 431, 569), as illustrated, for example, by the series $\text{Me}_{4-n}\text{Sn}[\text{cpFe}(\text{CO})_2]_n$ ($n = 0-2, 4$) (Table XLII, compounds 1, 3, 20, 40), $\text{Ph}_{4-n}\text{Sn}[\text{cpFe}(\text{CO})_2]_n$ ($n = 0-4$) (Table XLII, compounds 2, 5, 22, 32, 40), $\text{Me}_{4-n}\text{Sn}[\text{Mn}(\text{CO})_5]_n$ ($n = 0-3$) (Table XLII, compounds 1, 6, 26, 35), $\text{Cl}_{4-n}\text{Sn}[\text{cpFe}(\text{CO})_2]_n$ ($n = 0-2, 4$) (Table XLII, compounds 40, 42, 48, 62), and $\text{Br}_{4-n}\text{Sn}[\text{cpFe}(\text{CO})_2]_n$ ($n = 0-2, 4$) (Table XLII, compounds 40, 43, 50, 63). This trend has been interpreted (64, 226, 431, 569) in terms of an increased $5s$ character of the Sn-M bond as opposed to alkyl-, phenyl-, or halide-tin bonds. Support for this interpretation is derived from proton NMR data for $\text{Me}_n\text{SnM}_{4-n}$ ($n = 1-4$) species which show a decrease in $J_{\text{H-Sn-CH}_3}$ (226, 431) and, hence, in $5s$ character of the Me-Sn bond with decreasing n . Further, X-ray diffraction data reveal a tendency for larger than tetrahedral M-Sn-M bond angles and smaller than tetrahedral C-Sn-C and X-Sn-X bond angles, and also for relatively short Sn-M and long Sn-C and Sn-X bond lengths [(288) and references quoted therein]. All these trends are those expected for a high $5s$ character in the Sn-M bond.

The series of compounds $\text{R}_{3-n}\text{X}_n\text{SnMn}(\text{CO})_5$ ($\text{R} = \text{Me}, \text{Ph}$; $\text{X} = \text{Cl}, \text{Br}$; $n = 0-3$) (Table XLII) show an increase in center shift as R is replaced by X (431). This suggests (431) that $\text{Mn}(\text{CO})_5$ is a stronger electron donor than methyl, phenyl, or halogen and the more halogen atoms that are attached to the tin atom, the more σ electrons are transferred from manganese to tin. Support for this interpretation is provided by proton and ^{55}Mn NMR data, which show a decrease both in $J_{\text{H-Sn-CH}}$ and in the ^{55}Mn chemical shift with increasing center shift (431).

Although the center shift data discussed above provide convincing evidence that the metal moieties are better σ donors than alkyl or phenyl groups, such a conclusion is at variance with quadrupole splitting data, which indicates that the metal moieties are poorer σ donors than phenyl or alkyl (Section IV, A, b). At present, the most satisfactory explanation for this apparent discrepancy involves a difference in degree of utilization of the $5s$ and $5p$ orbitals (437). The quadrupole splitting measures the p donor capacity, whereas the center shift is most sensitive to the s

TABLE XLII

SOME CENTER SHIFT DATA FOR TIN-TRANSITION METAL SPECIES

Code No. ^a	Compound	C.S. ^b	Ref.
1	Me ₄ Sn	1.31	(516)
2	Ph ₄ Sn	1.22	(516)
3	Me ₃ SnepFe(CO) ₂ ^c	1.38	(65, 149)
4	BuSnepFe(CO) ₂	1.47	(288)
5	Ph ₃ SnepFe(CO) ₂	1.44	(149, 275, 324, 331)
6	Me ₃ SnMn(CO) ₅	1.40	(431, 569)
7	Ph ₃ SnMn(CO) ₅	1.46	(364, 431, 569)
8	Ph ₃ SnCo(CO) ₄	1.50	(364)
9	Ph ₃ SnRe(CO) ₅	1.45	(364)
10	Ph ₃ SnRe(CO) ₄ PPh ₃	1.50	(364)
11	Me ₃ SnepCr(CO) ₃	1.41	(65)
12	Me ₃ SnepMo(CO) ₃	1.43	(65)
13	Me ₃ SnepW(CO) ₃	1.36	(65)
14	Me ₃ SnIrHCl(CO)(PPh ₃) ₂	1.84	(65)
15	Me ₃ SnIrDCl(CO)(PPh ₃) ₂	1.84	(65)
16	Ph ₃ SnIrHCl(CO)(PPh ₃) ₂	1.42	(65)
17	Ph ₃ SnIrHCl(CO)(PPh ₂ Me) ₂	1.46	(65)
18	R ₃ SnepFe(CO)L ^d	1.39–1.50	(149)
19	R ₃ SnepFeL ₂ ^e	1.47–1.71	(149)
20	Me ₂ Sn[epFe(CO) ₂] ₂	1.68	(324)
21	Et ₂ Sn[epFe(CO) ₂] ₂	1.74	(324)
22	Ph ₂ Sn[epFe(CO) ₂] ₂	1.74	(275)
23	Ph ₂ Sn[Co(CO) ₄] ₂	1.68	(364)
24	Ph ₂ Sn[Mn(CO) ₅]Co(CO) ₄	1.65	(364)
25	Ph ₂ Sn[Re(CO) ₅] ₂	1.70	(364)
26	Me ₂ Sn[Mn(CO) ₅] ₂	1.68	(569)
27	Me ₂ ClSnMn(CO) ₅	1.54	(431)
28	Me ₂ BrSnMn(CO) ₅	1.54	(431)
29	Ph ₂ ClSnMn(CO) ₅	1.60	(364, 431)
30	Ph ₂ BrSnMn(CO) ₅	1.59	(431)
31	Ph ₂ ClSnCo(CO) ₄	1.56	(364)
32	PhSn[epFe(CO) ₂] ₃	2.00	(275)
33	PhSn[Co(CO) ₄] ₃	1.54	(226)
34	PhSn[Re(CO) ₅] ₃	1.75	(364)
35	MeSn[Mn(CO) ₅] ₃	1.83	(569)
36	MeCl ₂ SnMn(CO) ₅	1.67	(288, 431)
37	MeBr ₂ SnMn(CO) ₅	1.69	(431)
38	PhCl ₂ SnMn(CO) ₅	1.68	(431)
39	PhBr ₂ SnMn(CO) ₅	1.80	(431)
40	Sn[epFe(CO) ₂] ₄	2.14	(275)
41	Sn[Co(CO) ₄] ₄	1.96	(227)
42	SnCl ₄	0.85	(139)
43	SnBr ₄	1.14	(139)
44	SnI ₄	1.45	(139)
45	(NH ₄)[SnCl ₃]	3.71	(64)

TABLE XLII—*continued*

Code No. ^a	Compound	C.S. ^b	Ref.
46	(NH ₄)[SnBr ₃]	3.79	(64)
47	(NH ₄)[SnI ₃]	4.03	(64)
48	Cl ₃ SnepFe(CO) ₂	1.70	(64, 149, 275, 331)
49	Cl ₃ SnepFe(CO)PPh ₃	1.88	(149)
50	Br ₃ SnepFe(CO) ₂	1.75	(64)
51	I ₃ SnepFe(CO) ₂	1.88	(64)
52	Cl ₃ SnMn(CO) ₅	1.66	(288, 364, 431, 569)
53	Br ₃ SnMn(CO) ₅	1.79	(364, 431, 569)
54	Cl ₃ SnRh(PPh ₃) ₃	1.78	(227)
55	Cl ₃ SnIr(C ₈ H ₁₂) ₂	1.80	(227)
56	[(Cl ₃ Sn) ₂ RuCl ₂] ²⁻	1.94	<i>f</i>
57	[(Cl ₃ Sn) ₂ PtCl ₂] ²⁻	1.75	<i>f,g</i>
58	[(Cl ₃ Sn) ₅ Pt] ³⁻	1.65	<i>h</i>
59	[(Cl ₃ Sn) ₂ Pt ₃ (C ₈ H ₁₂) ₃ MeNO ₂]	1.50	(227)
60	[(Cl ₃ Sn) ₂ PdCl ₂] ²⁻ -(Me ₄ N ⁺) ₂	1.52	(46)
61	[(Cl ₃ Sn) ₄ Rh ₂ Cl ₂] ⁴⁻ -(Me ₄ N ⁺) ₄	1.90	(227)
62	Cl ₂ Sn[cpFe(CO) ₂] ₂	1.99	(64, 275, 288, 324, 331)
63	Br ₂ Sn[cpFe(CO) ₂] ₂	1.99	(64)
64	I ₂ Sn[cpFe(CO) ₂] ₂	2.00	(64)
65	Cl ₂ Sn[Mn(CO) ₅]cpMo(CO) ₃	1.98	(364)
66	Cl ₂ Sn[Mn(CO) ₅]Re(CO) ₅	1.96	(364)
67	ClSn[Mn(CO) ₅] ₃	1.92	(275, 364)
68	ClSn[Re(CO) ₅] ₃	1.82	(275)
69	BrSn[Re(CO) ₅] ₃	1.82	(364)
70	ClSn[Mn(CO) ₅][cpFe(CO) ₂] ₂	2.10	(275)
71	(NCS) ₂ Sn[cpFe(CO) ₂] ₂	1.85	(64, 288)
72	(HCO ₂) ₂ Sn[cpFe(CO) ₂] ₂	1.61	(64)
73	(MeCO ₂) ₂ Sn[cpFe(CO) ₂] ₂	1.63	(64)
74	(NCS) ₃ SnepFe(CO) ₂	1.65	(64)
75	(HCO ₂) ₃ SnepFe(CO) ₂	1.09	(64)
76	(MeCO ₃) ₃ SnepFe(CO) ₂	1.17	(64)
77	Me ₄ Sn ₃ Fe ₄ (CO) ₁₆	2.20, 1.45	(169)
78	Bu ₂ SnFe(CO) ₈ SnBu ₂	1.70	(169)

^a Code number will be preceded by Table number in text.

^b Data given in mm/sec relative to SnO₂ at liquid nitrogen temperature, assuming that center shift of BaSnO₃ is zero and that of α -tin is 2.10 mm/sec. When appropriate, data are an unweighted average.

^c cp = π -Cyclopentadienyl.

^d Range of data for R = Me or Ph, L = Ph₃M (M = P, As, Sb), Ph₂PCF₃, Ph₂PMe, PhPMe₂, f₆fos [Ph₂P·C=C(PPh₂)(CF₂)₂CF₂], Ph₂AsCF₃, or (C₆H₅O)₃P.

^e Range of data for R = Me, L = SbPh₃, $\frac{1}{2}$ Ph₂P(CH₂)₂PPh₂; R = Ph, L = Ph₂PMe, PhPMe₂.

^f Cation = Me₄N⁺ (46, 227).

^g Cation = Et₄N⁺, δ = 1.56 mm/sec (227).

^h Average of cations = Me₄N⁺ (46) and Et₄N⁺ (227).

donor capacity. As indicated by the crystal structure data, bonds to the metal moiety involve considerably more $5s$ character than $5p$ character relative to an alkyl or phenyl or halide group. If the bonds between Sn and the alkyl, phenyl, and halide groups involve mainly $5p$ electrons on Sn in these compounds, a strong donor such as alkyl would then increase the $5p$ electron density and decrease $[\Psi(O)_s]^2$ and the center shift relative to a halide as is observed (28). Onaka *et al.* (431) suggest π -bonding effects may be important, but this seems unlikely. Thus, π bonding will have only a secondary effect on quadrupole splitting due to the large $5d$ radial function. Further, as noted by Fenton and Zuckerman (227), π donation would be expected to give a decrease in center shift (from shielding effects); and from the data in Table XLII, it is evident that if π -bonding effects are present at all, they are not the dominant factor in the center shift trends.

Fenton and Zuckerman (226) have concluded that as the center shift for SnCl_3 transition metal derivatives (Table XLII, compounds 48–61) are smaller than that of α -tin (C.S. = 2.1 mm/sec), they should be regarded as derivatives of Sn^{IV} . However, Bird *et al.* (65) have argued that this more properly indicates the *valence state* rather than the formal oxidation state of the tin atom. Thus, when SnCl_3^- acts as a ligand, the involvement of the lone pair in bonding means that the tin atom cannot be regarded as bivalent. It is probable that the concepts of formal oxidation state have little meaning in these systems.

Finally, perhaps one of the most elegant experiments recently reported is the correlation found by Barber and Swift (47) between center shift and the $4d$ binding energy of tin (as measured by high-energy photoelectron spectroscopy) for the series $\text{Y}_2\text{Sn}(\text{ox})_2$ ($\text{Y} = \text{Et}, \text{Ph}, \text{Cl}, \text{Br}, \text{or I}$). This correlation is illustrated in Fig. 12, and indicates the potential of combining these two techniques.

3. Temperature Dependence of the Mössbauer Effect and the Goldanskii-Karyagin Effect

In early studies of ^{119}Sn Mössbauer spectra, it was realized that certain compounds give rise to a room temperature Mössbauer effect, while such an effect is absent from other species. It was suggested (323, 531) that the observation of a room temperature effect can be taken as evidence for a polymeric structure. This has been confirmed by Stöckler and Sano (529), who have demonstrated that both the Debye temperature and characteristic temperatures are higher for polymeric materials than monomeric species. Stöckler *et al.* (531) have also concluded that the recoil free fraction (f) has no simple dependence on; (a) the nearest neighbor atom mass, (b) the nearest neighbor ligand mass, (c) the

molecular weight, (*d*) the coordination number, (*e*) the macro properties of the material, or (*f*) its center shift and quadrupole splitting.

Further studies on the correlation between a room temperature Mössbauer effect and molecular structure have been reported by Poller *et al.* (464). These authors measured the ratio (*R*) of the room temperature effect to that at liquid nitrogen for a series of organotin compounds and the *R* values obtained are summarized in Table XLIII. For compounds 1-11 in Table XLIII, which are believed to have polymeric structure, finite *R* values were observed; whereas the compounds 17-26,

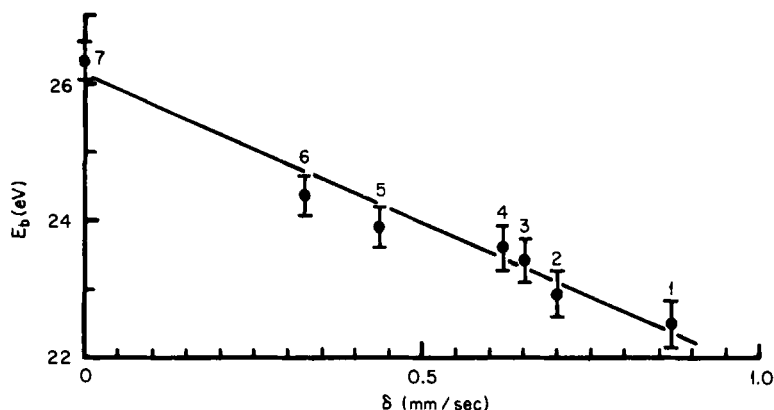


FIG. 12. The 4*d* binding energies of tin, E_b (eV) against Mössbauer center shifts for compounds 1-7. (1) $\text{Et}_2\text{Sn}(\text{OX})_2$; (2) $\text{Ph}_2\text{Sn}(\text{OX})_2$; (3) $\text{SnBr}_4 \cdot 2\text{oXH}$; (4) $\text{SnI}_2(\text{OX})_2$; (5) $\text{SnBr}_2(\text{OX})_2$; (6) $\text{SnCl}_2(\text{OX})_2$; and (7) SnO_2 (47).

which are probably monomeric, and compound 16, which is thought to be trimeric, did not give a significant *R* value. The compound 12 in Table XLIII is of particular interest as the observed *R* value is in conflict with infrared evidence (467), which suggests a monomeric five-coordinate structure.

The work of Poller *et al.* (464) and Stöckler *et al.* (529, 531) strongly suggests that the observation of a room temperature Mössbauer effect may be taken as firm evidence for a polymeric structure, and this criterion has been exploited by, for example, Ford *et al.* (242, 572, 573) in assigning polymeric structures to the species $(\text{Me}_3\text{Sn})_2\text{XO}_4$ (*X* = Se, Cr), Me_2SnXO_4 (*X* = S, Se), $\text{Me}_2\text{Sn}(\text{SO}_3\text{X})$ (*X* = F, Cl, CF_3 , Me, Et), $\text{Sn}(\text{SO}_3\text{F})_4$, and $\text{SnCl}_2(\text{SO}_3\text{F})_2$. It should, however, be emphasized that the absence of a room temperature effect for a compound in no way allows the elimination of an associated structure. For example,

there are excellent reasons to assign associated structures to the compounds $(\text{Me}_3\text{Sn})_2\text{SO}_4$ (206), $\text{Bu}_3\text{SnO}_2\text{CMe}$ (240), and Me_3SnNCO (383), none of which shows a detectable room temperature Mössbauer effect. Another example is provided by the compounds (464) $\text{PhSn}(\text{OCOCX}_3)\text{O}$

TABLE XLIII
R VALUES FOR SOME ORGANOTIN COMPOUNDS^a

Code No. ^b	Compound ^c	R^c	Ref.
1	$\text{Me}_3\text{SnL} \cdot \text{H}_2\text{O}$	0.035	(468)
2	$\text{Bu}_3\text{SnL} \cdot \text{H}_2\text{O}$	0.044	(468)
3	$\text{Ph}_3\text{SnL} \cdot \text{H}_2\text{O}$	0.045	(468)
4	$\text{Bu}_2\text{SnCl}_2 \cdot 4,4'\text{-bipy}$	0.057	(466)
5	$\text{Ph}_2\text{SnCl}_2 \cdot 4,4'\text{-bipy}$	0.040	(466)
6	$\text{Ph}_2\text{SnCl}_2 \cdot \text{pyrazine}$	0.035	(466)
7	$\text{Ph}_2\text{SnCl}_2 \cdot t\text{-DTDO}$	0.159	(467)
8	$\text{Ph}_3\text{SnO}_2\text{CMe}$	0.078	(240)
9	$\text{Ph}_3\text{SnO}_2\text{CEt}$	0.110	(240)
10	$\text{Ph}_3\text{SnO}_2\text{C} \cdot \text{CHMe}_2$	0.080	(241)
11	$\text{Ph}_3\text{SnO}_2\text{C} \cdot \text{CH}_2\text{Cl}$	0.183	(464)
12	$\text{Ph}_2\text{SnCl}_2 \cdot c\text{-DTDO}$	0.091	(467)
13	$\text{PhSn}[\text{O}_2\text{C} \cdot \text{CMe}_3]\text{O}$	0.385	(464)
14	$\text{PhSn}[\text{O}_2\text{C} \cdot \text{CCl}_3]\text{O}$	0.057	(464)
15	$\text{PhSn}[\text{O}_2\text{C} \cdot \text{CF}_3]\text{O}$	0	(464)
16	Oct_2SnL	0	(468)
17	$\text{Me}_2\text{Sn}(\text{ox})_2$	0	(462, 505)
18	$\text{Bu}_2\text{Sn}(\text{ox})_2$	0	(462)
19	$\text{Oct}_2\text{Sn}(\text{ox})_2$	0	(462)
20	$\text{Ph}_2\text{Sn}(\text{ox})_2$	0	(462)
21	$\text{Bu}_2\text{SnCl}_2 \cdot 2(4\text{-phepy})$	0	(466)
22	$\text{Ph}_2\text{SnCl}_2 \cdot 2,2'\text{-bipy}$	0	(465)
23	$\text{Ph}_2\text{SnCl}_2 \cdot 2\text{DTO}$	0	(467)
24	$\text{Ph}_2\text{SnCl}_2 \cdot 2\text{Me}_2\text{SO}$	0	(464)
25	$\text{Me}_2\text{SnCl}_2 \cdot 2\text{Me}_2\text{SO}$	0	(353)
26	$\text{Ph}_3\text{SnO}_2\text{C} \cdot \text{CMe}_3$	0	(240)

^a Data from (464), in which reference will be found values of center shift and quadrupole splitting.

^b In text code number will be preceded by table number.

^c See text for definition.

^d References are to structural studies.

^e LH_2 = Bis(8-hydroxy-5-quinolyl)methane; oxH = 8-hydroxyquinoline; 4,4'-bipy = 4,4'-bipyridine; 4-phepy = 4-phenylpyridine; 2,2'-bipy = 2,2'-bipyridine; *t*-DTDO = *trans*-1,4-dithiane 1,4-dioxide; *c*-DTDO = *cis*-1,4-dithiane 1,4-dioxide; DTO = 1,4-dithiane 1-oxide.

(X = H, Cl and F). All three of these compounds are very high melting solids (m.p. > 360°) indicative of polymeric structures, but the *R* factor falls dramatically from R = H to R = Cl and is equal to zero when R = F.

Studies of the variation of the magnitude of the Mössbauer effect over a wide range of temperatures have been reported by Stöckler and Sano (526) for the compounds $\text{Me}_3\text{SnCl}\cdot\text{py}$, Me_3SnF , Ph_3SnF , and $\text{Me}_3\text{SnO}_2\text{CH}$. As might be anticipated, the Mössbauer effect varied much more markedly with temperature for the monomeric compound Me_3SnClpy (348) than for the polymeric species Me_3SnF and $(\text{C}_6\text{H}_5)_3\text{SnF}$, while the compound $\text{Me}_3\text{SnO}_2\text{CH}$ showed a temperature dependence between the two extremes. This type of study has been extended by Herber (326) to the compounds $(\text{Bu}_3\text{Sn})_2\text{SO}_4$, $\text{Bu}_3\text{SnO}_2\text{CH}_3$, Bu_3SnF , and Bu_2SnF_2 . In these cases the ratios of the temperature dependence of the Mössbauer effect (as measured by the area under the resonance curve) are $(\text{Bu}_3\text{Sn})_2\text{SO}_4$: $\text{Bu}_3\text{SnO}_2\text{CMe}$: Bu_3SnF : Bu_2SnF_2 = 1 : 0.918 : 0.576 : 0.302. These ratios clearly indicate that the tributyl- and dibutyl-tin fluorides have stronger polymeric lattices than either $\text{Bu}_3\text{SnO}_2\text{CMe}$ or $(\text{Bu}_3\text{Sn})_2\text{SO}_4$, and Herber (326) has taken these data as further evidence in favor of a monomeric structure for $(\text{Bu}_3\text{Sn})_2\text{SO}_4$. However, infrared (355) and Mössbauer (240) evidence clearly show the presence of intermolecular association in the compound $\text{Bu}_3\text{SnO}_2\text{CMe}$, and the similarity of the temperature dependence of the Mössbauer effect in $\text{Bu}_3\text{SnO}_2\text{CMe}$ and $(\text{Bu}_3\text{Sn})_2\text{SO}_4$ makes it difficult to eliminate the possibility of association in $(\text{Bu}_3\text{Sn})_2\text{SO}_4$. Herber *et al.* (112, 383) have also used the temperature dependence of the Mössbauer effect to assign polymeric structures to the compounds Me_3SnN_3 and Me_3SnNCO .

Another phenomenon, which is of interest in studying polymeric materials, is the Goldanskii-Karyagin effect (365). This effect, which arises from a lattice dynamic anisotropy in the recoil free fraction, is manifested in an asymmetry in the intensities of the components of a quadrupole doublet. The presence of this effect was detected by Stöckler and Sano (527) for the polymeric materials $(\text{Me}_3\text{SnF})_n$ and $(\text{Me}_3\text{SnOH})_n$, whereas it was found (527) to be absent for the monomeric species Ph_3SnCl . However, the absence of a significant effect in $\text{Me}_3\text{SnO}_2\text{CH}$ demonstrates that polymeric structure is not a sufficient criterion to produce a significant Goldanskii-Karyagin effect (526). Stöckler and Sano (526, 527) and Herber *et al.* (326–329) have exploited the temperature dependence of this effect in the study of lattice dynamics for the species Me_3SnOH (527), Me_3SnF (328, 527), Ph_3SnF (526), Bu_3SnF (326), Bu_2SnF_2 (326), Me_2SnF_2 (327), and Me_3SnCN (329, 525), and Herber (326) has noted its absence in the Mössbauer spectrum of $(\text{Bu}_3\text{Sn})_2\text{SO}_4$.

B. Fe^{II} LOW-SPIN COMPOUNDS

In the absence of π bonding, an octahedral low-spin Fe^{II} compound can be represented by the simple molecular orbital picture illustrated in Fig. 13. The metal $3d$ electrons form a t_{2g}^6 configuration, while ligand donation from appropriate σ orbitals populates the molecular orbitals formed by overlap with the iron $3d_{z^2}$, $3d_{x^2-y^2}$, $4s$, and $4p$ orbitals. In hybridization terms, the σ bonding can be represented by overlap between d^2sp^3 hybrids of the iron atom with the σ orbitals of the ligands.

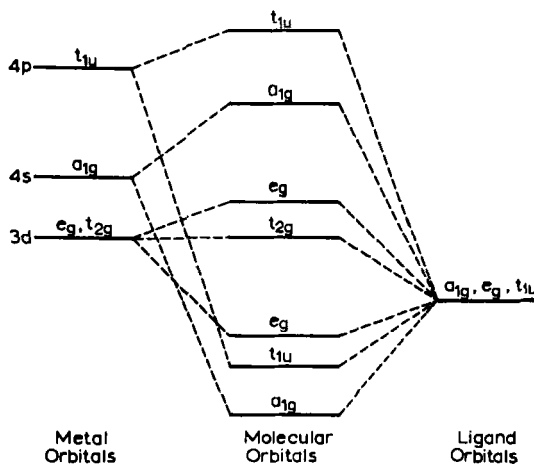


FIG. 13. Molecular orbital diagram for an octahedral MX_6 molecule considering only σ bonding.

In many cases the ligands also have empty antibonding π^* orbitals, which have suitable symmetry for overlap with the t_{2g}^6 electrons of the metal atom. Such overlap results in a donation of charge from the metal to the ligand.

As the t_{2g}^6 shell has cubic symmetry and is diamagnetic, any variations in center shift and quadrupole splitting found for octahedral compounds must arise from variations in the nature of the ligands, and Mössbauer spectroscopy has proved a very powerful means of studying the variations of metal-ligand interactions in low-spin Fe^{II} systems. This is in contrast to many other oxidation states of iron (*vide infra*) for which the asymmetry of the free ion electrons obscures the dependence of the C.S. and Q.S. on ligand properties.

1. Quadrupole Splitting

As for Sn^{IV} compounds, the quadrupole splittings for Fe^{II} low-spin compounds are due to q_{lat} and/or $q_{\text{m.o.}}$, and the quadrupole splitting will be sensitive to changes in both the nature and geometric distribution of the ligands. In Section II, D, it was shown that for contributions to the EFG arising from σ -bonding asymmetry, the additivity model should provide a realistic guide to the variation of quadrupole splitting with structure. However, for contributions from π -bonding asymmetries, some deviation from additivity might be anticipated. Table XLIV lists a wide range of quadrupole splittings for low-spin Fe^{II} compounds. We will first discuss the relationship between quadrupole splitting and structure, derive empirical partial quadrupole splittings, and comment on the nature of the metal-ligand bonds, particularly the Fe-N_2 bond as deduced from p.q.s. values.

a. Derivation of p.q.s. Values and Structural Determination. Berrett and Fitzsimmons (55) first showed that a *trans*- FeA_2B_4 isomer has twice the Q.S. of the corresponding *cis*- FeA_2B_4 isomer. They studied compounds of the type *trans*- and *cis*- $\text{Fe}(\text{CN})_2(\text{CNR})_4$ and $[\text{Fe}(\text{CN})(\text{CNR})_5]^+\text{ClO}_4^-$ ($\text{R} = \text{Et}, \text{Me}, \text{CH}_2\text{Ph}$) (Table XLIV, compounds 12, 39, 40) and used the point charge model to show that the observed magnitudes correspond reasonably well to the predicted 2:1:1 ratio. Bancroft *et al.* (44) extended the additivity model to a wide range of compounds and calculated empirical p.q.s. values for a wide range of ligands (p.q.s. = $\frac{1}{2}e^2Q[\text{L}]$ and Table IV). To calculate p.q.s. values it was necessary to assign structures to key compounds. For example, the exact 2:1 ratio for the isomers of $\text{FeCl}_2(\text{ArNC})_4$ (Table XLIV, compounds 1, 30) and $\text{Fe}(\text{SnCl}_3)_2(\text{ArNC})_4$ (Table XLIV, compounds 3, 32) allows the immediate assignment of structures to these four compounds, and the similarity of the quadrupole splittings of $\text{FeX}_2(\text{depe})_2$ ($\text{X} = \text{Cl}, \text{Br}, \text{I}$) and $\text{FeCl}_2(\text{dmpe})_2$ (Table XLIV, compounds 2, 4-6) to that of *trans*- $\text{FeCl}_2(\text{ArNC})_4$ suggests *trans*-octahedral structures for these compounds. Although the quadrupole splitting of $\text{FeCl}_2(\text{depb})_2$ (Table XLIV, compound 7) is too low to make an unambiguous assignment of structure, Chatt and Hayter (109) have used NMR and dipole moment data to assign *trans* structures to $\text{FeHCl}(\text{depe})_2$, $\text{FeHI}(\text{depe})_2$, $\text{FeCl}_2(\text{depe})_2$, and $\text{FeCl}_2(\text{depb})_2$ in solution, and it is a reasonable assumption that these compounds have *trans* structures in the solid state. All the quadrupole splittings of the pseudohalides $\text{FeY}_2(\text{depe})_2$ ($\text{Y} = \text{NCO}, \text{NCS}, \text{N}_3$) compounds (Table XLIV, compounds 9-11) are rather smaller, but it appears likely that they are also *trans* like the other bisdiphosphine complexes.

TABLE XLIV
QUADRUPOLE SPLITTINGS FOR Fe^{II} LOW-SPIN COMPOUNDS^a

Code No. ^b	Compound ^d	Quadrupole splitting ^c		Ref.
		Obs.	Calc.	
1	<i>trans</i> -FeCl ₂ (ArNC) ₄	+1.55	—	(34, 44)
2	<i>trans</i> -FeCl ₂ (depe) ₂	+1.29	—	(34, 44)
3	<i>trans</i> -Fe(SnCl ₃) ₂ (ArNC) ₄	(+)1.05	—	(34, 44)
4	<i>trans</i> -FeCl ₂ (dmpe) ₂	(+)1.51	—	(34, 44)
5	<i>trans</i> -FeBr ₂ (depe) ₂	(+)1.37	—	(34, 44)
6	<i>trans</i> -FeI ₂ (depe) ₂	(+)1.33	—	(34, 44)
7	<i>trans</i> -FeCl ₂ (depb) ₂	(+)1.13	—	(34, 44)
8	<i>trans</i> -FeH ₂ (depb) ₂	(-)1.84	—	(34, 44)
9	<i>trans</i> -Fe(NCO) ₂ (depe) ₂	(+)0.49	—	(34, 44)
10	<i>trans</i> -Fe(NCS) ₂ (depe) ₂	(+)0.53	—	(34, 44)
11	<i>trans</i> -Fe(N ₃) ₂ (depe) ₂	(+)0.98	—	(34, 44)
12	<i>trans</i> -Fe(EtNC) ₄ (CN) ₂	-0.60	—	(34, 55)
13	Na ₂ [Fe(CN) ₅ NO] · 2H ₂ O	+1.73	—	(34, 161, 238)
14	Na ₃ [Fe(CN) ₅ NH ₂] · H ₂ O	+0.67	—	(34, 44, 76, 238)
15	K ₃ [Fe(CN) ₅ H ₂ O] · 7H ₂ O	+0.80	—	(34, 44)
16	Na ₅ [Fe(CN) ₅ SO ₃] · 9H ₂ O	(+)0.76	—	(142, 238)
17	(Na, K) ₄ [Fe(CN) ₅ NO ₂]	(+)0.85	—	(76, 142, 238)
18	Fe(CNH) ₄ (CN) ₂	~0.0	—	(312)
19	Fe(CNH) ₄ (CNBF ₃) ₂	~0.0	—	(312)
20	Na ₃ [Fe(CN) ₅ P(C ₆ H ₅) ₃]	(+)0.62	—	(239)
21	Na ₃ [Fe(CN) ₅ As(C ₆ H ₅) ₃]	(+)0.92	—	(239)
22	Na ₃ [Fe(CN) ₅ Sb(C ₆ H ₅) ₃]	(+)0.94	—	(239)
23	<i>cis</i> -Fe(CO) ₄ Cl ₂	(-)0.25	—	(39)
24	K ₂ PcFe(CN) ₂	(+)0.56	—	(156)
25 ^e	PcFe(py) ₂	+2.04	—	(156, 347)
26	PcFe(Im) ₂	(+)1.77	—	(156, 347)
27	PcFe(but) ₂	(+)1.94	—	(156)
28	PcFe(pip) ₂	(+)2.21	—	(156)
29	Fe(niox) ₂ (NH ₃) ₂	(+)1.75	—	(156, 347)
		(η = large)		
30	<i>cis</i> -FeCl ₂ (ArNC) ₄	-0.78	-0.78	(34, 44)
31	[FeCl(ArNC) ₅]ClO ₄	0.73	+0.78	(44)
32	<i>cis</i> -Fe(SnCl ₃) ₂ (ArNC) ₄	0.50	-0.52	(44)
33	<i>cis</i> -FeCl(SnCl ₃)(ArNC) ₄	0.61	-0.65	(44)
34	[Fe(SnCl ₃)(ArNC) ₅]ClO ₄	0.32	+0.52	(44)
35	<i>trans</i> -FeHCl(depe) ₂	<0.12	-0.20	(44)
36	<i>trans</i> -FeHI(depe) ₂	<0.19	-0.18	(44)
37	<i>trans</i> -FeClSnCl ₃ (depe) ₂	1.28	+1.02	(44)
38	<i>trans</i> -FeBr ₂ (depb) ₂	1.22	+1.20	(44)
39	<i>cis</i> -Fe(CN) ₂ (EtNC) ₄	0.29	+0.30	(55)
40	[Fe(CN)(EtNC) ₅]ClO ₄	0.17	-0.30	(55)

TABLE XLIV—*continued*

Code No. ^b	Compound ^d	Quadrupole splitting ^c		Ref.
		Obs.	Calc.	
41	Fe(niox) ₂ (Im) ₂	1.38	+1.64 (156)	
42	Fe(niox) ₂ (py) ₂	1.75	+1.92 (156)	
43	Fe(niox) ₂ (but) ₂	1.83	+1.84 (156)	
44	K ₂ Fe(niox) ₂ (CN) ₂	0.80	+0.44 (156)	
45	KFe(niox) ₂ Im·CN	0.93	+1.04 (156)	
46	Fe(niox) ₂ Im·CO	0.77	+1.86 (156)	
47	[FeH(ArNC)(depe) ₂] ⁺ BPh ₄ ⁻	-1.14	-0.98 (34, 37)	
48	[FeH(CO)(depe) ₂] ⁺ BPh ₄ ⁻	(-)1.00	-0.46 (37, 39)	
49	<i>cis</i> -FeH ₂ (CO) ₄	0.55	+1.22 (39, 44)	
50	[FeH(P(OMe) ₃)(depe) ₂] ⁺ BPh ₄ ⁻	(-)0.90	— (37)	
51	[FeH(P(OPh) ₃)(depe) ₂] ⁺ BPh ₄ ⁻	(-)0.72	— (37)	
52	[FeH(PhCN)(depe) ₂] ⁺ BPh ₄ ⁻	(-)0.58	— (37)	
53	[FeH(MeCN)(depe) ₂] ⁺ BPh ₄ ⁻	(-)0.46	— (37)	
54	[FeH(N ₂)(depe) ₂] ⁺ BPh ₄ ⁻	(-)0.33	— (37)	
55	Fe(DMG) ₂ ·2py	1.84	— (3, 236)	
56	Fe(DMG) ₂ ·2β-pic	1.62	— (3, 236)	
57	Fe(DMG) ₂ ·2α-pic	0.7	— (3, 236)	
58	Fe(DMG) ₂ ·22,4-lut	0.5	— (3, 236)	
59	[Fe(DTOH ₂) ₂]Cl ₂	0.66	— (1, 236)	
60	[Fe(DTOH) ₂]	2.02	— (1, 236)	
61	[Fe(DTOCH ₃) ₂]	0.88	— (1, 236)	
62	Fe(NCS) ₂ (qp)	0.86	— (237)	
63	Fe(CN) ₂ (qp)	1.29	— (237)	

^a Data given in mm/sec at room temperature. Many "octahedral" complexes such as K₄Fe(CN)₆, Fe(phen)₃(ClO₄)₂ and others usually have zero or very small splittings. They are not given here. See Refs. (135, 195, 209, 215, 397, 404)

^b Code Number will be preceded by table number in the text.

^c Signs without brackets have been determined (see Table XLV), those with brackets have not been determined, but deduced in the references by analogy with the compounds of known sign. Calculated values use the p.q.s. values in Table XLVI. Many of these are reported for the first time.

^d ArNC = *p*-Methoxyphenylisocyanide; depe = 1,2-bis(diethylphosphino)ethane; dmpe = 1,2-bis(dimethylphosphino)ethane; depb = *o*-phenylenebis-diethylphosphine; Pc = phthalocyanine; py = pyridine; Im = imidazole; but = *n*-butylamine; pip = piperidine; niox = 1,2-cyclohexanedione dioxime; DMG = dimethylglyoxime; 2β-pic = 2β-picoline; 2α-pic = 2α-picoline; 22,4-lut = 22,4-lutidine; DTOH₂ = diacetylthiosemicarbozoneoxime; DTOCH₃ = *O*-methyl-di-acetylthiosemicarbozoneoxime; qp = tris-(*O*-diphenylphosphinophenyl)phosphine.

^e Similar quadrupole splittings are given for other PcFeX₂ compounds (347). (X = β-picoline, γ-picoline, or α-picoline).

As the original calculations of p.q.s. values were undertaken before any measurement of the signs of the Q.S., it was necessary to make assumptions for certain key compounds. For example, consider the compounds *trans*-FeX₂B₄ (X = Cl, Br, I; L = RNC, depe/2, etc.). It is a reasonable assumption, supported by center shift data (*vide infra*) and general chemistry, that halide ligands carry a higher negative charge and are poorer σ donor and π acceptors than the neutral B ligands. It would therefore be expected (Section I, C) that the q_{lat} and π -bonding inequalities would give negative contributions to the Q.S., whereas the σ bonding inequalities would give a positive contribution to the Q.S. Clearly, both the sign and the magnitude of these Q.S. values depends on the relative importance of these contributions. Originally, Bancroft *et al.* (44) assumed that the q_{lat} contribution was most important after calculating the q_{lat} contribution to the Q.S. from a *trans*-FeCl₂ linkage to be -1.2 mm/sec, in reasonable agreement with the Q.S. values for most of the *trans*-FeCl₂B₄ compounds. The reference p.q.s. value for Cl⁻ was thus taken as -0.30 mm/sec, the signs of *trans*-FeX₂B₄ compounds taken as negative, and p.q.s. values for other ligands derived. Predicted values were compared with observed, and good agreement obtained in most cases (Table XLIV, compounds 30-40) demonstrating that the additivity model provides a reasonable guide to variations of the Q.S. with structure. The predicted values calculated originally (44) are identical with those calculated in Table XLIV.

Measurement of the signs of the Q.S. of a number of Fe^{II} low-spin compounds using the magnetic field technique (36) showed that the wrong signs had been assumed. For example, Fig. 14 illustrates the spectra of *cis*- and *trans*-FeCl₂(ArNC)₄ in an applied magnetic field. These spectra indicate that the *trans* and *cis* isomers have positive and negative Q.S. values, respectively. These measurements provide an elegant confirmation of the opposite signs of the *trans* and *cis* isomers predicted by the additivity model, but show that the initially assumed signs of the Q.S. were incorrect.

Other signs have been measured (Table XLV), and have been invaluable in calculating p.q.s. values for a wide variety of ligands using the first twenty-nine compounds in Table XLIV. Using these p.q.s. values (Table XLVI), the quadrupole splitting values for compounds 30-49 have been calculated. In deriving the p.q.s. values, it was assumed that all the *trans*-FeX₂B₄ compounds have positive quadrupole splittings. Some of the signs of other compounds (such as compounds 20-22 in Table XLIV) were deduced by analogy with similar compounds to give reasonable p.q.s. values for such ligands as P(C₆H₅)₃. In addition, when some doubt exists about the sign of the quadrupole splitting, the

ambiguity can be eliminated by comparing quadrupole splittings for similar compounds. For example, the sign of the quadrupole splitting in *trans*-Fe(SnCl₃)₂(ArNC)₄ is not known, and p.q.s. values of SnCl₃⁻ of -0.43 and -0.95 mm/sec can be calculated from this compound assuming a positive and negative sign, respectively. However, the calculated quadrupole splitting for the compound *trans*-FeClSnCl₃(depe)₂ (observed

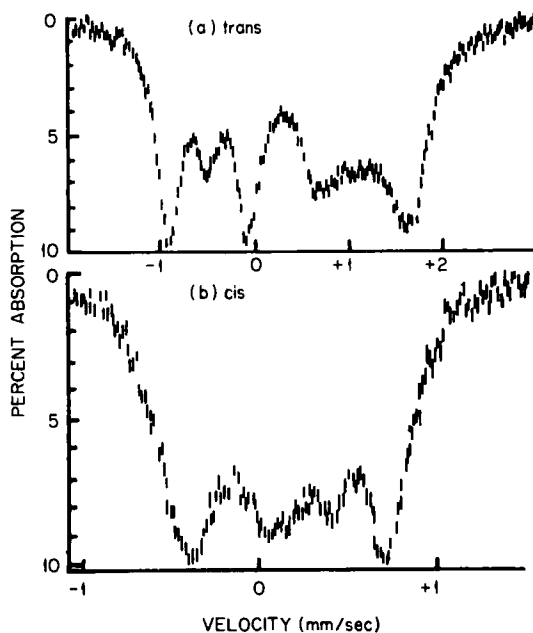


FIG. 14. Mössbauer spectra of (a) *trans*-FeCl₂(*p*-MeO·C₆H₄·NC)₄ at 4°K in a longitudinal magnetic field of 36kG; (b) *cis*-FeCl₂(*p*-MeO·C₆H₄·NC)₄ at 4°K in a longitudinal field of 28 kGauss (36).

1.28 mm/sec) is +1.02 mm/sec with (p.q.s.)_{SnCl₃⁻} = -0.43, and -0.02 mm/sec with (p.q.s.)_{SnCl₃⁻} = -0.95 mm/sec, clearly indicating a positive sign for the Q.S. of *trans*-Fe(SnCl₃)₂(ArNC)₄. Similarly, the positive sign of *trans*-FeCl₂(depe)₂, and the very small Q.S. for *trans*-FeHCl(depe)₂ allows the assignment of a negative sign to the Q.S. of *trans*-FeH₂(depb)₂. This sign is confirmed by the measured negative sign observed for *trans*-[FeH(ArNC)(depe)₂]⁺BPh₄⁻ (Table XLV), and the predicted Q.S. for the above compound is in good agreement with the observed value (Table XLIV, compound 47). The measured negative sign for *trans*-[FeH(ArNC)(depe)₂]⁺BPh₄⁻ makes it highly probable that all the other *trans*-[FeHL(depe)₂]⁺ species [L = CO, Me₃CNC, P(OMe)₃, P(OPh)₃,

TABLE XLV
SIGNS OF THE EFG FOR Fe^{II} LOW-SPIN COMPLEXES

Compound No.	Compound	Q.S.	Ref.
1	PcFe(Py) ₂	+1.96	(157)
2	Fe ^{II} (niox) ₂ (im) ₂	1.30 (η = large)	(157)
3	Fe ^{II} (niox) ₂ (NH ₃) ₂	1.72 (η = large)	(157)
4	<i>trans</i> -[FeH(ArNC)(depe) ₂ ⁺]BPh ₄ ⁻	-1.14	(34)
5	<i>trans</i> -FeCl ₂ (ArNC) ₄	+1.55	(34, 36)
6	<i>cis</i> -FeCl ₂ (ArNC) ₄	-0.83	(34, 36)
7	<i>trans</i> -FeCl ₂ (depe) ₂	+1.29	(34)
8	<i>trans</i> -Fe(CN) ₂ (EtNC) ₄	-0.60	(34)
9	Na ₃ [Fe(CN) ₅ NH ₃] · H ₂ O	+0.67	(34)
10	K ₃ [Fe(CN) ₅ H ₂ O] · 7H ₂ O	+0.80	(34)
11	Na ₂ [Fe(CN) ₅ NO] · 2H ₂ O	+1.73	(34, 161)

N₂, PhCN, and MeCN] (Table XLIV, compounds 48, 50–54) also have negative signs.

It is apparent from the general agreement between predicted and observed Q.S. values in Table XLIV that the additivity model holds rather well. We take satisfactory agreement to mean that predicted and observed values are within ± 0.2 mm/sec. These p.q.s. values should now be extremely useful for rationalizing Q.S. values for other Fe^{II} compounds containing these ligands in different combinations (*vide infra*; the carbonyl compounds), as well as rationalizing signs and magnitudes of Q.S. values in Co^{III}, Ru^{II}, and Ir^{III} compounds (*vide infra*).

However, there are at least three types of compounds where the agreement between predicted and observed values might be expected to be unsatisfactory. First, for cationic or anionic compounds, a q_{lat} contribution from the anion or cation, respectively, or a significant lowering or raising of the Fe *d* orbitals relative to the ligand orbitals might lead to discrepancies. The agreement for such cationic compounds as *trans*-[FeH(ArNC)(depe)₂]BPh₄, [Fe(CN)(EtNC)₅]ClO₄, and [Fe(SnCl₃)(ArNC)₅]ClO₄ is generally not as good as that for most of the analogous neutral compounds (Table XLIV, compounds 30–40).

Second, satisfactory agreement for such compounds as Fe^{II}(niox)₂L₂ (Table XLIV, compounds 41–46) is not always observed, but this might be due to large distortions from regular symmetry. The large values of η for these compounds (157) are consistent with this interpretation.

TABLE XLVI

PARTIAL QUADRUPOLE SPLITTINGS FOR Fe^{II} LIGANDS^a

$\text{NO}^+ = +0.02$	$\text{NCO}^- = 0.50$
$\text{Br}^- = -0.28$	$\text{NH}_3 = -0.51$
$\text{I}^- = -0.29$	$\text{PPh}_3 = -0.53$
$\text{Cl}^- = -0.30$	$\text{im} = -0.54$
$\text{SbPh}_3 = -0.37$	$\text{depb}/_2 = -0.58$
$\text{AsPh}_3 = -0.38$	$\text{depe}/_2 = -0.62$
$\text{N}_3^- = -0.38$	$\text{dmpe}/_2 = -0.67$
$\text{NO}_2^- = -0.41$	$\text{RNC} = -0.69$
$\text{SnCl}_3^- = -0.43$	$\text{CNH} = \sim 0.8$
$\text{pip} = -0.43$	$\text{CNBF}_3 = \sim 0.8$
$\text{CO} = -0.43$	$\text{CN}^- = -0.84$
$\text{H}_2\text{O} = -0.44$	$\text{niox}/_2 = -0.95$
$\text{SO}_3^{2-} = -0.46$	$\text{Pc}/_4 = -0.98$
$\text{py} = -0.47$	$\text{H}^- = -1.04$
$\text{NCS}^- = -0.49$	
$\text{but} = -0.49$	

^a These are derived from compounds 1-28 in Table XLV. Data given in mm/sec. Some of these values are given in Ref. (34); the others are newly calculated values.

Chelating ligands, in general, would be expected to give more variable p.q.s. values owing to steric effects. One interesting anomaly to the additivity model predictions concerns the compounds *cis*- and *trans*- $\text{Fe}(\text{phen})_2(\text{CN})_2$ and $\text{K}_2\text{Fe}(\text{phen})(\text{CN})_4$. The existence of the two isomers is based on infrared evidence (135, 504). Preliminary Mössbauer data show that all the Q.S. values are positive with values of ~ 0.6 mm/sec (35). Since the nitrogens in $\text{K}_2\text{Fe}(\text{phen})(\text{CN})_4$ must certainly be *cis*-, the predicted Q.S. ratios for the species *trans*- $\text{Fe}(\text{phen})_2(\text{CN})_2$, *cis*- $\text{Fe}(\text{phen})_2(\text{CN})_2$, and $\text{K}_2\text{Fe}(\text{phen})(\text{CN})_4$ is 2: - 1:1. Clearly these pre-predicted ratios are incompatible with the near equality in the sign and magnitude of the observed quadrupole splittings. Even if it is assumed that the *cis* and *trans* isomers of $\text{Fe}(\text{phen})_2(\text{CN})_2$ are, in fact, the same compound, it is still difficult to explain the data. Thus, if $\text{Fe}(\text{phen})_2(\text{CN})_2$ is *cis*, the magnitude of the quadrupole splitting is as expected, but the sign is anomalous, while a *trans* structure gives a correct prediction of sign, but an anomalous magnitude. Analogous bipyridyl complexes (76) show similar quadrupole splittings, although measurements of the signs are not available. At present no clear explanation of these data is apparent, although one possible cause might be distortions from a regular geometry owing to the steric properties of the phenanthroline.

A similar explanation has been used to rationalize the anomalous signs for Sn^{IV} complexes (439).

Finally, for strong π -accepting groups such as CO or NO^+ , we might expect considerable variations in p.q.s. values, leading to marked discrepancies between predicted and observed values (Table XLIV, compounds 46, 48, 49). For example, taking the sign of the Q.S. of *cis*- $\text{Fe}(\text{CO})_4\text{X}_2$ compounds ($\text{X} = \text{Cl}, \text{Br}, \text{I}$) to be negative, the p.q.s. for CO is -0.43 mm/sec. Using this value to predict the Q.S. for *trans*- $[\text{FeH}(\text{CO})\text{-(depe)}_2]^+\text{BPh}_4^-$ (compound 48), we obtain -0.46 mm/sec which is not in satisfactory agreement with the observed value. This compound perhaps represents one of the most extreme cases, since the very low CO

TABLE XLVII

Q.S. VALUES FOR CARBONYL COMPOUNDS AT 80°K^a

Compound No.	Compound	Q.S.
1	<i>cis</i> - $\text{Fe}(\text{CO})_4\text{I}_2$	0.31
2	<i>cis</i> - $\text{Fe}(\text{CO})_4\text{Br}_2$	0.31
3	<i>cis</i> - $\text{Fe}(\text{CO})_4\text{Cl}_2$	0.25
4	$\text{Fe}(\text{CO})_3\text{I}_2(\text{PPh}_2\text{Et})$	0.43
5	$\text{Fe}(\text{CO})_2\text{I}_2(\text{PPh}_2\text{Me})_2$	0.39
6	$\text{Fe}(\text{CO})_2\text{Br}_2(\text{PPh}_2\text{Me})_2$	0.56
7	$\text{Fe}(\text{CO})_2\text{Cl}_2(\text{PPh}_2\text{Me})_2$	0.60

^a From Ref. (39). Data given in mm/sec.

stretching frequency (45) indicates that the bonding properties (and, thus, the p.q.s. value) of CO have changed markedly. To examine the effect of a strong π -accepting ligand such as CO, the spectra of such compounds as $\text{Fe}(\text{CO})_3\text{X}_2\text{P}$ and $\text{Fe}(\text{CO})_2\text{X}_2\text{P}_2$ ($\text{X} = \text{Cl}, \text{Br}, \text{I}$; $\text{P} = \text{PPh}_2\text{Me}, \text{PPh}_2\text{Et}, \text{P}(\text{OPh})_3$, etc.) are now being recorded (39). The latter compounds have five possible geometric isomers, some of which are extremely difficult to distinguish by other spectroscopic methods, and the p.q.s. treatment could be extremely useful. Results for a few compounds are given in Table XLVII and the components of the EFG are given in terms of p.f.g. values in Table IV. The two phosphine ligands give identical values within experimental error. The structure of $\text{Fe}(\text{CO})_3\text{I}_2(\text{PPh}_2\text{Et})$ is taken as in Table IV (structure 18), and a p.q.s. for PPh_2Et is calculated to be -0.51 mm/sec. Then the predicted Q.S. values for structures 20 and 22 (Table IV) (both possible from CO IR) for the iodide derivative (compound 5, Table XLVII) are -0.60 and

−0.39 mm/sec, respectively. The Q.S. for compound 5 suggests then that it has the all cis structure, while the Q.S. for compounds 6 and 7 suggest that they have the *trans*-PPh₂Me structure. However, the solution NMR data for all three compounds suggests *trans*-P configurations, and the Q.S. for the two compounds are not different enough to be conclusive about structural assignments, especially because we would expect the p.q.s. of CO to vary somewhat. The few results given above certainly indicate the potential power of the additivity model in predicting such structures once we can be more confident about variations in p.q.s. values for such ligands as CO.

b. Bonding Properties of Ligands. As we have mentioned previously, three possible factors may contribute to the quadrupole splitting in Fe^{II} compounds; inequalities in σ or π bonding ($q_{\text{M.O.}}$) and inequalities in ligand charge (q_{lat}). The q_{lat} term will be expected to make a significant contribution only for relatively ionic ligands such as the halogens. The measured positive signs for the compounds *trans*-FeCl₂(ArNC)₄ (36) and *trans*-FeCl₂(depe)₂ (34) clearly show that the q_{lat} contribution is not the dominant contribution to the EFG, and indicate that σ -bonding inequalities are more important than π -bonding inequalities. A dominance of the σ -bonding contribution may also be assumed for the species FeX₂B₄ [X = Cl, Br, I, B = depe/2, dmpe/2, depb/2 (34)], Fe(niox)₂L₂ (L = py, im, NH₃, but, CN) (156), and PcFeL₂ (L = im, but, pip, CN) (156). However, the strong π -accepting characteristics of NO⁺ and CO, for example, are obviously important in determining the positive Q.S. of Na₂Fe(CN)₅NO · 2H₂O, the probably positive Q.S. of Fe(niox)₂im · CO, and the large differences in Q.S. between corresponding Fe(CO)₄X₂ and Fe(ArNC)₄X₂ (X = Cl, Br, I) compounds (e.g., Table XLIV, compounds 23, 30). For example, the much smaller Q.S. of the CO compounds can be attributed to the better π -acceptor properties of CO relative to ArNC (*vide infra*). In addition, the fairly small differences in Q.S. between *trans*-FeCl₂B₄ compounds (B = ArNC, depe, dmpe, etc.) could be due to the differences in π -accepting ability of the neutral ligands. Similarly, a π -bonding interpretation has been suggested to explain the Q.S. variation in PcFeL₂ (L = py, im, etc.) species (347). However, as mentioned above, it seems more likely that σ -bonding inequalities play the dominant role in determining the Q.S. in these latter compounds.

The above discussion can be considered more quantitatively by considering the p.q.s. values. It is apparent from Section II,C that the p.q.s. values will become more negative as q_{lat} and σ_{L} for a ligand increases, but as π_{L} decreases (44), i.e.,

$$\text{p.q.s.} \propto [-q_{\text{lat}} + (\pi_{\text{L}} - \sigma_{\text{L}})] \quad (47)$$

Thus, considering the p.q.s. values in Table XLVI, it is apparent that H^- , the best σ donor, gives the most negative p.q.s., whereas NO^+ , the best π acceptor gives the most positive p.q.s. value. Comparing other neutral ligands such as ArNC , CO , and phosphines, the p.q.s. values indicate that $\pi_{\text{L}} - \sigma_{\text{L}}$ increases in the order $\text{ArNC} < \text{phosphines} < \text{CO}$. Thus, CO , a good π acceptor, gives a low p.q.s. value for a neutral ligand. Combined with center shift data (*vide infra*), which gives a measure of $\sigma_{\text{L}} + \pi_{\text{L}}$, we can qualitatively separate the σ_{L} and π_{L} contributions for a wide range of ligands.

To illustrate the above concepts, we now discuss the quadrupole splitting trend in two series of compounds: the $[\text{Fe}(\text{CN})_5\text{X}^{n-}]^{(3-n)-}$ (Table XLIV, compounds 13–17) species and the *trans*- $[\text{FeHL}(\text{depe})_2]^+\text{BPh}_4^-$ compounds (Table XLIV, compounds 48, 50–54). The quadrupole splittings for the $[\text{Fe}(\text{CN})_5\text{X}^{n-}]^{(3-n)-}$ series have been the subject of much discussion (76, 160, 238). The order of center shifts, $\text{L} = \text{NH}_3 > \text{H}_2\text{O} > \text{SO}_3^{2-} > \text{NO}_2^- > \text{CN}^- > \text{NO}^+$ paralleled the expected π -bonding ability of the ligands, and the magnitude of the Q.S. values observed $\text{L} = \text{NO}^+ > \text{NO}_2^- > \text{SO}_3^{2-} > \text{H}_2\text{O} > \text{NH}_3$ has also been attributed to the differing π -acceptor abilities of the above ligands. The sign of the Q.S. for $\text{Na}_2\text{Fe}(\text{CN})_5\text{NO} \cdot 2\text{H}_2\text{O}$ has been shown to be positive (Table XLV), as expected if NO^+ is a better π acceptor (and/or weaker σ donor) than CN^- , and Oosterhuis and Lang (432) have found that the magnitude of the Q.S. is consistent with the calculated t_{2g} orbital populations as expected by the π -bonding argument. However, for the other compounds, the above order of C.S. indicated that CN^- is a better π acceptor than the other ligands, and on a π -bonding argument, a negative Q.S. sign would be expected. In contrast, positive signs have been observed for $\text{Na}_3[\text{Fe}(\text{CN})_5\text{NH}_3]$ and $\text{K}_3[\text{Fe}(\text{CN})_5 \cdot \text{H}_2\text{O}]$ (34), indicating that the greater σ -donor ability of CN^- largely determines the Q.S. The Q.S. data for this series of compounds strongly indicate that both σ and π bonding can be important in determining the magnitude and signs of the Q.S., as was indicated previously when discussing the variations of p.q.s. values. Further, although the present results indicate that σ -bonding inequalities are usually dominant, it is apparent that the sign of the Q.S. for a series of compounds should be known before the results are interpreted. For example, the observed Q.S. values in the series $[\text{Fe}(\text{CN})_5\text{MPh}_3]^{3-}$ ($\text{M} = \text{P}, \text{As}, \text{Sb}$) (Table XLIV, compounds 20–22) (239) may not be a reflection of the decreasing π -bonding ability $\text{PPh}_3 > \text{AsPh}_3 > \text{SbPh}_3$ (239). The Q.S. for all these compounds is most likely positive since the p.q.s. values for phosphines are probably substantially less negative than for CN^- . A decrease in π bonding in the above order would give the PPh_3 compound the most positive of the Q.S. values, in opposition to

the observed values (taking the Q.S. values to be positive). More likely, the trend in Q.S. could be attributed to a decrease in σ -donor ability in the order $\text{PPh}_3 > \text{AsPh}_3 > \text{SbPh}_3$.

The cationic compounds $\text{trans}[\text{FeHL}(\text{depe})_2]^+\text{BPh}_4^-$ (Table XLIV, compounds 47, 48, 50–54) provide another interesting series from which the bonding of N_2 can be compared with a large number of other neutral ligands. The sign of the Q.S. for $\text{L} = p\text{-MeO}\cdot\text{C}_6\text{H}_4\cdot\text{NC}$ has been determined to be negative (37), but unfortunately the sign of the Q.S. for the N_2 compound could not be determined unambiguously because of its small magnitude. However, it is reasonable to assume that all signs are negative since the range of p.q.s. values observed for a large number of neutral ligands (-0.40 to -0.70) (Table XLVI) gives an expected range of Q.S. values for any $\text{trans}\text{-FeHL}(\text{depe})_2^+$ species of -0.40 to -1.00 mm/sec.

The N_2 complex has the most positive Q.S. indicating that it is the best $\pi_{\text{L}}\text{-}\sigma_{\text{L}}$ ligand, although in contrast, the center shift data (*vide infra*) indicate that it is one of the poorest $\sigma_{\text{L}} + \pi_{\text{L}}$ ligands; π acceptance relative to σ donation is more important in N_2 than in the other ligands. As discussed in more detail in the next section, these data suggest that N_2 is a moderate π acceptor, but a weak σ donor.

The compounds $\text{Fe}(\text{DMG})_2\text{L}_2$ where L is pyridine or a methyl-substituted pyridine (Table XLIC, compounds 55–58) show variations in both center shift and quadrupole splitting (3, 236), which have been discussed in terms of a quantitative molecular orbital description. Quantitative predictions (11, 12) of the electronic structure of these compounds have also been reported, and reasonable agreement between observed and calculated quadrupole splittings obtained. Goldanskii *et al.* (1) have considered the relative quadrupole splittings of the species $[\text{Fe}(\text{DToH}_2)_2]\text{Cl}_2$, $\text{Fe}(\text{DToH})_2$, and $\text{Fe}(\text{DTOMe})_2$, where DToH_2 is diacetylthiosemicarbazoneoxime and DToH and DTOMe are ionic derivatives formed by removal of a proton from the oximide ($=\text{NOH}$) or thiosemicarbazene ($=\text{N}\cdot\text{NH}\cdot\text{CS}\cdot\text{NH}_2$) group, respectively. A simple molecular orbital description (2) was used to rationalize the quadrupole splittings, but this is of doubtful validity as a dominant contribution from the diffuse $4p_z$ electrons was assumed.

2. Center Shifts

Variations of both the σ - and π -bonding abilities of the ligands will be expected to affect the center shifts of low-spin Fe^{II} compounds (44, 76, 142, 156, 238). An increase in the σ -donating power will result in an increased population of iron d^2sp^3 hybrids and, as the center shift is more sensitive to $4s$ augmentation than $3d$ or $4p$ augmentation, a net

decrease in center shift will result. Greater π -acceptor power of the ligand will produce a greater delocalization of the t_{2g} electrons, with a consequent reduction in the shielding of the s electrons and this will also lead to a decrease in center shift.

The first observation (76, 142, 238) of a systematic variation of center shift was for the ions $[\text{Fe}(\text{CN})_5\text{X}^{n-}]^{(3-n)-}$ (Table XLVIII, compounds 15, 17–20, 56), for which it was observed initially (142)* that the center shift order $\text{NH}_3 > \text{H}_2\text{O} > \text{SO}_3^{2-} > \text{NO}_2^- > \text{CN}^- > \text{NO}^+$ inversely parallels the π -accepting abilities of these ligands. Other indications of a dependence of center shift on ligand-iron bonds were found (156), for the compounds $\text{Fe}(\text{niox})_2\text{L}_2$ and FePcL_2 (Table XLVIII, compounds 26–32, 66–70), and generally the center shift decreased with increasing σ -donor ability of the ligands. In contrast, ring substituents in the compound $\text{Fe}(\text{L})_3^{2+}$ ($\text{L} = 1, 10$ -phenanthroline or dipyridyl) have only a small effect upon the isomer shift (135, 209).

a. Derivation of p.c.s. Values. A comprehensive survey of center shifts for Fe^{II} low-spin compounds has been reported by Bancroft *et al.* (44), and much of the data in this paper, as well as other Fe^{II} center shifts, are given in Table XLVIII. These values are all relative to nitroprusside. It was postulated (44) that the observed center shifts could be represented as an algebraic sum of contributions from each ligand. The contribution of each ligand to the center shift (C.S.) was termed the partial center shift (p.c.s.). Relative to nitroprusside, we obtain the equation:

$$\text{C.S.} = \sum_{i=1}^6 (\text{p.c.s.}) + 0.16 \quad (48)$$

The use of p.c.s. values involves certain assumptions similar to those used for the quadrupole splitting additivity model. The center shifts must not be sensitive to small distortions in geometry, and variations in center shift must be chiefly dependent on variations in isomer shift, i.e., the S.O.D. shift must remain relatively constant (319). There is some evidence for this last assumption in the observation of an almost constant temperature dependence of center shift. It is also necessary to assume that the p.c.s. of a particular ligand is not dependent on the other ligands, i.e., that p.c.s. values are additive.

Center shifts relative to stainless steel at 295°K were used in the calculation of p.c.s. values assuming that the p.c.s. value of ArNC is zero (44); p.c.s. values for thirty-nine ligands (Table XLIX) are derived (from *trans*- FeA_2B_4 compounds where possible), and these p.c.s. values are used to predict the C.S. values for 46 other compounds. Except for

* Examination of the more recent data in Table XLVIII shows that the order is slightly different.

ten of these compounds, agreement between predicted and observed values is excellent (within ± 0.05 mm/sec), and the data lend credence to an additivity model for the C.S. However, the significantly smaller C.S. of *cis*-FeCl₂(ArNC)₄ compared to *trans*-FeCl₂(ArNC)₄, indicates that the p.c.s. values of π -acceptor ligands such as ArNC do vary from compound to compound. The above discrepancy may be attributed to the increased π -acceptor properties of ArNC when it is *trans* to a chloride, as opposed to another ArNC ligand. More serious π -bonding discrepancies will be noted shortly. Variations in p.c.s. values of σ -bonding ligands from compound to compound seem to be small as illustrated by the good agreement of the calculated and observed center shifts for *trans*-FeHCl(depe)₂ (Table XLVIII, compound 45).

The availability of p.c.s. data allowed a more careful study of the relationship between center shift and bonding properties of the ligands first observed for the Fe(CN)₅X derivatives (76, 142, 238). As stated earlier, an increase in both the σ -donor and π -acceptor abilities of the ligands will be expected to produce a decrease in the p.c.s. values. In agreement with this expectation, the most positive p.c.s. values (I⁻, Br⁻, and Cl⁻) are associated with the most ionic ligands, while H⁻ (very strong σ donor) and NO⁺ (very strong π acceptor) have the most negative values. In fact, using the partial ligand field strengths of the ligands (δ) calculated from the optical spectra of Co^{III} compounds (524), a good general correlation was observed between p.c.s. value and the ranking of the ligand in the spectrochemical series (44). Although an exact relationship is not expected, the correlation demonstrates that p.c.s. values give a good guide to relative δ values. For example, the p.c.s. of H⁻ provides strong evidence that H⁻ occupies a position close to CN⁻

TABLE XLVIII
CENTER SHIFT VALUES FOR Fe^{II} LOW-SPIN COMPOUNDS^a

Code No.	Compound	Center shift		Ref.
		Obs.	Pred.	
1	<i>trans</i> -FeCl ₂ (ArNC) ₄	+0.36	—	(44)
2	<i>trans</i> -Fe(SnCl ₃) ₂ (ArNC) ₄	+0.24	—	(44)
3	<i>trans</i> -FeCl ₂ (depe) ₂	+0.59	—	(44)
4	<i>trans</i> -FeBr ₂ (depe) ₂	+0.66	—	(44)
5	<i>trans</i> -FeI ₂ (depe) ₂	+0.65	—	(44)
6	<i>trans</i> -FeCl ₂ (depb) ₂	+0.59	—	(44)
7	<i>trans</i> -FeH ₂ (depb) ₂	+0.23	—	(44)

continued

TABLE XLVIII—*continued*
 CENTER SHIFT VALUES FOR Fe^{II} LOW-SPIN COMPOUNDS^a

Code No.	Compound	Center shift		Ref.
		Obs.	Pred.	
8	<i>trans</i> - $\text{FeCl}_2(\text{dmpe})_2$	+0.54	—	(44)
9	<i>cis</i> - $\text{Fe}(\text{CO})_4\text{Cl}_2$	+0.24	—	(39)
10	<i>trans</i> - $\text{Fe}(\text{N}_3)_2(\text{depe})_2$	+0.56	—	(44)
11	<i>trans</i> - $\text{Fe}(\text{NCO})_2(\text{depe})_2$	+0.51	—	(44)
12	<i>trans</i> - $\text{Fe}(\text{NCS})_2(\text{depe})_2$	+0.49	—	(44)
13	$[\text{Fe}(\text{MeNC})_6](\text{HSO}_4)_2$	+0.14	—	(55)
14	$[\text{Fe}(\text{EtNC})_6](\text{ClO}_4)_2$	+0.16	—	(55)
15	$\text{K}_4\text{Fe}(\text{CN})_6$	+0.21	—	(215)
16	$[\text{Fe}(\text{PhCH}_2\text{NC})_6](\text{ClO}_4)_2$	+0.12	—	(55)
17	$\text{Na}_2[\text{Fe}(\text{CN})_5\text{NO}] \cdot 2\text{H}_2\text{O}$	0.00	—	(238)
18	$\text{Na}_4[\text{Fe}(\text{CN})_5\text{NO}_2]$	+0.26	—	(238)
19	$\text{Na}_5[\text{Fe}(\text{CN})_5\text{SO}_3]$	+0.22	—	(238)
20	$\text{Na}_3[\text{Fe}(\text{CN})_5\text{H}_2\text{O}]$	+0.31	—	(142)
21	$[\text{Fe}(\text{bipy})_3](\text{ClO}_4)_2$	+0.52	—	(215)
22	$[\text{Fe}(\text{phen})_3](\text{ClO}_4)_2$	+0.58	—	(215)
23	$\text{Na}_3[\text{Fe}(\text{CN})_5\text{P}(\text{C}_6\text{H}_5)_3]$	+0.23	—	(239)
24	$\text{Na}_3[\text{Fe}(\text{CN})_5\text{As}(\text{C}_6\text{H}_5)_3]$	+0.29	—	(239)
25	$\text{Na}_3[\text{Fe}(\text{CN})_5\text{Sb}(\text{C}_6\text{H}_5)_3]$	+0.26	—	(239)
26	$\text{Fe}(\text{niox})_2(\text{NH}_3)_2$	+0.46	—	(156)
27	$\text{Fe}(\text{niox})_2(\text{py})_2$	+0.46	—	(156)
28	$\text{K}_2[\text{Fe}(\text{noix})_2(\text{CN})_2]$	+0.34	—	(156)
29 ^b	$\text{PcFe}(\text{py})_2$	+0.51	—	(156)
30	$\text{Fe}(\text{niox})_2(\text{im})_2$	+0.49	—	(156)
31	$\text{Fe}(\text{niox})_2(\text{but})_2$	+0.47	—	(156)
32	$\text{PcFe}(\text{pip})_2$	+0.51	—	(156)
33	$\text{Fe}(\text{NCS})_2(\text{qp})$	+0.47	—	(237)
34	$[\text{Fe}(\text{pyim})_3]\text{X}_2$	+0.62	—	(195)
35	$[\text{Fe}(\text{tripyam})_2](\text{ClO}_4)_2$	+0.63	—	(406)
36 ^c	$\text{Fe}(\text{phen-derivatives})_3(\text{X})_2$	+0.52–+0.56	—	(135, 209, 236)
37 ^b	$\text{Fe}(\text{DMG})_2(\text{py})_2$	+0.39	—	(3, 236)
38	$\text{K}_4[\text{Fe}(\text{CNBF}_3)_6]$	+0.15	—	(312)
39	$\text{Fe}(\text{CNH})_4(\text{CN})_2$	+0.16	—	(312)
40	<i>cis</i> - $\text{FeCl}_2(\text{ArNC})_4$	+0.28	+0.36	(44)
41	<i>cis</i> - $\text{Fe}(\text{SnCl}_3)_2(\text{ArNC})_4$	+0.27	+0.24	(44)
42	<i>cis</i> - $\text{FeClSnCl}_3(\text{ArNC})_4$	+0.23	+0.30	(44)
43	$[\text{FeCl}(\text{ArNC})_5]\text{ClO}_4$	+0.22	+0.26	(44)
44	$[\text{Fe}(\text{SnCl}_3)(\text{ArNC})_5]\text{ClO}_4$	+0.18	+0.20	(44)
45	<i>trans</i> - $\text{FeHCl}(\text{depe})_2$	+0.39	+0.42	(44)
46	<i>trans</i> - $\text{FeHI}(\text{depe})_2$	+0.39	+0.45	(44)
47	<i>trans</i> - $\text{FeCl}(\text{SnCl}_3)(\text{depe})_2$	+0.55	+0.54	(44)
48	<i>trans</i> - $\text{FeBr}_2(\text{depb})_2$	+0.61	+0.66	(44)
49	<i>trans</i> - $\text{Fe}(\text{CN})_2(\text{MeNC})_4$	+0.16	+0.18	(55)
50	<i>cis</i> - $\text{Fe}(\text{CN})_2(\text{MeNC})_4$	+0.16	+0.18	(55)

TABLE XLVIII—*continued*

Code No.	Compound	Center shift		Ref.
		Obs.	Pred.	
51	<i>trans</i> -Fe(CN) ₂ (EtNC) ₄	+0.21	+0.18 (55)	
52	<i>cis</i> -Fe(CN) ₂ (EtNC) ₄	+0.21	+0.18 (55)	
53	[Fe(CN)(EtNC) ₅]ClO ₄	+0.20	+0.17 (55)	
54	<i>trans</i> -Fe(CN) ₂ (PhCH ₂ NC) ₄	+0.15	+0.14 (55)	
55	[Fe(CN)(PhCH ₂ NC) ₅]ClO ₄	+0.14	+0.12 (55)	
56	Na ₃ [Fe(CN) ₅ NH ₃]H ₂ O	+0.26	+0.28 (238)	
57	Fe(phen) ₂ (NO ₂) ₂	+0.53	+0.54 (372)	
58	K ₂ [CaFe(NO ₂) ₆]	+0.55	+0.46 (501)	
59	[Fe(bipy) ₂ (NCS)py]NCS	+0.61	+0.52 (372)	
60	K ₃ [Fe(CN) ₅ CO]	+0.15	+0.18 (215)	
61	K ₂ [Fe(bipy)(CN) ₄]	+0.32	+0.32 (215)	
62	K ₂ [Fe(phen)(CN) ₄]	+0.33	+0.34 (215)	
63	<i>cis</i> -Fe(bipy) ₂ (CN) ₂	+0.43	+0.42 (215)	
64	<i>cis</i> -Fe(phen) ₂ (CN) ₂	+0.42	+0.46 (215)	
65	<i>trans</i> -Fe(phen) ₂ (CN) ₂	+0.48	+0.46 (215)	
66	K ₂ [PcFe(CN) ₂]	+0.37	+0.38 (156)	
67	KFe(niox) ₂ Im·CN]	+0.34	+0.41 (156)	
68	Fe(niox) ₂ Im·CO	+0.26	+0.37 (156)	
69	PcFe(Im) ₂	+0.47	+0.52 (156)	
70	PcFe(but) ₂	+0.52	+0.50 (156)	
71	Fe(CN) ₂ (qp)	+0.31	+0.36 (237)	
72	Fe(CNH) ₄ (CNBF ₃) ₂	+0.14	+0.16 (312)	
73	<i>trans</i> -Fe(CNMe) ₄ (CNBF ₃) ₂	+0.18	+0.16 (312)	
74	<i>trans</i> -Fe(CNet) ₄ (CNBF ₃) ₂	+0.16	+0.16 (312)	
75	[FeH(ArNC)(depe) ₂] ⁺ BPh ₄ ⁻	+0.19	+0.32 (45)	
76	[FeH(CO)(depe) ₂] ⁺ BPh ₄	+0.12	+0.29 (45)	
77	<i>cis</i> -FeH ₂ (CO) ₄	+0.01	-0.12 (44)	
78	[Fe(DTOH ₂) ₂]Cl ₂	+0.50	— (1, 236)	
79	[Fe(DTOH) ₂]	+0.30	— (1, 236)	
80	[Fe(DTOCH ₃) ₂]	+0.53	— (1, 236)	
81	[FeHP(OMe) ₃ (depe) ₂] ⁺ BPh ₄ ⁻	+0.25	— (45)	
82	[FeHP(OPh) ₃ (depe) ₂] ⁺ BPh ₄ ⁻	+0.26	— (45)	
83	[FeH(PhCN)(depe) ₂] ⁺ BPh ₄ ⁻	+0.33	— (45)	
84	[FeH(MeCN)(depe) ₂] ⁺ BPh ₄ ⁻	+0.35	— (45)	
85	[FeHN ₂ (depe) ₂] ⁺ BPh ₄ ⁻	+0.32	— (45)	

^a Data given in mm/sec at room temperature relative to sodium nitroprusside. This table is largely taken from Table 5, Ref. (44). All C.S. values have been converted from stainless steel to nitroprusside. C.S. = 0.16 + \sum_i (p.c.s.)_i.

^b C.S. values for analogous compounds with py replaced by other N bases give very similar C.S. values (3, 236, 347).

^c Many substituted phenanthroline compounds with different X groups have been run with very similar results (135, 209, 236).

in the spectrochemical series, and not a position between H_2O and NH_3 as previously suggested (434, 537). The relationship between p.c.s. and δ also suggests (44) that there may be a limiting value of C.S. for low-spin Fe^{II} compounds (~ 0.5 relative to stainless steel; ~ 0.7 relative to nitroprusside), above which there is a transition from low-spin to high-spin Fe^{II} .

As with the p.q.s. treatment, there are situations where the p.c.s. values may vary widely, thus leading to large discrepancies between observed and predicted values. For strong π -accepting ligands such as

TABLE XLIX
PARTIAL CENTER SHIFT VALUES FOR Fe^{II} LOW-SPIN COMPOUNDS^a

$\text{NO}^+ = -0.20$	$\text{SnCl}_3^- = 0.04$	$\text{py} = 0.07$
$\text{H}^- = -0.08$	$\text{qp}/_4 = 0.05$	$\text{NH}_3 = 0.07$
$\text{CO} = -0.03$	$\text{niox}/_2 = 0.04$	$\text{but} = 0.07$
$\text{PhCH}_2\text{NC} = -0.01$	$\text{SbPh}_3 = 0.05$	$\text{AsPh}_3 = 0.08$
$\text{CNBF}_3 = 0.00$	$\text{NO}_2^- = 0.05$	$\text{pip} = 0.08$
$\text{CNH} = 0.00$	$\text{Pc}/_4 = 0.05$	$\text{pyim}/_2 = 0.08$
$\text{ArNC} = 0.00$	$\text{dmpe}/_2 = 0.05$	$\text{tripyam}/_3 = 0.08$
$\text{MeNC} = 0.00$	$\text{NCS}^- = 0.05$	$\text{Im} = 0.08$
$\text{EtNC} = 0.00$	$\text{NCO}^- = 0.06$	$\text{N}_3^- = 0.08$
$\text{CN}^- = 0.01$	$\text{depe}/_2 = 0.06$	$\text{H}_2\text{O} = 0.10$
$\text{SO}_3^{2-} = 0.01$	$\text{depb}/_2 = 0.06$	$\text{Cl}^- = 0.10$
$\text{P}(\text{C}_6\text{H}_5)_3 = 0.02$	$\text{bipy}/_2 = 0.06$	$\text{Br}^- = 0.13$
$\text{DMG}/_2 = 0.03$	$\text{phen}/_2 = 0.07$	$\text{I}^- = 0.13$

^a Data given in mm/sec. Most of these values are taken from Ref. (44).

CO , it has become apparent that the C.S. values are not additive. For example, consider $[\text{FeHCO}(\text{depe})_2]^+$ (Table XLVIII, compound 76). Although a *trans*- CO compound was not available to derive $(\text{p.c.s.})_{\text{CO}}$ initially, the predicted C.S. value using the p.c.s. in Table XLIX is 0.29 mm/sec, while the observed value is 0.12 mm/sec. Similarly, for compounds such as $\text{Fe}(\text{CO})_2\text{X}_2\text{P}_2$ and $\text{Fe}(\text{CO})_3\text{X}_2\text{P}$ ($\text{X} = \text{Cl}, \text{Br}, \text{I}$; $\text{P} = \text{PPh}_2\text{Me}$, etc.) (39), the C.S. values are not additive. The CO group tends to "draw off" any excess charge on the Fe atom, and this effect, of course, results in a lowering of the CO stretching frequency.

In anionic compounds, there is also some evidence that the cation has an effect on the C.S. For example, a series of $\text{M}_4\text{Fe}^{\text{II}}(\text{CN})_6$ and $\text{M}_2\text{Fe}^{\text{II}}(\text{CN})_5\text{NO}$ ($\text{M} = \text{H}, \text{Li}, \text{Na}, \text{K}$, etc.) complexes (255, 404) shows a systematic trend in C.S. This trend has been attributed to a change in S.O.D. shift (404), although the changing polarizing power of the cation

may also be a factor. A small difference in C.S. has also been observed between $\text{K}_4\text{Fe}(\text{CN})_6 \cdot 3\text{H}_2\text{O}$ and $\text{H}_4\text{Fe}(\text{CN})_6$ (500).

Despite these discrepancies, it appears that for the majority of six-coordinate Fe^{II} low-spin compounds which do not contain strong π acceptors such as CO or NO^+ , the p.c.s. treatment should provide a reasonably accurate guide to C.S. values. For series of compounds such as the *trans*- $[\text{FeHL}(\text{depe})_2]^+\text{BPh}_4^-$ series, where some of the L are π acceptors, it is probably more informative to discuss variations in C.S. from compound to compound rather than derive p.c.s. for ligands.

b. Bonding Properties from C.S. and Q.S. Data. As discussed previously, p.c.s. values decrease with increasing σ bonding and π back-bonding, while the p.q.s. values become more positive with increasing π back-bonding, but more negative with increasing q_{lat} . Thus (44),

$$\text{p.c.s.} = k(\sigma_{\text{L}} + \pi_{\text{L}}) \quad (49)$$

$$\text{p.q.s.} = q_{\text{lat}} + c(\pi_{\text{L}}' - \sigma_{\text{L}}') \quad (50)$$

These two equations provide a very useful method for at least qualitatively characterizing both the σ -donor and π -acceptor properties of ligands. As expected from the above equations, H^- and NO^+ , the best σ -donor and π -acceptor ligands, respectively, give the most negative p.c.s. values of all ligands (Table XLIX), but have the most negative and positive p.q.s. values, respectively (Table XLVI). Considering some of the neutral ligands, the p.c.s. values show that $\sigma + \pi$ increases in the order $\text{H}_2\text{O} < \text{NH}_3 < \text{depe}/_2 \sim \text{depb}/_2 < \text{dmpe}/_2 < \text{ArNC} < \text{CO}$, whereas the p.q.s. values show that $\pi - \sigma$ increases in the order $\text{RNC} < \text{dmpe}/_2 < \text{depe}/_2 < \text{depb}/_2 < \text{NH}_3 < \text{H}_2\text{O} \sim \text{CO}$ (Fig. 15). For the first five ligands, the σ -donor properties probably dominate both the p.c.s. and p.q.s. values, and a correlation of p.c.s. *vs.* p.q.s. is observed (Fig. 15). However, RNC and CO (and NO^+) lie to the left of the line, because the π -acceptor properties are becoming more important in the order $\text{RNC} < \text{CO} < \text{NO}^+$. In the extreme case where the π -acceptor ability dominates both the p.c.s. and p.q.s. values, a line of opposite slope to that observed for the " σ -bonding" ligands would be observed.

For charged ligands, it is more difficult to evaluate σ and π because of possible q_{lat} effects.

Similarly, for the *trans*- $[\text{FeHL}(\text{depe})_2]^+\text{BPh}_4^-$ series of compounds, a plot of C.S. *vs.* Q.S. (Fig. 15) gives a reasonable correlation for all ligands but CO and N_2 . The slope of the line indicates that, except for CO and N_2 , the σ -donor properties are dominant in determining both the C.S. and Q.S. The C.S. data indicate that $\sigma + \pi$ increases in the order: $\text{MeCN} < \text{PhCN} < \text{N}_2 < \text{P}(\text{OPh})_3 < \text{P}(\text{OMe})_3 < \text{Me}_3\text{CNC} < p\text{-MeO} \cdot \text{C}_6\text{H}_4 \cdot$

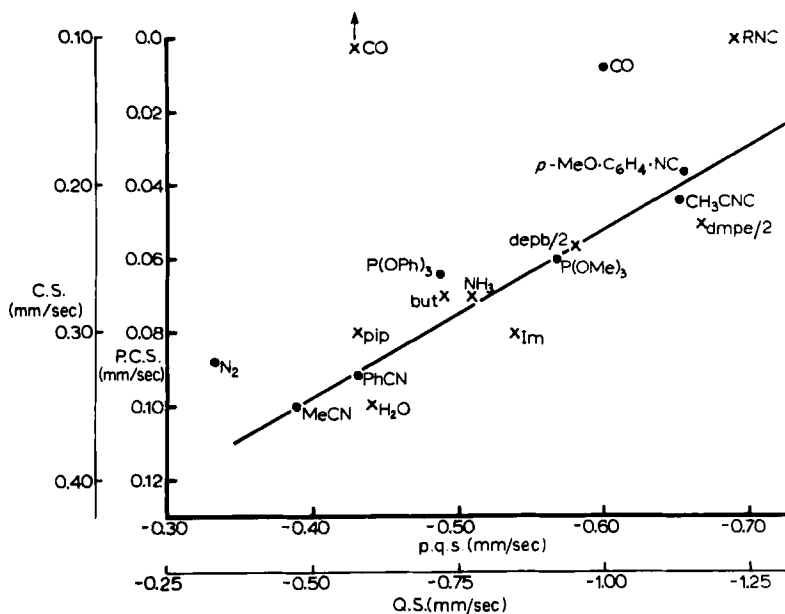


FIG. 15. Plots of (a) C.S. vs. Q.S. for $[\text{FeHL}(\text{depe})_2] \text{BPh}_4$ compounds (denoted \bullet); (b) p.q.s., vs. p.q.s. for a number of neutral ligands (Tables XLIV, XLVI, XLVIII, and XLIX) (denoted \times).

$\text{NC} < \text{CO}$, while π - σ (from the Q.S.) increases in the order $p\text{-MeO} \cdot \text{C}_6\text{H}_4 \cdot \text{NC} < \text{Me}_3\text{CNC} < \text{CO} < \text{P}(\text{OMe})_3 < \text{P}(\text{OPh})_3 < \text{PhCN} < \text{MeCN} < \text{N}_2$. The correlation for all ligands but CO and N_2 again indicates that N_2 is a very poor (relatively) σ donor and a moderate π acceptor, whereas CO is a good π acceptor and moderately good σ donor (37).

C. Ru^{II} AND Ir^{III} COMPOUNDS

It would seem likely that the p.c.s. and/or p.q.s. treatments might be applicable to other analogous t_{2g}^6 systems such as Co^{III} , Ru^{II} , and Ir^{III} . Although Co does not have a Mössbauer nuclide, NQR data on Co^{III} compounds can be compared with Mössbauer data for Fe^{II} low-spin compounds discussed previously to obtain the sign of the Q.S. for Co^{III} compounds (22). The sign of the Co Q.S. cannot be obtained from NQR. Using the p.q.s. values derived from Fe^{II} low-spin compounds, the expected Q.S. for a Co^{III} species such as $[\text{Co}(\text{NH}_3)_4\text{Cl}_2]^+$ is given by

$$(e^2qQ)_{\text{Co cpd}} = \frac{e^2q_{3d(\text{Co})}Q_{\text{Co}}}{e^2q_{3d(\text{Fe})}Q_{\text{Fe}}} (e^2qQ)_{\text{Fe cpd}} \quad (51)$$

assuming that the bonding in the analogous Co and Fe compounds is the same. For example, the expected Q.S. for a low-spin *trans*-Fe(NH₃)₄Cl₂ species is 0.84 mm/sec, and the Q.S. for *trans*-[Co(NH₃)₄Cl₂]⁺ should also be positive, instead of negative as calculated previously (517). Q.S. values for Fe compounds should be about one-third that of the Co

TABLE L
MÖSSBAUER PARAMETERS FOR Ru^{II} COMPOUNDS AT 4.2°K^a

Code No. ^b	Compound	C.S. ^c	Q.S.	Ref.
1	Ru(NH ₃) ₆ Cl ₂	-0.82	—	(470, 472)
2	[Ru(NH ₃) ₅ CH ₃ CN](ClO ₄) ₂	-0.71	—	(472)
3	[Ru(NH ₃) ₅ N ₂]Cl ₂	-0.62	0.20	(472)
4	[Ru(NH ₃) ₅ N ₂]X ₂ ^d	-0.81	0.26	(470)
5	[Ru(NH ₃) ₅ SO ₂]Cl ₂	-0.61	0.30	(472)
6	[Ru(NH ₃) ₅ CO]Br ₂	-0.54	—	(472)
7	[Ru(NH ₃) ₅ NO]Cl ₃ ·nH ₂ O	-0.18	0.36	(294, 470, 472)
8	[Ru(NH ₃) ₄ (SO ₂)Cl]Cl	-0.50	0.56	(470)
9	[Ru(NH ₃) ₄ (NO)(OH)]X ₂ ^d	-0.16	0.27	(470)
10	K ₄ [Ru(CN) ₆]	-0.24	—	(129, 362)
11	K ₂ [Ru(CN) ₅ NO]·2H ₂ O	-0.06	0.42	(129, 294, 470)
12	K ₄ [Ru(CN) ₅ NO ₂]	-0.37	0.28	(129, 470)
13	M ₂ [RuCl ₅ (NO)] ^d	-0.37	0.21	(294, 470)
14	Cs ₂ [RuBr ₅ (NO)]	-0.47	0.08	(294)
15	Rb ₂ [Ru(NCS) ₅ (NO)]	-0.30	0.24	(294)

^a Data given in mm/sec. C.S. and Q.S. values quoted are averages of available data.

^b Code number will be preceded by table number in text.

^c Relative to Ru metal at 4.2°K.

^d X = Cl, Br and/or I; M = K, Rb.

compounds (mainly due to $Q_{Co} \sim 0.4$ barns, and $Q_{Fe} \sim 0.2$ barns), and it should be possible to use the above equation to calculate approximate e^2qQ values for either Fe or Co compounds, if the e^2qQ value for the corresponding Co or Fe compound is known, or can be predicted from the p.q.s. values in Table XLVI (22).

For Ru^{II} and Ir^{III}, the bonding characteristics of ligands cannot be assumed identical in the analogous Ru^{II}, Ir^{III}, and Fe^{II} compounds, but it should still be possible to use the relative p.q.s. values in Table XLVI to predict the signs and relative magnitudes of Q.S. values in Ru^{II} and Ir^{III} compounds containing the ligands in Table XLVI. Recent data for Ru^{II} compounds (Table L) provides an excellent

framework to discuss the possibilities of this idea. It should be recognized, however, that the Ru^{II} quadrupole splittings are rather small and have relatively large errors.

For example, the averaged Q.S. values for $\text{K}_2[\text{Ru}(\text{CN})_5\text{NO}] \cdot 2\text{H}_2\text{O}$ (129, 294, 470) and $\text{K}_4[\text{Ru}(\text{CN})_5\text{NO}_2]$ (129, 470) are 0.42 and 0.28 mm/sec, respectively, while the corresponding Fe compounds have quadrupole splittings of +1.72 and 0.85 mm/sec (most likely positive), respectively. The ratios of the splittings are similar, and it would seem most likely that the signs of the Ru Q.S. values are positive. From the Fe^{II} p.q.s. values for NO^+ , Br^- , Cl^- , NCS^- , and CN^- (Table XLVI), we would predict that

TABLE LI
Q.S. VALUES FOR
 $\text{XYIr}^{\text{III}}\text{Cl}(\text{CO})(\text{PPh}_3)_2$ COMPOUNDS^a

X	Y	Q.S. ^b
H	H	4.76
H	Cl	1.44
Cl	Cl	3.10

^a From Ref. (562).

^b Data given in mm/sec.

the signs of the Q.S. in the series $[\text{Ru}(\text{X}_5)\text{NO}]^{2-}$ ($\text{X} = \text{Br}^-$, Cl^- , NCS , CN^-) (Table L, compounds 11, 13–15) are positive, and that the magnitudes would vary in the observed order $\text{X} = \text{CN}^- > \text{NCS}^- > \text{Cl}^- > \text{Br}^-$. Similarly, with the ammonia derivatives (Table L, compounds 1–9), we would expect a large positive Q.S. for $[\text{Ru}(\text{NH}_3)_5\text{NO}]^{3+}$, and a very small positive Q.S. for $[\text{Ru}(\text{NH}_3)_5\text{CO}]^{2+}$, because of the very similar p.q.s. values for NH_3 and CO (Table XLVI). In addition, it seems likely that the sign of the Q.S. in $[\text{Ru}(\text{NH}_3)_5\text{N}_2]\text{Cl}_2$ is positive, since N_2 should have a more positive p.q.s. than NH_3 from the Fe^{II} low-spin work. This positive sign would be expected since N_2 is likely a poorer σ donor and a better π acceptor than NH_3 .

Q.S. values reported recently for Ir^{III} compounds (Table LI) (562) should obey the additivity model reasonably well, and from the Fe^{II} p.q.s. values (Table XLVI), it would seem possible that the H,H and Cl,Cl derivatives have negative and positive V_{zz} , respectively, with the H,Cl derivative probably having a negative V_{zz} (assuming trans X and Y groups).

Little systematic C.S. work on series of Ru and Ir compounds has yet been carried out, but recent interesting Ru Mössbauer studies indicate that the order of C.S. values is similar to that expected from the Fe^{II} low-spin work. The C.S. values for the series [Ru(NH₃)₅X] (Table L, compounds 1–7) decrease in the order NO⁺ > CO > SO₂ > N₂ > CH₃CN > NH₃. Although attributed to a decrease in π -acceptor properties of X (470, 472, 473), the above order probably reflects a decrease in $(\sigma + \pi)$ of these ligands. Thus, as concluded from the [Fe^{II}HL(depe)₂]⁺BPh₄ series, N₂ is a poorer $(\sigma + \pi)$ ligand than CO, but slightly better than nitriles. Combined with the Q.S. data, N₂ appears to be a better π acceptor, but poorer σ donor than nitriles. This result is also consistent with that deduced from the Fe^{II} low-spin data (37). As with the Fe^{II} low-spin compounds, there is a correlation of the C.S. values for the [RuX₅NO]²⁻ compounds (Table L, compounds 11, 13–15) with the spectrochemical ranking of the X ligands (294).

D. IODINE COMPOUNDS

1. General Principles

Mössbauer spectra of iodine compounds may be obtained by utilizing either the 57.6 keV $\frac{7}{2} + \rightarrow \frac{5}{2}$ + transition of ¹²⁷I or the 27.7 keV $\frac{5}{2} + \rightarrow \frac{3}{2}$ + transition of ¹²⁹I. Unfortunately, both isotopes present problems. In the case of ¹²⁷I, the resolution of the spectra is often poor, and detailed computer analysis is needed to extract meaningful parameters; although the resolution of ¹²⁹I spectra is excellent, the necessity of synthesizing all absorbers from active ¹²⁹I presents a formidable experimental inconvenience. The majority of work published so far deals with ¹²⁹I spectra, although considerable effort has also been given to ¹²⁷I. For both isotopes the spins of the ground and excited states allow the determination of the sign and magnitude of e^2qQ , as well as η and the center shift. The values of e^2qQ and η are, of course, complimentary to values available from ¹²⁷I NQR spectroscopy, but the extra parameters (i.e., the center shift and the sign of e^2qQ) available from Mössbauer spectra often enable a more meaningful analysis of the data.

In this section we will discuss the general principles used in the interpretation of the iodine Mössbauer spectra and in the following section we will survey the experimental data.

The quadrupole coupling parameter e^2qQ and η are usually analyzed using the Townes–Dailey theory (163, 540) developed for the interpretation of NQR spectra. The basic assumption of this theory is that the major contributions of the EFG arise from an aspherical distribution of the electronic charge of the valence shell. Neglecting contributions

from $5d$ electrons and cross-terms, q for an iodine atom is given by Eq. (9), and e^2qQ is given by:

$$e^2qQ = e^2QK_p [-N_{p_x} + \frac{1}{2}(N_{p_x} + N_{p_y})] \quad (52)$$

where Q is the quadrupole moment of ^{129}I and is negative. The term $[-N_{p_x} + \frac{1}{2}(N_{p_x} + N_{p_y})]$ is often referred to as U_p and, hence,

$$e^2qQ = e^2QK_p U_p \quad (53)$$

The asymmetry parameter is given by the expression

$$\eta = \frac{3}{2}(N_{p_x} - N_{p_y})/U_p \quad (54)$$

For an iodine atom with a single I-A bond, e^2qQ may be related to bonding parameters. Thus, the I-A bond can be described by a molecular orbital (ψ) formed by a linear combination of atomic orbitals of I(ϕ_I) and A(ϕ_A). This molecular orbital may be written

$$\psi = \frac{a\phi_I + b\phi_A}{(a^2 + b^2 + 2abS)^{1/2}} \quad (55)$$

where $S = \int \phi_I \phi_A \delta I$. The parameters a and b determine the relative importance of ϕ_I and ϕ_A in the molecular orbital and are often expressed in terms of the ionic character I .

$$I = \frac{1 - b^2/a^2}{1 + b^2/a^2} = \frac{a^2 - b^2}{a^2 + b^2} \quad (56)$$

Thus, if $a = b = 1$, the bond is completely covalent, whereas if $a = 0$, $I = -1$ and the bond is completely ionic in the sense I^+A^- . For $b = 0$, the bond is ionic in the sense I^-A^+ .

The atomic orbital of ϕ_I may be written as a linear combination of the $5s$, $5p_z$, and $5d_{z^2}$ orbitals.

$$\phi_I = (1 - s^2 - d^2)^{1/2} \phi_{p_z} + s\phi_s + d\phi_{d_{z^2}} \quad (57)$$

while the involvement of $5s$ electrons in ϕ_I means that the $5s$ lone pair will be contained in an orbital of type

$$\phi_t = (1 - s^2)^{1/2} \phi_s + s\phi_{p_z} \quad (58)$$

The population of ϕ_I is given to a first approximation [i.e., neglecting $2abS$ (292)] by $2a^2/(a^2 + b^2)$ and, hence, N_{p_z} may be written as

$$N_{p_z} = \frac{2a^2}{a^2 + b^2} (1 - s^2 - d^2) + 2s^2 \quad (59)$$

From the definition of I (Eq. 56),

$$I + 1 = \frac{2a^2}{a^2 + b^2} \quad (60)$$

and, hence,

$$N_{p_z} = 1 + I + s^2 - d^2 - I(s^2 + d^2) \quad (61)$$

The term $I(s^2 + d^2)$ is normally neglected and, hence,

$$N_{p_z} = 1 + I + s^2 - d^2 \quad (62)$$

In the absence of π bonding, N_{p_x} and N_{p_y} will be equal to 2, but if π bonding removes π electrons from the p_x and p_y orbitals, then

$$N_{p_y} = N_{p_x} = 2 - \pi \quad (63)$$

Substitution from Eqs. (62) and (63) into Eq. (52) yields

$$\frac{e^2qQ}{e^2QK_p} = 1 - I - \pi - s^2 + d^2 \quad (64)$$

From Eq. (64) the relationship of e^2qQ to the iodine bonding may be assessed. Thus, e^2qQ will have a maximum negative value ($q = +ve$) for an I^+ ion ($a^2 = 0$, $I = -1$) and a minimum value for an I^- ion ($b^2 = 0$, $I = 1$). In the case of I_2 ($a^2 = b^2$, $I = 0$), V_{ZZ} will be equal to $K_p(1 - s^2 + d^2)$ and, hence, in the limiting case of pure p bonding with $\pi = 0$, e^2qQ will be equal to e^2QK_p . The quantity e^2QK_p has been found to be equal to -2293 Mc/sec (354) and this value allows $1 - I - \pi - s^2 + d^2$ (U_p) to be expressed in number of electrons.

The type of argument outlined above may be extended to more complex iodine bonding and these situations will be discussed as they arise.

The center shifts of iodine compounds will depend directly on the number of $5s$ electrons and indirectly (via shielding effects) on the number of $5p$ electrons. If h_s and h_p are the magnitudes of the s and p electron holes in the closed I^- valence shell, then the center shift with respect to an arbitrary source may be written (310, 452)

$$\text{C.S.} = K[-h_s + \gamma(h_p + h_s)(2 - h_s)] + S \quad (65)$$

where the term h_s represents the direct contribution from the loss of $5s$ electrons and the second term in the square brackets represents the increased s density at the nucleus resulting from the change in h_p and h_s . S is the center shift of the source from I^- and the constant K will depend

on the value of $\Delta R/R$. Assuming $h_s \ll 1$ and, hence, neglecting terms in h_s^2 and $h_s h_p$, Eq. (65) reduces to

$$\text{C.S.} = Ah_s + Bh_p + C \quad (66)$$

where $A = K - 2K\gamma$ and $B = 2K\gamma$.

For compounds in which the iodine atoms have single or two colinear bonds, a relationship between center shift and e^2qQ may be derived (203). Thus, neglecting π bonding,

$$h_p = 6 - (N_{p_x} + N_{p_y} + N_{p_z}) = |U_p| = 2 - N_{p_z} \quad (67)$$

and as

$$\begin{aligned} N_{p_z} &= (1 + s^2 - d^2 + I) & [\text{Eq. (62)}] \\ h_p &= (1 - s^2 + d^2 - I) \end{aligned} \quad (68)$$

If the effect of d -orbital participation is also neglected, expressions for h_p and h_s may be derived from the orbitals ϕ_I [Eq. (57)] and ϕ_t [Eq. (58)] which will have populations of $2a^2$ and 2 electrons, respectively. Thus,

$$h_p = 2 - 2a^2(1 - s^2) - 2s^2 = s^2(2a^2 - 2) + 2 - 2a^2 \quad (69)$$

and

$$h_s = 2 - 2a^2 s^2 - 2(1 - s^2) = s^2(2 - 2a^2) \quad (70)$$

and, hence,

$$h_p + h_s = 2 - 2a^2 \quad (71)$$

and

$$\frac{h_s}{h_p + h_s} = \frac{s^2(2 - 2a^2)}{(2 - 2a^2)} = s^2 \quad (72)$$

The equations derived above allow, at least in principle, the determination of the parameters h_p , h_s , s^2 , and I from a combination of quadrupole coupling and center shift data and, thus, provide a framework for the discussion of the iodine Mössbauer spectra.

2. Experimental Data

The majority of the available ^{127}I and ^{129}I Mössbauer data are summarized in Table LII. All values of e^2qQ have been expressed relative to the quadrupole moment of ^{127}I , and values of U_p have been calculated assuming $e^2qQ_p = -2293$ Mc/sec. Also included in Table LII are some NQR data; in general, the agreement with the Mössbauer results is excellent, especially as the Mössbauer and NQR measurements are often taken at different temperatures.

One of the most important tasks in the interpretation of the data in Table LII is the calibration of the center shifts in terms of h_p and h_s . This was first attempted by Hafemeister *et al.* (310) for ^{129}I using the

data for the alkali iodides (Table LII, compounds 1–5). Independent estimates of h_p for these species are available from NMR (68) and dynamic quadrupole coupling (408) measurements, and the variations of h_p reflect those of the center shifts. From these data, Hafemeister *et al.* (310) concluded that $\Delta R/R$ for ^{129}I is 3×10^{-5} . Pasternak *et al.* (443), assuming pure p bonding, took the center shifts of crystalline I_2 (Table LII, compound 9) to represent $h_p = 1$. Combination of the data for I_2 with those of the alkali iodides, gives the equation

$$\text{C.S.}(\text{ZnTe})^{129} = 0.136 h_p - 0.054 \text{ (cm/sec)} \quad (73)$$

More recent measurements (89) of frozen solutions of iodine in hexane, carbon tetrachloride, and argon (Table LII, compounds 10–12) have shown increased center shifts compared with crystalline iodine. This increase in center shift is probably due to intermolecular association in the solid and, hence, the frozen solution data provide a better guide to the center shift for $h_p = 1$. Interpretation of frozen solution data modifies Eq. (73) to give

$$\text{C.S.}(\text{ZnTe})^{129} = 0.15 h_p - 0.054 \text{ (cm/sec)} \quad (74)$$

The effect of variations in h_s has been assessed (445) by consideration of the center shifts of the ions IO_3^- , IO_4^- , and IO_6^{5-} (Table LII, compounds 21–29). The iodine atoms in the ions IO_4^- and IO_6^{5-} have a formal oxidation of VII and are situated in regular tetrahedral and octahedral environments. In contrast, IO_3^- contains an IV atom situated on top of a pyramid with an O-I-O angle close to 90° . Assuming pure p bonding in IO_3^- , Pasternak and Sonnino (445) deduced from Eq. (73) that $h_p = 1.54$, which can be interpreted in terms of the removal of 0.51 electrons from the I^- configuration per I-O bond. The value of A in Eq. (66) was then deduced from the center shifts of IO_4^- and IO_6^{5-} assuming that $s^2 = \frac{1}{4}$ and $\frac{1}{6}$, respectively, and that each I-O bond withdraws 0.51 electrons. A mean value of $A = -0.82$ was obtained and Eq. (74) may be extended to give

$$\text{C.S.}(\text{ZnTe})^{129} = -0.92 h_s + 0.15 h_p - 0.054 \text{ (cm/sec)} \quad (75)$$

where the original formula of Pasternak and Sonnino (445) has been modified as suggested by Bukshpan *et al.* (89). Equation (75) shows that the effect on the center shift of removing an s electron is of opposite sign and six times as large as that of removing a p electron.

The first calibration of the center shift scale for ^{127}I was by Perlow and Perlow (452). These authors, assuming pure p bonding in the interhalogen compounds, used the quadrupole coupling data of HI , ICl , $\text{KICl}_4 \cdot \text{H}_2\text{O}$, and $\text{KICl}_2 \cdot \text{H}_2\text{O}$ (Table LII, compounds 13, 14, 18, 20)

TABLE LII
MÖSSBAUER DATA FOR SOME IODINE COMPOUNDS

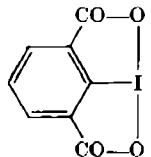
Code No. ^a	Compound ^b	Isotope	Mössbauer data					NQR data		
			C.S. ^c	e^2qQ^d	η	U_p^e	Ref. ^f	e^2qQ^d	η	Ref. ^g
1	LiI	129	-0.38 ^h	—	—	—	(310)	—	—	—
2	NaI	129	-0.46 ^h	—	—	—	(310)	—	—	—
		127	+0.14 ⁱ	—	—	—	(452)	—	—	—
3	KI	129	-0.51 ^h	—	—	—	(310)	—	—	—
		127	+0.14 ⁱ	—	—	—	(452)	—	—	—
4	RbI	129	-0.43 ^h	—	—	—	(310)	—	—	—
5	CsI	129	-0.37 ^h	—	—	—	(310)	—	—	—
		127	+0.12 ⁱ	—	—	—	(452)	—	—	—
6	AgI	129	-0.22 ^h	—	—	—	(419)	—	—	—
7	CuI	129	-0.38 ^h	—	—	—	(153)	—	—	—
8	HI(aq.)	127	+0.16 ⁱ	—	—	—	(452)	—	—	—
9	I ₂	127	-0.58 ⁱ	-2238 ⁱ	0.12	0.98	(452)	2153 ^k	0.15 ^k	(173)
		129	+0.83 ^h	-2156 ^h	0.16	0.94	(445)	—	—	—
10	I ₂ /hexane	129	+0.98 ⁱ	-2263 ⁱ	—	0.99	(89)	—	—	—
11	I ₂ /CCl ₄	129	+0.91 ⁱ	-2273 ⁱ	—	0.99	(89)	—	—	—
12	I ₂ /argon	129	+0.93 ^m	-2231 ^m	—	0.97	(89)	—	—	—
13	HI(anhydrous)	127	-0.62 ^{i,j}	-1640 ⁱ	—	0.72	(452)	-1831 ⁿ	—	(144)
14	ICl	127	-0.62 ⁱ	-2868 ⁱ	—	1.25	(452)	3008 ^o	0.02 ^o	(371)
		129	+1.73 ^h	-3131 ^h	0.06	1.36	(445)	-3046 ^h	0.03 ^h	(571)
15	IBr	129	+1.23 ^h	-2892 ^h	0.06	1.26	(445)	—	—	—
16	ICN	129	+1.19 ^p	-2640 ^p	—	1.15	(446)	-2549 ^k	—	(105)
17	I ₂ Cl ₆	129	+3.50 ^h	+3060 ^h	0.06	-1.33	(445)	3035 ^h	0.08 ^h	(571)
18	KICl ₄ ·H ₂ O	127	-1.39 ⁱ	+3094 ⁱ	—	-1.35	(452)	3059 ^q	—	(571)
19	I ₂ Cl ₄ Br ₂ ^r	129	+3.48	+3040 ^h	0.06	-1.33	(445)	—	—	—
			+2.82	+2916 ^h	0.06	-1.27	(445)	—	—	—

G. M. BANCROFT AND R. H. PLATT

20	KICl ₂ ·H ₂ O	127	-0.58 ⁱ	-3189 ⁱ	—	1.39	(452)	3140 ^a	—	(571)
21	KIO ₃	129	+1.56 ^h	—	—	—	(310)	996 ^a	—	(392)
22	NH ₄ IO ₃	129	+1.31 ^h	—	—	—	(310)	—	—	—
23	Ba(IO ₃) ₂	129	+1.11 ^h	+1030 ^h	—	-0.45	(310)	—	—	—
24	NaIO ₃	127	-0.44 ⁱ	+1089 ^{i,s}	—	-0.47	(361)	—	—	—
25	NaIO ₃ ·H ₂ O	127	-0.41 ⁱ	+1107 ^{i,s}	—	-0.48	(361)	—	—	—
26	Na ₂ Mn(IO ₃) ₆	127	-0.55 ⁱ	+1080 ^{i,s}	—	-0.47	(361)	—	—	—
27	KIO ₄	129	-2.34 ^h	—	—	—	(310)	—	—	—
		127	+0.70 ⁱ	—	—	—	(452)	—	—	—
28	NaIO ₄	127	+0.85 ⁱ	—	—	—	(361)	—	—	—
29	Na ₃ H ₂ IO ₆	127	+1.02 ⁱ	—	—	—	(361)	—	—	—
30	GeI ₄	129	+0.48 ⁱ	-1500 ⁱ	—	0.65	(88)	1492 ^{h,u}	—	(493)
31	SiI ₄	129	+0.26 ⁱ	-1335 ⁱ	—	0.58	(88)	1329 ^{h,u}	—	(493)
32	SnI ₄	129	+0.43 ⁱ	-1364 ⁱ	—	0.59	(91)	1389 ^{h,u}	—	(493)
33	Cl ₄	129	+0.20 ⁱ	-2102 ⁱ	—	0.92	(93)	2130 ^h	—	(493)
		127	-0.35 ⁱ	-2160 ⁱ	—	0.94	(293)	—	—	—
34	CHI ₃	129	+0.53 ⁱ	-2029 ⁱ	—	0.88	(93)	2056 ^{h,v}	0.02	(493)
		129	+0.52 ⁱ	-2065 ⁱ	—	0.90	(203)	—	—	—
		127	-0.21 ⁱ	-2060 ⁱ	—	0.90	(203)	—	—	—
35	CH ₂ I ₂	127	-0.14 ⁱ	-1920 ⁱ	—	0.84	(203)	1897 ^h	0.09	(493)
36	CH ₃ I	129	+0.20 ⁱ	-1739 ⁱ	—	0.76	(93)	1766 ^h	0.03	(493)
		127	-0.01 ⁱ	-1775 ⁱ	—	0.77	(203)	—	—	—
37	IF ₅	129	+3.00 ^w	+1073 ^w	—	-0.47	(90)	—	—	—
38	IF ₇	129	-4.56 ^w	-148 ^w	—	0.06	(90)	—	—	—
39	IF ₆ ⁺ AsF ₆ ⁻	129	-4.68 ⁱ	—	—	—	(92)	—	—	—
40	CsIF ₆	129	+2.45 ⁱ	-1414 ⁱ	—	0.62	(92)	—	—	—
41	I ₂ /benzene	129	+0.76 ⁱ	-2412 ⁱ	—	1.05	(89)	—	—	—
42	I ₂ ·PH	129	+0.93 ⁱ	-2223 ⁱ	—	0.97	(350)	—	—	—
43	I ₂ ·AC ^r	129	+1.64 ⁱ	-2840 ⁱ	—	1.24	(350)	—	—	—
			+0.29 ⁱ	-1308 ⁱ	—	0.57	—	—	—	—
44	I ₂ HMTA ^r	129	+1.51 ⁱ	-2582 ⁱ	—	1.13	(350)	—	—	—
			+0.28 ⁱ	-1272 ⁱ	—	0.55	—	—	—	—

continued

TABLE LII—*continued*
MÖSSBAUER DATA FOR SOME IODINE COMPOUNDS

Code No. ^a	Compound ^b	Isotope	Mössbauer data					NQR data		
			C.S. ^c	e^2qQ^d	η	U_p^e	Ref. ^f	e^2qQ^d	η	Ref. ^g
45	2(I ¹²⁷ Br)2,2'-bipy	129	+1.35 ⁱ	-2910 ⁱ	0.15	1.27	(570)	—	—	—
46	2(I ¹²⁷ Br)4,4'-bipy	129	+1.48 ⁱ	-3110 ⁱ	—	1.36	(570)	—	—	—
47	I ¹²⁷ Br·py	129	+1.61 ⁱ	-3224 ⁱ	—	1.41	(570)	—	—	—
48	2(I ¹²⁷ Cl)2,2'-bipy	129	+1.90 ⁱ	-3424 ⁱ	—	1.49	(570)	—	—	—
49	2(I ¹²⁷ Cl)4,4'-bipy	129	+1.43 ⁱ	-3428 ⁱ	—	1.49	(570)	—	—	—
50	ICl·py	129	+1.74 ⁱ	-3310 ⁱ	—	1.44	(570)	—	—	—
51	ICl·PMT	129	+1.90 ⁱ	-3395 ⁱ	—	1.48	(570)	—	—	—
42	PhI	127	-0.27 ⁱ	-1840 ⁱ	—	0.80	(205)	—	—	—
53	PhICl ₂	127	-0.78 ⁱ	+2525 ⁱ	0.70	-1.10	(205)	—	—	—
54	PHIO	127	-0.73 ⁱ	+2345 ⁱ	0.60	-1.02	(205)	—	—	—
55	PhIO ₂	127	-0.75 ⁱ	+1050 ⁱ	0.18	-0.46	(205)	1046 ^z	0.17 ^z	(392)
56		127	-0.83 ⁱ	+2585 ⁱ	0.92 ⁱ	-1.13	(205)	—	—	—
57	CsI ₃ ^y	129	+1.40 ⁱ	-2500 ⁱ	—	1.09	(204)	2477 ^h	—	(502)
				-1460 ⁱ	—	0.64	—	1436 ^h	0.04	—
				-830 ⁱ	—	0.36	—	819 ^h	0.02	—
58	Benz-HI ₃ ^r	129	+1.33 ⁱ	-2460 ⁱ	—	1.07	(204)	—	—	—
				-1180 ⁱ	—	0.51	—	—	—	—
59	Am-HI ₃ ^r	129	+1.31 ⁱ	-2450 ⁱ	—	1.07	(204)	—	—	—
				-930 ⁱ	—	0.41	—	—	—	—

60	CrI ₃	129	+0.23 ^h	+662 ^h	0.35	-0.29	(285)	—	—	—
61	SaI ₃	129	-0.25 ^h	—	—	—	(153)	—	—	—
62	GdI ₃	129	-0.38 ^h	—	—	—	(153)	—	—	—
63	ErI ₃	129	-0.29 ^h	—	—	—	(153)	—	—	—

^a Code number will be prefixed by Table number in the text.

^b PH = Phenazine; AC = acridine; HMTA = hexamethyltetramine; 2,2'bipy = 2,2'bipyridyl; 4,4'-bipy = 4,4'-bipyridyl; py = pyridine; PMT = pentamethylene tetrazole; Benz = benzamide; Am = amylose.

^c Data given in mm/sec relative to ZnTe.

^d Mc/sec for ¹²⁷I ground state, values quoted relative to ¹²⁹I have been converted assuming $Q(129)/Q(127) = 0.701$.

^e Calculated assuming $eQKp = -2292.7$ (354).

^f Reference to Mössbauer data.

^g Reference to NQR data.

^h At 77°K.

ⁱ At 4°K.

^j Converted from H₆TeO₆ source by addition of +0.95 mm/sec. This conversion is an average of the data for compounds, which were measured relative to both sources in Ref. (458).

^k At 300°K.

^l At 88°K.

^m At 22°K.

ⁿ Data for gaseous compound obtained by microwave spectroscopy.

^o At 295°K.

^p At 100°K.

^q At 298°K.

^r Spectrum shows two nonequivalent iodine atoms.

^s Converted from mm/sec.

^t At 85°K.

^u Average of two frequencies.

^v Spectrum of CHI₃·3S₈.

^w At 90°K.

^x At 274°K.

^y Spectrum shows three inequivalent iodine atoms.

to obtain values of h_p . Thus, for the species $\text{KICl}_2 \cdot \text{H}_2\text{O}$, ICl , and HI , assuming no π bonding, Eq. (67) gives

$$h_p = |U_p| \quad (76)$$

whereas for $\text{KICl}_4 \cdot \text{H}_2\text{O}$ which is square-planar

$$h_p = |2U_p| \quad (77)$$

For I_2 , h_p was taken as 1.11 to allow for an 11% admixture of p^4d character (493) in the bonding. These values of h_p gave a good linear relationship with center shift, from which it was deduced that $B = 2K\gamma = -0.56 \text{ mm/sec}/h_p$. Thus,

$$\text{C.S.}(\text{I}^-)^{127} = -0.56h_p \text{ (mm/sec)} \quad (78)$$

Then, taking $\gamma = 0.1$, $B = -K + 2K\gamma = 2.2 \text{ mm/sec}/h_s$, and Eq. (78) becomes

$$\text{C.S.}(\text{I}^-)^{127} = 2.2h_s - 0.56h_p \text{ (mm/sec)} \quad (79)$$

From Eq. (79) it will be noted that $\Delta R/R$ for ^{127}I is negative and, thus, has an opposite sign to that for ^{129}I . Ruby and Shenoy (498) have calculated the ratio of $\Delta R/R(^{127}\text{I})/\Delta R/R(^{129}\text{I})$ to be -0.78 , while a combination of the results of Pasternak *et al.* (443) and Perlow and Perlow (452) yields a ratio of -0.85 (498).

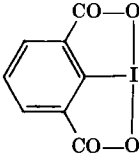
The combination of center shift and quadrupole coupling data for an iodine molecule provides a good means of determining the degree of s hybridization in the iodine bonds. Thus, for linear or square-planar arrangements of the bonds (neglecting π bonding), values of h_p calculated from U_p data [Eqs. (76) and (77), together with Eqs. (74) and (78)] should give a reasonable prediction of center shift. However, as the center shift caused by an s -electron hole is six times the shift due to a p -electron hole, even a small degree of s hybridization will lead to large inaccuracies in using Eqs. (74) and (78) to calculate center shifts. In Table LIII are given calculated center shifts for the ^{129}I spectra of IBr , I_2 , ICN , ICl , and I_2Cl_4 , together with the observed values. In all cases, save ICl , good agreement is obtained confirming pure p bonding (445, 446). The parameters for ICl may indicate some degree of π bonding. However, the extent of the π bonding required ($\pi = 10\%$) seems far too large, and Pasternak and Sonnino (445) have concluded that the value of U_p for ICl is not a good measure of the p -electron density.

Ehrlich and Kaplan (205) have made a detailed study of the bonding in the species in Table LII, compounds 52–56. The crystal structure (16) of PhICl_2 shows a linear ICl_2 group at an angle of 85° to the phenyl plane. The bonding of this compound may be described either by

dsp^3 hybridization with two equatorial lone pairs or by a p -bonding scheme utilizing a three-center two-electron molecular orbital between the iodine and two chlorine atoms. The former bonding scheme, which would involve a minimum value of $h_s = 0.37$ (205) is not compatible with either the center shift or the values of e^2qQ and η found for PhICl_2 and must, therefore, be rejected. Assuming, as required for a p -bonding

TABLE LIII

CALCULATED AND OBSERVED CENTER SHIFTS FOR SOME IODINE COMPOUNDS

Compound ^a	Isotope	Obs. C.S. ^b	h_p ^c	Calc. C.S.	π
IBr	129	+1.23	1.26	+1.35 ^d	—
ICl	129	+1.73	1.36	+1.50 ^d	10 ^g
ICN	129	+1.19	1.15	+1.19 ^d	—
I ₂ Cl ₆	129	+3.50	2.66	+3.45 ^d	—
PhI	127	-0.27	0.80	-0.29 ^e , -0.24 ^f	—
PhICl ₂	127	-0.78	1.91	-0.91 ^e , -0.80 ^f	—
PhIO	127	-0.73	1.78	-0.84 ^e , -0.73 ^f	—
	127	-0.83	1.98	-0.95 ^e , -0.83 ^f	—
PhIO ₂	127	-0.75	2.74	-1.37 ^e , -1.21 ^f	—
I ₂ /benzene	129	+0.76	1.05	+1.04 ^d	—
GeI ₄	129	+0.48	0.65	+0.44 ^d	—
SiI ₄	129	+0.26	0.58	+0.33 ^d	—
SnI ₄	129	+0.43	0.59	+0.35 ^d	—
2(IBr)2,2'-bipy	129	+1.35	1.27	+1.37 ^d	4 ^g
2(IBr)4,4'-bipy	129	+1.48	1.36	+1.50 ^d	4 ^g
IBrpy	129	+1.61	1.41	+1.58 ^d	6 ^g
2(ICl)2,2'-bipy	129	+1.90	1.49	+1.70 ^d	7 ^g
2(ICl)4,4'-bipy	129	+1.43	1.49	+1.70 ^d	0 ^g
IClpy	129	+1.74	1.44	+1.62 ^d	4 ^g
IClPMT	129	+1.90	1.48	+1.68 ^d	10 ^g

^a 2,2'-bipy = 2,2'-Bipyridyl; 4,4'-bipy = 4,4'-Bipyridyl; py = pyridine; PMT = pentamethylene tetrazole.

^b Data from Table LII, mm/sec relative to ZnTe.

^c h_p derived from e^2qQ and Table LII as described in text.

^d Using Eq. (74).

^e Using Eq. (78), assuming center shift of I⁻ is +0.16.

^f Assuming $2K\gamma = 0.50$ and center shift of I⁻ is +0.16.

^g Reference (570).

scheme, a filled p_z orbital perpendicular to the molecular plane, e^2qQ and η are given (205) by the expressions

$$\frac{e^2qQ \text{ (Mc/sec)}}{2293 \times 1.15} = \frac{2525}{2637} = 2 - \frac{1}{2}(N_{p_x} + N_{p_y}) \quad (80)$$

$$\eta = 0.70 = \frac{\frac{3}{2}(N_{p_x} - N_{p_y})}{2 - \frac{1}{2}(N_{p_x} + N_{p_y})} \quad (81)$$

where the correction term 1.15 has been applied to e^2qQ_p to allow for a change in $\langle r^{-3} \rangle$ resulting from the positive charge on the iodine atom. Solution of Eqs. (80) and (81) yields

$$N_{p_z} = 2.00, \quad N_{p_x} = 1.27, \quad N_{p_y} = 0.82 \quad (82)$$

from which it follows that $h_p = 1.91$. Similar analysis may be applied to the e^2qQ and η values of PhIO, PhIO₂, and iodosodilactone assuming a C-I-O bond angle of 90° in PhIO and T-shaped IO₂ groupings in both PhIO₂ and iodosodilactone; for iodobenzene $U_p = h_p$. Values of h_p and calculated center shifts using Eq. (78) are contained in Table LIII. In all cases except PhIO₂, good agreement with experimental center shift is obtained confirming pure p bonding. The discrepancy between the observed and calculated center shifts for PhIO₂ is probably due to s hybridization and a value of $h_s = 0.16$ (205) would be sufficient to account for the observed center shift.

The probability of pure p bonding in Table LII, compounds 52-54 and 56 provides a further means of calibrating the ¹²⁷I center shift scale. A plot of C.S. against h_p gives (205) a value of $2K\gamma = -0.50 \text{ mm/sec}/h_p$ compared with $-0.56 \text{ mm/sec}/h_p$ from Eq. (78) and $-0.47 \text{ mm/sec}/h_p$ from Eq. (73) when converted to ¹²⁷I units.

No π bonding would be expected in the series CH_{*n*}I_{4-*n*} ($n = 0-3$) (Table LII, compound 33-36) and, hence, it would be anticipated that $|U_p| = h_p$. The calculated center shifts for the ¹²⁷I spectra using Eq. (78) show an increasing deviation from the observed values as n increases, indicative of an increasing degree of s hybridization from $n = 0$ to $n = 3$. Erhlich and Kaplan (203) have calculated, using Eqs. (68)-(72), values of h_p , h_s , s^2 , and I for these compounds, and the results are given in Table LIV. Calculations using both available values of $2K\gamma$ (205, 452) have been made as well as calculations using the ¹²⁹I data of Bukshpan and Sonnino (93). For Cl₄ and CHI₃, values of s^2 from ¹²⁹I and ¹²⁷I agree with the uncertainty of the calibration constant, but for CH₃I a large discrepancy of experimental origin is observed. The data in Table LIV also show (as noted above) a trend to increasing s^2 and I as n increases from 0→3.

The calculated center shifts, using Eq. (74) assuming $U_p = h_p$, for the species MI_4 ($M = \text{Si, Ge, or Sn}$) (Table LII, compounds 30–32) are summarized in Table LIII. For GeI_4 the agreement with the experimental value is good, indicating pure p bonding; while for SiI_4 , the data suggest a small degree of s hybridization. In the case of SnI_4 , the calculated center shift is rather low, perhaps indicating a small degree of π bonding (91).

Wynter *et al.* (570) have reported ^{129}I Mössbauer spectra of the addition complexes of IBr and ICl with nitrogen bases (Table LII,

TABLE LIV
BONDING PARAMETERS FOR SOME IDOMETHANES^a

Compound	$2K\gamma = -0.56 \text{ mm/sec}$				$2K\gamma = -0.50 \text{ mm/sec}$			
	h_p	h_s	$s^2\%$	$I\%$	h_s	$s^2\%$	$I\%$	$s^2\%^b$
CI_4	0.94	0.004	0.4	6	-0.012	-1.3	7	0.6
CHI_3	0.90	0.034	3.6	6	0.022	2.4	8	1.8
CH_2I_2	0.84	0.046	5.2	11	0.036	4.1	12	—
CH_3I	0.77	0.071	8.5	14	0.066	7.9	15	4.4

^a Taken from Ref. (203), see text for definition of parameters.

^b Data from Ref. (93), recalculated in Ref. (203).

compounds 45–51). For the IBr complexes the p -orbital imbalance (U_p) increases linearly with the basicity of the amine, suggesting a linear N-I-Br linkage (570). The center shifts also increase with basicity, and calculated center shifts using Eq. (74) are in good agreement with the observed values confirming pure p bonding (Table LIII). A systematic relationship between Mössbauer parameters and basicity is not observed for the ICl derivatives, and there is also substantially worse agreement between observed and calculated center shifts (Table LIII). This is not altogether surprising as difficulty has been encountered in interpreting the Mössbauer data for ICl itself. Wynter *et al.* (570) have also calculated the percent π -bonding character (π) for the iodine bonds in these complexes. Thus, deriving U_p from e^2qQ and h_p from Eq. (74), a value of π may be calculated from the relationship

$$\pi = \frac{1}{3}(h_p - U_p) \quad (83)$$

The values of π obtained are listed in Table LIII, but in view of the

uncertainties in the calibration of the center shift, it is doubtful if they have more than qualitative significance.

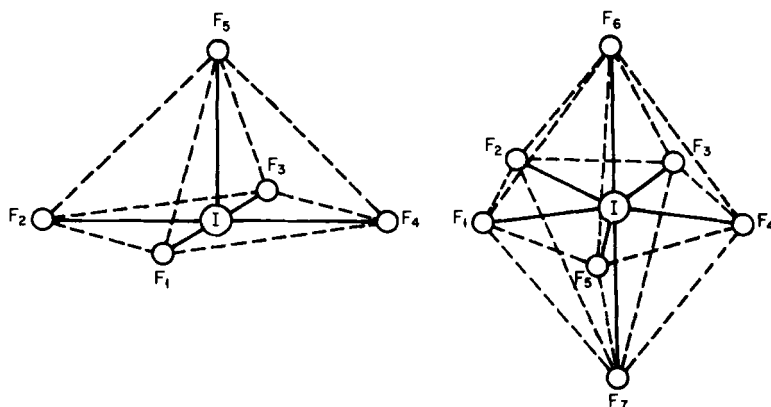
An increase in e^2qQ and, hence, U_p is observed for an I_2 solution in benzene (Table LII, compounds 35–41) as compared with crystalline iodine or solutions of iodine in inert matrices (Table LII, compounds 9–12) (89, 445). This is rather surprising as a transfer of electrons from the benzene ring to the iodine bond would be expected. Further, the calculated center shift, using Eqs. (74) and $h_p = U_p$ (Table LIII) is much higher than the experimental value and corresponds to $h_s = \text{ca. } 0.03$. Bukshpan *et al.* (89) have calculated a value of $h_p = 0.87$ by substituting experimental values of center shift into Eq. (74) and have used this result to infer the transfer of 0.26 electrons from the ring to the iodine atoms. This conclusion is, however, of doubtful validity. Thus, use of Eq. (74) implies that $h_s = 0$ and, hence, $h_p = U_p$. This is clearly not the case for the I_2 /benzene solution in which h_p from Eq. (74) is equal to 0.87, while $U_p = 1.05$.

The Mössbauer spectrum of I_2 -phenazine (Table LII, compound 42) (350) indicates only one type of iodine atom in agreement with the crystal structure (544), which shows a straight-chain configuration of alternating iodine and phenazine molecules resulting in equivalent N–I bonds. In contrast, I_2 -acridine and I_2 -hexamethylenetetramine (Table LII, compounds 43, 44) show two chemically inequivalent iodine atoms in the Mössbauer spectrum (350), indicative of only one N–I bond per iodine molecule. Ichiba *et al.* (350) have derived orbital populations for these complexes assuming pure p bonding.

In agreement with NQR data (502), Erlich and Kaplan found evidence for three nonequivalent iodine atoms in the Mössbauer spectrum of CsI_3 (Table LII, compounds 35–37). Assuming a linear structure, the largest value of e^2qQ may be assigned to the terminal iodine atoms. A sum of U_p for all three types of iodine is remarkably close to 2, indicating pure p bonding. Inequivalent iodine atoms are also indicated in the species benzamide- HI_3 (Table LII, compound 58) and amylose- HI_3 (Table LII, compound 59), although it was not possible to resolve separate spectra for the two terminal atoms. These data are in agreement with the structural studies of Robin *et al.* (475, 492).

The Mössbauer parameters of the fluoride species IF_7 , IF_5 , IF_6^- , and IF_6^+ (Table LII, compounds 37–40) (90, 92) are of interest because of the very high oxidation states and coordination numbers. The structures of IF_5 (521) and IF_7 (521) have been determined by use of X-ray diffraction and are illustrated in Fig. 16, while a regular octahedral structure may be inferred for IF_6^+ (117).

Bukshpan *et al.* (90, 92) have reported a detailed analysis of the

FIG. 16. Molecular structures of IF₅ and IF₇ (90).

Mössbauer parameters of these species. Thus, assuming that for IF₇ $N_{p_z} = 0$, it follows that $N_{p_x} + N_{p_y} = 2U_p = 0.13$. These populations give a value of $h_p = 5.87$ and from Eq. (75), $h_s = 1.56$.^{*} The total number of electrons transferred from the iodine to fluorines is, therefore, 6.43, and each fluorine atom can be considered to have removed 0.92 electrons. If it is now assumed that the fluorine atoms also remove 0.92 electrons from the iodine atom in IF₅, the experimental center shift and U_p may be used to derive the parameters $h_p = 5.08$, $h_s = 0.5$, $N_{p_z} = 0.62$, $N_{p_x} = N_{p_y} = 0.3$. These results seem realistic as they indicate a lone pair directed along the C_4 axes as would be expected from the stereochemistry (90). The Mössbauer spectrum of IF₆⁺ is a single line, as expected for an octahedral structure. From the experimental center shift, assuming $h_p = 6$, h_s equals 1.60, which corresponds to a loss of 5.60 electrons to the fluorine atoms, i.e., 0.93 electrons per fluorine atom. The spectrum of IF₆⁻ shows a positive value of U_p suggesting a similar structure to IF₇ with one of the equatorial fluorine atoms replaced by a lone pair. Assuming $N_{p_z} = 0$, $h_p = 4.76$, $h_s = 0.50$ and, hence, 0.88 electrons are removed per I-F bond (92).

E. Sn^{II} COMPOUNDS

The crystal structures of many tin(II) compounds [e.g., SnS (341), SnF₂ orthorhombic (188), Na₂Sn₂F₅ (394), K₂SnCl₄ (363), SnSe (429), SnCl₂ (499), and SnSO₄ (488)] show a distorted octahedral environment

^{*} In this, and other calculations of h_s , the authors (90, 92) have used C.S. (ZnTe)¹²⁹ = $-0.82h_s + 0.15h_p - 0.054$ (cm/sec) instead of Eq. (75).

with three short tin–ligand bonds, resulting in pyramidal coordination of the tin atom, and three longer tin–ligand distances completing the octahedron. This situation is often considered (182) in terms of sp^3 hybridization in which three orbitals form covalent bonds to the nearest neighbor atoms and the fourth orbital contains the lone pair and prevents the close approach of the atoms along the direction in which it points. The pyramidal bond angles would be expected to be reduced by lone pair–bond pair repulsions and in the limiting case of pure p bonding, bond angles of ca. 90° are anticipated. It is, however, difficult to deduce any information about bonding characteristics from the experimental bond angles owing to both the partial ionic character of the bonding and the unknown effect of lattice forces (182). The crystal structure of tetragonal SnO (409) shows a square-pyramidal arrangement of the oxygen atoms suggesting sp^3d_z hybridization resulting in four covalent bonds and a lone pair perpendicular to the plane.

As a result of the $5s^2$ electrons, a “perfect” Sn^{2+} ion would be expected to have a much greater center shift than gray α -tin. For Sn^{II} compounds, although the involvement of the $5s$ electrons in bonding will produce a reduction in center shift compared with an Sn^{2+} ion, the presence of a lone pair of electrons in an orbital of reasonably high $5s$ character should always ensure center shifts in excess of that of gray tin.

Table LV contains a collection of data for Sn^{II} compounds and, as anticipated, all center shifts are much larger than that of gray tin. From these data, attempts have been made to assess the relationship between bond character and center shift and, hence, obtain an estimate of the center shift of an Sn^{2+} ion ($\delta_{\text{Sn}^{2+}}$).

Early workers (74, 137) regarded SnCl_2 as ionic and took the center shift of this compound as a value of $\delta_{\text{Sn}^{2+}}$. However, as noted by Donaldson (190), the structure, volatility, and any estimate of the bonding of SnCl_2 are inconsistent with an ionic formalism. As a result, this estimate of $\delta_{\text{Sn}^{2+}}$ is probably too low.

An alternative approach by Lees and Flinn (381) uses a plot of quadrupole splitting against center shift. Most of the compounds considered lie on one of two straight lines, the gradients of which differ by a factor of two. It was assumed that the steeper of these two lines [SnSO_4 , $\text{SnCl}_2 \cdot 2\text{H}_2\text{O}$, SnC_2O_4 , SnF_2 , $\text{Sn}_2\text{P}_2\text{O}_7$, $\text{Sn}(\text{MeCO}_2)_2$, $\text{Sn}(\text{C}_4\text{H}_4\text{O}_6)_2$, $\text{Sn}_3(\text{PO}_4)_2$, and $\text{Sn}_3(\text{AsO}_4)_2$], which shows an approximately linear increase in quadrupole splitting with decreasing center shift, refers to compounds in which sp_z hybridization is important, while the other slope (SnBr_2 and SnS) refers to compounds in which equal amounts of p_x and p_y character are used in hybridization. Extrapolation of both lines to zero quadrupole splitting gave a value of 4.76 mm/sec

for $\delta_{\text{Sn}^{++}}$. Recent work (182, 271), however, has shown that the EFG of compounds lying on both lines [SnF_2 , $\text{Sn}_3(\text{PO}_4)_2$, SnC_2O_4 , $\text{Sn}(\text{O}_2\text{CMe})_2$, SnC_2O_4 , SnS , and SnSO_4] have the same sign, thus rendering Lees and Flinn's interpretation untenable.

A third approach to the problem has been described by Donaldson and Senior (190). These authors plotted the center shift of the Sn^{II} halides and chalcogenides, corrected for shielding effects, against the percentage sp^3 character estimated from the electronegatives of Hinze

TABLE LV
MÖSSBAUER PARAMETERS FOR SOME TIN COMPOUNDS

Compound	C.S. ^{a,b,e}	Q.S. ^a	Ref. ^c	Ref. ^d
SnF_2 (monoclinic)	3.67	+1.73	(74, 137, 189, 190, 381)	(271)
SnF_2 (orthorhombic)	3.30	2.18	(189)	—
NaSnF_3	3.17	+1.83	(191)	(183)
NaSn_2F_5	3.37	+1.86	(191)	(183)
SnCl_2	4.08	—	<i>f</i>	—
$\text{SnCl}_2 \cdot 2\text{H}_2\text{O}$	3.72	1.15	(137, 381)	—
SnBr_2	3.92	—	<i>f</i>	—
SnI_2	4.02	—	(182, 190, 303)	—
SnO (tetragonal)	2.80	+1.48	(74, 137, 190, 381)	(271)
SnO (orthorhombic)	2.70	2.20	(74)	—
SnS	3.41	+0.89	(74, 137, 190, 381)	(271)
SnSe	3.40	0.60	(190)	(271)
SnTe	3.33	0.50	(82, 190)	—
$\text{Sn}_3(\text{PO}_4)_2$	3.18	+1.75	(137, 381)	(271)
$\text{Sn}_2\text{P}_2\text{O}_7$	3.35	1.61	(381)	—
Sn_3AsO_4	2.97	2.03	(381)	—
$\text{Sn}(\text{O}_2\text{CMe})_2$	3.33	+1.72	(184, 381)	(183)
SnC_2O_4	3.75	+1.46	(137, 381)	(271)
$\text{SnC}_4\text{H}_4\text{O}_6$	3.11	1.97	(381)	—
$\text{Sn}(\text{HCO}_2)_2$	3.15	+1.56	(184)	—
$\text{K}_2\text{Sn}(\text{C}_2\text{O}_4)_2 \cdot \text{H}_2\text{O}$	—	+1.97	(183)	(183)
SnSO_4	3.99	+1.21	(137, 183, 187, 381)	(183)

^a Data given in mm/sec.

^b Relative to SnO_2 assuming center shift of α -tin is 2.1 mm/sec and that of PdSn is 1.52; data from Ref. (381) have converted from Mg_2Sn (77°K) using the value of the center shift SnO_2 quoted in this reference.

^c Reference to measurement of C.S., Q.S.

^d Reference to measurement of sign of $\frac{1}{2}e^2qQ$.

^e When appropriate an unweighted average has been taken.

^f Only recent data included. Refs. (187, 194, 303, 185).

and Jaffe (339, 340). A straight-line relationship was obtained for all compounds save SnO and SnF₂, and extrapolation to zero sp^3 character yielded a center shift of 7.7 mm/sec for an Sn²⁺ ion. As mentioned previously (Section IV, A, 2), this value is close to that expected from consideration of the probable center shift of an Sn⁴⁺ ion. Donaldson and Senior have suggested that the anomalously low center shifts of SnO and SnF₂ are due to extra sp mixing arising from crystal field effects. As such effects are very sensitive to the tin-anion bond length, they are only expected to be important for the oxide and fluoride.

The origins of the quadrupole splittings found for Sn^{II} compounds has been the subject of some discussion. The crystal structure of tetragonal SnO leaves little doubt that the lone-pair electrons are contained in a dsp^3 hybrid orbital perpendicular to the plane of the oxygen atoms. Because of the axial symmetry, the p contribution to the lone pair will be entirely p_z and, thus, a negative value of V_{zz} is anticipated. Boyle *et al.* (74) deduced from the asymmetry in the intensities of the spectrum of an oriented sample that the sign of $\frac{1}{2}e^2qQ$ for SnO was positive, thus allowing a negative sign to be assigned to Q for the excited state of ¹¹⁹Sn.

For compounds with pyramidal structures the presence of a lone pair in an approximately sp^3 -hybridized orbital would also be expected to give a positive sign for $\frac{1}{2}e^2qQ$, and this has been confirmed by application of a large magnetic field for the compounds SnF₂ (271), NaSnF₃ (183), NaSn₂F₅ (183), SnS (271), Sn₃(PO₄)₂ (271), Sn(O₂CMe)₂ (183), SnC₂O₄ (271), Sn(HCO₂)₂ (183), K₂Sn(C₂O₄)₂·H₂O (183), and SnSO₄ (183).

An alternative interpretation of the origins of the quadrupole splittings in pyramidal Sn^{II} compounds has been suggested by Donaldson and Senior (192), who noted that for compounds of known structure (SnF₂, NaSn₂F₅, SnS, K₂SnCl₄·H₂O, SnSO₄, and SnCl₂) the largest quadrupole splittings seem to be found for compounds (SnF₂, NaSn₂F₅) with the greater degree of asymmetry in the bond lengths. In contrast, there does not seem to be any correlation between quadrupole splitting and center shift, which might be expected if quadrupole splitting is chiefly dependent on lone-pair electrons. From these observations, Donaldson and Senior suggested that the EFG is produced primarily from inequalities in the tin-ligand bonds. Using the assumption that the lone-pair electrons make no contribution to the EFG, these authors calculated values of the p -orbital imbalance for the compounds SnF₂, NaSn₂F₅, SnS, K₂SnCl₄·H₂O, SnSO₄, and SnCl₂, which are a reasonable reflection of quadrupole splitting trends. However, the calculations predict opposite signs of $\frac{1}{2}e^2qQ$ for SnS and SnF₂ and such a change is not observed experimentally.

Although the available evidence seems to favor an interpretation of quadrupole splitting in terms of a dominant contribution from the lone pair, the lack of a general relationship between center shift and quadrupole splitting is surprising (183). Further, no rationalization of the relative magnitudes of the quadrupole splittings has been possible. For example, the point charge model (183) does not account for the widely different quadrupole splittings of SnSO_4 and $\text{Na}_2\text{Sn}_2\text{F}_5$. Clearly it is not yet possible to gain a complete understanding of the origins of the EFG's found for Sn^{II} compounds.

Mössbauer center shifts of a wide range of Sn^{II} complexes have been reported and a selection of the data is given in Table LVI. These compounds show a consistent trend to decreasing center shift compared with the parent compounds, and this shift has been associated (106, 185–187, 194, 303) with an increase in sp^3 character caused by the replacement of a bridging tin–ligand bond in the parent compound with a terminal bond in the complex. Another example of this effect (191) is found for the $[\text{Sn}_2\text{F}_5]^{2-}$ ions, which have consistently higher shifts than $[\text{SnF}_3]^-$ species. Coordination of a second ligand results in a further decrease in center shift—indicative of further participation of the $5s$ orbital in bonding. Two five-coordinate complexes have been reported ($\text{SnCl}_2 \cdot \text{terpyridyl}$ and $\text{SnCl}_2 \cdot \text{PMAQ}$), and these species have lower center shifts than four-coordinate analogs (194).

The amount by which the center shift is decreased on complex formation can be taken as a guide to the Sn–ligand bond strengths. For example, the sequence (186, 303) found for the amine complexes with SnCl_2 — N -methylmorpholine > morpholine ~ piperidine ~ piperazine > pyridine ~ α -picoline > γ -picoline > 1,10-phenanthroline ~ 2,2'-bipyridyl—roughly parallels the basic strength of the ligands as measured by pK values. Donaldson and Nicholson (185) have used the center shifts of 1:1 complexes with SnCl_2 to deduce the order of bond strengths: triphenylarsine oxide > triphenylphosphine oxide > pyridine > thiourea > pyridine 1-oxide > diglyme > urea > water.

The complexes in Table LVI and related species (106, 185–187, 194, 303) show quadrupole splittings in the range 0–2.25 mm/sec. However, very little correlation between quadrupole splitting and the nature of the complexes has been possible. This is probably due to the influence of the lone-pair electrons, as a result of which the quadrupole splitting is no longer an additive function of the ligands.

Mössbauer data for the species $\text{Sn}(\text{O}_2\text{CR})_2$ [$R = \text{H}, \text{Me}, \text{Et}, n\text{-Pr}, i\text{-Pr}, i\text{-Bu}, t\text{-Bu}, \text{CH}_n\text{Cl}_{3-n}$ ($n = 0\text{--}2$), $\text{CH}_n\text{F}_{3-n}$ ($n = 0\text{--}2$), $\text{CH}_3 \cdot \text{CHCl}$, and $\text{ClCH}_2 \cdot \text{CH}_2$] allow the assignment (184) of polymeric structures with pyramidally coordinated Sn^{II} units, and the Mössbauer parameters

for the ions $\text{Sn}(\text{O}_2\text{CR}')_3^-$ ($\text{R}' = \text{H}, \text{Me}, \text{ClCH}_2, \text{and FCH}_2$) (184) and $[\text{Sn}(\text{HPO}_3)_3]^{4-}$ (166) are also consistent with pyramidal coordination. Mössbauer data has also proved useful in the study of the products of the tin(II)-thiourea-anion system (106) and the decomposition products of trihydroxystannates (165).

The ternary halides of type SnXF ($\text{X} = \text{Cl}, \text{Br}, \text{I}$) comprise an interesting series of compounds (193). The Mössbauer spectra show only one type of tin environment. Structures based on the parent halides are, therefore, indicated. The center shifts of the SnXF ($\text{X} = \text{Cl}, \text{Br}, \text{I}$) species (3.64–3.78 mm/sec) are much closer to the value for SnF_2 (C.S. = 3.67 mm/sec) than SnCl_2 (C.S. = 4.17 mm/sec), SnBr_2 (C.S. = 4.03 mm/sec) or SnI_2 (C.S. = 3.95 mm/sec) suggesting a pyramidal structure with bridging fluorine atoms and terminal X atoms. Similarly, the center shifts of SnIX ($\text{X} = \text{Cl}, \text{Br}$) (C.S. = 3.76 mm/sec) are close to that of SnI_2 , indicating a structure with bridging iodine atoms. These types of arguments have been extended to assign structures to the more complex species Sn_2XF_3 ($\text{X} = \text{Cl}, \text{I}$), Sn_2BrCl_3 , Sn_3BrF_5 , and Sn_2NCSX_3 ($\text{X} = \text{F}, \text{Cl}, \text{Br}, \text{I}$).

TABLE LVI

SELECTION OF CENTER SHIFT DATA FOR TIN(II) COMPLEXES^a

Compound ^b	C.S. ^c	Ref.
SnF_2	3.67	(187)
MSnF_3^d	3.03–3.29	(191)
MSn_2F_5	3.17–3.44	(191)
$\text{SnF}_2 \cdot \text{py}$	3.24	(187)
SnCl_2	4.08	(185, 187, 194, 303)
$(\text{pyH})\text{SnCl}_3$	3.12	(187)
$\text{SnCl}_2 \cdot \text{py}$	3.29	(187)
$\text{SnCl}_2 \cdot 2\text{py}$	3.12	(187)
$\text{SnCl}_2 \cdot \text{Ph}_3\text{PO}$	3.21	(185)
$\text{SnCl}_2 \cdot 2\text{Ph}_3\text{PO}$	3.34	(185)
$\text{SnCl}_2 \cdot \text{pyO}$	3.50	(185)
$\text{SnCl}_2 \cdot 2\text{pyO}$	3.30	(185)
$\text{SnCl}_2 \cdot \text{Ph}_3\text{AsO}$	3.00	(185)
$\text{SnCl}_2 \cdot \text{CO}(\text{NH}_2)_2$	3.70	(185)
$\text{SnCl}_2 \cdot \text{CS}(\text{NH}_2)_2$	3.41	(106)
$\text{SnCl}_2 \cdot \text{H}_2\text{O}$	3.87	(185)
$2\text{SnCl}_2 \cdot \text{dg}$	3.58	(185)
$\text{SnCl}_2 \cdot \text{ppz}$	2.92	(186)
$\text{SnCl}_2 \cdot 2\text{morph}$	2.91	(186, 303)
$\text{SnCl}_2 \cdot \text{Me-morph}$	2.45	(303)

TABLE LVI—*continued*

Compound ^b	C.S. ^c	Ref.
SnCl ₂ ·2pip	2.86	(186)
SnCl ₂ ·bipy	3.53	(194, 303)
SnCl ₂ ·phen	3.59	(194, 303)
SnCl ₂ ·2 <i>p</i> -tol	3.47	(194)
SnCl ₂ ·2(γ -pic) ₂	3.40	(303)
SnCl ₂ ·2(α -pic) ₂	3.27	(303)
SnCl ₂ ·terp	3.17	(194)
SnCl ₂ ·PMAQ	3.33	(194)
SnBr ₂	3.92	(185, 187, 194, 303)
(pyH)SnBr ₃	3.65	(187)
SnBr ₂ ·py	3.45	(187)
SnBr ₂ ·2py	3.36	(187)
Sn(NCS) ₂	3.52	(187)
(pyH)Sn(NCS) ₃	3.28	(187)
Sn(NCS) ₂ ·2py	3.29	(187)
Sn(HCO ₂) ₂	3.15	(187)
MSn(HCO ₂) ₃ ^e	2.90–3.13	(184)
Sn(HCO ₂) ₂ ·py	3.05	(187)
Sn(HCO ₂) ₂ ·2py	3.04	(187)
SnSO ₄	4.00	(187)
SnSO ₄ ·py	3.52	(187)

^a Further data for similar complexes may be found in Refs. (106, 184–187, 194, 303).

^b dg = Diglyme; ppz = piperazine; morph = morpholine; Me-morph = *N*-methylmorpholine; *p*-tol = *p*-toluidine; pic = picoline; terp = terpyridyl; PMAQ = 8-(2-pyridylmethyleamine)quinoline.

^c Data given in mm/sec at liquid nitrogen temperature relative to SnO₂, assuming the center shifts of Pd(Sn) and α -tin are +1.52 and +2.10 mm/sec, respectively; when appropriate an unweighted average has been taken.

^d Range of data for M = NH₄, Na, K, Rb, Cs, Sr, and Ba.

^e Range of data for M = Rb, Cs, NH₄.

Clark *et al.* (124) have reported the Mössbauer spectra of the ions SnX₃[−] (X = F, Cl, Br, or I) and SnX₂Y[−] (X, Y = Cl, Br, or I). Although the SnX₃[−] species do show some correlation between center shift and ligand electronegativity, a linear relationship is not observed and the correlation does not extend to the mixed salts. This is in marked contrast to the octahedral Sn^{IV} halide complexes (Section IV, A, 2), and probably illustrates the ability of the lone pair to mask the effect of the ligands.

F. OTHER OXIDATION STATES OF IRON

An enormous number of Mössbauer spectra of Fe compounds have been recorded, and these spectra have been extremely useful in describing the structure and bonding in many of these compounds. For Fe^{II} and Fe^{III} high spin, $q_{\text{C.F.}} = 0$, and any quadrupole splitting will be due to q_{lat} and/or $q_{\text{M.O.}}$ [Eqs. (6)–(11)]. In contrast, for Fe^{II} high-spin and Fe^{III} low-spin compounds, the major part of the Q.S. is due to $q_{\text{C.F.}}$ [Eq. (11)]. The magnitudes of these Q.S. values over a wide range of temperature have been interpreted with varying degrees of success using models developed by Ingalls (351) and Golding [281–283]. Bonding information is usually more difficult to extract for these two species than for other Mössbauer compounds containing Fe^{II} low spin, Sn^{IV} , or Fe^{II} for which $q_{\text{C.F.}} = 0$. For other oxidation states of iron, i.e., Fe^0 , Fe^{-1} , and intermediate spin states of Fe^{II} and Fe^{III} , the separation of q into lattice and valence contributions [Eq. (6)], and the separation of q_{val} into $q_{\text{M.O.}}$ and $q_{\text{C.F.}}$ [Eq. (11)] no longer appears to be useful. Both $q_{\text{M.O.}}$ and $q_{\text{C.F.}}$ are of similar magnitudes. As a result, rationalization of Q.S. values—except on the purely empirical level—has usually not been possible.

In this section, we will review very briefly what we consider to be some interesting Mössbauer applications for iron compounds. Enough recent data is presented to enable the interested reader to find easily most of the papers in this area. A recent review of magnetic data (479) has recently been published, and as noted in the Preface, the very interesting magnetic properties of many of these iron compounds will not be discussed here. Many iron spectra have also been discussed recently (110).

1. Fe^{II} Compounds

Mössbauer spectra of a number of Fe^{II} (formally) compounds have been obtained, and a selection of data is given in Table LVII. Fe^{II} has the spherically symmetric electronic configuration d^6 , and the partial quadrupole splitting treatment outlined in Section II should be applicable to Fe^{II} quadrupole splittings. Indeed, Mazak and Collins (402) were among the first to apply a point charge treatment. All the compounds in Table LVII contain strong π -accepting ligands such as CO or NO^+ , and as noted previously for Fe^{II} low-spin compounds (Section IV, B), the partial quadrupole splitting treatment may not be as useful for such ligands. However, the p.q.s. treatment still should be useful for rationalizing the signs of the Q.S. values, and their approximate magnitudes.

The bonding in tetrahedral $\text{Fe}^{-\text{II}}$ compounds can be considered to be a combination of σ donation to the sp^3 Fe hybrids and π acceptance from the t_{2g} $3d$ orbitals. Because of the smaller $\langle r^{-3} \rangle$ for $4p$ electrons than $3d$ electrons, we would expect that σ donation in $\text{Fe}^{-\text{II}}$ compounds would not affect the Q.S. values as much as in Fe^{II} low-spin compounds.

Mazak and Collins (406) determined the signs of the Q.S. for $\text{KFe}(\text{CO})_3\text{NO}(+ve)$, $\text{Fe}(\text{CO})_2(\text{NO})_2(-ve)$, and $\text{Fe}(\text{Ph}_3\text{P})_2(\text{NO})_2(-ve)$. The first sign is expected from the p.q.s. values for Fe^{II} low-spin compounds (Table XLVI). NO^+ has a much more positive p.q.s. than CO, mainly due to the very strong π -acceptor properties of NO^+ . The magnitude of the Q.S. for $\text{Fe}(\text{CO})_2(\text{NO})_2$ is similar to that of $\text{KFe}(\text{CO})_3\text{NO}$. η should be 1 for this compound (Table IV, compound 3), but the negative Q.S.

TABLE LVII

MÖSSBAUER PARAMETERS FOR $\text{Fe}^{-\text{II}}$ COMPOUNDS^a

Compound ^b	C.S. ^c	Q.S.	Ref.
$\text{Hg}\{\text{Fe}(\text{CO})_2\text{NO}[\text{P}(\text{C}_6\text{H}_5)_3]\}_2$	0.26	1.42	(333)
$\text{Hg}\{\text{Fe}(\text{CO})_3\text{NO}\}_2$	0.26	1.26	(333)
	0.28	1.32	(406)
$\text{Fe}(\text{CO})_2(\text{NO})_2$	0.32	-0.33 ($\eta \sim 0.85$)	(406)
	0.32	0.34	(146)
$\text{NaFe}(\text{CO})_3\text{NO}$	0.16	0.37	(406)
$\text{KFe}(\text{CO})_3\text{NO}$	0.18	+0.36	(406)
$\text{Fe}(\text{Ph}_3\text{P})(\text{CO})(\text{NO})_2$	0.20	0.55	(406)
$\text{Fe}(\text{Ph}_3\text{P})_2(\text{NO})_2$	0.35	0.69	(406)
	0.33	0.70	(146)
$\text{Fe}(\text{Ph}_2\text{MeP})_2(\text{NO})_2$	0.30	0.60	(146)
$\text{Fe}[(\text{PhO})_3\text{P}]_2(\text{NO})_2$	0.29	0.50	(146)
$\text{Fe}(\text{Ph}_3\text{As})_2(\text{NO})_2$	0.42	0.59	(146)
$\text{Fe}(\text{Ph}_3\text{As})(\text{CO})(\text{NO})_2$	0.34	0.64	(146)
$\text{Fe}(\text{diphos})(\text{NO})_2$	0.29	0.54	(146)
$\text{Fe}(\text{arphos})(\text{NO})_2$	0.36	0.58	(146)
$\text{Fe}(\text{arphos})(\text{CO})(\text{NO})_2$	0.28	0.47	(146)
$\text{Fe}(f_4\text{fos})(\text{NO})_2$	0.35	0.29	(146)
$\text{Fe}(f_6\text{fos})(\text{NO})_2$	0.33	0.29	(146)

^a Data given in mm/sec at 80°K.

^b diphos = $\text{Ph}_2\text{PCH}_2\text{CH}_2\text{PPh}_2$; arphos = $\text{Ph}_2\text{PCH}_2\text{CH}_2\text{AsPh}_2$; $f_4\text{fos}$ = Ph_2P
 $\text{C} = \text{C P}(\text{Ph})_2\text{CF}_2\text{CF}_2$; $f_6\text{fos}$ = $\text{Ph}_2\text{P C} = \text{C P}(\text{Ph})_2(\text{CF}_2)_2\text{CF}_2$.

^c With respect to sodium nitroprusside; unfortunately, Mazak and Collins (406) do not give their C.S. standard. To bring their values into line with the others, it appears as if the values in (406) were quoted relative to Fe metal. 0.26 mm/sec has been added to these values.

implies that the C-Fe-C angle is greater than 109° . The substantially larger and more negative Q.S. for $\text{Fe}(\text{Ph}_3\text{P})_2(\text{NO})_2$ implies that the p.q.s. value for Ph_3P is more negative than that for CO, and that the P-Fe-P bond angle is greater than 109° . These results suggest that the order of p.q.s. values in tetrahedral Fe^{II} compounds is $(\text{p.q.s.})_{\text{NO}^+} > (\text{more positive than}) (\text{p.q.s.})_{\text{CO}} > (\text{p.q.s.})_{(\text{PhO})_3\text{P}} > (\text{p.q.s.})_{\text{Ph}_3\text{As}} \sim (\text{p.q.s.})_{\text{Ph}_3\text{MeP}} > (\text{p.q.s.})_{\text{Ph}_3\text{P}}$. For the ligands NO^+ , CO, and Ph_3P , the above order is the same as that found for these ligands in Fe^{II} low-spin compounds (Table XLVI). Since the Q.S. is probably most sensitive to π -bonding inequalities, the above order probably reflects a decrease in π -acceptor properties from NO^+ to Ph_3P (406).

The C.S. values for the compounds in Table LVII become more positive in the order $\text{NO}^+ < \text{CO} < \text{PR}_3 < \text{AsPh}_3$. This order reflects a decrease in σ donor and/or π acceptor properties from NO^+ to AsPh_3 .

For the compounds containing the chelating ligands such as diphos (146), the Q.S. values are substantially smaller than for the phosphine-NO compounds such as $\text{Fe}(\text{Ph}_3\text{P})_2(\text{NO})_2$. These smaller values have been attributed to distortions (146), although it is quite possible that the bonding properties of NO vary appreciably from one compound to another and give rise to these significant differences and/or that the bonding properties of diphos are appreciably different than Ph_3P .

2. Fe^{III} High-Spin Compounds

Fe^{III} high spin has the electronic configuration $(t_{2g})^3(e_g)^2$. Any Q.S. is thus due to q_{lat} or $q_{\text{M.O.}}$ and, in general, Q.S. values should be small (Table LVIII). The octahedral and tetrahedral species (Table LVIII, compounds 1, 2, 5-7) should all have small or zero quadrupole splittings as is observed (41, 125, 201). However, the quite large splitting for $(\text{NEt}_4)\text{Fe}(\text{NCO})_4$ (201) shows that considerable distortion from tetrahedral symmetry is present. Mössbauer spectroscopy appears to be able to detect such distortions more easily than infrared in this case (245).

The C.S. values for six-coordinate complexes (Table LVIII, compounds 1, 2) are about 0.20 mm/sec larger than for four-coordinate complexes containing the same ligand (Table LVIII, compounds 5, 6) and this difference can be used to distinguish six-coordinate from four-coordinate species. For example, the very similar C.S. values for $\text{M}(\text{acac})_3\text{FeCl}_4$ ($\text{M} = \text{Si}, \text{Ge}$) (compounds 3 and 4) to those of the FeCl_4^- species strongly indicates (41) that the FeCl_4^- anion is present in the acac compounds, and no bridging acac groups are present. Similarly, the C.S. values in frozen solution for ferric bromide and thiocyanate species (Table LVIII, compounds 8, 10) allowed the assignment of a tetra-

hedral structure to the bromide species (HFeBr_4), but an octahedral structure to the thiocyanate species (399). These differences in C.S. probably reflect the different bond lengths in tetrahedral and octahedral coordination. For example, $r_{\text{Fe-Cl}}$ in NaFeCl_4 and FeCl_3 are 2.19 (484) and 2.48 Å (304), respectively.

Clausen and Good (125, 126) have studied extensively a number of tetrahedral ferric systems. The Q.S. in the $(\text{R}_n\text{NH}_{4-n})\text{FeX}_4$ species (125) (Table LVIII, compounds 13–23) has been attributed to hydrogen bonding. The identical solid and solution spectra strongly support this suggestion and tend to rule out lattice effects. Spectra of $[\text{FeCl}_{4-n}\text{Br}_n]^-$ species (126) show that the C.S. increases from 0.55 mm/sec for FeCl_4^- to 0.62 for FeBr_4^- , but very little, if any, line broadening is observed. This indicates that the q_{lat} contributions from Cl^- and Br^- are very similar.

A combination of Mössbauer and other spectroscopic data has provided good evidence in EDTA and DTPA complexes (Table LVIII, compounds 27–31) that the coordination number changes (313, 519). It was concluded that compounds 27 and 29 contain six-coordinate Fe; compounds 28 and 30, seven-coordinate Fe; and compound 31, eight-coordinate iron.

A number of substituted ferric acetylacetonates (Table LVIII, compounds 39–43) have been prepared, and their Mössbauer spectra recorded (32, 42, 256, 405). Very broad lines are usually obtained, and these have been attributed to relaxation effects. Surprisingly, γ irradiation (32) narrows the line width for $\text{Fe}(\text{acac})_3$ markedly. The most likely reason for the small and variable Q.S. in these compounds is π acceptance from the Fe d orbitals to the acac ring.

Several groups have recorded spectra of Fe^{III} compounds containing the N,N' -ethylenebis(salicylaldiminato)anion (salen) (43, 54, 56, 86, 87, 480, 481). The crystal structure of $[\text{Fe}(\text{salen})\text{Cl}]_2$ (261) proves that this is a dimer; and the magnetic susceptibilities and molecular weights suggest that $[\text{Fe}(\text{salen})]_2\text{O}$ and related compounds are dimers. However, the structure of a nitromethane adduct of $\text{Fe}(\text{salen})\text{Cl}$ (260) showed that this was monomeric. The magnetic susceptibilities have been fit rather successfully to a simple binuclear model involving exchange between $S = \frac{5}{2}$ iron ions in the dimeric species (54, 259, 387). However, for $\text{Fe}(\text{salen})\text{Cl} \cdot \frac{1}{3}\text{MeNO}_2$ (86), the magnetic and Mössbauer data strongly suggest that this is a dimer instead of the monomeric nitromethane adduct reported earlier (260). For example, no enhancement of the external magnetic field was observed at low temperatures in large magnetic fields (86). This appears to be conclusive proof that there is a spin zero ground state originating from antiferromagnetic coupling

TABLE LVIII

MÖSSBAUER PARAMETERS FOR Fe^{III} HIGH-SPIN COMPOUNDS^a

Code No.	Compound ^b	C.S. ^c	Q.S.	Ref.
1	$\text{FeCl}_3(\text{anhydrous})$	+0.76	—	(41)
2	$[\text{Co}(\text{NH}_3)_6][\text{FeCl}_6]$	+0.75	—	(41)
3	$\text{Si}(\text{acac})_3\text{FeCl}_4$	+0.55	>0	(41)
4	$\text{Ge}(\text{acac})_3\text{FeCl}_4$	+0.55	>0	(41)
5	$(\text{NMe}_4)\text{FeCl}_4$	+0.55	0.00	(125, 201)
6	$(\text{NEt}_4)\text{FeCl}_4$	+0.55	0.00	(125, 201)
7	$(\text{NEt}_4)\text{FeBr}_4$	+0.62	0.00	(201)
8	HFeBr_4^d	+0.61	0.00	(399)
9	$(\text{NEt}_4)\text{Fe}(\text{NCO})_4$	+0.60	0.86	(201)
10	$\text{Fe}(\text{SCN})_4\text{X}_2^{-e}$	+0.76	0.56	(399)
11	$\text{FeCl}_3 \cdot \text{TPA}$	+0.54	0.21	(58)
12	$\text{FeCl}_3 \cdot \text{TPP}$	+0.57	0.23	(58)
13	$\text{MeNH}_3\text{FeCl}_4$	+0.54	0	(125)
14	$\text{Me}_2\text{NH}_2\text{FeCl}_4$	+0.53	0.33	(125)
15	$\text{Me}_3\text{NHFeCl}_4$	+0.52	0	(125)
16	$\text{BuNH}_3\text{FeCl}_4^f$	+0.55	0.41	(125)
17	$\text{Bu}_2\text{NH}_2\text{FeCl}_4^f$	+0.55	0.37	(125)
18	$\text{Bu}_3\text{NHFeCl}_4^f$	+0.55	0.28	(125)
19	$\text{Bu}_4\text{NFeCl}_4^f$	+0.52	0	(125)
20	$\text{BuNH}_3\text{FeBr}_4^d$	+0.61	0.32	(125)
21	$\text{Bu}_2\text{NH}_2\text{FeBr}_4^d$	+0.61	0.30	(125)
22	$\text{Bu}_3\text{NHFeBr}_4^d$	+0.62	0.22	(125)
23	$\text{Bu}_4\text{NFeBr}_4$	+0.56	0	(125)
24	$\alpha\text{-FephenCl}_3$	+0.68	0.85	(56)
25	$\beta\text{-FephenCl}_3$	+0.70	0.80	(56)
26	$[\text{Fe}(\text{phen})_2\text{Cl}_2]\text{ClO}_4$	+0.65	0.05	(56)
27	$\text{HFe}(\text{OH}_2)\text{Y}^b$	+0.71	0.42	(519)
28	$\text{KFe}(\text{OH}_2)\text{Y} \cdot \text{H}_2\text{O}^b$	+0.83	0.81	(519)
29	$\text{H}_2\text{FeDTPA} \cdot 2\text{H}_2\text{O}^t$	+0.63	0.84	(313)
30	$\text{NH}_4\text{HFeDTPA} \cdot \text{H}_2\text{O}^t$	+0.62	1.10	(313)
31	$\text{K}_2\text{FeDTPA} \cdot 2\text{H}_2\text{O}^t$	+0.66	0.99	(313)
32	$[\text{Fe}_3(\text{RCOO})_6(\text{OH})_2]\text{X}' \cdot \text{H}_2\text{O}^t$	+0.66	0.63	(403)
33	$[\text{Fe}_3(\text{RCOO})_6](\text{CH}_3\text{COO})_3$	+0.63	0.62	(403)
34	$\text{Fe}(\text{sul})_3 \cdot 3\text{H}_2\text{O}$	+0.79	1.06	(211)
35	$\text{Fe}(\text{ac})_3$	+0.79	1.06	(211)
36	$\text{Fe}(\text{ol})_3$	+0.74	0.81	(211)
37	$\text{Fe}(\text{nic})_3 \cdot \text{H}_2\text{O}$	+0.77	1.05	(211)
38	$\text{Fe}(\text{AcNH})_3$	+0.32 ^g	0.90	(256)
39	$\text{Fe}(\text{acac})_3$	+0.78	0.67 ^h	(32, 42, 405)
40	$\text{Fe}(\text{BzAc})_3$	+0.86	0.33	(42)

TABLE LVIII—continued

Code No.	Compound ^b	C.S. ^c	Q.S.	Ref.
41	Fe(TfAc) ₃	+0.78	0.67	(42)
42	Fe(dbm) ₃	+0.67	0.60	(401)
		+0.81	—	(42)
43	Fe(tta) ₃	+0.78	0.39	(401)
44	Fe(salen) ₂ O	+0.66	0.83	(43, 56, 480)
45	[Fe(salen)Br] ₂	+0.74	1.64	(43)
46	[Fe(salen)Cl] ₂	+0.67	1.40	(43, 54, 87, 405)
47	Fe(salen)Cl · 2MeNO ₂	+0.65	1.33	(43, 481)
48	Fe(salen)Cl · 2Y ^f	+0.70	1.42	(43)
49	Fe(salen)Cl · MeCN	+0.63	0.85	(43)
50	Fe(salen)Br · 2Z ^f	+0.71	1.62	(43)
51	Fe(salen)Br · MeNO ₂	+0.72	1.12	(43)
52	Fe(salen)Br · MeCN	+0.74	0.54	(43)
53	Fe(salen)Br · 2MeOH	+0.76	0.86	(43)
		+0.72	1.65	
54	Fe(salen)Cl · $\frac{1}{2}$ MeNO ₂	+0.64	1.40	(86)
55	Fesal- <i>N</i> -(2 hydroxyphenyl)Cl ^k	+0.65	1.42	(54)
		+0.60	0.95	
56	Fe[N(SiMe ₃) ₂] ₃	+0.43	5.12	(13)

^a Data given in mm/sec at 80°K except where noted.

^b acac = acetylacetonate; TPA = triphenylarsine; TPP = triphenylphosphine; Y = anion of ethylenediaminetetraacetic acid; DTPA = anion of diethylenetriaminepentaacetic acid; sal = salicylhydroxamate; ac = acetylhydroxamate; ol = oleylhydroxamate; nic = nicotinyhydroxamate; AcNH = acetoacetanilide; BzAc = benzoylacetylacetate; TfAc = trifluoroacetylacetate; dbm = dibenzoylmethane; tta = thenocyltrifluoroacetate; salen = *N,N'*-ethylenebis-(salicylaldimate)anion.

^c With respect to sodium nitroprusside.

^d In frozen solutions.

^e In frozen solution; X = nitrobenzene or H₂O.

^f These spectra were run in frozen benzene solution with very similar results (125).

^g This shift appears to be erroneous.

^h After γ irradiation this splitting was resolved (32). Other spectra did not resolve the Q.S.

ⁱ At room temperature.

^j Y = MeOH, CHCl₃ and C₅H₅N; Z = CHCl₃, C₅H₅N, MeNO₂. An average of values is given.

^k Other similar compounds give very similar four-line spectra.

^l R = CH₃, CH₂Cl, CHCl₂, CCl₃; an average of the very similar results has been taken.

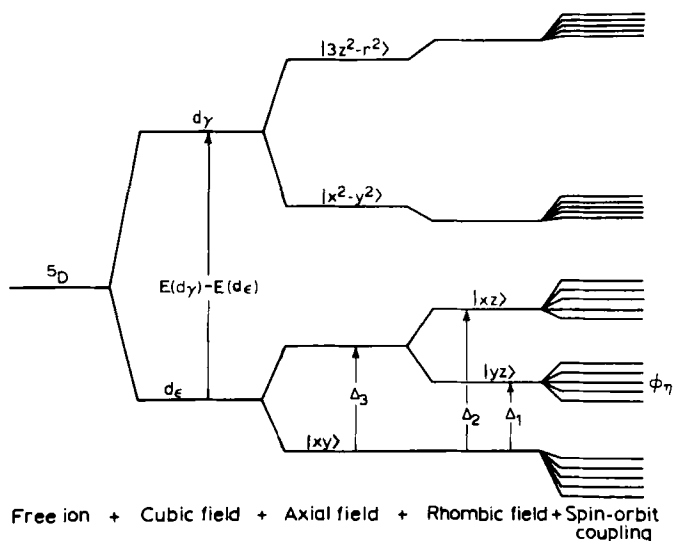
between two iron ions. Apparently, yet another MeNO_2 adduct was prepared (43), and Mössbauer and infrared evidence was consistent with a monomeric species. Indeed, a very recent communication (478) shows that *rapid* crystallization of $[\text{Fe}(\text{salen})\text{Cl}]_2$ in MeNO_2 or $\text{C}_5\text{H}_5\text{N}$ yields products which are almost certainly monomeric. Application of small magnetic fields results in large internal fields in contrast to the dimeric compounds $[\text{Fe}(\text{salen})\text{Cl}]_2$ and $[\text{Fe}(\text{salen})]_2\text{O}$ (476). On the basis of Mössbauer and infrared evidence, monomeric structures were assigned to compounds 47, 49, 51, and 52 in Table LVIII (43), while from this evidence, most of the others appear to be dimeric. However, some compounds (Table LVIII, compounds 53, 55) gave at least two doublets. These two doublets could be due to a mixture of monomeric and dimeric species, or two iron atoms in a dimeric unit which are not in identical environments with respect to the neighboring units in the crystal (54). It is apparent from the above results that there is a delicate balance between the monomeric and dimeric species, and much more work needs to be done to obtain pure products of one form in all cases.

Finally, the very unusual spectrum of $\text{Fe}[\text{N}(\text{SiMe}_3)_2]_3$ should be noted. This compound contains three-coordinate iron [(13) and references], V_{zz} is positive and $\mu = 5.91$ B.M. The quadrupole splitting (5.12 mm/sec) is by far the largest observed for any iron compound to date and the C.S. is the smallest yet observed for Fe^{III} high-spin compounds. Interesting magnetic properties have also been observed at low temperatures (13).

3. Fe^{II} High-Spin and Fe^{III} Low-Spin Compounds

As noted in Section II of this review, a large q_{val} contribution [specifically $q_{\text{C.F.}}$ in Eq. (11)] becomes dominant when considering Q.S. values in Fe^{II} high-spin ($t_{2g}^4 e_g^2$) and Fe^{III} low-spin (t_{2g}^5) compounds. Normally, a large temperature-dependent Q.S. is observed. The $q_{\text{C.F.}}$ contribution often masks changes in Q.S. owing to differences in covalency of the iron-ligand bonds, but at least for some Fe^{II} high-spin compounds, the Q.S. values appear to be useful for estimating bonding properties of ligands (19, 320, 321). The theoretical bases for interpreting Fe^{II} high-spin and Fe^{III} low-spin quadrupole splittings are similar, and a brief outline of the method (351) for Fe^{II} high-spin compounds will now be made.

The energy level diagram for Fe^{II} high spin is given in Fig. 17. The primary effect of the crystal field is to remove the degeneracy of the d orbitals. If the sixth d electron exclusively occupied the low-energy d_{xy} orbital, then $q_{\text{val}} = \frac{4}{7}\langle r^{-3} \rangle_{3d}$ which should give rise to a Q.S. of over 4 mm/sec. However, the Q.S. is reduced from this value by (a) thermal population of the other t_{2g} levels, (b) spin orbit coupling, (c) covalency

FIG. 17. Energy level diagram for Fe^{II} high spin (351).

effects, and (d) contributions from q_{int} . q_{val} can be written as (351)

$$q_{\text{val}} = (1 - R) \frac{4}{7} \langle r^{-3} \rangle_{3d} F(\Delta_1, \Delta_2, \alpha^2 \lambda_0, T) \alpha^2 \quad (84)$$

where the function F expresses the decrease in q_{val} due to thermal population and spin-orbit coupling; λ_0 is the spin orbit coupling constant; and α^2 is the covalency parameter and takes the values 0.6 to 0.9. Neglecting spin-orbit coupling, and taking $\Delta_1 = \Delta_2 \equiv \Delta_3$, then

$$F(\Delta_3, T) = \frac{1 - \exp(-\Delta_3/kT)}{1 + 2 \exp(-\Delta_3/kT)} \quad (85)$$

If the orbital doublet is lowest in energy, then

$$F(\Delta_3, T) = - \left[\frac{1 - \exp(-\Delta_3/kT)}{2 + \exp(-\Delta_3/kT)} \right] \quad (86)$$

A similar expression (390) is easily derived for the Boltzmann population for tetrahedral Fe^{II} species.

The spin-orbit coupling lifts the fivefold degeneracy of each orbital state (Fig. 17). This decreases F by an amount depending on the ratios Δ_1/λ and Δ_2/λ . Ingalls has computed the decrease of F as a function of these ratios (351). The Q.S. is also decreased directly and indirectly by the expansion of the radial part of the 3d wave function on bonding. The covalency parameter α^2 takes this into account.

The lattice contribution for the axial compression and elongation considered in Eqs. (85) and (86) is given as (351):

$$q_{\text{lat}} = \pm (1 - \gamma) \frac{14\Delta_3}{3e^2\langle r^2 \rangle} \quad (87)$$

The lattice contribution is always of opposite sign to q_{val} , and has often been neglected. However, for square-planar complexes of Fe^{II} , (121) the lattice contribution can be larger than q_{val} .

There are several difficulties in applying this method. The Q.S. for one d electron is still not precisely known, and it is not always obvious whether the decrease in Q.S. from the large value of 4 mm/sec is due to covalency, q_{lattice} , or spin-orbit coupling.

Some Q.S. and C.S. values for Fe^{II} high-spin compounds are given in Table LIX, and the crystal field splittings calculated using Ingall's

TABLE LIX
MÖSSBAUER PARAMETERS FOR Fe^{II} HIGH-SPIN COMPOUNDS^a

Code No.	Compound ^b	C.S. ^c	Q.S.	Ref.
1	(NMe ₄) ₂ FeCl ₄	1.26	2.61	(202)
2	(NEt ₄) ₂ FeCl ₄	1.27	2.59	(202, 268)
3	(PQ)FeCl ₄	1.25	2.99	(202)
4	(Cat)Fe(NCSe) ₄	1.24	2.69	(202)
5	(NMe ₄) ₂ Fe(NCS) ₄	1.22	2.10	(202)
6 ^d	FeLCl ₂	1.08	2.71	(94)
7 ^d	FeLBr ₂	1.08	2.42	(94)
8 ^d	FeLI ₂	1.07	1.83	(94)
9	Fe(quin) ₂ Cl ₂	1.23	3.06	(390)
10 ^d	Fe(quin) ₂ Cl ₂	1.12	2.72	(95)
11 ^d	Fe(quin) ₂ Br ₂	1.08	2.71	(95)
12 ^d	(Et ₄ N)Fe(quin)Cl ₃	1.13	2.08	(95)
13 ^d	Fe(Ph ₃ PO) ₂ Cl ₂	1.22	0.80	(95)
14 ^d	Fe(Ph ₃ PO) ₂ Br ₂	1.26	2.21	(95)
15 ^d	Fe(IQ) ₄ Cl ₂	1.29	3.18	(97)
16 ^d	Fe(IQ) ₄ Br ₂	1.26	2.21	(97)
17 ^d	Fe(IQ) ₄ I ₂	1.23	0.40	(97)
18 ^d	Fe(IQ) ₄ (NCS) ₂	1.37	1.50	(97)
19 ^d	Fe(IQ) ₄ (NCO) ₂	1.29	2.47	(96)
20 ^d	Fe(IQ) ₄ (NCSe) ₂	1.30	1.41	(96)
21 ^d	Fe(γ -pic) ₄ Cl ₂	1.31	2.98	(97)
22 ^d	Fe(γ -pic) ₄ Br ₂	1.25	1.28	(97)
23 ^d	Fe(γ -pic) ₄ I ₂	1.19	0.19	(97)
24 ^d	Fe(γ -pic) ₄ (NCS) ₂	1.33	1.67	(97)
25 ^d	Fe(py) ₄ Cl ₂	1.30	3.11	(97, 284)

TABLE LIX—*continued*

Code No.	Compound ^b	C.S. ^c	Q.S.	Ref.
26 ^d	Fe(py) ₄ (NCO) ₂	1.35	2.49	(96, 284)
27 ^d	Fe(py) ₄ (NCSe) ₂	1.30	0.71	(96)
28 ^d	Fe(py) ₄ (NCS) ₂	1.35	1.54	(97, 220, 284)
29 ^d	FeL ₃ (ClO ₄) ₂	1.29	2.37	(94)
30 ^d	FeL ₂ Cl ₂	1.28	2.23	(94)
31 ^d	FeL ₂ Br ₂	1.27	2.12	(94)
32	FeCl ₂ ·2AM	1.55	2.80	(58)
33	FeCl ₂ ·2FA	1.59	3.00	(58)
34	FeCl ₂ ·BM	1.54	2.87	(58)
35	FeCl ₂ ·AN	1.49	2.18	(58)
36	Fe(phen) ₂ (N ₃) ₂	1.20	3.02	(135, 372)
37	Fe(phen) ₂ Cl ₂	1.27	3.23	(135, 372, 390)
38	Fe(phen) ₂ I ₂	1.30	2.80	(135)
39	Fe(phen) ₂ (SCN) ₂	1.28	2.96	(135, 284)
40	Fe(phen) ₂ Br ₂	1.29	3.14	(135, 284, 372)
41	FeCl ₂ ·4H ₂ O	1.49	3.05	(135)
42	Fe(phen) ₂ (SeCN) ₂	1.26	2.61	(135)
43	Fe(phen) ₂ (OCN) ₂	1.20	3.15	(284, 372)
44	Fe(phen) ₂ (HCOO) ₂	1.21	3.03	(284, 372)
45	Fe(phen) ₂ (CH ₃ COO) ₂	1.12	3.17	(372)
46	Fe(Htcz) ₂ (NCS) ₂ ^d	1.25	2.98	(98)

^a Data in mm/sec at 80°K unless otherwise noted.

^b PQ = *N,N'*-Dimethyl-4,4'-dipyridyl; Cat = α,α -(bistriphenylphosphonium)-*p*-xylene; L = di-2-pyridylamine; quin = quinoline; IQ = isoquinoline; γ -pic = γ -picoline; AM = acetamide; FA = formamide; BM = benzamide; AN = aniline; Htcz = thiocarbonylhydrazide.

^c Relative to sodium nitroprusside.

^d Room temperature results.

method are given in Table LX along with the ground state orbital. The Q.S. values are very sensitive to small distortions from tetrahedral or octahedral symmetry, and the Mössbauer spectra of the FeX₄²⁻ species (X = Cl⁻, Br⁻, NCS⁻, NCSe⁻) all indicate small distortions from tetrahedral symmetry which had gone undetected (202, 268). As outlined in the introduction (Section II), a perfect tetrahedral or octahedral species would give no splitting. Neglecting spin-orbit coupling and g_{int} , the Q.S. as a function of T for the tetrahedral compounds gave a reasonable fit for most compounds to Ingalls treatment (202). Many of the crystal field splittings for the octahedral species were calculated from the Q.S. at only one temperature, and it has been shown recently (390) that the Q.S. does not fit the theory well over a large temperature range. The

more rigorous calculations given by Ingalls for such compounds as $\text{FeSiF}_6 \cdot 6\text{H}_2\text{O}$, $\text{FeSO}_4 \cdot 7\text{H}_2\text{O}$, and others gave more acceptable agreement.

Golding *et al.* (199, 284) have correlated Q.S. and magnetic moments for $\text{Fe}(\text{py})_4\text{X}_2$ compounds ($\text{X} = \text{Cl}^-$, Br^- , I^- , NCO^- , NCS^- , etc.). The quadrupole splitting is very sensitive to small distortions from cubic symmetry, whereas the average magnetic moment is not sensitive to small distortions.

TABLE LX
CRYSTAL FIELD SPLITTINGS IN Fe^{II} HIGH-SPIN COMPOUNDS

Compound	Δ_3 (cm^{-1}) (or Δ_1 and Δ_2)		Ground state orbital	Ref.
PQFeCl_4	470		d_z^2	(202)
$(\text{Cat})\text{Fe}(\text{NCSe})_4$	292		d_z^2	(202)
$(\text{NEt}_4)_2\text{FeCl}_4$	135		d_z^2	(202)
	185		d_z^2	(268)
$(\text{NMe}_4)_2\text{FeCl}_4$	125		d_z^2	(202)
$(\text{NEt}_4)_2\text{FeBr}_4$	96		d_z^2	(202)
$(\text{NMe}_4)_2\text{Fe}(\text{NCS})_4$	101		d_z^2	(202)
$\text{Fe}(\text{quin})_2\text{Cl}_2$	~600		d_{xy}	(390)
$\text{Fe}(\text{IQ})_4\text{Cl}_2$	600		d_{xy}	(97)
$\text{Fe}(\text{IQ})_4\text{Br}_2$	360		d_{xy}	(97)
$\text{Fe}(\text{IQ})_4\text{I}_2$	80		d_{xy}	(97)
$\text{Fe}(\gamma\text{-pic})_4\text{Cl}_2$	520		d_{xy}	(97)
$\text{Fe}(\gamma\text{-pic})_4\text{Br}_2$	200		d_{xy}	(97)
$\text{Fe}(\gamma\text{-pic})_4\text{I}_2$	40		d_{xy}	(97)
$\text{Fe}(\gamma\text{-pic})_4(\text{NCS})_2$	~500		d_{xz}, d_{yz}	(97)
$\text{FeSiF}_6 \cdot 6\text{H}_2\text{O}$	760		d_z^2	(351)
$\text{FeSO}_4 \cdot 7\text{H}_2\text{O}$	480	1300	d_{xy}	(351)
$\text{Fe}(\text{NH}_4\text{SO}_4)_2 \cdot 6\text{H}_2\text{O}$	240	320	d_{xy}	(351)
$\text{FeC}_2\text{O}_4 \cdot 2\text{H}_2\text{O}$	100	960	d_{xy}	(351)
FeSO_4	360	1680	$d_{x^2-y^2} + \delta d_z^2$	(351)
FeF_2	1000	2200	$d_{x^2-y^2} + \delta d_z^2$	(351)

From linear correlations of Q.S. and isomer shift (corrected for S.O.D. shift) for Fe^{II} high-spin compounds (19, 320, 321), Hazony *et al.* have suggested that the main cause of variation in the Q.S. in a series of compounds such as FeF_2 , FeCl_2 , FeBr_2 , and FeI_2 is due to a variation in α^2 in Eq. (84). Using the value of $\alpha^2 = 0.60$ for FeF_2 from ESR data (539), they obtained (19) $\alpha^2 = 0.34, 0.39$, and 0.42 for the iodide, bromide, and chloride, respectively, in contrast to the much higher values given previously. This order parallels the nephelauxetic series. Also, the

variation in C.S. values shows an excellent correlation with the nephelauxetic series, in contrast to the correlation with the spectrochemical series for Fe^{II} low-spin (44) and Au compounds (49).

Similarly (321), for $[\text{FeCl}_{6-n} \cdot n\text{H}_2\text{O}]^{(n-4)}$ compounds, plots of Q.S. and isomer shift versus n are reasonably linear, and the correlation of Q.S. with I.S. has been attributed to central field covalency—the expansion of the radial portion of the $3d$ wave function due to the reduction of the metal ion's effective charge via σ and π bonding. Hazony *et al.* have shown that it should be possible to estimate both σ - and π -bonding properties of ligands from these correlations. They have also recently extended these ideas to other iron species (320). These papers should be very important for further interpretation of Fe^{II} high-spin data.

The degeneracy of the 2T_2 ground state in Fe^{III} low spin is lifted by the combined effects of spin-orbit coupling and the ligand field. Unfortunately, application of Golding's method (281, 282) for explaining the temperature dependence of Fe^{III} low-spin Q.S. values has not proven to be very successful [for example, see (480) and (489)]. The most serious disagreement apparently arises from the neglect of lattice contributions and from inadequate recognition of covalency. Qualitatively, however, Fe^{III} low-spin quadrupole splittings should be larger than Fe^{III} high-spin and Fe^{II} low-spin quadrupole splittings, and examination of Table LXI shows that this is indeed true. The very large splittings for compounds 8, 22, and 23, however, cannot be reconciled with Golding's estimate of a maximum Q.S. of 2.54 mm/sec in Fe^{III} low-spin compounds.

A very small selection of the Fe^{III} low-spin data is given in Table LXI, mainly because the C.S. is remarkably insensitive to variations in ligand properties within similar series of compounds (e.g., Table LXI, compounds 1–5, 19–23), and because the Q.S. values have not been readily rationalized because of the difficulty in estimating the relative magnitudes of such contributions as covalency and q_{lat} . Recent determinations of signs of the Q.S. for such compounds as $\text{Fe}(\text{bipy})_3(\text{ClO}_4)_3$ and $\text{Fe}(\text{ethylenediamine})_3\text{Cl}_3$ (477) should enable a more rigorous interpretation of these Q.S. values. For example, the positive sign of V_{zz} in the above two compounds indicates an orbital doublet ground state, with the magnitude of the Q.S. being reduced by covalency.

The magnetic properties of, and the relaxation effects in, these compounds have perhaps been of much greater interest (145, 432, 487–489), but they are beyond the scope of this article.

The dithiocarbamate compounds, $\text{Fe}(\text{RR}'\text{NCS}_2)_3$, are of considerable interest because the strength of the ligand field is close to the value of the mean pairing energy of the d electrons. The magnetic susceptibilities

(485 and references) indicate that compound 15 is pure high spin, while the others exhibit high spin-low spin equilibria. However, all compounds show a single spectrum at all temperatures. The time of change from one spin state to another must be less than 1.5×10^{-7} sec, and the C.S. and Q.S. are, therefore, averages which depend on the proportion of high-spin to low-spin species (246, 485). This thermal admixture makes it even more difficult to interpret variations in Q.S. The sign of the EFG in these compounds is negative (485), and the very large C.S. values result from electron donation from ligand σ orbitals into metal d orbitals (485).

TABLE LXI
MÖSSBAUER PARAMETERS FOR Fe^{III} LOW-SPIN COMPOUNDS^a

Code No. ^b	Compound ^c	C.S. ^d	Q.S.	Ref.
1	$\text{K}_3\text{Fe}(\text{CN})_6^e$	+0.14	0.28	(135, 142)
2	$\text{Cu}_3[\text{Fe}(\text{CN})_6]_2^e$	+0.10	0.48	(142)
3	$\text{Ag}_3\text{Fe}(\text{CN})_6^e$	+0.12	0.76	(142)
4	$\text{Na}_2[\text{Fe}(\text{CN})_5\text{H}_2\text{O}]^e$	+0.12	1.82	(238)
5	$\text{Na}_2[\text{Fe}(\text{CN})_5\text{NH}_3] \cdot \text{H}_2\text{O}^e$	+0.12	1.78	(238)
6	$[\text{Fe}(\text{phen})_3](\text{ClO}_4)_3$	+0.35	1.67	(135)
		+0.31 ^e	1.62 ^e	(56)
7	$[\text{Fe}(\text{dipy})_3](\text{ClO}_4)_3$	+0.32	1.76	(135)
8	$[\text{Fe}(\text{terpy})_2](\text{ClO}_4)_3$	+0.32	3.43	(480)
9	$\text{Na}_2[\text{Fe}(\text{CN})_5\text{PPh}_3]^e$	+0.14	1.04	(239)
10	$\text{Na}_2[\text{Fe}(\text{CN})_5\text{AsPh}_3]^e$	+0.20	1.00	(239)
11	$\text{Na}_2[\text{Fe}(\text{CN})_5\text{SbPh}_3]^e$	+0.26	0.94	(239)
12	$[\text{Fe}(\text{bipy})_2(\text{CN})_2]\text{ClO}_4^e$	+0.24	1.63	(56)
13	$\text{Fe}(\text{SacSac})_3$	+0.55	1.90	(53)
14	$\text{Fe}(\text{Sacac})_3$	+0.57	1.47	(145)
15	$\text{Fe}[(\text{CH}_2)_4\text{NCS}_2]_3$	+0.76	0.42	(485)
16	$\text{Fe}[(\text{CH}_3)_2\text{NCS}_2]_3$	+0.71	0.73	(213, 485)
17	$\text{Fe}[(i\text{-C}_4\text{H}_9)_2\text{NCS}_2]_3$	+0.73	0.64	(213, 485)
18	$(\text{Ph}_4\text{P})_3[\text{Fe}\{\text{S}_2\text{C}_2(\text{CN})_2\}_3]$	+0.66	1.85	(489)
19	$(\text{Et}_4\text{N})_2[\text{Fe}\{\text{S}_2\text{C}_2\text{Ph}_2\}_2]_2$	+0.61	2.37	(61)
20	$(\text{Et}_4\text{N})_2[\text{Fe}\{\text{S}_2\text{C}_2(\text{CF}_3)_2\}_2]_2$	+0.59	2.50	(61)
21	$(\text{Et}_4\text{N})_2[\text{Fe}\{\text{S}_2\text{C}_2(\text{CN})_2\}_2]_2$	+0.59	2.76	(61)
22	$(\text{Bu}_4\text{N})_2[\text{Fe}\{\text{S}_2\text{C}_6\text{H}_3\text{Me}\}_2]_2$	+0.60	2.95	(61)
23	$(\text{Bu}_4\text{N})_2[\text{Fe}\{\text{S}_2\text{C}_6\text{Cl}_4\}_2]_2$	+0.58	3.02	(61)

^a Data given in mm/sec at 80°K unless otherwise noted.

^b Code number will be preceded by Table number in text.

^c SacSac = Dithioacetylacetonate; Sacac = monothioacetylacetonate.

^d Relative to sodium nitroprusside.

^e At room temperature.

In contrast, $\text{Fe}(\text{Sacac})_3$ did show two resolvable patterns (145), indicating a longer relaxation time in this compound compared with that in the dithiocarbamate complexes. The high-spin form of $\text{Fe}(\text{Sacac})_3$ gave a very similar Q.S. (0.56 mm/sec) to $\text{Fe}(\text{acac})_3$ (Table LVIII), whereas the low spin isomer gave the very much larger splitting due to the q_{val} contribution. Similarly, $\text{Fe}(\text{SacSac})_3$ gave a larger splitting (53) indicating a more substantial splitting of the ground 2T_2 state than in $\text{Fe}(\text{Sacac})_3$.

A larger number of spectra of dithiolene complexes have been reported (59, 61, 489), but because of the complications outlined earlier, even a qualitative description of trends in Q.S. has been hampered. For $(\text{Ph}_4\text{P})_3[\text{Fe}\{\text{S}_2\text{C}_2(\text{CN})_2\}_3]$, the sign of the Q.S. is -ve (489), and this has been taken to be a d_{xy} hole well separated by higher states. Application of Golding's theory to the Q.S. values over a wide range of temperatures did not give good agreement. One series of these compounds (Table LXI, compounds 19-23) shows a very large variation in Q.S., but no change in C.S. (59). No adequate explanation for this phenomenon can be given at the present time.

4. Fe^0 , Fe^{-1} , and π -cpFe Complexes

An enormous number of Mössbauer spectra of Fe^0 , Fe^{-1} , and π -cpFe compounds have been reported. A very small selection of data is given in Table LXII. Much of the earlier work is reviewed in reference (110). Generally, variations in C.S. and Q.S. within isostructural and iso-electronic series of compounds are comparatively small. Variations in C.S. have been successfully related to qualitative differences in bonding properties of ligands, and in some cases, useful empirical correlations have been noted between the Q.S. and coordination number of the iron. However, the variations in Q.S. for fairly similar groups of compounds have not proved to be amenable to any consistent qualitative or semi-quantitative treatment (with the exception of some π -cp complexes noted later). These difficulties are probably largely due to the large and variable q_{val} term for Fe^0 (d^8) and Fe^{-1} (d^9). The relative energies of the Fe atomic orbitals and ligand orbitals probably vary greatly in fairly similar compounds. This situation is in direct contrast to another d^8 system of considerable Mössbauer interest, Au^{III} , whose energy levels have greater stability, giving rise to large and predictable changes in Q.S. with variations in ligand (see Section IV, G, 1).

Herber, King, and Wertheim (333) first proposed that center shifts could be expressed as a sum of partial center shifts [Eq. (48)]. They derived p.c.s. values for a large number of ligands, and calculated C.S. values for Fe compounds of varying coordination number and formal

TABLE LXII

⁵⁷Fe MÖSSBAUER PARAMETERS FOR Fe⁰, Fe⁻¹, and π -cpFe COMPLEXES^a

Code No. ^b	Compound ^c	C.S. ^d	Q.S.	Ref.
1	Fe(CO) ₅	0.17	2.57	(134, 224, 333)
2	(Et ₄ N) ₂ [Fe ₂ (CO) ₈]	0.18	2.22	(224)
3	(Et ₄ N)[Fe(CO) ₄ H]	0.09	1.36	(224)
4	Na ₂ {Fe(CO) ₄ }	0.08	<0.18	(224)
		0.01 ^e	~0 ^e	(218)
5	Fe ₂ (CO) ₉	0.39	0.48	(224, 333)
6	Fe ₃ (CO) ₁₂	1. 0.37	1.13	(224)
		2. 0.30	0.13	—
7	(Et ₄ N)[Fe ₂ (CO) ₈ H]	0.33	0.50	(224)
8	[Fe(CO) ₃ (PMe ₂) ₂]	0.21	0.69	(267)
9	[Fe(CO) ₃ (SMe) ₂]	0.30	0.89	(333)
10	[Fe(CO) ₃ (SPh) ₂]	0.32	1.07	(267)
11	[Fe(CO) ₃ I(PMe ₂) ₂]	0.26	0.99	(267)
12	[Fe(CO) ₄ (PMe ₂) ₂]	0.23	2.58	(267)
13	[Fe(CO) ₃ SC(Me) ₃] ₂	0.29	0.93	(333)
14	<i>cis</i> -[Fe(CO) ₂ cp(PMe ₂) ₂]	0.40	1.61	(267)
15	<i>trans</i> -[Fe(CO) ₂ cp(PMe ₂) ₂]	0.42	1.64	(267)
16	<i>cis</i> -[Fe(CO) ₂ cp(PPh ₂) ₂]	0.52	1.65	(332)
17	<i>trans</i> -[Fe(CO) ₂ cp(PPh ₂) ₂]	0.52	1.66	(332)
18	[Fe(CO) ₂ cp(SPh) ₂]	0.61	1.67	(267)
19	[Fe(CO) ₂ cp(SMe) ₂]	0.56	1.65	(267, 333)
20	Fe(CO) ₂ cpI	0.48	1.83	(333)
21	[Fe(CO) ₂ cpI] ₂	0.48	1.89	(333)
22	Fe(CO) ₂ cpCl	0.49	1.88	(333)
23	Fe(CO) ₂ cpSnPh ₃	0.35	1.82	(149)
24	Fe(CO) ₂ cp(PPh ₃)SnPh ₃	0.46	1.84	(149)
25	Fe(CO) ₂ cp(AsPh ₃)SnPh ₃	0.53	1.90	(149)
26	Fe(CO) ₂ cp(SbPh ₃)SnPh ₃	0.55	1.90	(149)
27	Fe(CO) ₂ cp(PPh ₂ CF ₃)SnPh ₃	0.46	1.83	(149)
28	Fe(CO) ₂ cp(PMe ₂ Ph)SnPh ₃	0.43	1.71	(149)
29	PPh ₃ Fe(CO) ₄	0.17	2.54	(133)
30	P(OEt) ₃ Fe(CO) ₄	0.13	2.31	(133)
31	AcNpFe(CO) ₄	0.24	1.78	(133)
32	MaAFe(CO) ₄	0.27	1.41	(133)
33	[π -AllylFe(CO) ₄] ⁺ BF ₄ ⁻	0.32	1.01	(133)
34	<i>f</i> ₈ fosFe(CO) ₃	0.20	2.34	(147)
35	diphosFe(CO) ₃	0.19	2.12	(147)
36	<i>ff</i> fosFe(CO) ₄	0.21	2.80	(147)
37	diphosFe ₂ (CO) ₈	0.16	2.47	(147)
38	diarsFe ₂ (CO) ₈	0.19	2.68	(147)
39	(cp) ₂ Fe	0.77	2.39	(208, 382, 561)
40	cpFe(C ₅ H ₄)COCH ₃	0.71	2.27	(533)
41	cpFe(C ₅ H ₄)CH ₃	0.77	2.39	(382)

TABLE LXII—*continued*

Code No. ^b	Compound ^c	C.S. ^d	Q.S.	Ref.
42	cpFe(C ₅ H ₄)Cl	0.67	2.42	(533)
43	[cpFe(C ₅ H ₄)] ₂ CH ⁺ BF ₄ ⁻	0.79	2.11	(325)
44	[(cp) ₂ Fe] ⁺ Br ⁻	0.70	~0.2	(561)
45	[(cp) ₂ Fe] ⁺ BF ₄ ⁻	0.62	0.65	(533)
46	[Me ₄ N] ₂ [Fe(C ₂ B ₉ H ₁₁) ₂]	0.56	2.80	(60)
47	(Me ₄ N)[Fe(C ₂ B ₉ H ₁₁) ₂]	0.50	0.64	(60)
48	(cp)Fe(C ₂ B ₉ H ₁₁) ^f	0.61	0.53	(325)
49	[BrFe(NO) ₂] ₂	0.67	1.76	(146)
50	[IFe(NO) ₂] ₂	0.60	1.68	(146)
51	(C ₅ H ₁₁ N)Fe(NO) ₂ Br	0.60	1.12	(146)
52	Ph ₃ PFe(NO) ₂ Br	0.50	1.02	(146)
53	Ph ₃ AsFe(NO) ₂ Br	0.52	1.28	(146)
54	Ph ₃ SbFe(NO) ₂ Br	0.55	1.49	(146)

^a Data given in mm/sec at 80°K unless otherwise noted.

^b Code number will be preceded by table number in the text.

^c AcNp = acenaphthalene; MaA = maleic anhydride;

$f_6fos = \text{Ph}_2\text{PC} = \text{CP}(\text{Ph})_2(\text{CF}_2)_2\text{CF}_2$; $\text{diphos} = \text{Ph}_2\text{PCH}_2\text{CH}_2\text{PPh}_2$;

$\text{diars} = \text{Ph}_2\text{AsCH}_2\text{CH}_2\text{AsPh}_2$; and $ffos = \text{Ph}_2\text{PC} = \text{CP}(\text{Ph})_2(\text{CF}_2)\text{CF}_2$.

^d Relative to sodium nitroprusside.

^e At room temperature.

^f Temperature = 140°K.

valencies. Although the agreement between predicted and observed values was quite good for a number of compounds, the p.c.s. value for cp varied markedly, and the Fe^{II} low-spin work discussed previously strongly indicates that the C.S. values for compounds containing CO are not additive. Also, it appears that the coordination number and valency of the iron should be a constant for a meaningful application of the p.c.s. treatment.

From a general structural point of view, Greenwood and co-workers have made several important empirical generalizations (224, 267). First, five-coordinate Fe⁰ compounds (Table LXII, compounds 1–3, 12) have much larger quadrupole splittings than four-coordinate compounds (Table LXII, compound 4) and six-coordinate Fe⁰ compounds (Table LXII, compounds 6, 8, and 9), while seven-coordinate values (Table LXII, compounds 6 and 7) are also generally small. A lone pair is considered in compounds 8 and 9 to occupy an effective ligand site and complete the octahedral coordination of the metal. Greenwood *et al.* also

noted that the C.S. value is reduced as the anionic charge on the metal cluster increases, e.g., for the series $\text{Fe}_2(\text{CO})_9$, $\text{Fe}_2(\text{CO})_8\text{H}^-$, and $\text{Fe}_2(\text{CO})_8^{2-}$, the C.S. decreases from 0.42 to 0.33 to 0.18 mm/sec. It is also generally true that the C.S. increases as the coordination number increases. Thus, the C.S. for $\text{Na}_2\text{Fe}(\text{CO})_4$, $\text{Fe}(\text{CO})_5$, and $\text{Fe}_2(\text{CO})_9$ are 0.08, 0.17, and 0.39 mm/sec, respectively.

From compounds 8, 9, and 14–19 in Table LXII, it is apparent that replacement of S by P in a bridging position lowers the C.S. (267). This is consistent with P being a stronger σ donor than S. However, the Q.S. for compounds 14–19 are all somewhat surprisingly within experimental error.

In the $\text{Fe}(\text{CO})\text{LcpX}$ ($\text{L} = \text{CO}$, PPh_3 , AsPh_3 etc.; $\text{X} = \text{Cl}^-$, I^- , SnPh_3^-) compounds, the C.S. has a small and measurable trend, but the Q.S. values are again remarkably constant. The trend in C.S. values is consistent with an increase in $\sigma + \pi$ in the order (149) $\text{SbPh}_3 < \text{AsPh}_3 < \text{PPh}_3 \sim \text{PPh}_2\text{CF}_3 < \text{PMe}_2\text{Ph} < \text{CO}$.

Perhaps the largest variations in Q.S. within a series of compounds is given by compounds 29–33 in Table LXII (133). An increase in C.S. is paralleled by a large decrease in Q.S. These C.S. observations are consistent with $\sigma + \pi$ decreasing in the order $\text{P}(\text{OEt})_3 > \text{PPh}_3 > \text{AcNp} > \text{MaA} > \pi$ allyl, although an adequate explanation for the Q.S. trend has not yet been proposed.

In compounds 34–38 and other similar complexes (147), the $\text{LFe}(\text{CO})_4$ derivatives give larger Q.S. than the corresponding $\text{L}_2\text{Fe}(\text{CO})_3$ derivatives. In contrast, other similar compounds show the reverse trend (133, 333). Possible explanations of these trends have been discussed (147), but the signs of the Q.S. should be determined for a meaningful rationalization.

Very interesting studies on π -cyclopentadienyl and analogous carborane species have appeared (Table LXII, compounds 39–48) (60, 132, 154, 174, 514, 561). The very large splitting in $(\text{cp})_2\text{Fe}$ and its almost complete collapse in $(\text{cp}_2\text{Fe})^+$ species has been a subject of considerable discussion. The sign of the Q.S. in $(\text{cp})_2\text{Fe}$ has been found to be positive using both the magnetic field technique (132) and single crystals (174). Using molecular orbital calculations (154, 514), this large positive splitting has been attributed mainly to an electron localized in d_{xy} . The removal of this electron on going to $[(\text{cp})_2\text{Fe}]^+$ fortuitously collapses the splitting. The analogous carbollyl complexes (Table LXII, compounds 46–48) give slightly larger splittings than their cyclopentadienyl counterparts, indicating that the three B atoms in the C_2B_3 face of the carborane icosahedron have very similar bonding characteristics to those of the replaced carbon atoms. The smaller C.S. in the boranes

indicates greater s electron density at the Fe nucleus in the carboranes than π -cp compounds. This has been attributed to the stronger π -acceptor properties of the boranes (60).

Finally, in this section, we mention a few of the $\text{Fe}^{-\text{I}}$ compounds whose spectra have been recorded (146). The order of C.S. gives a measure of $(\sigma + \pi)$ for these ligands; i.e., $\text{C}_5\text{H}_5\text{N} < \text{Ph}_3\text{Sb} < \text{Ph}_3\text{As} < \text{Ph}_3\text{P}$. $\text{Fe}^{-\text{I}}$ compounds have larger Q.S. values than their $\text{Fe}^{-\text{II}}$ analogs because of the $q_{\text{C.F.}}$ term in $\text{Fe}^{-\text{I}}$ compounds (146). Rather surprisingly, $\text{Fe}^{-\text{I}}$ compounds have a larger C.S. than $\text{Fe}^{-\text{II}}$ compounds. This is probably due to the fact that on going from $\text{Fe}^{-\text{II}}$ to $\text{Fe}^{-\text{I}}$ we have replaced strong $\sigma + \pi$ ligands such as CO by weak $\sigma + \pi$ ligands such as Cl and Br (146).

5. Fe Intermediate Spins

A number of interesting papers have appeared which discuss the Mössbauer parameters of intermediate spin ($S = 1$) Fe^{II} compounds and $S = \frac{3}{2}$ Fe^{III} compounds. A selection of the available data is given in Table LXIII. Much of the interest in the bis(N,N -disubstituted dithiocarbamate)iron(III) compounds (Table LXIII, compounds 8–11) has centered around the interpretation of magnetic and relaxation phenomena of these compounds [(486, 563, 565) and references in (564)]. These papers have been of considerable interest and importance, but as discussed at the beginning of this chapter, they are beyond the scope of this article.

The first six compounds in Table LXIII have magnetic moments at 295°K of about 3.9 B.M., and this has been attributed (372, 375) to two unpaired electrons with a contribution of ~ 1.0 B.M. from the second-order Zeeman effect. The Mössbauer spectra, however, are of very little use in characterizing the spin state of these compounds. Thus, both the C.S. and Q.S. are very similar to those of Fe^{II} low-spin compounds, although the quadrupole splittings are rather small. The magnetic data, and other spectral data strongly suggests that these compounds do have the $S = 1$ configuration.

FePc has long been of great interest. The magnetic moment of this complex is much above that expected for two unpaired electrons [see references in (158)]. Both an $S = 1$ state and a thermal admixture of $S = 2$ and $S = 0$ states are possible explanations for this unusual magnetic moment. The complex obeys a Curie–Weiss law and gives an almost temperature-independent susceptibility (384). The temperature independence of the Q.S. (155, 179, 410) down to 4°K indicates that there are no low-lying excited states within about 4 cm^{-1} of the ground state (410). More recently, Dale *et al.* (155, 158) have obtained magnetic data

down to 1.25°K and shown that the susceptibility is virtually independent of temperature between 1.25° and 20°K. Their results are compatible with the iron atom having an orbital singlet with a real spin triplet state. This $S = 1$ state is split by second-order spin-orbit coupling into a singlet ground state and a doublet state at 70 cm⁻¹. Mössbauer spectra in large magnetic fields (155) show that the field gradient is positive. Most of the very large Q.S. can be attributed to the strong in-plane covalent bonding (155), and reasonable agreement between predicted and observed values has been obtained (155, 179), using the M.O. calculations used by Zerner *et al.* (575) for Fe^{II} porphyrin complexes, which should be closely analogous to FePc.

The pentacoordinate dithiocarbamate complexes have an orbitally degenerate spin quartet ground term as indicated by the magnetic

TABLE LXIII

MÖSSBAUER PARAMETERS FOR INTERMEDIATE SPIN Fe^{II} AND Fe^{III} COMPOUNDS^a

Code No. ^b	Compound	C.S. ^c	Q.S.	Ref.
1	[Fe(phen) ₂ OX] · 5H ₂ O ^{c,d}	+0.58	0.21	(372, 375)
2	[Fe(phen) ₂ mal] · 7H ₂ O	+0.52	0.18	(372, 375)
3	[Fe(phen) ₂ F ₂] · 4H ₂ O	+0.55	0.16	(372, 375)
4	[Fe(dip) ₂ OX] · 3H ₂ O ^d	+0.52	0.26	(372, 375)
5	[Fe(4,7-dmph) ₂ OX] · 4H ₂ O ^d	+0.54	0.21	(372, 375)
6	[Fe(4,7-dmph) ₂ mal] · 7H ₂ O	+0.52	0.21	(372, 375)
7	FePc ^d	+0.78	2.67	(155, 347, 410)
		+0.83 ^e	2.67 ^e	(155, 179, 410)
8	(R ₂ NCS ₂) ₂ FeCl ^h	~+0.64 ^g	2.64	(212)
			2.68 ^f	(564)
9	(R ₂ NCS ₂) ₂ FeBr ^h	~+0.64 ^g	2.82	(212)
			2.88 ^f	(564)
10	(R ₂ NCS ₂) ₂ FeI ^h	~+0.64 ^g	2.92	(212)
11	(R ₂ NCS ₂) ₂ FeSCN ^h	~+0.64 ^g	2.56	(212)

^a Data given in mm/sec at 80°K unless otherwise noted.

^b Code number will be preceded by table number in the text.

^c At room temperature.

^d phen = Phenanthroline; dip = 2,2'-dipyridyl; 4,7-dmph = 4,7-dimethyl-1,10-phenanthroline; Pc = phthalocyanine; ox = oxalate; mal = malonate.

^e At ~4°K.

^f At 1.2°K.

^g These C.S. values are averages for all R and X values for the compounds (R₂NCS₂)₂FeX (212).

^h R = CH₃, C₂H₅, C₆H₁₂, C₆H₁₁, C₈H₁₄, etc. [212].

ⁱ Values quoted relative to nitroprusside.

susceptibility, ESR, and Mössbauer results [(563, 564) and references]. Most of the compounds are simple paramagnets, although $[(C_2H_5)_2NCS_2]_2FeCl$ has shown magnetic ordering at low temperatures (563). The large positive Q.S. values (564) cannot be readily explained because the q_{lat} contribution to the EFG cannot be calculated. It is likely (564) that an appreciable q_{val} contribution arises from the ground quartet term. The variations in Q.S. (Table LXIII, compounds 8–11) could be due to the variation in q_{lat} (212, 564).

G. OTHER MÖSSBAUER ISOTOPES

In the preceding parts of this chapter we have discussed Mössbauer results for ^{57}Fe , ^{119}Sn , ^{99}Ru , ^{193}Ir , ^{129}I , and ^{127}I compounds. Despite the fact that there are over thirty isotopes which exhibit this effect, we restrict the discussion in this final section to four isotopes which have yielded useful and interesting chemical information: ^{197}Au , ^{121}Sb , ^{125}Te , and ^{129}Xe . Interesting chemical information has also been obtained on many rare earth isotopes [for a review see (427)] and ^{237}Np [for a review see (458)], while other isotopes such as ^{61}Ni (214, 518), and many heavy isotopes such as ^{177}Hf , ^{181}Ta , ^{182}W , ^{186}Os , and ^{195}Pt have not yet yielded useful chemical information [for a review see (270, 512)]. A recent paper on ^{182}W Mössbauer (33) indicates that useful chemical information should be readily obtained from tungsten compounds.

1. ^{197}Au

Mössbauer spectra of ^{197}Au compounds were first reported by Roberts (491) and Shirley (511). Although the natural linewidth of the 77.3 keV ($\frac{1}{2} \rightarrow \frac{3}{2}$) resonance is about 50 times that of ^{57}Fe , the changes in C.S. and Q.S. are two to three times those observed for ^{57}Fe compounds. The sign of $\delta R/R$ has recently been shown to be positive (490), and the quadrupole moment of the ground nuclear state has the value +0.586 barns (67). Because of the liquid He temperatures required to obtain reasonable spectra, and the very short half-life (~ 18 hr) of the ^{195}Pt precursor, very little quantitative data had been reported until very recently. Three recent papers (49, 108, 222) demonstrate the considerable utility of Mössbauer parameters for discussing structure and bonding in Au compounds. A selection of data (49, 108, 222) for Au^I and Au^{III} compounds is given in Tables LXIV and LXV, respectively.

a. *Center Shifts.* Au^I compounds contain linear L–Au–L' units in the first coordination sphere of the gold atom [see references in (49)]. The electron configuration of Au^{+1} ion is $5d^{10}$, and the ligands donate electrons to the $6s6p$ Au hybrid orbitals. Since the C.S. is usually more

TABLE LXIV

MÖSSBAUER PARAMETERS FOR SOME RECENTLY MEASURED Au^I COMPOUNDS^a

Code No. ^b	Compound	C.S. ^c	Q.S.	Ref.
1	AuCl	~-1.4	~4.6	(49, 108, 222)
2	AuBr	-1.47	4.23	(222)
3	AuI	-1.28	~4.1	(49, 108, 222)
4	AuCN	+2.11	8.16	(49, 108, 222)
5	As(C ₆ H ₅) ₄ Au(N ₃) ₂	+1.43	6.84	(49)
6	KAu(CN) ₂	+3.12	10.12	(49)
7	(C ₁₀ H ₁₂)AuCl	+0.83	6.04	(49)
8	(C ₁₈ H ₃₆)AuCl	+0.91	6.41	(49)
9	(C ₁₆ H ₃₂)AuCl	+1.03	6.29	(49)
10	Me ₂ SAuCl	+1.26	6.42	(108)
11	C ₅ H ₅ NAuCl	+1.7	6.4	(108)
12	Ph ₃ AsAuCl	+1.92	7.00	(108)
13	Ph ₃ PAuCl	+2.96	7.47	(108)
14	(C ₆ F ₅ Ph ₂ P)AuCl	+2.93	7.87	(108)
15	Ph ₃ PAuN ₃	+3.3	8.4	(108)
16	Ph ₃ PAu(OCOMe)	+3.3	7.6	(108)
17	Ph ₃ PAuCN	+3.9	10.5	(108)
18	Ph ₃ PAuMe	+4.93	10.35	(108)

^a At 4.2°K/(mm/sec). In many cases, averages of the available recent data (see references) are given.

^b Code number will be preceded by table number in text.

^c Relative to the source Au/Pt at 4.2°K.

sensitive to the *s* electron augmentation than *p* electron augmentation and $\delta R/R$ is positive, we would expect that an increase in the σ -donor characteristics of the two ligands would increase $[\Psi(O)_s]^2$ and the C.S. π -accepting ligands would decrease the 5*d* electron density and also result in an increase in the C.S. However, π -bonding effects are usually not considered to be very important in Au compounds.

Au^{III} compounds are known to be square-planar [see references in (49)] and the bonding involves *dsp*² hybrid orbitals on the gold. Assuming again that the C.S. is most sensitive to 6*s* orbital augmentation, the C.S. should again increase with increased σ -donor characteristics of the ligands. In addition, it might be expected that Au^{III} would have larger C.S. values than Au^I because of the smaller *d* electron density in Au^{III} compounds and resultant increase in $[\Psi(O)_s]^2$. However, the increased shielding of *s* electrons from a larger 6*p* electron density in Au^{III} compounds would tend to offset the *d*-electron density effect.

TABLE LXV

MÖSSBAUER PARAMETERS FOR SOME RECENTLY MEASURED Au^{III} COMPOUNDS^a

Code No. ^b	Compound	C.S. ^c	Q.S.	Ref.
1	AuF ₃	-1.07	2.74	(222)
2	AuCl ₃	+0.57	0.75	(222)
		+0.83	—	(108)
3	AuBr ₃	+0.79	1.27	(222)
		+0.48	—	(49)
		+0.18	1.8	(108)
4	[BrF ₂] ⁺ [AuF ₄] ⁻	-0.69	1.82	(222)
5	MAuF ₄ ^d	+0.03	<1.0	(49, 108)
6	KAuI ₄	+0.43	1.28	(49)
7	KAuBr ₄	+0.64	1.13	(49, 222)
8	KAuCl ₄ · 2H ₂ O	+0.71	~1.3	(49, 108, 222)
9	Ph ₄ AsAuCl ₄	+1.09	1.88	(108)
10	KAu(SCN) ₄	+1.63	2.04	(49)
11	As(C ₆ H ₅) ₄ Au(N ₃) ₄	+1.66	2.89	(49)
12	Na ₃ AuO ₃	+2.45	3.02	(49)
13	KAu(CN) ₂ X ₂ ^d	~+2.7	~5.5	(49, 222)
14	KAu(CN) ₄	+4.12	6.93	(49, 222)
15	Ph ₃ PAuCl ₃	2.06	3.25	(108)
16	C ₅ H ₅ NAuCl ₃	1.45	—	(108)
17	Me ₂ SAuCl ₃	1.26	2.20	(108)
18	<i>p</i> -MeC ₆ H ₄ NCAuCl ₃	0.75	2.00	(108)

^a At 4.2°K (mm/sec). In many cases, averages of the available recent data (see references) are given.

^b Code number will be preceded by table number in text.

^c Relative to the source Au/Pt at 4.2°K.

^d M = alkali metal; X = Cl, Br, I.

In agreement with the above considerations, it is apparent from the data in Tables LXIV and LXV that the C.S. values for both Au^I and Au^{III} compounds increase as the σ -donor characteristics of the ligands increase. Thus, for Au^I halides, azide, and cyanide (Table LXIV, compounds 1–5) the C.S. becomes more positive in the order Cl⁻ < Br⁻ < I⁻ < N₃⁻ < CN⁻. Similarly, in the LAuCl compounds (Table LXIV, compounds 10–14), the C.S. increases in the order L = Me₂S < C₅H₅N < Ph₃As < Ph₃P ~ (C₆F₅)Ph₂P. Again, in the Ph₃P AuX series (Table LXIV, compounds 15–18), the C.S. increases in the order X = N₃⁻ ~ OCOMe⁻ < CN⁻ < Me. The order of these C.S. values agrees with generally recognized bonding characteristics, and it is apparent that the C.S. should be useful for placing ligands in a σ -bonding order.

For the Au^{III} compounds, a similar order of C.S. values is found (Table LXV) (except for the halides), and the order of center shifts correlates very well with the spectrochemical ranking of ligands (49). A similar correlation has been noted previously in this chapter for Fe^{II} low-spin compounds (44). Thus, in the AuX_4^- series, (Table LXV, compounds 5-8, 10-12, 14), the C.S. values increase in the order $\text{F}^- < \text{I}^- < \text{Br}^- < \text{Cl}^- < \text{SCN}^- \sim \text{N}_3^- < \text{O}^{2-} < \text{CN}^-$. For the LAuCl_3 compounds (Table LXV, compounds 15-17), the order of C.S. is identical to that of the Au^{I} compounds, i.e., $\text{L} = \text{Me}_2\text{S} < \text{C}_5\text{H}_5\text{N} < \text{Ph}_3\text{P}$, indicating again that Ph_3P is the strongest σ donor in this series.

It is interesting to note that the C.S. value for $\text{KAu}(\text{CN})_2\text{X}_2$ ($\text{X} = \text{Cl}, \text{Br}, \text{I}$) compounds ($\sim +2.7$ mm/sec) is close to the arithmetic mean of the C.S. values for KAuX_4 compounds (~ 0.9 mm/sec) and that for $\text{KAu}(\text{CN})_4$ (~ 4.1 mm/sec). It is possible then that a partial center shift approach would be useful for predicting and rationalizing Au^{III} C.S. data. It is also noticeable from Tables LXIV and LXV that Au^{III} compounds generally have more positive C.S. values than their Au^{I} analogs, consistent with considerations outlined above. Thus, the C.S. of $\text{KAu}(\text{CN})_4 > \text{KAu}(\text{CN})_2$ and the C.S. of $\text{AuCl}_3 > \text{AuCl}$. However, this generalization is not always true; for example, $\text{C}_5\text{H}_5\text{NAuCl}_3$ has a smaller C.S. than $\text{C}_5\text{H}_5\text{NAuCl}$. It is often difficult then to distinguish Au^{I} from Au^{III} on the basis of C.S. alone (49, 108, 222).

b. Quadrupole Splittings. The quadrupole splittings also show a large range of values, and they can also be interpreted qualitatively using the simple bonding considerations outlined in the previous section. The signs of the quadrupole splittings have not been determined, but they can be predicted with considerable confidence. For Au^{I} compounds, the Z EFG axis lies through the bond axes, and σ bonding involves donation of electrons to the $6s$ and $6p_z$ orbitals. V_{zz} then should be negative, and since Q is $+ve$, e^2qQ for Au^{I} compounds is negative. Since the $6s$ population should be proportional to the $6p$ population, then an increase in σ -donor power of a ligand should increase the magnitude of the Q.S., while also increasing the C.S. Inspection of Table LXIV shows that an increase in C.S. is paralleled usually by an increase in Q.S. Indeed, Faltens and Shirley (222) have fit a Q.S.-C.S. plot for compounds 1-4 and 6 (Table LXIV) to a straight line with the equation:

$$\text{C.S.} = 0.872\text{Q.S.} - 0.474(\text{cm/sec}) \quad (88)$$

For Au^{III} , the situation is slightly more complicated. The Z EFG axis lies along the 4-fold symmetry axis. The $d_{x^2-y^2}$ hole in a Au^{3+} ion would then produce a negative e^2qQ since there is a concentration of electron density (two d_z electrons) along the Z EFG axis. Covalent

bonding, however, to the $5d_{x^2-y^2}$, $6p_x$ and $6p_y$ orbitals produces a positive contribution to the field gradient, and calculations show (222) that, except for the most ionic Au^{III} compounds, the latter contribution should dominate and give a positive e^2qQ . Thus, for the more ionic auric fluorides (Table LXV, compounds 1, 4, and 5), the sign of e^2qQ is taken to be negative, whereas for all the other compounds, the sign of e^2qQ is taken as positive (222). Supporting these assignments, a plot of C.S. versus Q.S. for a number of auric compounds (222) is reasonably linear with an equation:

$$\text{C.S.} = 0.532 \text{ Q.S.} + 0.016 \text{ (cm/sec)} \quad (89)$$

Faltens and Shirley noted that the C.S. and Q.S. taken together could be used to determine the oxidation state of gold unambiguously.

Like the C.S. values, the Q.S. for $\text{KAu}(\text{CN})_2\text{X}_2$ compounds (~ 5.5 mm/sec) is intermediate between that of the AuX_4^- species (~ 1.5 mm/sec) and the $\text{Au}(\text{CN})_4^-$ species (~ 6.9 mm/sec). The Q.S. value for *trans*- $\text{Au}(\text{CN})_2\text{X}_2^-$ compounds would be expected to be considerably larger than the average value of the two end members because of the large η in $\text{Au}(\text{CN})_2\text{X}_2^-$ (222). It would appear that partial quadrupole splittings could be derived and used successfully for such compounds.

Faltens and Shirley (222) have attempted to interpret the C.S. and Q.S. variations more quantitatively with very little success. Fortunately, it seems that even the qualitative interpretation is of considerable bonding and structural use in these gold compounds.

2. ^{121}Sb

A large number of Sb Mössbauer spectra have been recorded using the $37.2 \text{ keV } \frac{7}{2}^+ \rightarrow \frac{5}{2}^+$ transition. The majority of the data for Sb^{III} and Sb^{V} stoichiometric compounds containing one oxidation state of Sb are given in Tables LXVI and LXVII. Spectra of simple compounds can be obtained at 80°K , but liquid He temperatures are desirable to obtain good spectra and to extract more meaningful center shifts and quadrupole splittings (524). The quadrupole splittings are never well resolved, and most of the discrepancies in C.S. values are probably due to fitting one Lorentzian to an asymmetric peak.

The C.S. values are very sensitive both to the oxidation state of Sb, and the type of ligand. This is due to the very large value of $\delta\langle R^2\rangle/\langle R^2\rangle(\rho)$ (Table LXVIII) for ^{121}Sb , in comparison with other Mössbauer nuclei discussed in this chapter. The values in Table LXVIII were obtained in two ways. In the first method, (498, 510) experimentally determined C.S. values for tin, antimony, tellurium, iodine, and xenon have been compared with atomic Hartree-Fock density calculations to give values

TABLE LXVI
MÖSSBAUER PARAMETERS FOR Sb^{III} COMPOUNDS^a

Compound	C.S. ^b	e^2qQ	Ref.
SbF_3	-14.6	+19.6	(72, 496, 522)
SbCl_3^c	-13.8	+12.2	(72, 496, 522)
SbBr_3^c	-13.9	+9.4	(72, 522)
SbI_3^c	-15.9	—	(72, 522)
Sb_2O_3	-11.4	~18.0	(62, 72, 496, 522)
Sb_2S_3	-14.4	—	(62, 72, 522)
Sb_2Te_3	-15.3	—	(62)
$\text{Co}(\text{NH}_3)_6\text{SbCl}_6$	-19.7	—	(63)
K_3SbCl_6	-18.2	—	(63)
Cs_3SbCl_6	-18.1	—	(63)
$(\text{NH}_4)_3\text{SbCl}_6$	-17.2	—	(63)
$(\text{NH}_4)_2\text{SbCl}_5$	-15.2	—	(63)
Sb^{III} in $\text{Rb}_4[\text{Sb}^{\text{III}}\text{Sb}^{\text{V}}\text{Cl}_{12}]$	-19.6	—	(63)
Ph_3Sb	-9.69	+17.5	(389)
$(p\text{-ClC}_6\text{H}_4)_3\text{Sb}$	-9.3	—	(307)
$(p\text{-CH}_3\text{OC}_6\text{H}_4)_3\text{Sb}$	-9.0	—	(307)

^a Data given in mm/sec with both source and absorber at 80°K except for Ph_3Sb . This spectrum was recorded with both source and absorber at 4.2°K.

^b Center shift values are quoted relative to $^{121}\text{SnO}_2$ or $\text{Ca}^{121}\text{SnO}_3$, taking these compounds to have identical C.S. values. The C.S. of InSb w.r.t. from these sources is -8.5 ± 0.1 mm/sec.

^c Russian work (377, 513) has yielded substantially more negative values for the C.S. For example, the C.S. values (377) for SbCl_3 , SbBr_3 , and SbI_3 are -15.5, -15.85, and -16.5 mm/sec, respectively.

of $\delta\langle R^2\rangle/\langle R^2\rangle$ for each nucleus. In the second, the center shifts for isoelectronic pairs of compounds were compared to obtain ratios of $\delta\langle R^2\rangle/\langle R^2\rangle$ for adjacent nuclei. Taking the value of ρ for ^{119}Sn to be 2.4×10^{-4} , as deduced by a comparison of center shifts with calculated charge densities (496), the values of ρ for the other Mössbauer nuclei could be determined. It is important to note that ρ is negative for ^{121}Sb . The very large differences in C.S. between Sb^{III} compounds (C.S. ranges from -9 to -19 mm/sec) and Sb^{V} compounds (C.S. ranges from -7 to +4 mm/sec) have been very useful in detecting the existence of Sb^{III} and Sb^{V} in mixed oxides and sulfides of Sb (62, 71, 388), as well as in complex chlorides such as $\text{Rb}_4[\text{Sb}_2\text{Cl}_{12}]$ (63). The large range of C.S. values within one oxidation state (Tables LXVI and LXVII) has been useful in obtaining structural and bonding information (*vide infra*). Because ρ is negative, an increase in $[\psi(O)_s]^2$ decreases the C.S. Sb^{V} , then,

TABLE LXVII
MÖSSBAUER PARAMETERS FOR Sb^{V} COMPOUNDS^a

Compound	C.S. ^c	e^2qQ	Ref.
SbF_5	+2.23	—	(72, 522)
SbCl_5	-3.12	-4.4	(72, 522)
	-3.5	—	(513)
Sb_2O_5	+1.2	-4.3	(72, 496, 522)
RbSbCl_6	-2.7	—	(63)
$\text{HSbCl}_4 \cdot \text{XH}_2\text{O}$	-3.0	—	(513)
NaSbF_6	+1.7	—	(496, 513)
KSbF_6	+3.8	—	(496)
$\text{NaSb}(\text{OH})_6$	+0.5	—	(513)
Ph_5Sb	-4.6	—	(389)
Ph_4SbF	-4.5	—	(389)
Ph_4SbF^b	-4.56	-7.2	(389)
Ph_4SbCl^b	-5.26	-6.0	(389)
Ph_4SbBr^b	-5.52	-6.8	(389)
$\text{Ph}_4\text{SbNO}_3^b$	-5.49	-6.4	(389)
$\text{Ph}_3\text{SbF}_2^b$	-4.69	-22.0	(389, 523)
$\text{Ph}_3\text{SbCl}_2^b$	-6.02	-20.6	(389, 523)
$\text{Ph}_3\text{SbBr}_2^b$	-6.32	-19.8	(389, 523)
$\text{Ph}_3\text{SbI}_2^b$	-6.72	-18.1	(389, 523)
$(\text{PhCH}_2)_3\text{SbCl}_2^b$	-5.86	-23.0	(389)
$(\text{CH}_3)_3\text{SbCl}_2^b$	-6.11	-24.0	(389, 523)
$(\text{CH}_3)_3\text{SbBr}_2^b$	-6.40	-22.1	(389, 523)
$\text{Ph}_4\text{SbClO}_4$	-5.9	—	(389)

^a Data given in mm/sec with both source and absorber at 80°K unless otherwise noted.

^b Spectra recorded with both source and absorber at 4.2°K.

^c Center shift values are quoted relative to $^{121}\text{SnO}_2$ or $\text{Ca } ^{121}\text{SnO}_3$ (^{121}Sb), taking these two compounds to have identical C.S. values. The center shift of InSb w.r.t. from these sources is -8.5 ± 0.1 mm/sec.

has a more positive C.S. than Sb^{III} . In contrast, because ^{119}Sn has a positive ρ , Sn^{IV} has more negative C.S. values than Sn^{II} (Section III, A).

The quadrupole splittings are never well resolved; only for the largest Q.S. values for spectra at 4.2°K (such as the spectra of $\text{R}_{5-n}\text{SbX}_n$ ($\text{R} = \text{Ph, Me}$; $\text{X} = \text{F}^-, \text{Cl}^-, \text{Br}^-, \text{I}^-$; $n = 0-2$) can more than two of the eight lines be visually resolved. As a result, the quadrupole splittings (if detectable) normally have large errors. From spectra of the alkyl and aryl halides, the ratio of quadrupole moments $Q_{\text{ex}}/Q_{\text{gr}}$ has been determined to be 1.34 ± 0.01 (523), but the value of Q_{gr} is not nearly as well defined. Ruby *et al.* (496) concluded from a number of widely varying Q_{gr} values

and their calculated value (496), that $Q_{gr} = -0.28 \pm 0.1$ barns. It should be noted here that both Q_{ex} and Q_{gr} have negative values. Thus, as for ^{119}Sn , an excess charge density along the Z EFG direction gives a negative q , but a positive e^2qQ .

TABLE LXVIII
VALUES OF $\rho = \delta\langle R^2 \rangle / \langle R^2 \rangle \times 10^4$ FOR VARIOUS NUCLEI^a

	From comparison of isoelectronic structures	From density calibration
^{119}Sn	—	2.4
^{121}Sb	-14.6	-17.0
^{125}Te	1.9	—
^{127}I	-4.8	-5.6
^{129}I	6.2	6.6
^{129}Xe	0.55	0.66

^a From Refs. (498, 510).

a. Experimental Data. For Sb^{III} halides and oxide, a linear relationship has been noted between C.S. values and the difference in Pauling electronegativity ($\Delta\chi$) between Sb and the ligand (72, 522). The least-squares fit to the data gives:

$$\text{C.S.} = -18.3 + 4.35\Delta\chi \quad (90)$$

SbF_3 lies well off this line. A plot of C.S. versus Q.S. for SbI_3 , SbBr_3 , SbCl_3 , and Sb_2O_3 gives another straight line (72).

$$\text{C.S. (mm/sec)} = -18.0 + 0.011e^2qQ (\text{MHz}) \quad (91)$$

These correlations indicate that a "bare" Sb^{3+} ion should have a C.S. of about -18 mm/sec. As the electronegativity of the ligand increases, $[\Psi(O)_s]^2$ decreases, causing the C.S. to become more positive. The C.S. values for Ph_3Sb and related compounds, using the above correlation Eq. (90), are somewhat anomalous, since the electropositive Ph group might be expected to increase $[\Psi(O)_s]^2$ more than in SbI_3 , and give a very negative C.S. value. In fact, the most positive values for Sb^{III} compounds are observed. The structures of SbI_3 and Ph_3Sb are, however, not analogous. SbI_3 is essentially octahedral (542), whereas Ph_3Sb is trigonal-pyramidal with C-Sb-C bond angles of $\sim 113^\circ$ (101), implying that Ph_3Sb has σ bonds which are essentially sp^3 hybrids with sufficient p_z electron density in the lone pair to give the large positive Q.S. (389).

It has also been suggested that there may be some resonance between Sb and Ph groups (148, 389) which permits some of the *s* electron density of the lone pair to be dissipated into the aromatic rings and give the unexpected C.S. values.

Some of the C.S. values for the SbCl_6^{3-} species in Table LXVI are more negative than the -18 mm/sec suggested (72, 522) as the C.S. value for a "bare" Sb^{3+} ion from Eqs. (90) and (91). These very negative values imply (63) that the $5s$ pair is not being used greatly in the bonding to the six chlorides and/or that the value of -18 mm/sec is inaccurate and that the C.S. value for a bare Sb^{3+} is considerably more negative than this value.

As for Sb^{III} compounds, it is apparent from Table LXVII that the C.S. values for Sb^{V} compounds become more positive as the electronegativity of the ligands increases. The center shifts for analogous compounds vary as follows: $\text{SbCl}_5 < \text{Sb}_2\text{O}_5 < \text{SbF}_5$; $\text{SbCl}_6^- < \text{SbF}_6^-$; $\text{Ph}_4\text{SbBr} < \text{Ph}_4\text{SbCl} < \text{Ph}_4\text{SbF}$; and $\text{Ph}_3\text{SnI}_2 < \text{Ph}_3\text{SbBr}_2 < \text{Ph}_3\text{SbCl}_2 < \text{Ph}_3\text{SbF}_2$. Also, the C.S. values for the Ph_3SbX_2 compounds are more negative than for the Ph_4SbX compounds. It should be noted here that Gukasyan and Shpinel (307) have quoted substantially more negative values for the C.S. of Ph_3SbF_2 and Ph_3SbCl_2 than those given in Table LXVII. This discrepancy is probably due to fitting one peak to the asymmetric spectrum. The above trends in C.S. are again consistent with the increased withdrawal of *s* electron density as the electronegativity of the ligand increases.

Considerable structural and bonding information can be obtained for the $\text{Ph}_{5-n}\text{SbX}_n$ species, and this series of spectra are the most interesting Sb spectra yet reported (389). The sign and magnitude of the Q.S. values for the R_3SbX_2 species is expected from the known trigonal-bipyramidal structure (72, 469, 522) and the signs and magnitudes of the Q.S. for the isoelectronic Sn compounds (Table XXII). In fact, it should be possible to use the isoelectronic Sn and Sb compounds along with Eq. (51) to derive an accurate value of $Q_{119\text{sn}}/Q_{121\text{sb}}$. The positive q values observed (negative e^2qQ) are expected from the excess negative charge lying in the XY plane due to the strong σ -donor properties of the R groups. As with Sn compounds (Table XX), as the electronegativity of the halide decreases (from F to I), the e^2qQ values become more negative. It is also apparent that the methyl compounds have larger Q.S. values than the phenyl compounds [$\text{Ph}_3\text{SbCl}_2 = -20.6$ mm/sec; $(\text{CH}_3)_3\text{SbCl}_2 = -24.0$ mm/sec] indicating that methyl is a better σ donor than phenyl. Once again, the same trend is noticed in the isoelectronic Sn^{IV} species. Thus, $[\text{Me}_3\text{SnCl}_2]^-$ and $[\text{Ph}_3\text{SnCl}_2]^-$ (Table XXII) have Q.S. values of -3.31 and -3.02 mm/sec, respectively, and the p.q.s. value for methyl is

substantially more negative than phenyl. The C.S. values for the methyl compounds are slightly more negative than those for the phenyl compounds. Again, this is consistent with Me being a better donor than Ph, and once again the Sn^{IV} compounds show the analogous trend (Table XX).

The Ph_4SbX compounds are of some considerable structural interest. Although recent X-ray structures of Ph_4SbOH (52) and $\text{Ph}_4\text{SbOCH}_3$ (509) have shown five-coordinate trigonal-bipyramidal coordination about Sb, the Ph_4Sb group has often been taken as ionic, i.e., Ph_4Sb^+ . Recent infrared evidence has been shown to be consistent with this cation being present (396). A tetrahedral species would be expected to give little or no quadrupole splitting, and little or no variation in C.S. as the counterion is varied. In contrast, the C.S. varies from -4.56 (Ph_4SbCl) to -5.9 mm/sec ($\text{Ph}_4\text{SbClO}_4$), and the Q.S. values of ~ 7 mm/sec (except for $\text{Ph}_4\text{SbClO}_4$) approach those expected from a point charge model taking the Sb-X bond to be identical in character in both R_3SbX_2 and R_4SbX compounds. Taking structures 8 and 10 in Table IV, and assuming $[\text{L}]^{\text{tbe}} \equiv [\text{L}]^{\text{tba}}$, the ratio of Q.S. for R_3SbCl_2 : R_4SbCl is expected to be greater than 2 : 1 in comparison to the ~ 3 : 1 observed. The quadrupole splittings strongly indicate that except for $\text{Ph}_4\text{SbClO}_4$, a strong covalent bond is formed between the Sb and X ligand, and that these compounds are five-coordinate in the solid state. The narrow single-line spectrum of $\text{Ph}_4\text{SbClO}_4$, the large absorption, and the negative C.S. all are consistent with this compound being formulated as $\text{Ph}_4\text{Sb}^+(\text{ClO}_4)^-$ (389). Solution conductance data indicate that whereas Ph_4SbF and Ph_4SbCl are essentially undissociated, Ph_4SbNO_3 could be a 1 : 1 electrolyte (389) in solution.

The Mössbauer spectra of SbF_5 and SbCl_5 have not been very useful for structural elucidation (72, 522). For example, two proposed structures for the low temperature phase of SbCl_5 are: a dimeric structure with Sb in six coordination, and an ionic $[\text{SbCl}_4]^+[\text{SbCl}_6]^-$ structure (430, 508). The Mössbauer spectrum of SbCl_5 is consistent with essentially octahedral coordination about Sb. A two-peak fit gave an equally good fit to the data (72) and the ionic structure cannot be ruled out from this spectrum.

3. ^{125}Te

Several papers have appeared which discuss the Mössbauer spectra of Te compounds using the $35.48 \text{ KeV } \frac{3}{2}^+ \rightarrow \frac{1}{2}^+$ transition. The majority of data for tellurium halide and oxygen complexes are given in Tables LXIX and LXX. All spectra have been obtained at 80°K , but many

absorbers have been enriched to obtain reasonable spectra. Because of the very large line widths (~ 5.3 mm/sec), the quadrupole splittings are usually not well resolved. More seriously, however, agreement of C.S. values among various workers has been extremely poor (Tables LXIX and LXX), and this has made it extremely difficult to obtain meaningful chemical bonding information, or for that matter, the sign and magnitude of $\delta R/R$. For example, as summarized by Gibb *et al.* (266), Russian work

TABLE LXIX

MÖSSBAUER PARAMETERS FOR Te HALIDES AND HALIDE COMPLEXES^a

Compound	C.S. ^c	Q.S.	Ref.
TeF ₄	+0.4	7.0	(546)
	+0.4	6.8	(547)
TeCl ₄	+1.2	4.0	(361)
	+2.7	5.4	(545)
TeBr ₄	+1.1	3.8	(361)
	+1.6	5.0	(545)
TeI ₄	+1.0	3.0	(547)
	+1.8	~ 4	(361)
	+1.0	6.0	(546)
M ₂ TeCl ₆ ^b	+1.95	0.0	(266)
	+1.4	0.0	(85, 513)
	+1.8	0.0	(545)
	+1.70 ^d	0.0	(306)
M ₂ TeBr ₆ ^b	+1.74	0.0	(266)
	+1.7	0.0	(85, 513)
	+2.2	0.0	(545)
	+1.56 ^d		(306)
M ₂ TeI ₆ ^b	+1.59	0.0	(266)
	+2.0	0.0	(85, 513)
	+1.27 ^d		(306)
TeF ₆ ²⁻ ?	+0.0	0.0	(513)
	+0.97	5.6	(306)
MTeF ₅ ^b	+0.89	5.98	(266)
TeCl ₂	+0.5	6.5	(361)
	+1.3	6.5	(545)
TeBr ₂	+0.6	6.3	(545)

^a Data given in mm/sec at 80°K.

^b M = NH₄, Rb, Cs, K, NMe₄.

^c Relative to ¹²⁵I/Cu as source.

^d These values were quoted relative to ZnTe. ZnTe has a C.S. very close to zero relative to ¹²⁵I/Cu source (266, 361).

(85, 513) for the hexahalogen complexes of tellurium, M_2TeX_6 ($X = Cl, Br, I$), showed that the C.S. of these complexes increased in the order $Cl < Br < I$, i.e., in the same order for the hexahalogen complexes of Sn indicating that like Sn, $\delta R/R$ is positive. However, more recent and precise work (266, 306) shows that the trend is just the opposite. The C.S. varies in the order $I < Br < Cl$. The explanation of this trend will be examined shortly. However, it has been concluded (266, 306, 361) that $\delta R/R$ is positive for ^{125}Te .

Calculations of the quadrupole moment of the excited state of ^{125}Te (99, 548) indicate that Q is negative (99) and that its magnitude is about 0.2 barns.

Some information of chemical interest can be obtained from the results in Tables LXIX and LXX. For example, Te^{VI} has substantially more negative C.S. values than Te^{IV} , and this difference has been used by Erickson and Maddock (219) to calculate the amount of TeO_2 in α - TeO_3 . The lack of quadrupole splittings in the M_2TeX_6 species is consistent with the known regular octahedral structure of some of the anions (78, 162, 266). The far-infrared spectra of these anions also indicate octahedral symmetry (301). In contrast, the compounds $MTeF_5$ ($M = NH_4^+, Cs^+$) have a large quadrupole splitting, consistent with the square-pyramidal structure deduced from IR and Raman spectroscopy (302). The agreement between the recently reported parameters for supposed TeF_6^{2-} species (306) and the parameters for the TeF_5^- species (266) strongly suggests that Gukasyan *et al.* (306) measured spectra of TeF_5^- and not TeF_6^{2-} (266).

The trend in C.S. values for the M_2TeX_6 series is of considerable bonding interest. The structural data described above indicate that the lone pair in Te is stereochemically inactive and, thus, has a very high s character. The very positive C.S. values for this species are consistent with this observation. Also, the trend in C.S. $I < Br < Cl$ (opposite to that for Sn species) suggests that little s character is involved in the Te-X bonds. If the bonding mainly involves Te p electrons, then an electronegative ligand would cause an increase in $[\Psi(O)_s]^2$ (the lone pair contracts from deshielding) (266), and the C.S. decreases as is observed for Xe (454) and iodine (445) compounds having regular 90° and 180° bond angles.

Any other bonding information is very difficult to extract from present data because of the large discrepancies in C.S. values between workers. Erickson and Maddock (219) have suggested that agreement is improved between workers if TeO_2 is used as the C.S. standard. However, even if all the data are converted to TeO_2 , large discrepancies are still observed.

4. ^{129}Xe

The Perlows have published several interesting papers on the Mössbauer spectra of Xe compounds using the $39.58 \text{ keV } \frac{3}{2}^+ \rightarrow \frac{1}{2}^+$ transition in ^{129}Xe . Much of the interest in this work has stemmed from the "production" of novel xenon compounds from their iodine precursors. This aspect of the work has been outlined in Section III,E of this chapter. In addition, however, useful bonding information has been

TABLE LXX
MÖSSBAUER PARAMETERS FOR Te OXYGEN COMPOUNDS^a

Compound	C.S. ^c	Q.S.	Ref.
$\text{Te}(\text{OH})_6$ (monoclinic)	-0.98	0	(266)
	-1.01	0	(219)
	-1.15	0	(361)
	-0.8	0	(545)
BaH_4TeO_6	-0.87	0	(266)
$\text{Na}_2\text{H}_4\text{TeO}_6$	-0.94	0	(219)
$\text{Na}_2\text{TeO}_4 \cdot 2\text{H}_2\text{O}$	-0.95	0	(266)
Na_2TeO_4	-1.26	0	(219)
MTeO_4^b	~ -0.9	0	(266)
	-0.9	0	(361, 545)
H_2TeO_3	+1.3	7.7	(545)
Na_2TeO_3	+0.42	6.65	(266)
	+0.35	5.94	(219)
	+0.22	5.78	(361)
	+0.66	5.97	(266)
SrTeO_3	+0.66	5.97	(266)
TeO_2	+0.91	6.25	(266)
	+0.91 ^d	6.63	(219)
	+0.72	6.54	(361)
	+1.3	6.8	(545)
Te_2O_4	+0.78	7.3	(546)
	+0.89	6.65	(266)
	+1.7	6.0	(545)
	+1.01	—	(219)
$\beta\text{-TeO}_3$	+1.01	—	(219)
$\alpha\text{-TeO}_3$	-0.90	0	(219)
	-1.07	2.6	(361)
	-0.1	0	(545)

^a Data given in mm/sec at 80°K

^b M = K₂, Ca, Sr, Co, Ni.

^c Relative to $^{125}\text{I}/\text{Cu}$ as source.

^d This value and all other C.S. values from Ref. (219) are taken after fixing this TeO_2 value at +0.91 mm/sec.

obtained using the Townes–Dailey Q.S. approach outlined for iodine in Section IV, D. A summary of most of the xenon work is given by Perlow (449).

Although some xenon–oxygen compounds have been studied (449), examination of the data for xenon halides (Table LXXI) will illustrate the useful bonding information obtainable from xenon Mössbauer.

For ^{129}Xe , ρ is positive and comparatively small (Table LXVIII), giving rise to rather small changes in C.S. with rather large errors (Table

TABLE LXXI
MÖSSBAUER PARAMETERS FOR XENON HALIDES^a

Substance ^b	C.S. ^c	$\frac{1}{2}e^2qQ$ (mm/sec) ^d	e^2qQ (Mc/sec) ^d	U_p	h_p	Electron transfer/ bond
XeF_4	$+0.40 \pm 0.04$	41.04	(+)2620	1.50	3.00	0.75
$[\text{XeCl}_4]$	$+0.25 \pm 0.08$	25.62	(+)1640	0.94	1.88	0.47
XeF_2	$+0.10 \pm 0.12$	39.00	(−)2490	1.43	1.43	0.72
$[\text{XeCl}_2]$	$+0.17 \pm 0.08$	28.20	(−)1800	1.03	1.03	0.52
$[\text{XeBr}_2]$	-0.03 ± 0.07	22.2	(−)1415	0.81	0.81	0.41

^a From Ref. (454). Data given in mm/sec at 4.2°K.

^b Those compounds in brackets were prepared from the corresponding I compound and used as sources. For example, XeCl_4 was prepared from KICl_4 .

^c Relative to xenon clathrate at 4.2°K.

^d e^2qQ for one p_z electron in ^{129}Xe is +1742 Mc/sec or +54.6 mm/sec, taking $E_\gamma = 39.58$ keV.

LXXI). An increase in $[\Psi(O)_z]^2$ should thus increase the C.S. The quadrupole moment of ^{129}Xe has been determined to be $Q = -0.41 \pm 0.06$ barns (448, 449). The e^2qQ value for one Xe $5p_z$ electron is equal to +1740 Mc/sec or +54.6 mm/sec (448). It should be recognized that q is negative for one p_z electron, but the negative sign of Q gives a positive e^2qQ for an excess of negative charge along the Z EFG direction.

XeF_2 is known to be linear, and the linear and square-planar structures of ICl_2^- and ICl_4^- are probably preserved in XeCl_2 and XeCl_4 [see references in (453)]. The center shifts and quadrupole splittings are consistent with pure p bonding, perhaps expected from the 90° and 180° bond angles in linear and square-planar structures (454). On the assumption of pure p bonding, we would expect that the XeX_4 compounds would have a more positive C.S. than the XeX_2 compounds owing to the lower p -electron density and the resulting higher $[\Psi(O)_z]^2$ owing to deshielding in XeX_4 . This order is found experimentally (Table LXXI). Also, on the basis of pure p bonding we would expect the

order of C.S. values to be $F^- > Cl^- > Br^-$, and this is generally true, although the differences are very small and are often within the errors. This same trend holds for the analogous iodine compounds (Section IV, D). Appreciable s character in the bonds would lead to the opposite trend in C.S. values, i.e., $F^- < Cl^- < Br^-$. More negative C.S. values for the xenon oxides (453) implies that the Xe-O bonding involves appreciable s electron density on the xenon atom—as has been concluded for iodine-oxygen compounds [(445) and Section IV, D].

Since e^2qQ for one p_z electron has been determined, Eq. (53) can be used along with known Q.S. values to derive U_p , and these are given in Table LXXI. The signs of e^2qQ cannot be determined directly [although the Goldanskii-Karyagin asymmetry is helpful in assigning the sign of e^2qQ (449)], but it is apparent that the signs of the square-planar and linear compounds will be the same as those for the isoelectronic and isostructural iodine species (Table LII). The square-planar tetrahalides have a positive e^2qQ ($q = -ve$), and the linear dihalides a negative e^2qQ ($q = +ve$). In the square-planar compounds, the bonding involves the p_x and p_y orbitals and $h_p = 2U_p$, while in the dihalides, $h_p = U_p$. The assumption of pure p bonding can be tested using the C.S. data, which can be thought of as measuring h_p directly [for example, in the ^{129}I case, see Eq. (73)]. Unfortunately, the xenon C.S. values are not precisely known, but a plot of h_p (from Q.S.) versus C.S. gives a reasonable straight line through the origin. The change in center shift per p electron hole (0.13 mm/sec) was obtained from the slope of this line.

The Mössbauer data suggests, then, that as for the isoelectronic iodine compounds, the bonding from xenon to the halides involves mainly xenon p electrons. The p -electron transfer/bond given in the last column of Table LXXI is consistent with this interpretation. The two chlorides and the two fluorides display very similar electron transfers per bond (449).

ACKNOWLEDGMENTS

We are very grateful to Dr. M. G. Clark for helpful comments.

REFERENCES

1. Ablov, A. V., Belozerskii, G. N., Goldanskii, V. I., Makarov, E. F., Trukhtanov, V. A., and Khrapov, V. V., *Dokl. Phys. Chem.* **151**, 712 (1963) (Russ.: *Dokl. Akad. Nauk SSSR, Phys. Chem. Sect.* p. 1352).*
2. Ablov, A. V., Bersuker, I. B., and Goldanskii, V. I., *Dokl. Phys. Chem.* **152**, 934 (1963) (Russ., p. 1391).

* Hereafter the Russian journals will be designated by "Russ." and the page number will follow.

3. Ablov, A. V., Goldanskii, V. I., Stukan, R. A., and Makarov, E. F., *Dokl. Phys. Chem.* **170**, 565 (1966) (Russ. p. 128).
4. Alcock, N. W., and Timms, R. E., *J. Chem. Soc., A* 1876 (1968).
5. Aleksandrov, A. Yu., Delyagin, N. N., Mitrofanov, K. P., Polak, L. S., and Shpinel, V. S., *Dokl. Phys. Chem.* **148**, 1 (1963) (Russ. p. 126).
6. Aleksandrov, A. Yu., Delyagin, N. N., Mitrofanov, K. P., Polak, L. S., and Shpinel, V. S., *Sov. Phys. JETP* **16**, 879 (1963).
7. Aleksandrov, A. Yu., Dorfman, Ya. G., Lependina, O. L., Mitrofanov, K. P., Plotnikova, M. V., Polak, L. S., Temkin, A. Ya., and Shpinel, V. S., *Russ. J. Phys. Chem.* **38**, 1185 (1964).
8. Aleksandrov, A. Yu., Mitrofanov, K. P., Okhlobystin, O. Yu., Polak, L. S., and Shpinel, V. S., *Dokl. Phys. Chem.* **153**, 974 (1963) (Russ. p. 370).
9. Aleksandrov, A. Yu., Okhlobystin, O. Yu., Polak, L. S., and Shpinel, V. S., *Dokl. Phys. Chem.* **157**, 768 (1964) (Russ. p. 934).
10. Ali, K. M., Cunningham, D., Frazer, M. J., Donaldson, J. D., and Senior, B. J., *J. Chem. Soc., A* 2836 (1969).
11. Alti, G. De., Galasso, V., and Bigotto, A., *Inorg. Chim. Acta* **3**, 527 (1969).
12. Alti, G. De., Galasso, V., Bigotto, A., and Costa, G., *Inorg. Chim. Acta* **3**, 533 (1969).
13. Alyea, E. C., Bradley, D. C., Copperthwaite, R. G., Sales, K. D., Fitzsimmons, B. W., and Johnson, C. E., *Chem. Commun.* 1715 (1970).
14. "An Introduction to Mössbauer Spectroscopy" (L. May, ed.). Plenum, New York, 1971.
15. Araujo, F. T. de, Dufresne, A., Lima, G. C. de, and Knudsen, J. M., *Chem. Phys. Lett.* **7**, 333 (1970).
16. Archer, E. M., and van Schalkwyk, T. G. D., *Acta Crystallogr.* **6**, 88 (1953).
17. Artman, J. O., in "Mössbauer Effect Methodology" (I. J. Gruverman, ed.). Vol. 7. Plenum, New York, 1971.
18. Attridge, C. J., *Organometal. Chem. Rev. Sect. A* **5**, 323 (1970).
19. Axtmann, R. C., Hazony, Y., and Hurley, J. W. Jr., *Chem. Phys. Lett.* **2**, 673 (1968).
20. Bancroft, G. M., *Phys. Lett. A* **26**, 17 (1967).
21. Bancroft, G. M., *Chem. Geol.* **5**, 255 (1970).
22. Bancroft, G. M., *Chem. Phys. Lett.* **10**, 449 (1971).
23. Bancroft, G. M., and Burns, R. G., 1966 *Int. Mineral Assoc. Pap. Proc., 5th Gen. Meeting Mineral Soc., London* 36 (1968).
24. Bancroft, G. M., and Burns, R. G., *Mineral Soc. Amer. Spec. Pap.* **2**, 137 (1969).
25. Bancroft, G. M., Burns, R. G., and Howie, R. A., *Nature (London)* **213**, 1221 (1967).
26. Bancroft, G. M., Burns, R. G., and Maddock, A. G., *Amer. Mineral.* **52**, 1009 (1967).
27. Bancroft, G. M., Burns, R. G., and Stone, A. J., *Geochim. Cosmochim. Acta* **32**, 547 (1968).
28. Bancroft, G. M., Butler, K. D., Dale, B., and Rake, A. T., *J. Chem. Soc., Dalton Trans.* (1972). In press.
29. Bancroft, G. M., Butler, K. D., and Rake, A. T., *J. Organometal. Chem.* (1972). **34**, 137 (1972).
30. Bancroft, G. M., Dharmawardena, K. G., and Maddock, A. G., *J. Chem. Soc., A* 2914 (1969).

31. Bancroft, G. M., Dharmawardena, K. G., and Maddock, A. G., *Inorg. Chem.* **9**, 223 (1970).
32. Bancroft, G. M., Dharmawardena, K. G., and Stone, A. J., *Chem Commun.* **6** (1971).
33. Bancroft, G. M., Garrod, R. E. B., and Maddock, A. G., *Inorg. Nucl. Chem. Lett.* **7**, 1157 (1971).
34. Bancroft, G. M., Garrod, R. E. B., and Maddock, A. G., *J. Chem. Soc., A* 3165 (1971).
35. Bancroft, G. M., Garrod, R. E. B., and Maddock, A. G., unpublished observations.
36. Bancroft, G. M., Garrod, R. E. B., Maddock, A. G., Mays, M. J., and Prater, B. E., *Chem. Commun.* 201 (1970).
37. Bancroft, G. M., Garrod, R. E. B., Maddock, A. G., Mays, M. J., and Prater, B. E., *J. Amer. Chem. Soc.* **94**, 647 (1972).
38. Bancroft, G. M., Garrod, R. E. B., Poliakoff, M., and Turner, J. J., unpublished observations.
39. Bancroft, G. M., and Libbey, E. T., unpublished results.
40. Bancroft, G. M., Maddock, A. G., Burns, R. G., and Strens, R. G. J., *Nature (London)* **212**, 913 (1966).
41. Bancroft, G. M., Maddock, A. G., Ong, W. K., and Prince, R. H., *J. Chem. Soc., A* 723 (1966).
42. Bancroft, G. M., Maddock, A. G., Ong, W. K., Prince, R. H., and Stone, A. J., *J. Chem. Soc., A* 1966 (1967).
43. Bancroft, G. M., Maddock, A. G., and Randl, R. P., *J. Chem. Soc., A* 2939 (1968).
44. Bancroft, G. M., Mays, M. J., and Prater, B. E., *J. Chem. Soc., A* 956 (1970).
45. Bancroft, G. M., Mays, M. J., Prater, B. E., and Stefanini, F. P., *J. Chem. Soc., A* 2146 (1970).
46. Baranovskii, V. I., Sergeev, V. P., and Dzevitskii, B. E., *Dokl. Phys. Chem.* **184**, 55 (1969) (Russ. p. 632).
47. Barber, M., and Swift, P., *Chem. Commun.* 1338 (1970).
48. Barger, C. B., and Drickamer, H. G., *J. Chem. Phys.* **55**, 3471 (1971).
49. Bartunik, H. D., Potzel, W., Mössbauer, R. L., and Kaindl, G., *Z. Phys.* **240**, 1 (1970).
50. Bearden, A. J., Marsh, H. S., and Zuckerman, J. J., *Inorg. Chem.* **5**, 1260 (1966).
51. Beattie, I. R., and McQuillan, G. P., *J. Chem. Soc., A* 1519 (1963).
52. Beauchamp, A. L., Bennett, M. J., and Cotton, F. A., *J. Amer. Chem. Soc.* **91**, 297 (1969).
53. Beckett, R., Heath, G. A., Hoskins, B. F., Kelly, B. P., Martin, R. L., Roos, I. A. G., and Weickhardt, P. L., *Inorg. Nucl. Chem. Lett.* **6**, 257 (1970).
54. Bergen, A. Van den, Murray, K. S., West, B. O., and Buckley, A. N., *J. Chem. Soc., A* 2051 (1969).
55. Berrett, R. R., and Fitzsimmons, B. W., *J. Chem. Soc., A* 525 (1967).
56. Berrett, R. R., Fitzsimmons, B. W., and Owusu, A. A., *J. Chem. Soc., A* 1575 (1968).
57. Bilevich, K. A., Goldanskii, V. I., Rochev, V. Ya., and Khrapov, V. V., *Izv. Akad. Nauk SSSR Ser. Khim.* 1583 (1969) (Russ. p. 1705).
58. Birchall, T., *Can. J. Chem.* **47**, 1351 (1969).
59. Birchall, T., *Can. J. Chem.* **47**, 4563 (1969).

60. Birchall, T., and Drummond, I., *Inorg. Chem.* **10**, 399 (1971).
61. Birchall, T., and Greenwood, N. N., *J. Chem. Soc.*, A 286 (1969).
62. Birchall, T. and Valle B. D., *Chem. Commun.* 675 (1970).
63. Birchall, T., Valle, B. D., Martineau, E., and Milne, J. B., *J. Chem. Soc.*, A 1855 (1971).
64. Bird, S. R. A., Donaldson, J. D., Holding, A. F. LeC., Senior, B. J., and Tricker, M. J., *J. Chem. Soc.*, A 1616 (1971).
65. Bird, S. R. A., Donaldson, J. D., Keppie, S. A., and Lappert, M. F., *J. Chem. Soc.*, A 1311 (1971).
66. Biryukov, B. P., Unisimov, K. N., Struchkov, Yu. T., Kolobova, N. E., Osipova, O. P., and Zakharova, M. Ya., *J. Struct. Chem. (USSR)* **8**, 554 (1967).
67. Blackman, A. G., Landman, D. A., and Lurio, A., *Phys. Rev.* **161**, 60 (1967).
68. Bloembergen, N., and Sorokin, P. P., *Phys. Rev.* **110**, 865 (1958).
69. Blom, E. A., Penfold, B. R., and Robinson, W. T., *J. Chem. Soc.*, A 913 (1969).
70. Bokii, N. G., Zakharova, G. N., and Struchkov, Yu. T., *J. Struct. Chem. (USSR)* **11**, 828 (1970) (Russ. p. 895).
71. Bowen, L. H., Garrou, P. E., and Long, G. G., *J. Inorg. Nucl. Chem.* **33**, 953 (1971).
72. Bowen, L. H., Stevens, J. G., and Long, G. G., *J. Chem. Phys.* **51**, 2010 (1969).
73. Boylan, M. J., Nelson, S. M., and Deeney, F. A., *J. Chem. Soc.*, A 976 (1971).
74. Boyle, A. J. F., Bunbury, D. St. P., and Edwards, C., *Proc. Phys. Soc.* **79**, 416 (1962).
75. Boyle, A. J. F., and Hall, H. E., *Rep. Progr. Phys.* **25**, 441 (1962).
76. Brady, P. R., Duncan, J. F., and Mok, K. F., *Proc. Roy. Soc. Ser. A* **287**, 343 (1965).
77. Brändén, C. I., *Acta Chem. Scand.* **17**, 759 (1963).
78. Brown, I. D., *Can. J. Chem.* **42**, 2758 (1964).
79. Bryan, R. F., *J. Amer. Chem. Soc.* **86**, 733 (1964).
80. Bryan, R. F., *J. Chem. Soc.*, A 696 (1968).
81. Bryuchova, E. V., Semin, G. K., Goldanskii, V. I., and Khrapov, V. V., *Chem. Commun.* 491 (1968).
82. Bryukhanov, V. A., Delyagin, N. N., Kuzmin, R. N., and Shpinel, V. S., *Sov. Phys. JETP* **19**, 1344 (1964).
83. Bryukhanov, V. A., Goldanskii, V. I., Delyagin, N. N., Makarov, E. F., and Shpinel, V. S., *Sov. Phys. JETP* **15**, 443 (1962).
84. Bryukhanov, V. A., Goldanskii, V. I., Delyagin, N. N., Korytko, L. A., Makarov, E. F., Suzdalev, I. P., and Shpinel, V. S., *Sov. Phys. JETP* **16**, 321 (1963).
85. Bryukhanov, V. A., Iofa, B. Z., Opalenko, A. A., and Shpinel, V. S. *Zh. Neorg. Khim.* **12**, 1985 (1967).
86. Buckley, A. N., Rumbold, B. D., Wilson, G. V. H., and Murray, K. S., *J. Chem. Soc.*, A 2298 (1970).
87. Buckley, A. N., Wilson, G. V. H., and Murray, K. S., *Solid State Commun.* **7**, 471 (1969).
88. Bukshpan, S., *J. Chem. Phys.* **48**, 4242 (1968).
89. Bukshpan, S., Goldstein, C., and Sonnino, T., *J. Chem. Phys.* **49**, 5477 (1968).
90. Bukshpan, S., Goldstein, C., Soriano, J., and Shamir, J., *J. Chem. Phys.* **51**, 3976 (1969).
91. Bukshpan, S., and Herber, R. H., *J. Chem. Phys.* **46**, 3375 (1967).
92. Bukshpan, S., Soriano, J., and Shamir, J., *Chem. Phys. Lett.* **4**, 241 (1969).

93. Buskshpan, S., and Sonnino, T., *J. Chem. Phys.* **48**, 4442 (1968).
94. Burbridge, C. D., and Goodgame, D. M. L., *J. Chem. Soc.*, A 694 (1967).
95. Burbridge, C. D., and Goodgame, D. M. L., *J. Chem. Soc.*, A 1074 (1968).
96. Burbridge, C. D., and Goodgame, D. M. L., *Inorg. Chim. Acta* **4**, 231 (1970).
97. Burbridge, C. D., Goodgame, D. M. L., and Goodgame, M., *J. Chem. Soc.*, A 349 (1967).
98. Burns, G. R., *Inorg. Chem.* **7**, 277 (1968).
99. Buyrn, A. B., and Grodzins, L., *Bull. Amer. Phys. Soc.* **8**, 43 (1963).
100. Cameron, J. A., Keszthelyi, L., Nagy, G., and Kacsoh, L., *Chem. Phys. Lett.* **8**, 628 (1971).
101. Campbell, I. G. M., *J. Chem. Soc.* 3116 (1955).
102. Carty, A. J., Efratry, A., Ng, T. W., and Birchall, T., *Inorg. Chem.* **9**, 1263 (1970).
103. Carty, A. J., Hinsperger, T., Mihichuk, L., and Sharma, H. D., *Inorg. Chem.* **9**, 2573 (1970).
104. Carty, A. J., Ng, T. W., Carter, W., Palenik, G. J., and Birchall, T., *Chem. Commun.*, 1101 (1969).
105. Casabella, P. A., and Bray, P. J., *J. Chem. Phys.*, **28**, 1182 (1958).
106. Cassidy, J. E., Moser, W., Donaldson, J. D., Jelen, A., and Nicholson, D. G., *J. Chem. Soc.*, A 173 (1970).
107. Champion, A. R., Vaughan, R. W., and Drickamer, H. G., *J. Chem. Phys.* **47**, 2583 (1967).
108. Charlton, J. S., and Nichols, D. I., *J. Chem. Soc. A* 1484 (1970).
109. Chatt, J., and Hayter, R. G., *J. Chem. Soc.* 5507 (1961).
110. "Chemical Applications of Mössbauer Spectroscopy" (V. I. Goldanskii and R. H. Herber, eds.). Academic Press, New York, 1968.
111. *Chem. Soc. Spec. Publ. No. 11* (1958); *No. 18* (1965).
112. Cheng, H. S., and Herber, R. H., *Inorg. Chem.* **9**, 1686 (1970).
113. Cheng, H. S., and Herber, R. H., *Inorg. Chem.* **10**, 1315 (1971).
114. Chivers, T., and Sams, J. R., *Chem. Commun.* 249 (1969).
115. Chivers, T., and Sams, J. R., *J. Chem. Soc.*, A 928 (1970).
116. Chow, Y. M., *Inorg. Chem.* **9**, 794 (1970).
117. Christe, K. O., and Sawodny, W., *Inorg. Chem.* **6**, 1783 (1967).
118. Clark, H. C., O'Brien, R. J., and Trotter, J., *J. Chem. Soc.* 2332 (1964).
119. Clark, M. G., *Mol. Phys.* **20**, 257 (1971).
120. Clark, M. G., *J. Chem. Phys.* **54**, 697 (1971).
121. Clark, M. G., Bancroft, G. M., and Stone, A. J., *J. Chem. Phys.* **47**, 4250 (1967).
122. Clark, M. G., Maddock, A. G., and Platt, R. H., *J. Chem. Soc., Dalton Trans.* 281 (1972).
123. Clark, R. J. H., Davies, A. G., and Puddephatt, R. J., *J. Chem. Soc.*, A 1828 (1968).
124. Clark, R. J. H., Maresca, L., and Smith, P. J., *J. Chem. Soc.*, A 2687 (1970).
125. Clausen, C. A., and Good, M. L., in "Mössbauer Effect Methodology" (I. J. Gruverman, ed.), Vol. 4. Plenum, New York, 1968.
126. Clausen, C. A., and Good, M. L., *Inorg. Chem.* **9**, 220 (1970).
127. Clausen, C. A., and Good, M. L., *Inorg. Chem.* **9**, 817 (1970).
128. Clausen, C. A., Prados, R. A., and Good, M. L., *Chem. Commun.* 1188 (1969).
129. Clausen, C. A., Prados, R. A., and Good, M. L., *J. Amer. Chem. Soc.* **92**, 7483 (1970).

130. Clausen, C. A., Prados, R. A., and Good, M. L., *Chem. Phys. Lett.* **8**, 565 (1971).
131. Cody, V., and Corey, E. R., *J. Organomet. Chem.* **19**, 359 (1969).
132. Collins, R. L., *J. Chem. Phys.* **42**, 1072 (1965).
133. Collins, R. L., and Pettit, R., *J. Chem. Phys.* **39**, 3433 (1963).
134. Collins, R. L., and Pettit, R., *J. Amer. Chem. Soc.* **85**, 2332 (1965).
135. Collins, R. L., Pettit, R., and Baker, W. A., *J. Inorg. Nucl. Chem.* **28**, 1001 (1966).
136. Collins, R. L., and Travis, J. C., in "Mössbauer Effect Methodology" (I. J. Gruverman, ed.), Vol. 3. Plenum, New York, 1967.
137. Cordey Hayes, M., *J. Inorg. Nucl. Chem.* **26**, 915 (1964).
138. Cordey Hayes, M., *J. Inorg. Nucl. Chem.* **26**, 2306 (1964).
139. Cordey Hayes, M., in "Chemical Applications of Mössbauer Spectroscopy" (R. H. Herber and V. I. Goldanskii, eds.), p. 314. Academic Press, New York, 1968.
140. Cordey Hayes, M., Kemmitt, R. D. W., Peacock, R. D., and Rimmer, G. D., *J. Inorg. Nucl. Chem.* **31**, 1515 (1969).
141. Cordey Hayes, M., Peacock, R. D., and Vucelic, M., *J. Inorg. Nucl. Chem.* **29**, 1177 (1967).
142. Costa, N. L., Danon, J., and Xavier, R. M., *J. Phys. Chem. Solids* **23**, 1783 (1962).
143. Cotton, F. A., and Edwards, W. T., *J. Amer. Chem. Soc.* **91**, 843 (1969).
144. Cowan, M., and Gordy, W., *Phys. Rev.* **104**, 551 (1956).
145. Cox, M., Darken, J., Fitzsimmons, B. W., Smith, A. W., Larkworthy, L. G., and Rogers, K. A., *Chem. Commun.* 105 (1970).
146. Crow, J. P., Cullen, W. R., Herring, F. G., Sams, J. R., and Tapping, R. L., *Inorg. Chem.* **10**, 1616 (1971).
147. Cullen, W. R., Harbourne, D. A., Liengme, B. V., and Sams, J. R., *Inorg. Chem.* **8**, 1464 (1969).
148. Cullen, W. R., and Hochstrasser, R. M., *J. Mol. Spectrosc.* **5**, 118 (1960).
149. Cullen, W. R., Sams, J. R., and Thompson, J. A. J., *Inorg. Chem.* **10**, 843 (1971).
150. Cullen, W. R., Sams, J. R., and Waldman, M. C., *Inorg. Chem.* **9**, 1682 (1970).
151. Cullen, W. R., and Waldman, M. C., *Can. J. Chem.* **47**, 3093 (1969).
152. Cunningham, D., Frazer, M. J., and Donaldson, J. D., *J. Chem. Soc., A* 2049 (1971).
153. Da Costa, M. I., Fraga, E. F. R., and Sonnino, T., *J. Chem. Phys.* **52**, 1611 (1970).
154. Dahl, J. P. and Ballhausen, C. J., *Kgl. Dan. Vidensk. Selsk. Mat. Fys. Medd.* **33**, No. 5 (1961).
155. Dale, B. W., Williams, R. J. P., Edwards, P. R., and Johnson, C. E., *J. Chem. Phys.* **49**, 3445 (1968).
156. Dale, B. W., Williams, R. J. P., Edwards, P. R., and Johnson, C. E., *Trans. Faraday Soc.* **64**, 620 (1968).
157. Dale, B. W., Williams, R. J. P., Edwards, P. R., and Johnson, C. E., *Trans. Faraday Soc.* **64**, 3011 (1968).
158. Dale, B. W., Williams, R. J. P., Johnson, C. E., and Thorp, T. L., *J. Chem. Phys.* **49**, 3441 (1968).
159. Dalton, R. F., and Jones, K., *Inorg. Nucl. Chem. Lett.* **5**, 785 (1969).

160. Danon, J., in "Chemical Applications of Mössbauer Spectroscopy" (V. I. Goldanskii and R. H. Herber, eds.), p. 159. Academic Press, New York, 1968.
161. Danon, J., and Iannarella, L., *J. Chem. Phys.* **47**, 382 (1967).
162. Das, A. K., and Brown, I. D., *Can. J. Chem.* **44**, 939 (1966).
163. Das, T. P., and Hahn, E. L., "Nuclear Quadrupole Resonance Spectroscopy." Academic Press, New York, 1958.
164. Davies, A. G., personal communication.
165. Davies, A. G., and Donaldson, J. D., *J. Chem. Soc.*, A 946 (1968).
166. Davies, A. G., Donaldson, J. D., and Simpson, W. B., *J. Chem. Soc.*, A 417 (1969).
167. Davies, A. G., Milledge, H. J., Puxley, D. C., and Smith, P. J., *J. Chem. Soc.*, A 2862 (1970).
168. Davies, A. G., Smith, L., and Smith, P. J., *J. Organomet. Chem.* **23**, 135 (1970).
169. Davies, A. G., Smith, L., Smith, P. J., and McFarlane, W., *J. Organomet. Chem.* **29**, 245 (1971).
170. Debye, N. W. G., Fenton, D. E., Ulrich, S. E., and Zuckerman, J. J., *J. Organomet. Chem.* **28**, 339 (1971).
171. Debye, N. W. G., Rosenberg, E., and Zuckerman, J. J., *J. Amer. Chem. Soc.* **90**, 3234 (1968).
172. Deer, W. A., Howie, R. A., and Zussman, J., "Rock Forming Minerals." Longmans, Green, New York, 1963.
173. Dehmelt, H. G., *Naturwissenschaften* **37**, 398 (1950).
174. Dehn, J. T., and Mulay, L. N., *J. Inorg. Nucl. Chem.* **31**, 3103 (1969).
175. DeVoe, J. R., and Spijkerman, J. J., *Mössbauer Spectrometry, Anal. Chem. Ann. Rev.* **42**, 366R (1970) and previous years.
176. Devooght, J., Gielen, M., and Lejeune, S., *J. Organomet. Chem.* **21**, 333 (1970).
177. deVries, J. L. K. F., Trooster, J. M., and de Boer, E., *Chem. Commun.* 604 (1970).
178. deVries, J. L. K. F., Trooster, J. M., and de Boer, E., *Inorg. Chem* **10**, 81 (1971).
179. Dezsi, I., Balizs, A., Molnar, B., Gorobchenko, V. D., and Lukashevich, I. I., *J. Inorg. Nucl. Chem.* **31**, 1661 (1969).
180. Dezsi, I., Keszthelyi, L., Molnar, B., and Pocs, L., *Phys. Lett.* **18**, 28 (1965).
181. Dollase, W. A., *Amer. Mineral.* **56**, 447 (1971).
182. Donaldson, J. D., *Progr. Inorg. Chem.* **8**, 287 (1967).
183. Donaldson, J. D., Filmore, E. J., and Tricker, M. J., *J. Chem. Soc.*, A 1109 (1971).
184. Donaldson, J. D. and Jelen, A., *J. Chem. Soc.*, A 1448 (1968).
185. Donaldson, J. D., and Nicholson, D. G., *J. Chem. Soc.*, A 145 (1970).
186. Donaldson, J. D., and Nicholson, D. G., *Inorg. Nucl. Chem. Lett.* **6**, 151 (1970).
187. Donaldson, J. D., Nicholson, D. G., and Senior, B. J., *J. Chem. Soc.*, A 2928 (1968).
188. Donaldson, J. D., and Oteng, R., *Inorg. Nucl. Chem. Lett.* **3**, 163 (1967).
189. Donaldson, J. D., Oteng, R., and Senior, B. J., *Chem. Commun.* 618 (1965).
190. Donaldson, J. D., and Senior, B. J., *J. Chem. Soc.*, A 1796 (1966).
191. Donaldson, J. D., and Senior, B. J., *J. Chem. Soc.*, A 1798 (1966).
192. Donaldson, J. D., and Senior, B. J., *J. Inorg. Nucl. Chem.* **31**, 881 (1969).
193. Donaldson, J. D., and Senior, B. J., *J. Chem. Soc.*, A 2358 (1969).

194. Doskey, M. A., and Curran, C., *Inorg. Chim. Acta* **3**, 169 (1969).
195. Dosser, R. J., Eilbeck, W. J., Underhill, A. E., Edwards, P. R., and Johnson, C. E., *J. Chem. Soc., A* 810 (1969).
196. Drickamer, H. G., Lewis, G. K., and Fung, S. C., *Science* **163**, 885 (1969).
197. Dulaney, G. W., and Clifford, A. F., in "Mössbauer Effect Methodology" (I. J. Gruverman, ed.), p. 65. Vol. 5. Plenum, New York, 1970.
198. Duncan, J. F., and Golding, R. M., *Quart. Rev., Chem. Soc.* **19**, 36 (1965).
199. Duncan, J. F., Golding, R. M., and Mok, K. F., *J. Inorg. Nucl. Chem.* **28**, 1114 (1966).
200. Dundon, R. W., and Walter, L. S., *Earth Planet. Sci. Lett.* **2**, 372 (1967).
201. Edwards, P. R., and Johnson, C. E., *J. Chem. Phys.* **49**, 211 (1968).
202. Edwards, P. R., Johnson, C. E., and Williams, R. J. P., *J. Chem. Phys.* **47**, 2074 (1967).
203. Ehrlich, B. S., and Kaplan, M., *J. Chem. Phys.* **50**, 2041 (1969).
204. Ehrlich, B. S., and Kaplan, M., *J. Chem. Phys.* **51**, 603 (1969).
205. Ehrlich, B. S., and Kaplan, M., *J. Chem. Phys.* **54**, 612 (1971).
206. Emerson, G. F., Mahler, J. E., Pettit, R., and Collins, R., *J. Amer. Chem. Soc.* **86**, 3590 (1964).
207. Ensling, J., Gütlisch, P., Hassellbach, K. M., and Fitzsimmons, B. W., *J. Chem. Soc., A* 1940 (1971).
208. Epstein, L. M., *J. Chem. Phys.* **36**, 2731 (1962).
209. Epstein, L. M., *J. Chem. Phys.* **40**, 435 (1964).
210. Epstein, L. M., and Straub, D. K., *Inorg. Chem.* **4**, 1551 (1965).
211. Epstein, L. M., and Straub, D. K., *Inorg. Chem.* **8**, 453 (1969).
212. Epstein, L. M., and Straub, D. K., *Inorg. Chem.* **8**, 560 (1969).
213. Epstein, L. M., and Straub, D. K., *Inorg. Chem.* **8**, 784 (1969).
214. Erich, U., Frölich, F., Gütlisch, P., and Webb, G. A., *Inorg. Nucl. Chem. Lett.* **5**, 855 (1969).
215. Erickson, N. E., Ph.D. Thesis, Columbia Univ., New York, New York, 1964.
216. Erickson, N. E., in "Mössbauer Effect and Its Applications in Chemistry" (R. F. Gould, ed.), Amer. Chem. Soc. Publ., Washington, D.C., 1967. No. 68.
217. Erickson, N. E., *Chem. Commun.* 1349 (1970).
218. Erickson, N. E., and Fairhall, A. W., *Inorg. Chem.* **4**, 1320 (1965).
219. Erickson, N. E., and Maddock, A. G., *J. Chem. Soc., A* 1665 (1970).
220. Erickson, N. E., and Sutin, N., *Inorg. Chem.* **5**, 1834 (1966).
221. Evans, B. J., Ghose, S., and Hafner, S. S., *J. Geol.* **75**, 306 (1967).
222. Faltens, M. O., and Shirley, D. A., *J. Chem. Phys.* **53**, 4249 (1970).
223. Farmery, K., Kilner, M., Greatrex, R., and Greenwood, N. N., *Chem. Commun.* 593 (1968).
224. Farmery, K., Kilner, M., Greatrex, R., and Greenwood, N. N., *J. Chem. Soc., A* 2339 (1969).
225. Fenger, J., Maddock, A. G., and Siekierska, K. E., *J. Chem. Soc., A* 3255 (1970).
226. Fenton, D. E., and Zuckerman, J. J., *J. Amer. Chem. Soc.* **90**, 6226 (1968).
227. Fenton, D. E., and Zuckerman, J. J., *Inorg. Chem.* **8**, 1771 (1969).
228. Finger, L. W., *Mineral. Soc. Amer. Spec. Pap.* **2**, 95 (1969).
229. Finger, L. W., *Amer. Mineral.* **55**, 300 (1970).
230. Fischer, D. C., and Drickamer, H. G., *J. Chem. Phys.* **54**, 4825 (1971).
231. Fischer, K. F., *Amer. Mineral.* **51**, 814 (1966).
232. Fitzsimmons, B. W., *J. Chem. Soc., A* 3235 (1970).

233. Fitzsimmons, B. W., Owusu, A. A., Seeley, N. J., and Smith, A. W., *J. Chem. Soc., A* 935 (1970).
234. Fitzsimmons, B. W., Seeley, N. J., and Smith, A. W., *J. Chem. Soc., A* 143 (1969).
235. Fluck, E., *Advan. Inorg. Chem. Radiochem.* **6**, 433 (1964).
236. Fluck, E., in "Chemical Applications of Mössbauer Spectroscopy" (R. H. Herber and V. I. Goldanskii, eds.), Chap. 4. Academic Press, New York, 1968.
237. Fluck, E., and Brauch, K. F., *Z. Anorg. Chem.* **364**, 107 (1969).
238. Fluck, E., Kerler, W., and Neuwirth, W., *Angew. Chem. Int. Ed., Engl.* **2**, 277 (1963).
239. Fluck, E., and Kuhn, P., *Z. Anorg. Chem.* **350**, 263 (1967).
240. Ford, B. F. E., Liengme, B. V., and Sams, J. R., *J. Organomet. Chem.* **19**, 53 (1969).
241. Ford, B. F. E., and Sams, J. R., *J. Organomet. Chem.* **21**, 345 (1970).
242. Ford, B. F. E., Sams, J. R., Goel, R. G., and Ridley, D. R., *J. Inorg. Nucl. Chem.* **33**, 23 (1971).
243. Forder, R. A., and Sheldrick, G. M., *J. Organomet. Chem.* **21**, 115 (1970).
244. Forder, R. A., and Sheldrick, G. M., *J. Organomet. Chem.* **22**, 611 (1970).
245. Forster, D., and Goodgame, D. M. L., *J. Chem. Soc.* 262 (1965).
246. Frank, E., and Abeledo, C., *Inorg. Chem.* **5**, 1453 (1966).
247. Frauenfelder, H., "The Mössbauer Effect." Benjamin, New York, 1962.
248. Friedt, J. M., *J. Inorg. Nucl. Chem.* **32**, 431 (1970).
249. Friedt, J. M., and Adloff, J. P., *C. R. Acad. Sci. Ser. C* **264**, 1356 (1967).
250. Fung, S. C., and Drickamer, H. G., *J. Chem. Phys.* **51**, 4353 (1969).
251. Fung, S. C., and Drickamer, H. G., *J. Chem. Phys.* **51**, 4360 (1969).
252. Gabriel, J. R., and Ruby, S. L., *Nucl. Instrum. Methods* **36**, 23 (1965).
253. Gallagher, P. K., and Kurkjian, C. R., *Inorg. Chem.* **5**, 214 (1966).
254. Gancedo, R. R., Maddock, A. G., and Platt, R. H., unpublished observations.
255. Garg, A. N., and Goel, P. S., *Inorg. Chem.* **10**, 1344 (1971).
256. Garg, A. N., Shukla, P. N., and Goel, P. S., *Chem. Phys. Lett.* **7**, 494 (1970).
257. Garrod, R. E. B., Platt, R. H., and Sams, J. R., *Inorg. Chem.* **10**, 424 (1971).
258. Gassenheimer, B., and Herber, R. H., *Inorg. Chem.* **8**, 1120 (1969).
259. Gerloch, M., Lewis, J., Mabbs, F. E., and Richards, A., *J. Chem. Soc., A* 112 (1968) and references.
260. Gerloch, M., and Mabbs, F. E., *J. Chem. Soc., A* 1598 (1967).
261. Gerloch, M., and Mabbs, F. E., *J. Chem. Soc., A* 1900 (1967).
262. Ghose, S., *Acta Crystallogr.* **14**, 622 (1961).
263. Ghose, S., *Z. Kristallogr. Kristallgeometrie, Kristallphys. Kristallchem.* **122**, 81 (1965).
264. Ghose, S., and Hafner, S. S., *Z. Kristallogr., Kristallgeometrie, Kristallphys., Kristallchem.* **125**, 157 (1967).
265. Gibb, T. C., *J. Chem. Soc., A* 2503 (1970).
266. Gibb, T. C., Greatrex, R., Greenwood, N. N., and Sarma, A. C., *J. Chem. Soc., A* 212 (1970).
267. Gibb, T. C., Greatrex, R., Greenwood, N. N., and Thompson, D. T., *J. Chem. Soc., A* 1663 (1967).
268. Gibb, T. C., and Greenwood, N. N., *J. Chem. Soc.*, 6989 (1965).
269. Gibb, T. C., and Greenwood, N. N., *J. Chem. Soc., A* 43 (1966).
270. Gibb, T. C., and Greenwood, N. N., "Mössbauer Spectroscopy." Chapman & Hall, London, 1971.

271. Gibb, T. C., Goodman, B. A., and Greenwood, N. N., *Chem. Commun.* 774 (1970).
272. Glentworth, P., Nichols, A. J., Large, N. R., and Bullock, R. J., *Chem. Commun.* 206 (1971).
273. Goldanskii, V. I., *At. Energy Rev.* **1**, 3 (1963).
274. Goldanskii, V. I., "The Mössbauer Effect and Its Applications in Chemistry." Consultants Bureau, New York, 1964.
275. Goldanskii, V. I., Borshagovskii, B. V., Makarov, E. F., Stukan, R. A., Anisimov, K. N., Kolobova, N. E., and Shripkin, V. V., *Theor. Exp. Chem. (USSR)* **3**, 275 (1967) (Russ. p. 478).
276. Goldanskii, V. I., Gorodinskii, G. M., Karyagin, S. V., Korytko, L. A., Krizhanskii, L. M., Makarov, E. F., Suzdalev, I. P., and Khrapov, V. V., *Dokl. Phys. Chem.* **147**, 766 (1962) (Russ. p. 127).
277. Goldanskii, V. I., Khrapov, V. V., Stukan, R. A., *Organometal. Chem. Rev. Sect. A* **4**, 225 (1969).
278. Goldanskii, V. I., Makarov, E. F., Stukan, R. A., Sumarokova, T. N., Trukhtanov, V. A., and Khrapov, V. V., *Dokl. Phys. Chem.* **156**, 474 (1964) (Russ. p. 400).
279. Goldanskii, V. I., Makarov, E. F., Stukan, R. A., Trukhtanov, V. A., and Khrapov, V. V., *Dokl. Phys. Chem.* **151**, 598 (1963) (Russ. p. 357).
280. Goldanskii, V. I., Rochev, V. Ya., and Khrapov, V. V., *Dokl. Phys. Chem.* **156**, 571 (1964) (Russ. p. 909).
281. Golding, R. M., *Mol. Phys.* **12**, 13 (1967).
282. Golding, R. M., "Applied Wave Mechanics." Van Nostrand, Princeton, New Jersey, 1969.
283. Golding, R. M., Jackson, F., and Sinn, E., *Theor. Chim. Acta* **15**, 123 (1969).
284. Golding, R. M., Mok, K. F., and Duncan, J. F., *Inorg. Chem.* **5**, 774 (1966).
285. Goldstein, C., and Pasternak, M., *Phys. Rev.* **177**, 481 (1969).
286. Goldstein, M., and Unsworth, W. D., *Spectrochim. Acta Part A*, **27**, 1055 (1971).
287. Goodgame, D. M. L., and Machado, A. A. S. C., *Chem. Commun.* 1420 (1969).
288. Goodman, B. A., Greatrex, R., and Greenwood, N. N., *J. Chem. Soc., A* 1868 (1971).
289. Goodman, B. A., and Greenwood, N. N., *Chem. Commun.* 1105 (1969).
290. Goodman, B. A., and Greenwood, N. N., *J. Chem. Soc., A* 1862 (1971).
291. Goodman, B. A., Greenwood, N. N., Jaura, K. L., and Sharma, K. K., *J. Chem. Soc., A* 1865 (1971).
292. Gordy, W., *Discuss. Faraday Soc.*, **19**, 14 (1955).
293. Greatrex, R., and Greenwood, N. N., *Discuss. Farad. Soc.* **47**, 126 (1969).
294. Greatrex, R., Greenwood, N. N., and Kaspi, P., *J. Chem. Soc. A* 1873 (1971).
295. Greatrex, R., Greenwood, N. N., and Pauson, P. L., *J. Organomet. Chem.* **13**, 533 (1968).
296. Greene, P. T., and Bryan, R. F., *J. Chem. Soc., A* 1696 (1970); 2549 (1971).
297. Greenwood, N. N., *Chem. Brit.* **3**, 56 (1967).
298. Greenwood, N. N., in "Spectroscopic Properties of Inorganic and Organometallic Compounds," Chem. Soc., Specialist Periodical Rep. 1967 and annually afterwards.
299. Greenwood, N. N., Perkins, P. G., and Wall, D. H., *Symp. Farad. Soc.* **1**, 51 (1967).
300. Greenwood, N. N., and Ruddick, J. N. R., *J. Chem. Soc., A* 1679 (1967).
301. Greenwood, N. N., and Straughan, B. P., *J. Chem. Soc., A* 962 (1966).

302. Greenwood, N. N., Sarma, A. C., and Straughan, B. P., *J. Chem. Soc., A* 1446 (1966).
303. Greenwood, N. N., and Timnick, A., *J. Chem. Soc., A* 676 (1971).
304. Gregory, N. W., *J. Amer. Chem. Soc.* **73**, 472 (1951).
305. Grover, J. E., and Orville, P. M., *Geochim. Cosmochim. Acta* **33**, 205 (1969).
306. Gukasyan, S. E., Iofa, B. Z., Karasev, A. N., Semenov, S. I., and Shpinel, V. S., *Phys. Status Solidi* **37**, 91 (1970).
307. Gukasyan, S. E., and Shpinel, V. S., *Phys. Status Solidi* **29**, 49 (1968).
308. Gütlich, P., and Hassellbach, K. M., *Angew Chem.* **81**, 627 (1969).
309. Gütlich, P., Odar, S., Fitzsimmons, B. W., and Erickson, N. E., *Radiochim. Acta* **10**, 147 (1968).
310. Hafemeister, D. W., DePasquali, G., and DeWaard, H., *Phys. Rev.* **135**, B1089 (1964).
311. Hafner, S. S., Virgo, D., and Warburton, D., *Proc. Apollo 12 Lunar Sci. Conf.* 1972).
312. Hall, D., Slater, J. H., Fitzsimmons, B. W., and Wade, K., *J. Chem. Soc., A* 800 (1971).
313. Hall, L. H., Spijkerman, J. J., and Lambert, J. L., *J. Amer. Chem. Soc.* 2044 (1968).
314. Halsey, M. J., and Pritchard, A. M., *J. Chem. Soc., A* 2878 (1968).
315. Hansson, A., and Brunge, O., private communication quoted by I. Lindquist, "Inorganic Adduct Molecules of Oxo Compounds." Academic Press, New York, New York, 1963.
316. Harmon, K. M., Hesse, L. L., Klemann, L. P., Kocher, C. W., McKinley, S. V., and Young, A. E., *Inorg. Chem.* **8**, 1054 (1969).
317. Harrison, P. G., and Zuckerman, J. J., *J. Amer. Chem. Soc.* **91**, 6885 (1969).
318. Harrison, P. G., and Zuckerman, J. J., *Inorg. Chem.* **9**, 175 (1970).
319. Hazony, Y., *J. Chem. Phys.* **45**, 2664 (1966).
320. Hazony, Y., and Axtmann, R. C., *Chem. Phys. Lett.* **8**, 571 (1971).
321. Hazony, Y., Axtmann, R. C., and Hurley, J. W., Jr., *Chem. Phys. Lett.* **2**, 440 (1968).
322. Hazony, Y., and Herber, R. H., *J. Inorg. Nucl. Chem.* **33**, 961 (1971).
323. Herber, R. H., "Applications of the Mössbauer Effect in Chemistry and Solid State Physics," Int. At. Energy Agency, Tech. Dept., No. 50, p. 130. Vienna, 1965.
324. Herber, R. H., *Progr. Inorg. Chem.* **8**, 1 (1966).
325. Herber, R. H., *Inorg. Chem.* **8**, 174 (1969).
326. Herber, R. H., *J. Chem. Phys.* **54**, 3755 (1971).
327. Herber, R. H., and Chandra, S., *J. Chem. Phys.* **52**, 6045 (1970).
328. Herber, R. H., and Chandra, S., *J. Chem. Phys.* **54**, 1847 (1971).
329. Herber, R. H., Chandra, S., and Hazony, Y., *J. Chem. Phys.* **53**, 3330 (1970).
330. Herber, R. H., and Cheng, H. S., *Inorg. Chem.* **8**, 2145 (1969).
331. Herber, R. H., and Goscinnny, Y., *Inorg. Chem.* **7**, 1293 (1968).
332. Herber, R. H., and Hayter, R. G., *J. Amer. Chem. Soc.* **86**, 301 (1964).
333. Herber, R. H., King, R. B., and Wertheim, G. K., *Inorg. Chem.* **3**, 101 (1964).
334. Herber, R. H., and Parisi, G. I., *Inorg. Chem.* **5**, 769 (1966).
335. Herber, R. H., and Stapfer, C. H., *Inorg. Nucl. Chem. Lett.* **7**, 617 (1971).
336. Herber, R. H., Stöckler, H. A., and Reichle, W. T., *J. Chem. Phys.* **42**, 2447 (1965).
337. Hermodsson, Y., *Acta Crystallogr.* **13**, 656 (1960).

338. Hill, J. C., Drago, R. S., and Herber, R. H., *J. Amer. Chem. Soc.* **91**, 1644 (1969).
339. Hinze, J., and Jaffé, H. H., *J. Amer. Chem. Soc.* **84**, 540 (1962).
340. Hinze, J., and Jaffé, H. H., *J. Phys. Chem.* **67**, 1501 (1963).
341. Hofmann, W., *Z. Kristallogr.* **92**, 161 (1935).
342. Hogben, M. G., Gay, R. S., and Graham, W. A. G., *J. Amer. Chem. Soc.* **88**, 3457 (1966); Hogben, M. G., and Graham, W. A. G., *ibid.* **91**, 283 (1969); Hogben, M. G., Gay, R. S., Oliver, A. J., Thompson, J. A. J., and Graham, W. A. G., *ibid.* **91**, 291 (1969).
343. Hogg, C. S., and Meads, R. E., *Mineral. Mag.* **37**, 606 (1970).
344. Hoppe, R., and Dähne, W., *Naturwissenschaften* **49**, 254 (1962).
345. Hoy, G. R., and Chandra, S., *J. Chem. Phys.* **47**, 961 (1967).
346. Huang, H. H., and Hui, K. M., *J. Organomet. Chem.* **2**, 288 (1964).
347. Hudson, A., and Whitfield, H. J., *Inorg. Chem.* **6**, 1120 (1967).
348. Hulme, R., *J. Chem. Soc.* 1524 (1963).
349. Ichiba, S., Mishima, M., Sakai, H., and Negita, H., *Bull. Chem. Soc. Jap.* **41**, 49 (1968).
350. Ichiba, S., Sakai, H., Negita, H., and Maeda, Y., *J. Chem. Phys.* **54**, 1627 (1971).
351. Ingalls, R., *Phys. Rev.* **133 A**, 787 (1964).
352. Ingalls, R., Costan, C. J., DePasquali, G., Drickamer, H. G., and Pinajian, J. J., *J. Chem. Phys.* **45**, 1057 (1966).
353. Isaacs, N. W., and Kennard, C. H. L., *J. Chem. Soc.*, A 1257 (1970).
354. Jaccarino, V., King, J. G., Satten, R. A., and Stroke, H. H., *Phys. Rev.* **94**, 1798 (1954).
355. Janssen, M. J., Luijken, J. G. A., and Van Der Kerk, G. J. M., *Rec. Trav. Chim. Pays Bas.* **82**, 90 (1963).
356. Jesson, J. P., Weiher, J. F., and Trofimenko, S., *J. Chem. Phys.* **48**, 2058 (1968).
357. Johnson, C. E., *Symp. Faraday Soc.* **1**, 1 (1967).
358. Jones, C. H. W., and Warren, J. L., *J. Chem. Phys.* **53**, 1740 (1970).
359. Jones, M. T., *Inorg. Chem.* **6**, 1249 (1967).
360. Josephson, B. D., *Phys. Rev. Lett.* **4**, 341 (1960).
361. Jung, P., and Triftshauser, W., *Phys. Rev.* **175**, 512 (1968).
362. Kaindl, G., Potzel, W., Wagner, F. E., Zahn, U., and Mössbauer, R. L., *Z. Phys.* **226**, 103 (1969).
363. Kamenar, B., and Grdenic, D., *J. Inorg. Nucl. Chem.* **24**, 1039 (1962).
364. Karasyov, A. N., Kolobova, N. E., Polak, L. S., Shpinel, V. S., and Anisimov, K. N., *Teor. Eksp. Khim. Akad. Nauk Ukr. (Engl.)* **2**, 126 (1966).
365. Karyagin, S. V., *Sov. Phys. Dokl.* **148**, 110 (1963) (Russ. p. 1102); *Sov. Phys. Solid State* **5**, 1552 (1964) (Russ. p. 2128); *ibid.* **8**, 1387 (1966) (Russ. p. 1739).
366. Kasai, N., Yasuda, K., and Okawara, R., *J. Organomet. Chem.* **3**, 172 (1965).
367. Khrapov, V. V., Candidate Dissertation, Inst. Chem. Phys. Acad. Sci. USSR, Moscow, 1965.
368. Khrapov, V. V., Goldanskii, V. I., Prokof'ev, A. K., and Kostyanovskii, R. G. *J. Gen. Chem. USSR* **37**, 1 (1967) (Russ. p. 3).
369. Kistner, O. C., and Sunyar, A. W., *Phys. Rev. Lett.* **4**, 412 (1960).
370. Knight, J., and Mays, M. J., *J. Chem. Soc.*, A 654 (1970).
371. Kojima, S., Tsukada, K., Ogawa, S., and Shimauchi, A., *J. Chem. Phys.* **23**, 1963 (1955).

372. König, E., Hüfner, S., Steichele, E., and Madeja, K., *Z. Naturforsch. A* **22**, 1543 (1967).
373. König, E., and Kremer, S., *Chem. Phys. Lett.* **8**, 312 (1971).
374. König, E., and Madeja, K., *Inorg. Chem.* **6**, 48 (1967).
375. König, E., and Madeja, K., *Inorg. Chem.* **7**, 1848 (1968).
376. Korecz, L., and Burger, K., *J. Inorg. Nucl. Chem.* **30**, 781 (1968).
377. Kothekar, V., Iofa, B. Z., Semenov, S. I., and Shpinel, V. S., *Sov. Phys. JETP* **28**, 86 (1969).
378. Kriegsmann, V. H., and Geissler, H., *Z. Anorg. Chem.* **323**, 170 (1963).
379. Kriegsmann, V. H., and Pischtschan, S., *Z. Anorg. Chem.* **308**, 212 (1961).
380. Krizhanskii, L. M., Okhlobystin, O. Yu., Popov, A. V., and Rogozev, B. I., *Dokl. Phys. Chem.* **160**, 142 (1965) (Russ. p. 1121).
381. Lees, J. K., and Flinn, P. A., *J. Chem. Phys.* **48**, 882 (1968).
382. Lesikar, A. V., *J. Chem. Phys.* **40**, 2746 (1964).
383. Leung, K. L., and Herber, R. H., *Inorg. Chem.* **10**, 1020 (1971).
384. Lever, A. B. P., *J. Chem. Soc.* 1821 (1965).
385. Lewis, G. K., and Drickamer, H. G., *J. Chem. Phys.* **49**, 3782 (1968).
386. Lewis, G. K., and Drickamer, H. G., *Proc. Nat. Acad. Sci. U.S.* **61**, 414 (1968).
387. Lewis, J., Mabbs, F. E., and Richards, A., *J. Chem. Soc., A* 1014 (1967).
388. Long, G. G., Stevens, J. G., and Bowen, L. H., *Inorg. Nucl. Chem. Lett.* **5**, 799 (1969).
389. Long, G. G., Stevens, J. G., Tullbane, R. J., and Bowen, L. H., *J. Amer. Chem. Soc.* **92**, 4230 (1970).
390. Long, G. L., and Whitney, D. L., *J. Inorg. Nucl. Chem.* **33**, 1196 (1971).
391. Lucken, E. A. C., "Nuclear Quadrupole Coupling Constants." Academic Press, New York, 1969.
392. Ludwig, G. W., *J. Chem. Phys.* **25**, 159 (1956).
393. McClure, D. S., *Advan. Chem. Co-ord. Compounds* **498** (1961).
394. McDonald, R. R., Larson, A. C., and Cromer, D. T., *Acta Crystallogr.* **17**, 1104 (1964).
395. McGrady, M. M., and Tobias, R. S., *J. Amer. Chem. Soc.* **87**, 1909 (1965).
396. MacKay, K. M., Sowerby, D. B., and Young, W. C., *Spectrochim. Acta Part A* **24**, 611 (1968).
397. McWhinnie, W. R., Poller, R. C., and Thevarasa, M., *J. Chem. Soc., A* 1671 (1967).
398. Maddock, A. G., "Mössbauer Spectroscopy in the Study of Nuclear Reactions in Solids," MTP Publications, 1972. Butterworths, London, and University Park Press, State College, Pennsylvania.
399. Maddock, A. G., Medeiros, L. O., and Bancroft, G. M., *Chem. Commun.* 1067 (1967).
400. Maddock, A. G., and Platt, R. H., *J. Chem. Soc., A* 1191 (1971).
401. Maddock, A. G., and Platt, R. H., *J. Chem. Phys.* **55**, 1490 (1971).
402. Maddock, A. G., and Platt, R. H., unpublished observations.
403. Malathi, N., and Puri, S. P., *J. Phys. Soc. Jap.* **29**, 108 (1970).
404. Matas, J., and Zemeik, T., *Phys. Lett.* **19**, 111 (1965).
405. Matthews, C. K., *J. Inorg. Nucl. Chem.* **31**, 2853 (1969).
406. Mazak, R. A., and Collins, R. L., *J. Chem. Phys.* **51**, 3220 (1969).
407. Melson, G. A., Stokley, P. F., and Bryan, R. F., *J. Chem. Soc., A* 2247 (1970).
408. Menes, M., and Bolef, D. I., *J. Phys. Chem. Solids* **19**, 79 (1961).
409. Moore, W. J., and Pauling, L., *J. Amer. Chem. Soc.* **63**, 1392 (1941).

410. Moss, T. H., and Robinson, A. B., *Inorg. Chem.* **7**, 1692 (1968).
411. "Mössbauer Effect Data Index" (A. H. Muir, K. J. Ando, and H. M. Coogan, eds.) Wiley, New York, 1966.
412. "Mössbauer Effect Methodology" (I. J. Gruverman, ed.), Vols. 1-7. Plenum, New York, 1965-1971.
413. Mössbauer, R. L., *Naturwissenschaften* **45**, 538 (1958).
414. Mueller, R. F., *Mineral Soc. Amer. Spec. Paper* **2**, 83 (1969).
415. Mullins, F. P., *Can. J. Chem.* **48**, 1677 (1970).
416. Mullins, F. P., *Can. J. Chem.* **49**, 2719 (1971).
417. Mullins, M. A., and Curran, C., *Inorg. Chem.* **6**, 2017 (1967).
418. Mullins, M. A., and Curran, C., *Inorg. Chem.* **7**, 2584 (1968).
419. Murin, A. N., Lure, B. G., and Grushko, Yu. S., *Fiz. Tverd. Tela* **9**, 1820 (1967); *Chem. Abstr.* **67**, 69,093 (1967).
420. Naik, D. V., and Curran, C., personal communication, presented at the Int. Conf. Organometal. Chem. Moscow (1971).
421. Naik, D. V., and Curran, C., *Inorg. Chem.* **10**, 1017 (1971).
422. Nath, A., Harpold, M., Klein, M. P., and Kundig, W., *Chem. Phys. Lett.* **2**, 471 (1968).
423. Nath, A., Klein, M. P., Kundig, W., and Lichtenstein, D., in "Mössbauer Effect Methodology" (I. J. Gruverman, ed.), Vol. 5, p. 163. Plenum, New York, 1970.
424. Nesmeyanov, A. N., Goldanskii, V. I., Khrapov, V. V., Rochev, V. Ya., Kravtsov, D. N., and Rokhlina, E. M., *Bull. Acad. Sci. USSR* **4**, 763 (1968).
425. Nozik, A. J., and Kaplan, M., *J. Chem. Phys.* **47**, 2960 (1967).
426. O'Connor, J. E., and Corey, E. R., *Inorg. Chem.* **6**, 968 (1967).
427. Ofer, S., Nowik, I., and Cohen, S. G., in "Chemical Applications of Mössbauer Spectroscopy" (V. I. Goldanskii and R. H. Herber, eds.), p. 426. Academic Press, New York, 1968.
428. Okawara, R., Webster, D. E., and Rochow, E. G., *J. Amer. Chem. Soc.* **82**, 3287 (1960).
429. Okazaki, A., and Ueda, I., *J. Phys. Soc. Jap.* **11**, 470 (1956).
430. Olie, K., Smitskamp, C. C., and Gerding, H., *Inorg. Nucl. Chem. Lett.* **4**, 129 (1968).
431. Onaka, S., Sasaki, Y., and Sano, H., *Bull. Chem. Soc. Jap.* **44**, 726 (1971).
432. Oosterhuis, W. T., and Lang, G., *J. Chem. Phys.* **50**, 4381 (1969).
433. O'Rourke, M., and Curran, C., *J. Amer. Chem. Soc.* **92**, 1501 (1970).
434. Osborn, J. A., Gillard, R. D., and Wilkinson, G., *J. Chem. Soc.* 3168 (1964).
435. Panyushkin, V. N., DePasquali, G., and Drickamer, H. G., *J. Chem. Phys.* **51**, 3305 (1969).
436. Papike, J. J., and Clark, J. R., *Amer. Mineral.* **53**, 1156 (1968).
437. Parish, R. V., *Progr. Inorg. Chem.* **15**, 101 (1972).
438. Parish, R. V., and Johnson, C. E., *Chem. Phys. Lett.* **6**, 239 (1970).
439. Parish, R. V., and Johnson, C. E., *J. Chem. Soc., A* 1906 (1971).
440. Parish, R. V., and Platt, R. H., *J. Chem. Soc., A* 2145 (1969).
441. Parish, R. V., and Platt, R. H., *Inorg. Chim. Acta* **4**, 589 (1970).
442. Parish, R. V., and Platt, R. H., *Inorg. Chim. Acta* **4**, 65 (1970).
443. Pasternak, M., Simopoulos, A., and Hazony, Y., *Phys. Rev., A* **140**, 1892 (1965).
444. Pasternak, M., and Sonnino, T., *Phys. Rev.* **164**, 384 (1967).
445. Pasternak, M., and Sonnino, T., *J. Chem. Phys.* **48**, 1997 (1968).

446. Pasternak, M., and Sonnino, T., *J. Chem. Phys.* **48**, 2009 (1968).
447. Pelah, I., and Ruby, S. L., *J. Chem. Phys.* **51**, 383 (1969).
448. Perlow, G. J., *Phys. Rev.* **135**, B1102 (1964).
449. Perlow, G. J., in "Chemical Applications of Mössbauer Spectroscopy" (V. I. Goldanskii and R. H. Herber, eds.), p. 377. Academic Press, New York, 1968.
450. Perlow, G. J., and Perlow, M. R., *Rev. Mod. Phys.* **36**, 353 (1964).
451. Perlow, G. J., and Perlow, M. R., *J. Chem. Phys.* **41**, 1157 (1964).
452. Perlow, G. J., and Perlow, M. R., *J. Chem. Phys.* **45**, 2193 (1966).
453. Perlow, G. J., and Perlow, M. R., *J. Chem. Phys.* **48**, 955 (1968).
454. Perlow, G. J., and Yoshida, H., *J. Chem. Phys.* **49**, 1474 (1968).
455. Petrides, D., Mullins, F. P., and Curran, C., *Inorg. Chem.* **9**, 1270 (1970).
456. Petrov, A. A., Rogozev, B. I., Krizhanskii, L. M., and Zaugorodnii, V. S., *J. Gen. Chem. USSR* **38**, 1151 (1968) (Russ. p. 1196).
457. Philip, J., Mullins, M. A., and Curran, C., *Inorg. Chem.* **7**, 1895 (1968).
458. Pillinger, W. L., and Stone, J. A., in "Mössbauer Effect Methodology" (I. J. Gruverman, ed.), Vol. 4, p. 217. Plenum, New York.
459. Poder, C., and Sams, J. R., *J. Organometal. Chem.* **19**, 67 (1969).
460. Poeth, T. P., Harrison, P. G., Long, T. V., Willeford, B. R., and Zuckerman, J. J., *Inorg. Chem.* **10**, 522 (1971).
461. Poliakoff, M., and Turner, J. J., *J. Chem. Soc.*, A 654 (1971).
462. Poller, R. C., and Ruddick, J. N. R., *J. Chem. Soc.*, A 2273 (1969).
463. Poller, R. C., Ruddick, J. N. R., and Spillman, J. A., *Chem. Commun.* 680 (1970).
464. Poller, R. C., Ruddick, J. N. R., Taylor, B., and Toley, D. L. B., *J. Organometal. Chem.* **24**, 341 (1970).
465. Poller, R. C., Ruddick, J. N. R., Thevarasa, M., and McWhinnie, W. R., *J. Chem. Soc.*, A 2327 (1969).
466. Poller, R. C., and Toley, D. L. B., *J. Chem. Soc.*, A 1578 (1967).
467. Poller, R. C., and Toley, D. L. B., *J. Chem. Soc.*, A 2035 (1967).
468. Poller, R. C., and Toley, D. L. B., *J. Inorg. Nucl. Chem.* **31**, 2973 (1969).
469. Polynova, T. W., and Porai-Koshits, M. A., *J. Struct. Chem.* **7**, 691 (1966).
470. Potzel, W., Wagner, F. E., Zahn, U., Mössbauer, R. L., and Danon, J., *Z. Phys.* **240**, 306 (1970).
471. Potzel, W., Wagner, F. E., Mössbauer, R. L., Kaindl, G., and Selzter, H. E., *Z. Phys.* **241**, 179 (1971).
472. Prados, R. A., Ph.D. Thesis, Louisiana State Univ., Baton Rouge, Louisiana. Kindly communicated by M. L. Good.
473. Prados, R. A., Clausen, C. A., and Good, M. L., Abstr. Amer. Chem. Soc. 1971 Spring meeting, Los Angeles.
474. "Pyroxenes and Amphiboles; Crystal Chemistry and Phase Petrology." *Min. Soc. Amer. Spec. Paper No. 2*, (1969).
475. Reddy, J. M., Knox, K., and Robin, M. B., *J. Chem. Phys.* **40**, 1082 (1964).
476. Reiff, W. M., *J. Chem. Phys.* **54**, 4718 (1971).
477. Reiff, W. M., *Chem. Phys. Lett.* **8**, 297 (1971).
478. Reiff, W. M., *Inorg. Chim. Acta*. In press.
479. Reiff, W. M., *Coord. Chem. Rev.* In press.
480. Reiff, W. M., Baker, W. A., and Erickson, N. E., *J. Amer. Chem. Soc.* **90**, 4794 (1968).
481. Reiff, W. M., Long, G. J., and Baker, W. A., *J. Amer. Chem. Soc.* **90**, 6347 (1968).

482. Renovitch, G. A., and Baker, W. A., *J. Amer. Chem. Soc.* **89**, 6377 (1967).
483. Rentzeperis, P. J., *Z. Kristallogr.* **117**, 431 (1962).
484. Richards, R. R., and Gregory, N. W., *J. Phys. Chem.* **69**, 239 (1965).
485. Rickards, R., Johnson, C. E., and Hill, H. A. O., *J. Chem. Phys.* **48**, 5231 (1968).
486. Rickards, R., Johnson, C. E., and Hill, H. A. O., *Trans. Faraday Soc.*, **65**, 2847 (1969).
487. Rickards, R., Johnson, C. E., and Hill, H. A. O., *J. Chem. Phys.* **51**, 846 (1969).
488. Rickards, R., Johnson, C. E., and Hill, H. A. O., *J. Chem. Phys.* **53**, 3118 (1970).
489. Rickards, R., Johnson, C. E., and Hill, H. A. O., *J. Chem. Soc. A* 797 (1971).
490. Roberts, L. D., Patterson, D. O., Thomson, J. O., and Levey, R. P., *Phys. Rev.* **179**, 656 (1969).
491. Roberts, L. D., Pomerance, H., Thomson, J. O., and Dam, C. F., *Bull. Amer. Phys. Soc.* **7**, 565 (1962).
492. Robin, M. B., *J. Chem. Phys.* **40**, 3369 (1964).
493. Robinson, H., Dehmelt, H. G., and Gordy, W., *J. Chem. Phys.* **22**, 511 (1954).
494. Rogozev, B. I., Zavgorodnii, V. S., Krizhanskii, L. M., and Petrov, A. A., *J. Gen. Chem. USSR* **38**, 1999 (1968) (Russ. p. 2064).
495. Rother, P., Wagner, F., and Zahn, U., *Radiochim. Acta* **11**, 203 (1969).
496. Ruby, S. L., Kalvius, G. M., Beard, G. B., and Snyder, R. E., *Phys. Rev.* **159**, 239 (1967).
497. Ruby, S. L., and Selig, H., *Phys. Rev.* **147**, 348 (1966).
498. Ruby, S. L., and Shenoy, G. K., *Phys. Rev.* **186**, 326 (1969).
499. Rundle, R. E., and Olson, D. H., *Inorg. Chem.* **3**, 596 (1964).
500. Sano, H., and Hashimoto, F., *Bull. Chem. Soc. Jap.* **38**, 684 (1965).
501. Sano, H., and Kono, H., *Bull. Chem. Soc. Jap.* **38**, 1228 (1965).
502. Sasane, A., Nakamura, D., and Kubo, M., *J. Phys. Chem.* **71**, 3249 (1967).
503. Saxena, S. K., and Ghose, S., *Amer. Mineral.* **56**, 532 (1971).
504. Schilt, A. A., *Inorg. Chem.* **3**, 1323 (1964).
505. Schlemper, E. O., *Inorg. Chem.* **6**, 2012 (1967).
506. Schlemper, E. O., and Britton, D., *Inorg. Chem.* **5**, 507 (1966).
507. Schlemper, E. O., and Hamilton, W. C., *Inorg. Chem.* **5**, 995 (1966).
508. Schneider, R. F., and Di Lorenzo, J. V., *J. Chem. Phys.* **47**, 2343 (1967).
509. Shen, K., McEwen, W. E., LaPlaca, S. J., Hamilton, W. C., and Wolf, A. P., *J. Amer. Chem. Soc.* **90**, 1718 (1968).
510. Shenoy, G. K., and Ruby, S. L., in "Mössbauer Effect Methodology" (I. J. Gruverman, ed.), Vol. 5, p. 77. Plenum, New York, 1970.
511. Shirley, D. A., *Rev. Mod. Phys.* **36**, 339 (1964).
512. Shirley, D. A., in "Chemical Applications of Mössbauer Spectroscopy" (V. I. Goldanskii and R. H. Herber, eds.), p. 504. Academic Press, New York, 1968.
513. Shpinel, V. S., Bryukhanov, V. A., Kothekar, V., Iofa, B. Z., and Senov, S. I., *Symp. Faraday Soc.* **1**, 69 (1967).
514. Shustorovich, E. M., and Djatkina, M. E., *Dokl. Akad. Nauk. SSSR (Engl.)* **128**, 1234 (1959).
515. Simopoulos, A., Wickman, H. H., Kostikas, A., and Petrides, D., *Chem. Phys. Lett.* **7**, 615 (1970).
516. Smith, P. J., *Organometal. Chem. Rev. Sect. A* **5**, 373 (1970).
517. Spiess, H. W., Haas, H., and Hartmann, H., *J. Chem. Phys.* **50**, 3057 (1969).

518. Spijkerman, J. J., *Symp. Faraday Soc.* **1**, 134 (1967).
519. Spijkerman, J. J., Hall, L. H., and Lambert, J. L., *J. Amer. Chem. Soc.* **90**, 2039 (1968).
520. Stapfer, C. H., Leung, K. L., and Herber, R. H., *Inorg. Chem.* **9**, 970 (1970).
521. Stein, L., in "Halogen Chemistry" (V. Gutman, ed.), Vol. 1, p. 133 and refs. quoted therein. Academic Press, New York, 1967.
522. Stevens, J. G., and Bowen, L. H., in Mössbauer Effect Methodology" (I. J. Gruverman, ed.), Vol. 5, p. 27. Plenum, New York, 1970.
523. Stevens, J. G., and Ruby, S. L., *Phys. Lett.* **32 A**, 91 (1970).
524. Stevens, P. J., D. Phil. Thesis, Oxford Univ., Oxford, 1964.
525. Stöckler, H. A., and Sano, H., *Phys. Lett. A* **25**, 550 (1967).
526. Stöckler, H. A., and Sano, H., *Chem. Phys. Lett.* **2**, 448 (1968).
527. Stöckler, H. A., and Sano, H., *Phys. Rev.* **165**, 406 (1968).
528. Stöckler, H. A., and Sano, H., *Trans. Faraday Soc.* **64**, 577 (1968).
529. Stöckler, H. A., and Sano, H., *Chem. Commun.* 954 (1969).
530. Stöckler, H. A., Sano, H., and Herber, R. H., *J. Chem. Phys.* **45**, 1182 (1966).
531. Stöckler, H. A., Sano, H., and Herber, R. H., *J. Chem. Phys.* **47**, 1567 (1967).
532. Stukan, R. A., Goldanskii, V. I., Makarov, E. F., and Rukhadze, E. G., *J. Struct. Chem. (USSR)* **8**, 239 (1965).
533. Stukan, R. A., Gulein, S. P., Nesmeyanov, A. N., Goldanskii, V. I., and Makarov, E. F., *Teor. Eksp. Khim.* **2**, 805 (1966).
534. Sukhoverkhov, V. F., and Dzevitskii, B. E., *Dokl. Akad. Nauk SSSR Ser. Fiz.* **177**, 1089 (1967) (Russ. p. 6111).
535. Taft, R. W., in "Steric Effects in Organic Chemistry" (M. S. Newman, ed.), p. 556. Wiley, New York, 1956.
536. "The Mössbauer Effect and Its Applications in Chemistry." (R. F. Gould, ed.). Amer. Chem. Soc., Washington, D.C., 1967.
537. Thomas, K., Osborn, J. A., Powell, A. R., and Wilkinson, G., *J. Chem. Soc., A* 1801 (1968).
538. Thompson, J. B., *Amer. Mineral.* **54**, 341 (1969); **55**, 528 (1970).
539. Tinkham, M., *Proc. Roy. Soc., Ser. A* **236**, 549 (1956).
540. Townes, C. H., and Dailey, B. P., *J. Chem. Phys.* **17**, 782 (1949).
541. Triftshauser, W., and Craig, P. P., *Phys. Rev.* **162**, 274 (1967).
542. Trotter, J., and Zobel, T., *Z. Kristallogr.* **123**, 67 (1966).
543. Tsai, J. H., Flynn, J. J., and Boer, F. P., *Chem. Commun.* 702 (1967).
544. Uchida, T., *Bull. Chem. Soc. Jap.* **40**, 2244 (1967).
545. Unland, M. L., *J. Chem. Phys.* **49**, 4514 (1968).
546. Violet, C. E., in "The Mössbauer Effect and Its Applications in Chemistry" (R. F. Gould, ed.), p. 147. Amer. Chem. Soc., Washington, D.C., 1967.
547. Violet, C. E., and Booth, R., *Phys. Rev.* **144**, 225 (1966).
548. Violet, C. E., Booth, R., and Wooten, F., *Phys. Lett.* **5**, 230 (1963).
549. Virgo, D., and Hafner, S. S., *Mineral Soc. Amer. Spec. Paper* **2**, 67 (1969).
550. Virgo, D., and Hafner, S. S., *Amer. Mineral.* **55**, 201 (1970).
551. Vucelic, M., *Croat. Chem. Acta* **40**, 255 (1968).
552. Wagner, F., and Zahn, U., *Z. Phys.* **233**, 1 (1970).
553. Walker, L. R., Wertheim, G. K., and Jaccarino, V., *Phys. Rev. Lett.* **6**, 98 (1961).
554. Watanabe, N., and Niki, E., *Bull. Chem. Soc. Jap.* **43**, 3034 (1970).
555. Watson, R. E., and Freeman, A. J., *Phys. Rev.* **120**, 1125 (1960).
556. Wedd, R. W. J., and Sams, J. R., *Can. J. Chem.* **48**, 71 (1970).

557. Wei, C. H., and Dahl, L. F., *J. Amer. Chem. Soc.* **91**, 1351 (1969).
558. Wells, W. L., and Brown, T. L., *J. Organomet. Chem.* **11**, 271 (1968).
559. Wertheim, G. K., "Mössbauer Effect: Principles and Applications." Academic Press, New York, 1964.
560. Wertheim, G. K., and Buchanan, D. N. E., *Chem. Phys. Lett.* **3**, 87 (1969).
561. Wertheim, G. K., and Herber, R. H., *J. Chem. Phys.* **38**, 2106 (1963).
562. Wickman, H. H., and Silverthorn, W. E., *Inorg. Chem.* **10**, 2333 (1971).
563. Wickman, H. H., Trozzolo, A. M., Williams, H. J., Hull, G. W., and Merrett, F. R., *Phys. Rev.* **155**, 563 (1967).
564. Wickman, H. H., and Trozzolo, A. M., *Inorg. Chem.* **7**, 63 (1968).
565. Wickman, H. H., and Wagner, C. F., *J. Chem. Phys.* **51**, 435 (1969).
566. Williams, D. E., and Kocher, C. W., *J. Chem. Phys.* **52**, 1480 (1970).
567. Williams, D. E., and Kocher, C. W., *J. Chem. Phys.* **55**, 1491 (1971).
568. Williams, P. G. L., and Bancroft, G. M., "Mössbauer Effect Methodology" (I. J. Gruverman, ed.), Vol. 7, p. 39. Plenum, New York, 1971.
569. Wynter, C. I., and Chandler, L., *Bull. Chem. Soc. Jap.* **43**, 2115 (1970).
570. Wynter, C. I., Hill, J., Bledsoe, W., Shenoy, G. K., and Ruby, S. L., *J. Chem. Phys.* **50**, 3872 (1969).
571. Yamasaki, R. S., and Cornwell, C. D., *J. Chem. Phys.* **30**, 1265 (1959).
572. Yeats, P. A., Ford, B. F. E., Sams, J. R., and Aubke, F., *Chem. Commun.* 791 (1969).
573. Yeats, P. A., Poh, B. L., Ford, B. F. E., Sams, J. R., and Aubke, F., *J. Chem. Soc., A* 2188 (1970).
574. Yeats, P. A., Sams, J. R., and Aubke, F., *Inorg. Chem.* **9**, 740 (1970).
575. Zerner, M., Gouterman, M., and Kobayashi, H., *Theor. Chim. Acta* **6**, 363 (1966).
576. Zhdonov, Y. A., and Minkin, V. I., "Correlation Analysis in Organic Chemistry." Izd. Rostovsk Univ., 1961.
577. Zuckerman, J. J., *Advan. Organomet. Chem.* **9**, 21 (1970).